A novel paradigm for heart failure with preserved ejection fraction

A novel paradigm for heart failure with preserved ejection fraction

Working towards understanding the pathology of HFpEF

Ilona Jacquelina Nicola Maria Cuijpers

Cover

This cover shows that passion and devotion for science (depicted by the snapdragons and cornflowers, respectively), ambition and creativity (shown by the use a variety of purple colours), and the ability to grow and adapt to every possible circumstance (depicted by the edelweiss flowers) are essential for scientific and personal development. The small vessels, depicted as ferns and tree branches, show that there are multiple ways to reach the top (depicted by the gladiolus). As such, the shortest and best path is not always a straight line and each step (forward or backward) is important for scientific and personal growth.

Deze omslag toont dat passie en toewijding voor de wetenschap (uitgebeeld als een grote leeuwenbek en korenbloemen, respectievelijk), ambitie en creativiteit (uitgebeeld door het gebruik van paarstinten) en het zowel kunnen groeien in elke mogelijke omstandigheid als het aanpassen aan veranderende omstandigheden (uitgebeeld als een edelweiss) vereist zijn voor wetenschappelijke en persoonlijke ontwikkeling. De kleine vaten (uitgebeeld als de varens en vertakkingen) tonen dat er meerdere wegen naar de top zijn (uitgebeeld door de gladiolen). Rechtdoor is niet altijd de kortste of beste weg en elke stap (vooruit of achteruit) draagt bij aan een grotere wetenschappelijke en persoonlijke groei.

Cover design: Guillaume Gilbert

The research presented in this dissertation was performed at the center for molecular and vascular biology (CMVB, Katholieke Universiteit Leuven) and the department of Cardiology (Maastricht University). This doctoral research thesis was made possible by an Aspirant Fellowship from the Fonds Wetenschappelijk Onderzoek (FWO) Vlaanderen. We acknowledge the support from the European Research Area Network Cardiovascular disease (ERA-CVD), Innovative medicine initiatives (IMI), Netherlands Organization for Scientific Research (NWO), the Dutch Heart Foundation, and Boehringer Ingelheim International GmbH.

Printed by Proefschriftmaken.nl, The Netherlands.

Maastricht University

KU LEUVEN

DOCTORAL SCHOOL
BIOMEDICAL SCIENCES

A novel paradigm for heart failure with preserved ejection fraction

Working towards understanding the pathology of HFpEF

DISSERTATION

to obtain the degree of Doctor in Biomedical Sciences at Katholieke Universiteit Leuven and Doctor at Maastricht University, on the authority of the Rector Magnifici Prof. dr. Luc Sels and Prof. dr. Rianne Letschert in accordance with the decision of the Board of Deans, to be defended in public on Wednesday 28th of October 2020 at 13:00 hours in Maastricht

by

Ilona Jacquelina Nicola Maria Cuijpers

Promotors:

Prof. Dr. Ing. Elizabeth A.V. Jones, KU Leuven

Prof. Dr. Stephane Heymans, Maastricht University

Jury/assessment members:

Prof. Dr. Ronny Bruffaerts, KU Leuven, Chair reading examining committee

Prof. Dr. Aernout Luttun, KU Leuven

Prof. Dr. Massimiliano Mazzone, KU Leuven

Prof. Dr. Arantxa González Miqueo, Center for Applied Medical Research (CIMA), Spain

Prof. Dr. Simon Sedej, University of Graz, Austria

Prof. Dr. Ronit Shiri-Sverdlov, Maastricht University

Associate Prof. Dr. Kristiaan Wouters, Maastricht University

“No scorching sun nor freezing cold will stop me on my journey”

For the Dancing and the Dreaming

Gerard Butler

Table of contents

Words of Gratitude

Promoveren is een beproeving. Een beproeving die veel doorzettingsvermogen, passie, wilskracht, moed, nieuwsgierigheid, hoop, energie, zweet, tranen en (soms) een beetje magie vereist. Wetenschap is onvoorspelbaar en bestaat uit vallen en opstaan, bergen en dalen, positieve en negatieve data. Het vereist aanpassingsvermogen en het leren omgaan met kritiek en afwijzingen. Bovendien leerde ik naast mijn onderzoek studenten te begeleiden en coachen, experimenten te plannen, artikelen te reviewen, onderzoek te presenteren, samenwerkingen op te zetten, figuren te ontwerpen, onderzoek uit te dragen naar het brede publiek, beurzen, ethische projectaanvragen, verslagen, reviews, manuscripten en een thesis te schrijven, …. en nog veel meer.

Hoewel deze vier jaar niet de gemakkelijkste jaren waren, had ik ze nooit willen missen. Ik ben ontzettend trots op hoe ik op persoonlijk vlak gegroeid ben. Daarnaast ben ik ontzettend “fier” op al de vaardigheden die ik tijdens mijn promotie geleerd heb. Echter, is promoveren geen eenmanswerk en wil ik graag iedereen bedanken die mij heeft geholpen, gesteund en geïnspireerd.

First and foremost, **Elizabeth**, there is so much, I would like to thank you for. First of all, thank you so much for “adopting” me in your group and giving me the feeling of being at home. Thank you for all your excellent daily supervision and openness for every question. For being there for me whenever I needed your help. For supporting and calming me down when experiments did not work out as expected. For believing in me and teaching me that the only way you would get forward is to just give it a try. For making me even more critical and strengthen my arguments. For giving me the opportunity to learn a lot of new skills, the freedom to grow, and tips about future careers. For reminding me the important things in life and

showing me all your new chairs. Elizabeth, I am so proud to be part of your team that started off with 4 people and has grown to 9 people over the years.

Beste **Stephane**, bedankt dat ik mijn dubbel graad promotieonderzoek in uw team heb mogen uitvoeren. Dank voor uw kritische blik, waarbij u mij altijd herinnerde dat translatie van basis onderzoek naar de kliniek essentieel is. Daarnaast wil ik u bedanken voor het stimuleren van netwerken en samenwerken met andere medeonderzoekers door mij op verscheidene cursussen en congressen te laten presenteren. U toonde mij dat samenwerking de sleutel tot succes is.

Ευχαριστώ **Anna-Pia** om mij de kans te bieden om mijn droom, een doctoraat te behalen, mogelijk te maken. Onze eerste lange ontmoeting tijdens het sollicitatiegesprek in Leuven zal voor altijd in mijn geheugen gegrift staan. Onze ritjes van Maastricht naar Leuven waar werkelijk alles besproken kon worden, de tea time, onze gezellige lunches en je persoonlijke advies op wetenschappelijk, financieel en privégebied waren van onschatbare waarden. Toen je echter na 6 maanden je droom achteraan jaagde, voelde dit als een groot verlies. Natuurlijk had jij al een back-up plan geregeld om mijn promotie te verzekeren en stond je nog altijd voor mij klaar.

I would like to thank the members of the reading committee Prof. **Simon Sedej**, Prof. **Arantxa González Miqueo**, Prof. **Ronit Shiri-Sverdlov**, Prof. **Kristiaan Wouters**, Prof. **Aernout Luttun**, and Prof. **Massimiliano Mazzone** for their critical reading, constructive feedback, and proficient evaluation of the thesis. I would like to specially thank **Aernout** and **Massimiliano** for their commitment as my thesis advisory board members, who have given me suggestions during my whole PhD period. I also would like to thank all the members of the **corona**.

Daarnaast wil ik mijn **paranimfen** en lieve collega's bedanken.

Lieve **Paolo**, ik weet niet hoe ik jou moet bedanken. Tijdens onze eerste ontmoeting in Leuven raakte ik geïnspireerd door je passie, aanstekelijke enthousiasme en tijd speelt geen rol cultuur. Hoewel we in ons eerste half jaar tot alle hilariteit Engels met elkaar spraken, verzetten wij onze verdere vriendschap in twee talen dat vaak als fascinerend werd gezien door onze collega's. Jij was altijd in voor een discussie, een leuk weetje (vooral over bananen) en een lange lunch en had je altijd oor voor mij. Bij lab problemen kon ik altijd bij je terecht voor goed advies en kreeg ik ook meestal een lange uitgebreide uitleg en verschillende back-up plannen. Ook kon ik bij jou terecht als ik het even niet meer zag zitten, de experimenten allemaal niet leken te lukken of de publicatie druk zo oneerlijk was. Elkaar steunen werd ons hoger doel! Lieve Paolo, het einde van deze promotie zal zeker niet het einde van onze vriendschap betekenen. Ik wens je heel veel succes met je verdere PhD en veel liefde toe samen met Paolo in jullie nieuwe appartement. En vergeet niet.. Het komt in orde.

Dear **Steven**, o nee sorry ik mag geen Engels meer spreken haha. In december 2017 leerde ik jou kennen gedurende ons lab etentje. In het begin was je erg stil, maar dat veranderde snel. Samen vormde wij een hecht team, team HFpEF, dat met volle energie alle uitdagingen aanging. Tijdens onze tijdlijn experimenten waren wij vaak in de vroeg ochtenden samen te vinden in het lab, waarbij jij mij altijd bijstond bij. Als ik het moeilijk had herinnerde je mij altijd aan jouw eigen PhD en dat alles wel goed kwam. Naar onze lunch keek ik altijd uit; we bespraken Nederlandse artikels, vertaalde de horoscoop en maakte puzzels. Ook zal ik nooit ons reisje naar Pamplona vergeten; onze inmenging met de Spaanse cultuur tijdens de late stapavond, onze culinaire uitdagingen, de helikopter die personen opspoorde (Brexit) en tot slot onze verloren koffers. En dan natuurlijk ook nog ons late stapavondje in Leuven dat natuurlijk eindigt met nagelen in de Seven Oaks. Dank je wel voor al jouw hulp, vriendschap en Engelse humor waarom ik altijd zo hard om moet lachen.

I would like to thank all my lovely colleagues from **the Jones/Heymans** Lab. First, I would like to thank everyone for their support, willingness to help with everything, fun lunches, giggles in the hallways, and all our fun lab activities (drinks, bowling, diners, cooking experiences etc.).

Dear **Ashkan**, we started together our PhD adventure in 2016. We joined our forces to achieve all the milestones from our very first evaluation to our defense and article submission crises (using PhD memes). Thank you for all your technical PC assistance, cell culture advice, helpful discussions, and reminding all us to don't speak too much in jargon. Ashkan, I also would like to thank you for dragging me to gym, bringing too much sweets (which resulted in the need to go to the gym), and all your funny quotes, especially about managing a PI. I would like to wish you all the best and hope to visit you soon in Canada! **Hanna**, thank you so much for being there for me as a friend and colleague, making science fun, and reminding me of the important things in life. While you are not in the office anymore, your quotes on the wall are still making me smile. Enjoy your future with your beautiful family! **Nadèche**, dank je wel voor al je technisch advies, je hulp bij het kweken van muizen en gezellige lunchpauzes. **Margo**, ik wil je heel erg bedanken voor al je hulp tijdens het celkweek werk gedurende de laatste periode van de PhD. Jouw sterke motivatie en harde werk zullen zich belonen. Geniet van je PhD. **Bram en Jana**, het is super dat jullie ons team HFpEF versterken. Jullie kritische vragen vereiste soms heel wat denkwerk, maar waren altijd van grote waarde! Ik ben blij dat jullie twee met veel energie en enthousiasme mijn werk zullen voortzetten. Ik kijk uit naar jullie verdediging en wens jullie heel veel succes toe! Dear **Laia**, thank you so much for join our team. I would like to wish you all the best of luck during your Post Doc in our group! Enjoy the beautiful city Leuven and the rest of Belgium.

Dear **Emma**, thank you so much for being such a good friend and colleague. During the start of the PhD, you were always there for me to help me out, even while you were so busy. I

enjoyed our time working together in Leuven and was so happy when you started working in Stephane's group. Thank you for all your critical questions, helpful tips, our fun moments in the office, your lovely messages, and our great trips to congresses. Best of luck with your new position in Germany and Denver. **Quentin**, my Maastricht/Leuven PhD friend, it's great to have someone to discuss yours struggles and successes of working in multiple institutes. I enjoyed working, traveling, chatting (sometimes we even forgot that we were already in Liège), and attending workshops with you. Hope to see you soon and have again a reallyyyy long chat with you. Dear (tropical storm) **Vincenza**, while we only worked for a few months together, you taught me various technical skills, asked critical questions, and showed me how to be persistent. Your energy and enthusiasm were admiring. I would like to wish you, Craig, and Skye all the best. Hope to meet up soon in Maastricht. **Bartek**, thank you for our fun talks and lab activities. Good luck at your new position in Liège! I also would like to thank my students **Liene**, **Laura**, and **Daria**. Thank you for all our fun moments and all the contribution to my PhD research. **Liene**, een student begeleiden in het eerste halve jaar van mijn PhD was toch wel spannend, maar wat heb ik genoten van jouw enthousiasme, motivatie en de gezelligheid in het kantoor. **Laura**, it was pleasure to have you in our group. I would like to wish you good luck with your new study in Utrecht!

I would like to thank all members of the endothelial cell meeting group. I enjoyed chatting in a non-formal matter about our research and appreciated all your help and comments during my PhD. Ik wil specifiek graag **Aernout** zijn groep en **An** haar groep bedanken. **Petra** dank u wel voor onze gezellige FACS sorts en het toch een beetje (Belgisch) Limburg in de buurt te hebben. **Wouter**, **Willeke** en **Ljuba** dank jullie wel voor alle antibody zoektochten en hulp bij stainings. **An** dank u wel voor al uw hulp bij technische vragen, uw tips om het onderzoek nog beter te presenteren en uw motiverende en lieve woorden en e-mailtjes. **Michael** en **Willeke**, team

Nederland, dank je wel voor al je hulp tijdens mijn FACS avontuur en onze leuke anekdotes over Belgen bij het koffieapparaat! **Michael** dank je voor al je hulp bij mijn zoektocht voor een nieuwe functie.

Daarnaast wil ik graag alle (oud-)collega's van Maastricht bedanken. **Blanche, Marc, Annika, Jeremy, Emma, Monica, Steffie, Robin, Rick, Wouter, Arantxa, Michiel, Anne, Job, Jort** en **Eleni** dank jullie wel voor al jullie feedback tijdens de lab meetings en voor de gezellige uitjes en lunches met de groep. Lieve **Annika**, wat was het heerlijk om met jou samen te werken, meetings te bezoeken of gewoon gezellig te kletsen. Heel veel succes met je PhD. **Barbara** en **Lilian** dank je wel voor alle administratieve hulp.

I would like to thank all the (ex-)members of the Center for Molecular and Vascular Biology. **Ellen, Mara, Joseph, Ljuba, Tula, Denise, Kylie, Nathan, Severien, Lore, Christine, Annemie, Annick de Soete, Bianca, Ingrid,** en **Inge** dank jullie wel voor jullie vriendschap, alle gezelligheid en lunches waarbij heel wat afgelachen werd. **Mara**, **Ellen, Ljuba,** en **Nadèche** (het puzzelteam) dank jullie wel voor alle steun, jullie positiviteit en al onze giechelbuien in de gangen. **Joseph**, thank you for making me laugh and our adventures in the DelHaize. **Guillaume**, merci, for all your great drawings, which inspired me to start drawing! Good luck in France! **Chandan**, thank you for all our chats in the coffee room. **Peter**, köszönöm, I still remember the first day I met you when you told me that my name was Hungarian. Ik wil je bedanken voor al je hulp. I enjoyed our chats which mostly stated with how are you and ended up in endless other subjects (Hungary, echocardiography and PV loop discussions, or even Dutch conversations). **Annick de Soete** dank je voor alle administratieve hulp, de grappige telefoontjes naar Nederlandse bedrijven en onze gesprekken in de koffiekamer en jouw kantoor waarbij we soms de tranen in de ogen hadden van het lachen.

Ingrid ik wil ook jouw super bedanken voor al je administratieve hulp, maar ook de hulp bij het invullen van kruiswoordpuzzels.

I would like to thank all our **collaborators** and the **Lymit-dis ERA-net group** for all their help and feedback during my PhD.

Ik bedank graag al mijn vrienden en vriendinnen van de **carnavalsgroep**. Voor onze gezellige carnavalsdagen, tentfeestjes, uitjes, weekendjes weg, etentjes en drankjes, tussen al mijn drukke werk in Leuven en Maastricht. Ik zou ook graag **Luc**, **Joris** en **Carina** willen bedanken. Hoewel we ons minder zagen door ons drukke bestaan is het contact steeds gebleven. Dank jullie wel voor al jullie steun, interesse en de gezellige uitjes.

Daarnaast wil ik graag mijn familie bedanken, want zonder hun steun en liefde zou ik hier nooit hebben gestaan. **Mam en pap** bedankt om mich de kansen te geve die ich wou griepen, ummer ming eige paad te loate keeze um dees wereld te verkinnen en mich in alles te steune. Geer hub mich gelierd dat hel wirke ummer beloond weurd en dat opgeeve gein optie is. Al woar de aafstand no Leuven soms groter dan gedacht, geer zoog ummer waal ein maneer um mich te helpen en te steunen. **Rick** ich wil dich bedanken um ding interesse in ming werk, de veule discussies die ver heje euver medisch of neet medisch onderzeuk en ding hulp mit al ming computer problemen. **Petenonk Nico en Petetant Jacqueline** bedankt veur alle steun en interesse de aafgeloape joare. Al uch medische vroage en ming oetleg stimuleerde mich des te meer um de wetenschap meer openbaar veur het publiek te maken. **Oma Maike** wat bin ich blie dat ich uch bie ming promotie kin hubbe. Dank uch veur al die joare dat geer veur mich kloar stongt en nog ummer steit (mit meistal ein stuk vla), oze gezellige bezeukskes, winkeldaagskes en toertochtjes in de auto. Al woar het soms meuilijk te bevaten wat ich noe eigenlijk deech, geer stingt ummer veur mich kloar. **Oma en Opa "Sjin"** bedankt veur al uch interesse in "ming studie in Leuven" en het feit dat ger elke kier waal weer aan eederein vertilde

wie trots ger waal neet op mich woart. Hoewaal aafscheid numme ummer zwaor is, weit ich dat geer vanaf bove ummer op mich zult litte, trots op mich zut en samen auch zult mit vieren…. hopelijk hubbe ze genog vla doa bove. (**Schoon-)Familie** bedankt veur al uch begrip en hulp in de aafgelope joaren. **Noa** en **Aaron** bedankt voor al onze gezellige tekenavonturen en spellendagjes!

Leeve **Roel** in onze vief joar same hubbe veer al veule leuke en minder leuke dinger mitgemaakt. Toen ich wie ver 8 moand same woare vertilde dat ich geer minge dreum wool noagoan in Leuven, woars dich super gedreve um mich te steunen of dat noe via de telefoon, email, skype of daadwerkelijk samen zeen woar. Taxi Roel sting altied veur mich kloar: of ich nu weer urges vaststing umdat de trein neet wier reej, ich noa ein congres ging, of um gewoon ein verassing bezeukske te bringe in Leuven. Zonger dich hej ich hie nooit gestange, dich hub altied no mich geloesterd (zowaal as ich super enthousiast woar of jus klaagde), gerust gestild en gemotiveerd um neet op te geven, want ja as ein doctoraat mekkelijk woar dan woar waal eiderein doctor. Ding interesse in ming onderzeuk leet se ummer merken as se weer thoeskeems en weer nuje vroage veur mich hejs. Doe lierdes mich dat ontspanning auch belangrijk is en dat ein goeie wandeling mit oze leeve **Rhino** dich op nuje goeje gedachten kint bringen. Ich bin noe kloar veur ein nuj avontuur mit dich: geneten van oze toekomst samen in os eige huuske.

Ευχαριστώ	köszönöm	Thank you	Bedankt		
Graciasdziękuję	تشكر با	Grazie	Merci	Tack	Danke

Abbreviations

A	late mitral inflow peak velocity
A’	late diastolic mitral annulus peak velocity
ADMA	asymmetric dimethyl-L-arginine
AET	aortic ejection time
Akr1b1	aldo-keto reductase family 1 member B1
Angpt	angiopoietin
αSMA	alpha smooth muscle actin
AW	anterior wall
BSA	body surface area
CAMKII	calcium/calmodulin-dependent kinase-II
cAMP	cyclic adenosine monophosphate
CCL2	C-C motif chemokine ligand 2
cGMP	cyclic guanosine monophosphate
CI	cardiac index
CO	cardiac output
Col	collagen
CRP	C-reactive protein
CSA	cross-sectional area
DAP	diastolic arterial pressure
DCM	dilated cardiomyopathy
DEG	differentially expressed gene
dP/dt_{max}	maximum rate of pressure change in the left ventricle
dP/dt_{min}	minimum rate of pressure change in the left ventricle
DPP-4	dipeptidyl peptidase-4
E	early mitral inflow peak velocity
E’	early diastolic mitral annulus peak velocity
Ea	arterial elastance
ECG	electrocardiogram
EDD	end-diastolic diameter
EDP	end-diastolic pressure
EDPVR	end-diastolic pressure volume relationship
EDV	end-diastolic volume
EF	ejection fraction
eNOS	endothelial nitric oxide synthase
ERK2	extracellular signal-regulated kinase-2
ESD	end-systolic diameter
ESP	end-systolic pressure
ESPVR	end-systolic pressure-volume relationship
ESV	end-systolic volume
$F_{passive}$	passive stiffness
FS	fractional shortening
HDL	high-density lipoprotein
HF	heart failure
HFmrEF	heart failure with mid-range ejection fraction
HFpEF	heart failure with preserved ejection fraction
HFrEF	heart failure with reduced ejection fraction
HR	heart rate

HT	hypothyroidism
H_2O_2	hydrogen peroxide
HUVEC	human umbilical vein endothelial cell
GIP	glucose-dependent insulinotropic peptide
GLP-1	glucagon-like peptide-1
ICAM-1	intercellular adhesion molecule-1
Ier3	immediate early response 3
IL	interleukin
IP	intraperitoneal
IVCT	isovolumic contraction time
IVRT	isovolumic relaxation time
Ket/Xyl	ketamine/xylazine
LDL	low-density lipoprotein
LOX	lysyl oxidase
MAP	mean arterial pressure
MetS	metabolic syndrome
MHC	myosin heavy chain
MPI	myocardial performance index
Mmp	metalloproteinase
NFκB	nuclear factor kappa B
NFT	non-flow time
NG2	neuron-glial antigen 2
NMDA	N-methyl-D-aspartate
NO	nitric oxide
NOX	nicotinamide adenine dinucleotide phosphate oxidase
N2Bus	N2B unique sequence
$ONOO^-$	peroxynitrite
$O_2^{\cdot -}$	superoxide anion
PDE	phosphodiesterase
PDGFβ	platelet-derived growth factor beta
PDGFβR	platelet-derived growth factor beta receptor
P4ha1	prolyl-4-hydroxylase subunit alpha 1
PGE2	prostaglandin E2
PGF2α	prostaglandin F2 alpha
PK	protein kinase
PRSW	preload-recruitable stroke work
Ptges-1	prostaglandin E synthase 1
PV	pressure-volume
PW	posterior wall
ROS	reactive oxygen species
S’	systolic peak wave
SAMP	senescence-accelerated mouse-prone
SAP	systolic arterial pressure
sGC	soluble guanylate cyclase
SGLT2	sodium-glucose transport protein 2
SR	sarcoplasmic reticulum
SS-31	szeto-schiller-31
SV	stroke volume
TGFβ	transforming growth factor beta
Timp	tissue inhibitor of metalloproteinases

TL	tibia length
TNFα	tumor necrosis factor alpha
T2DM	type 2 diabetes mellitus
VCAM-1	vascular cellular adhesion molecule-1
VEGF	vascular endothelial growth factor
vSMC	vascular smooth muscle cell
ZDF	zucker diabetic fatty
ZSF1	zucker fatty spontaneously hypertensive heart failure F1 hybrid

English Summary

More than half of the patients with heart failure (HF) suffer from heart failure with preserved ejection fraction (HFpEF; ejection fraction >50%), a complex cardiovascular syndrome characterised by diastolic dysfunction and cardiac stiffening, fibrosis, inflammation, and hypertrophy. Due to the ageing population, as well as increased incidence of common comorbidities, such as type 2 diabetes mellitus, hypertension, and obesity, the prevalence of HFpEF is increasing dramatically. Alarmingly, there are no specific evidence-based therapies for HFpEF, likely due to the incomplete understanding of the pathology, heterogeneity in the patient population, and inadequate diagnosis. In this thesis, we therefore investigated the disease progression and established early characteristics of HFpEF in the obese ZSF1 rat, which mimics human pathology. This will facilitate risk stratification and the development of prevention and treatment strategies.

Chapter 1 introduces the current clinical challenges in the diagnosis, prevention, and treatment of HFpEF. This chapter gives a literature overview of the current diagnosis, pathological understanding of HFpEF, and rodent models for HFpEF and introduces potential therapeutic options for patients with HFpEF. **Chapter 2** describes the rationale and aims of thesis.

In **chapter 3**, we investigated the effects of the two most common anaesthetics, ketamine/xylazine and isoflurane, on cardiac function, especially diastolic dysfunction, in HFpEF-diseased obese ZSF1 rats. In echocardiography, ketamine/xylazine was able to demonstrate diastolic dysfunction in obese ZSF1 rats. In contrast to ketamine/xylazine, isoflurane impeded the reliable measurement of diastolic function, resulting in underdiagnosis of diastolic dysfunction in HFpEF-diseased obese ZSF1 rats. Well-considered evaluation of anaesthetics usage during the echocardiographical assessment of diastolic function is therefore required both in animal models and patients.

In **chapter 4**, we showed that active cardiac capillary regression caused by the loss of the mural support cells, called pericytes, is an early event in the development of HFpEF, leading to microvascular rarefaction in established HFpEF. Capillary regression coincided with endothelial activation and junctional remodelling and occurred before the development of other key pathological processes, including diastolic dysfunction, cardiac fibrosis, and cardiac and systemic inflammation. The reduced pericyte density at this early stage *in vivo* might be explained by an increased vulnerability of pericytes to metabolic stressors, including hyperglycaemia, hyperlipidaemia, and oxidative stress, compared to endothelial cells, as shown *in vitro*. Thus, targeting the microvasculature, especially stabilising pericytes, could be a potential new therapy for HFpEF.

In **chapter 5**, we demonstrated that the currently used anti-diabetic drug linagliptin prevents metabolic risk-induced cardiac stiffening by reducing the cardiomyocyte passive stiffness, the earliest manifestation of diastolic dysfunction. This was mediated by prevention of direct cleavage of the giant spring titin, which is responsible for cardiac relaxation. In addition, the indirect modulation of titin phosphorylation, titin isoform switching, and reduced cardiac fibrosis by linagliptin resulted in a reduced passive stiffness. Thus, reducing cardiomyocyte stiffness by administrating linagliptin could prevent the development of metabolic risk-induced diastolic dysfunction in patients.

To conclude, in **chapter 6**, we discuss the impact of the findings described in this thesis on the diagnosis and (early) pathophysiological understanding of HFpEF and development of novel preventive and therapeutic options in patients with HFpEF. Furthermore, we discuss that the development of novel animal models mimicking human pathophysiology are crucial for the development of early diagnostic markers and effective prevention and therapeutic strategies.

Nederlandse Samenvatting

Meer dan de helft van de patiënten met hartfalen (HF) lijdt aan hartfalen met een behouden ejectiefractie (ejectiefractie >50%), ook wel HFpEF genoemd. HFpEF is een complex cardiovasculair syndroom dat gekenmerkt wordt door diastolische dysfunctie en verstijving, fibrosis, ontsteking en hypertrofie van het hart. Veroudering en de toegenomen incidentie van veel voorkomende comorbiditeiten, zoals type 2 diabetes mellitus, hypertensie en obesitas, leiden tot een drastische toename van de prevalentie van HFpEF. Echter zijn er momenteel geen behandelingen voor HFpEF beschikbaar, doordat de onderliggende pathologie niet gekend is, de patiëntenpopulatie zeer heterogeen is en patiënten inadequaat gediagnosticeerd worden. In deze thesis onderzochten wij daarom het verloop van de ontwikkeling van HFpEF in een rat model dat de humane ziekte nabootst, de obese ZSF1 rat, om zo vroege ziekteverschijnselen te ontdekken. Dit onderzoek zal de risicostratificatie en de ontwikkeling van preventie- en behandelstrategieën vergemakkelijken.

Hoofdstuk 1 introduceert de huidige klinische uitdagingen voor de diagnose, preventie en behandeling van HFpEF. Dit hoofdstuk geeft een literatuuroverzicht over de huidige diagnose, ziekteontwikkeling in HFpEF en diermodellen voor HFpEF. Daarnaast worden potentiële behandelingen voorgesteld voor HFpEF patiënten. **Hoofdstuk 2** beschrijft de rationale en de doelstellingen van deze thesis.

In **hoofdstuk 3** hebben wij onderzocht wat de effecten van de twee meest gebruikte anesthetica (ketamine/xylazine en isofluraan) zijn op de hartfunctie, specifiek de diastolische functie, in obese ZSF1 ratten die lijden aan HFpEF. In obese ZSF1 ratten die geanestheseerd waren met ketamine/xylazine konden wij met behulp van echocardiografie diastolische dysfunctie diagnosticeren. Echter wanneer isofluraan als anestheticum werd gebruikt kon er met behulp van echocardiografie geen betrouwbare opname van de diastolische functie worden gemaakt.

Dit resulteerde in onderdiagnose van diastolische dysfunctie in obese ZSF1 ratten die lijden aan HFpEF. Dit toont aan dat er bij echocardiografie een goed overwogen evaluatie van het type anestheticum vereist is voor het diagnosticeren van diastolische dysfunctie in zowel diermodellen als patiënten.

In **hoofdstuk 4** toonden wij dat actieve regressie van de capillairen in het hart een vroeg verschijnsel is in de ontwikkeling van HFpEF. Deze actieve capillaire regressie werd veroorzaakt door het verlies van de ondersteunende cellen in de vaatwand, ook wel pericyten genoemd, en resulteerde in capillaire rarefactie nog voordat er klinische symptomen van HFpEF zichtbaar waren. Capillaire regressie ging tezamen met endotheel activatie en reorganisatie van endotheelcel junctie eiwitten, maar vond plaats voor de ontwikkeling van andere belangrijke pathologische processen (systemische ontsteking, diastolische dysfunctie en fibrose en ontsteking in het hart). De verminderde dichtheid van pericyten in dit vroeg stadium *in vivo* kan potentieel worden verklaard door het feit dat *in vitro* pericyten gevoeliger waren voor metabole stress factoren (hyperglycemie, hyperlipidemie en oxidatieve stress) in vergelijking met endotheelcellen. Therapieën die een positief effect hebben op de microvasculatuur door de pericyten te stabiliseren zouden mogelijk de ontwikkeling van HFpEF kunnen vertragen of zouden zelfs HFpEF kunnen genezen.

In **hoofdstuk 5** toonden wij aan dat het medicijn dat tegenwoordig wordt gebruikt voor de behandeling van type 2 diabetes, linagliptin genaamd, de ontwikkeling van metabool risico-geïnduceerde verstijving van het hart voorkomt. Dit was het gevolg van het verhinderen van de ontwikkeling van de vroegste manifestatie van diastolische dysfunctie, ook wel toegenomen passieve stijfheid van hartcellen genoemd. Titine, het grootste eiwit in het lichaam, is verantwoordelijk voor de relaxatie van het hart. De verminderde passieve stijfheid van de hartcellen was het gevolg van de verhinderde splitsing van titine. Daarnaast resulteerde toegenomen fosforylering van titine, het switchen van de titine isovormen en verminderde

fibrose in een afgenomen passieve stijfheid van de hartcellen. Linagliptin kan dus potentieel door middel van het verminderen van de stijfheid van hartcellen de ontwikkeling van diastolische dysfunctie voorkomen in patiënten met een verhoogd metabool risico.

Tot slot wordt in **hoofdstuk 6** de impact van de bevindingen van deze thesis op de diagnose, het begrip van de ziekteontwikkeling en de ontwikkeling van nieuwe preventie- en behandelingsmethoden besproken. Daarnaast wordt de urgentie voor het ontwikkelen van nieuwe diermodellen die de ziekteontwikkeling in HFpEF patiënten nabootsen besproken.

Chapter 1: General Introduction

Parts of this general introduction are adapted from my two shared first author review articles entitled "Cellular and Molecular Differences between HFpEF and HFrEF: A Step Ahead in an Improved Pathological Understanding." https://doi.org/10.3390/cells9010242 and "Microvascular and lymphatic dysfunction in HFpEF and its associated comorbidities." https://doi.org/10.1007/s00395-020-0798-y and our position paper of the ESC Working Group on Myocardial Function "Towards standardization of echocardiography for the evaluation of left ventricular function in adult rodents" https://doi.org/10.1093/cvr/cvaa110

1.1 Heart failure with preserved ejection fraction, an emerging clinical problem

1.1.1 Types of heart failure

Heart failure (HF) is the most prominent cause of hospitalisation globally, with 3.6 million newly diagnosed patients annually in Europe, resulting in a socioeconomic burden of billions of euros[1]. More than half of these HF patients suffer from **heart failure with preserved ejection fraction** (HFpEF; ejection fraction >50%). HFpEF is a complex cardiovascular syndrome characterised by diastolic dysfunction (impaired cardiac relaxation) and cardiac remodelling, including left ventricular stiffening, fibrosis, inflammation, and hypertrophy. The risk of developing HFpEF is especially increased in patients with a cluster of metabolic comorbidities, including obesity, hypertension, type 2 diabetes mellitus (T2DM), kidney disease, ageing, and chronic obstructive pulmonary disease, and its related systemic inflammation. In contrast to HFpEF, **heart failure with reduced ejection fraction** (HFrEF), defined by an ejection fraction of less than 40%, is characterised by substantial acute or chronic cardiomyocyte loss, due to ischemia, a genetic mutation, myocarditis, or valvular disease, resulting in the development of systolic dysfunction (impaired cardiac contraction)[2]. **Heart failure with mid-range or mildly reduced EF** (HFmrEF) is an intermediate stage with an ejection fraction between 40-49%, that generally progresses either to HFpEF (25% of cases) or HFrEF (33% of cases)[3]. With regard to ischaemic aetiology, HFmrEF resembles more HFrEF,

but HFmrEF has a higher frequency of underlying coronary artery disease and better overall prognosis[3-5].

1.1.2 Risk factors and gender predisposition associated with HFpEF development

Despite the fact that cardiovascular events associated with HFpEF, HFmrEF, and HFrEF share many risk factors[6], some risk factors are more prevalent in HFpEF than in HFrEF (Figure 1.1). Patients with HFpEF are more likely to be **older**[7]. In addition, HFpEF patients have a higher prevalence of **non-cardiac comorbidities**, including metabolic syndrome (MetS) components (hypertension, T2DM, hyperlipidaemia), anaemia, pulmonary disease, liver disease, sleep apnoea, gout, and cancer, than HFrEF patients[8]. The **inflammation** accompanied with these comorbidities is also associated with an increased risk for HFpEF development[8]. As such, the incidence of hospitalisation for comorbidity-related illness is higher in HFpEF compared to HFrEF[9]. Patients suffering from **autoimmune diseases**, such as rheumatoid arthritis, are also at increased risk for developing HFpEF[10].

In addition to the variation in risk factors, there are also gender-related differences in HFpEF compared to HFrEF patients. HFpEF is the most common form of HF in **women**, with a two-fold predominance of females[11,12]. This predominance might be the result of a greater susceptibility of men to develop HFrEF, specifically after myocardial infarction[7]. Additionally, men more easily develop eccentric left ventricular hypertrophy upon pressure-overload in HFrEF, while concentric hypertrophy, as observed in HFpEF, is more common in women[13]. HFpEF also develops mostly in postmenopausal women[14,15], suggesting a protective role for female sex hormones. Finally, a history of preeclampsia also predisposes to HFpEF development in middle aged women[16].

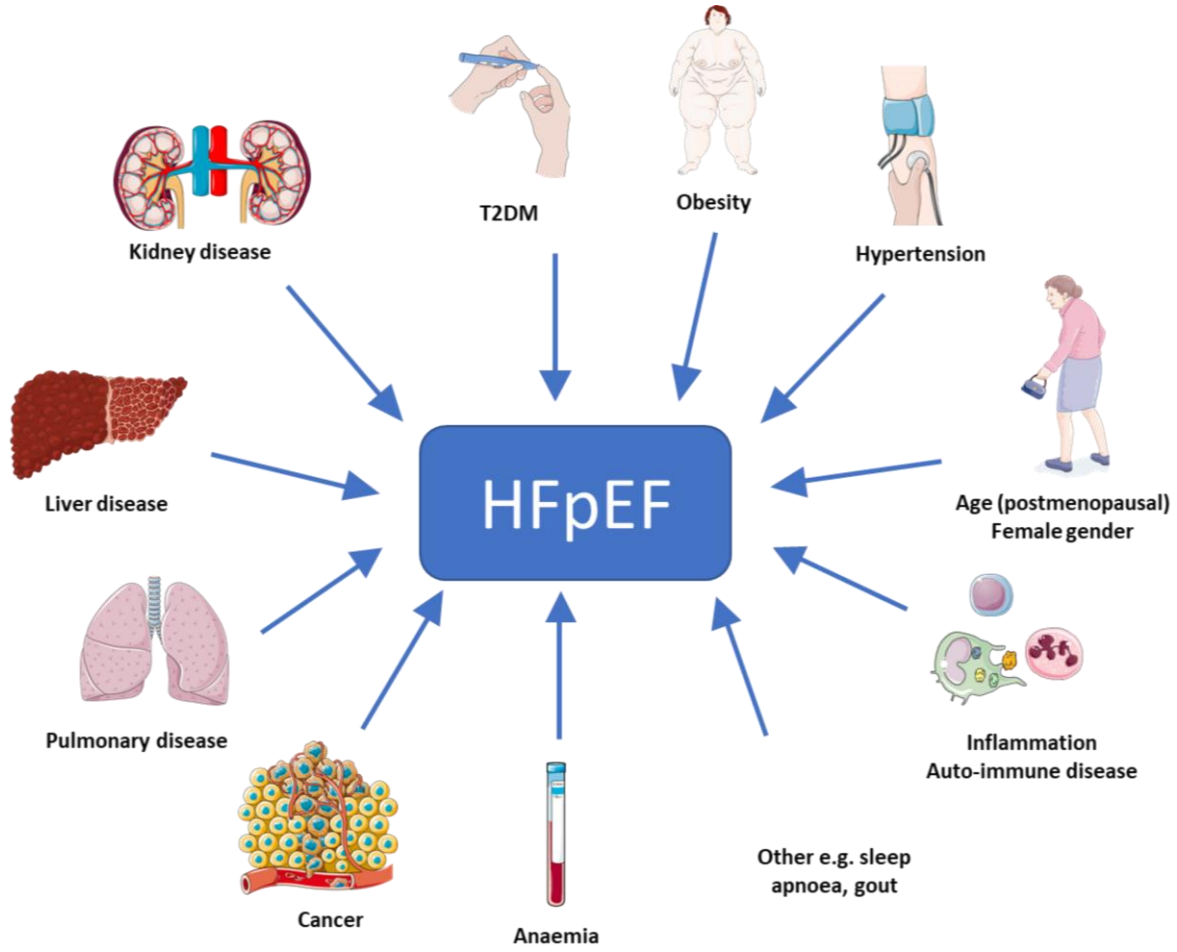

Figure 1.1 – Risk factors and comorbidities associated with the development of heart failure with preserved ejection fraction. *HFpEF, heart failure with preserved ejection fraction; T2DM, type 2 diabetes mellitus. Image was created using artwork from Servier Medical Art.*

1.1.3 Prevalence and prognosis of HFpEF

HFpEF accounts for 40 to 50% of incident HF overall and this is expected to rise even further[17,18]. More than half of patients with unexplained exertional dyspnoea that are referred to catherization laboratories are diagnosed with HFpEF and over 70% of patients with prevalent HF above the age of 65 years have a preserved ejection fraction[19]. HFpEF prognosis is poor with a 1-year hospital readmission and mortality rate ranging both between 20% and 35%, severely impaired health-related quality of life (score 40.9 out of 105), and a high premature life-years lost[20,21]. As a result, long-term costs for HFpEF are soaring due to increasing emergency rehospitalisations[22]. Despite emergence of HFpEF as an important clinical problem over the last two decades, little advancement has been made in identifying evidence-based

treatments or prevention strategies for HFpEF[23]. This is especially complicated by **incomplete understanding of the pathophysiology**, **patient population heterogeneity**, and **inadequate diagnosis**[24].

1.2 Diagnosis of HFpEF

Early reliable diagnosis is essential to determine the aetiology and stage of HFpEF, such that management strategies could be developed that delay or reverse disease progression. However, **symptoms**, such as poor exercise capacity and peripheral oedema, are **not disease-specific**[25,26] and may have a non-cardiac origin in many patients[27-30]. Furthermore, younger HFpEF patients often have a different clinical presentation, aetiology, and outcome compared to older patients[31].

1.2.1 Non-invasive assessment of diastolic dysfunction by echocardiography

In addition to the presence of symptoms, the diagnosis of HFpEF requires a normal or mildly abnormal systolic function and evidence of diastolic dysfunction and/or structural myocardial changes[25]. Diastolic dysfunction occurs when the left ventricle does not properly relax, resulting in decreased filling of the heart with blood. Diastolic dysfunction can be caused by stiffening of the left ventricular wall and/or abnormal relaxation as a result of excessive cardiac fibrosis and/or increased cardiomyocyte passive stiffness, which will be further discussed in section 1.3.

While several image modalities are available, **transthoracic echocardiography** is the preferred method for quantitative diagnosis of patients with suspected HFpEF, due to its non-invasiveness, accuracy, repeatability, low costs, safety, and wide availability[25]. It provides essential information on cardiac dimensions, hemodynamics, and systolic and diastolic function. To assess whether systolic function is preserved, ejection fraction is calculated based on the left ventricular end-diastolic and -systolic volume (EDV and ESV, respectively). For the diagnosis of diastolic dysfunction, **pulsed waved and tissue Doppler** are used to asses blood

flow and myocardial velocity, respectively. These techniques are based on the Doppler principle that states that the frequency of a wave will shift when it is emitted or reflected from a moving object, which is the blood for pulsed wave Doppler and the heart wall for tissue Doppler. Estimates of blood flow and myocardial velocity are subsequently calculated by comparing the frequency change between the transmitted and reflected sound waves, whereby an increase in Doppler shift indicates an increased velocity and *vice versa*[32].

The four distinct phases of diastole (Figure 1.2) are visible with Doppler imaging. During the first phase, the isovolumic ventricular relaxation (IVRT; pulse waved Doppler), the atrium fills actively, while the left ventricle is relaxed. This period spans from the closure of the aortic valve (end-systole) until the filling of the atrium[33].When the left ventricular pressure falls below the left arterial pressure, the mitral valve opens and blood flows passively from the left atrium to the ventricle during phase 2 (called rapid passive filling). This phase is responsible for approximately 80% of the total left ventricular filling. Both the peak velocity at which the blood flows in the left ventricle (E; early mitral inflow peak velocity) and the time form the peak of the E wave to baseline (mitral valve deceleration time) can be measured by pulsed wave Doppler. The velocity of the cardiac muscle movement during this early filling phase, the early diastolic mitral annulus peak velocity (E'), can be measured by tissue Doppler. During diastasis, the third phase, active left ventricular relaxation is completed and left atrial and ventricular pressures are almost in equilibrium, resulting in slow left atrial filling from pulmonary venous flow[33], which can be assessed by both pulsed wave and tissue Doppler. During the last phase, the arterial kick, the left atrium contracts, resulting in accelerated blood flow from the left atrium to the ventricle[33]. The peak velocity of blood (A; late mitral inflow velocity) and cardiac movement (A'; late diastolic mitral annulus peak velocity) can be assessed by pulsed wave and tissue Doppler, respectively. Alterations of any of these diastolic phases lead to diastolic dysfunction.

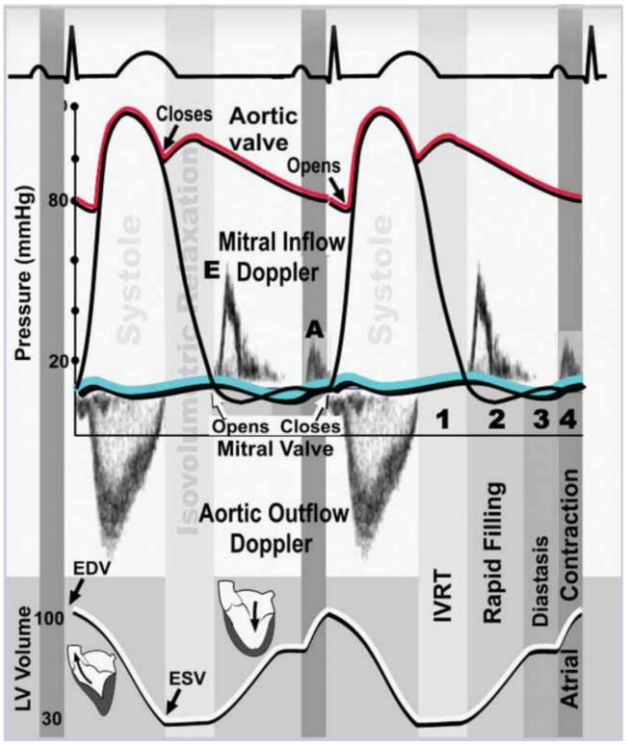

Figure 1.2 – Cardiac cycle with pulsed wave Doppler imaging and electrocardiogram*. The first phase of diastole, the isovolumic ventricular relaxation time (IVRT), comprises the left atrial filling from the closure of the aortic valve until the opening of the mitral valve. When the mitral valve opens, blood flows passively from the left atrium in the ventricle (rapid passive filling) with an early mitral inflow peak velocity (E). During diastasis, active left ventricular relaxation is completed. During arterial systole, the left atrium contracts to accelerate the blood flow from the left atrium to the ventricle. The peak velocity of blood during this period is called the arterial or "late" mitral inflow peak velocity (A). EDV, end-diastolic volume; ESV, end-systolic volume. From Ho CY. 2007.*[34]

1.2.2 Grades of diastolic dysfunction

There are three grades of diastolic dysfunction (Figure 1.3)[35]. **Grade I**, also called **impaired relaxation**, is the mildest form of diastolic dysfunction. In this is phase, there is greater impedance to blood flow from the left atrium to the left ventricle, resulting in a prolonged relaxation, including a prolonged mitral valve deceleration time (DT >160 ms) and IVRT (>90 ms) and a reduced E[33]. This results in increased A peak velocities, ultimately leading to a decreased E/A ratio < 1.0 and preserved E/E' ratio (<8.0)[35]. During **grade II**, called **pseudonormal**, the diastolic phase resembles a normal filling, reflected by a normal E/A ratio (1-2) and mitral valve deceleration time (DT <160 ms)[35]. However, progressive diastolic dysfunction causes the left atrial pressure to rise, which drives left ventricular filling and thereby superimposes upon the impaired left ventricular relaxation[35]. The decreased E' velocity

and resultant increased E/E' ratio, indicate a reduced cardiac relaxation and increased left atrial pressure[35]. During the most severe grade of diastolic dysfunction, **restrictive filling (Grade III)**, increased left atrial pressure results in a faster opening of the mitral valve, leading to a shortened IVRT (<70 ms) and increased E[35]. Due to left ventricular stiffening, early diastolic filling results in a fast rise of the left ventricular pressure, leading to an equilibrium of left atrial and ventricular pressure and a shortened mitral valve deceleration time (DT <160 ms)[35]. Due to the more rapid increase in left ventricular pressure in the stiff left ventricle, the atrial contraction results in a short small A wave, thereby increasing the E/A ratio (>2.0)[35]. Similar to the pseudonormal grade, the E/E' is increased (>15)[35].

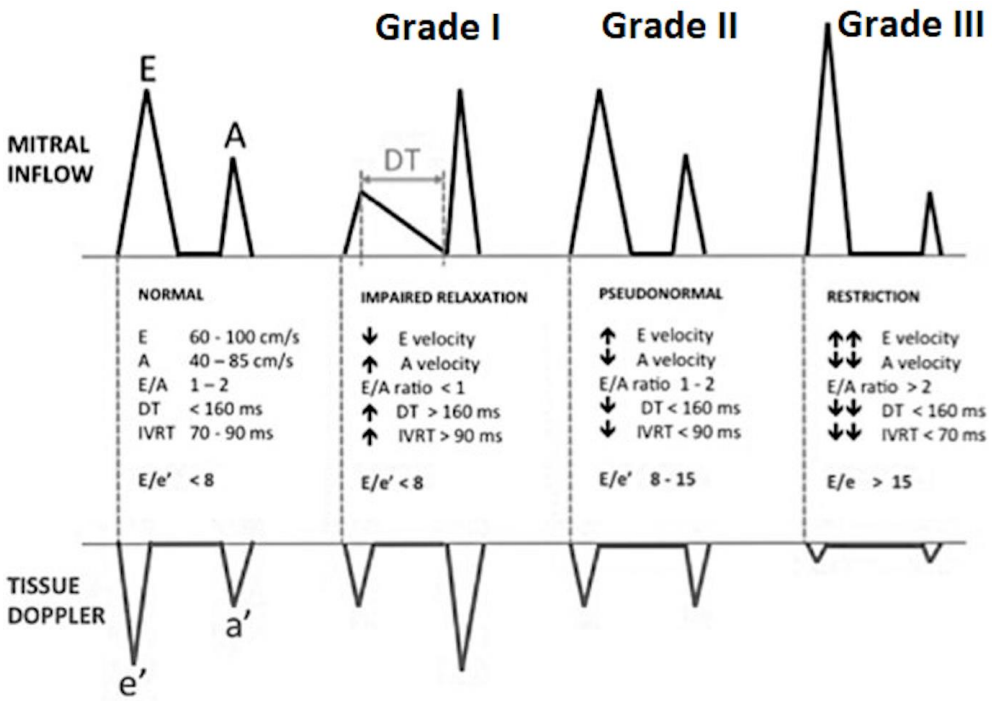

Figure 1.3- Grades of diastolic dysfunction. *A, late mitral inflow peak velocity; A', late diastolic mitral annulus peak velocity; DT, deceleration time; E, early mitral inflow peak velocity; E', early diastolic mitral annulus peak velocity; IVRT, isovolumic relaxation time. From Vermeiren GL et al.*[35]

Although the terms diastolic dysfunction and HFpEF are often used interchangeably, it is important to take into consideration that **diastolic dysfunction** is **not equivalent to HFpEF**. Declines in left ventricular relaxation and compliance occur during healthy ageing[36], but not all elderly patients with diastolic dysfunction have or will develop HFpEF. For example, only 12% of patients with severe diastolic dysfunction at initial echocardiographic evaluation developed

HFpEF during six years follow up[37]. HFpEF by definition requires the presence of elevated left ventricular filling pressures either at rest or with exertion, which are required to maintain systemic perfusion[38]. The pathophysiology of HFpEF is very heterogeneous with variable contributions from diastolic dysfunction, relative pericardial restraint, and impaired contractile reserve, atrial function, and ventricular-vascular coupling, all contributing to elevations in pulmonary venous and left ventricular filling pressures[39-42]. Increases in left ventricular pressure promote symptoms of dyspnoea, impair exercise capacity, and increase the risk for hospitalisation and mortality in HFpEF[43-45].

1.2.3 Invasive assessment of HFpEF by pressure-volume loops

Echocardiography is highly dependent on loading conditions and heart rate (HR). Invasive measurements of left ventricular filling, relaxation, diastolic distensibility, and stiffness by **pressure-volume (PV) loops** are considered as definite evidence for diastolic dysfunction during direct real-time cardiac functional assessment[46]. During PV loop acquisition, a high-fidelity micromanometer catheter is inserted in the left ventricle, which subsequently simultaneously measures both pressure and volume. Passive left ventricular relaxation is measured as IVRT (tau) and minimum rate of pressure change in the left ventricle (dP/dt_{min})[47]. Increased tau (>48 ms) and/or decreased dP/dt_{min} are associated with impaired active relaxation[48]. However, dP/dt_{min} is dependent on HR and load, therefore increased tau, as observed in HFpEF patients[49], is considered as a better parameter of decreased passive relaxation[47]. The slope of the load-independent end-diastolic pressure-volume relationship (EDPVR), called beta or chamber stiffness constant, is also a measure of left ventricular relaxation. It is the reciprocal of ventricular compliance, or also called ventricular stiffness, and is obtained by reducing the preload through a temporary occlusion of the inferior vena cava[47]. If the left ventricular compliance is decreased, the left ventricle is stiffer resulting in an

increased end-diastolic pressure (EDP) at every EDV. This is reflected by an upward and leftward shift of the EDPVR, as observed in HFpEF (Figure 1.4)[33,49].

Ejection fraction is the most universally accepted parameter in clinical practice for cardiac contractility, however, it is highly sensitive to afterload, cardiac size, and remodelling. Furthermore, it measures ventricular-arterial coupling rather than contractility alone. More specific measurements of contractility, such as maximal rate of pressure change in the left ventricle during isovolumic contraction (dP/dt_{max}) and slope of the end-systolic pressure-volume relationship (ESPVR), have been developed, but due to their complexity, they are mainly used in animal research.

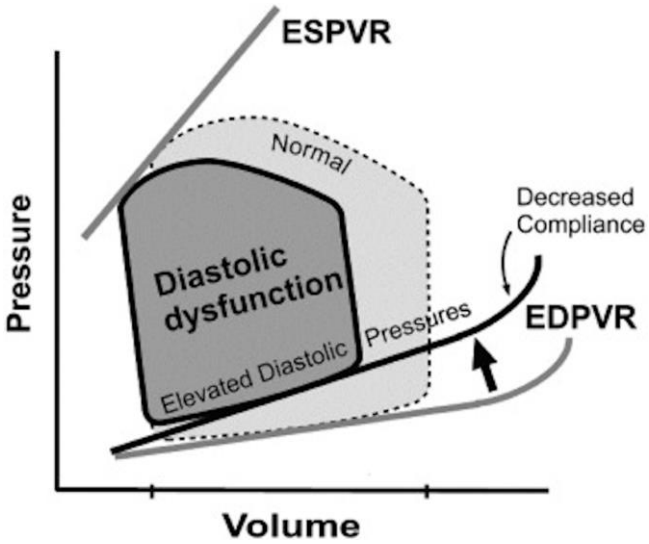

Figure 1.4- The left ventricular pressure-volume loop during diastolic dysfunction. *Diastolic dysfunction (stiffening) is reflected by an upward and leftward shift of the end-diastolic pressure-volume relationship (EDPVR), while the end-systolic pressure-volume relationship (ESPVR) is unaltered. From Ho CY. 2007*[34]

1.3 Left ventricular stiffness in HFpEF: fibrosis and passive stiffness

To improve the diagnosis, a better understanding of the pathophysiology of HFpEF is crucial. The **microvascular paradigm** proposes that the chronic low-grade inflammatory state induced by comorbidities is the cause of myocardial structural and functional alterations (Figure 1.5)[50]. In this model, comorbidities, such as obesity, T2DM, hypertension, trigger chronic low-grade systemic inflammation, characterised by elevated levels of circulating immune cells and pro-

inflammatory cytokines and upregulation of endothelial adhesion molecules, such as intercellular and vascular cellular adhesion molecule-1 (ICAM-1 and VCAM-1), and corresponding ligands on circulating leukocytes. The resultant increased myocardial infiltration of leukocytes, especially macrophages, elevates transforming growth factor beta (TGFβ) levels, thereby inducing cardiac fibrosis. Furthermore, the systemic pro-inflammatory state induces excessive reactive oxygen species (ROS) production by coronary microvascular endothelial cells, contributing to cardiac oxidative stress and resultant nitric oxide (NO) oxidation. Consequently, the reduced NO bioavailability leads to impaired nitric oxide/soluble guanylate cyclase/cyclic guanosine monophosphate/protein kinase G (NO/sGC/cGMP/PKG) signalling, causing vascular endothelial dysfunction and cardiomyocyte hypertrophy and stiffening. In HFpEF patients, both increases in **cardiac fibrosis** (excessive extracellular matrix deposition) and **cardiomyocyte stiffness** (titin modifications) impair cardiac relaxation and/or reduce left ventricular compliance, resulting in the development of diastolic dysfunction[51].

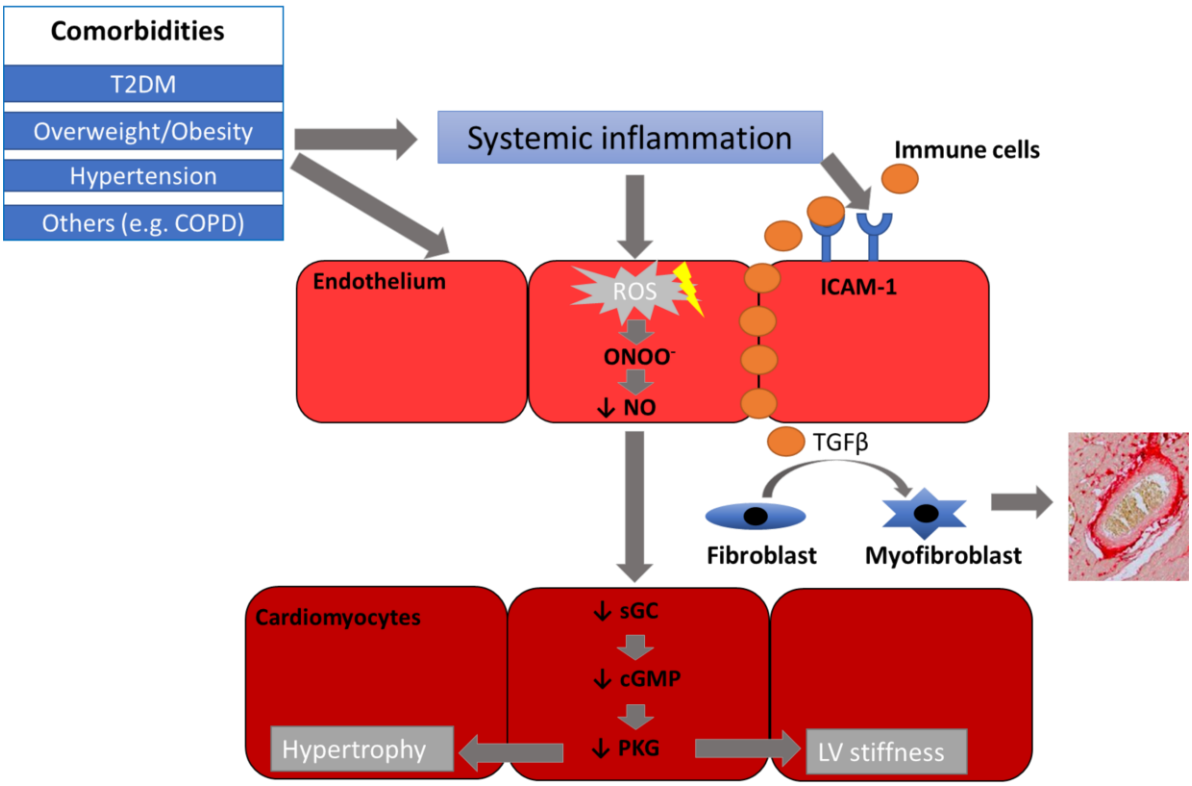

Figure 1.5- Microvascular paradigm. *Comorbidities, including type 2 diabetes mellitus (T2DM), obesity, hypertension, and chronic obstructive pulmonary disease (COPD), induce a systemic pro-inflammatory state and oxidative stress. Coronary endothelial cells subsequently produce reactive oxygen species (ROS), resulting in the*

formation of peroxynitrite ($ONOO^-$) and the resultant reduced nitric oxide (NO) bioavailability. Reduced soluble guanylate cyclase (sGC) activity in the adjacent cardiomyocytes leads to diminished cyclic guanosine monophosphate (cGMP) levels and protein kinase G (PKG) activity. Reduced PKG activity induces subsequently left ventricular (LV) stiffness and hypertrophy. In addition to inducing oxidative stress, systemic inflammation increases the expression of adhesion molecules, such as intercellular adhesion molecule-1 (ICAM-1), on coronary endothelial cells, thereby promoting the transmigration of immune cells through the endothelium. Immune cells, macrophages specifically, produce transforming growth factor beta (TGFβ), which promotes the conversion of fibroblasts to myofibroblasts, resulting in cardiac fibrosis. Figure based on Paulus WJ et al. 2013[50].

1.3.1. Increased stiffness: post-translational modifications and isotype switching of titin

The giant sarcomeric protein **titin**, a force-transducing bidirectional spring, is the main determinant of cardiomyocyte stiffness. Alternative splicing of *Titin* mRNA creates isoforms with differential stiffnesses: the short, stiffer N2B isoform, and the longer, more compliant N2BA isoform (Figure 1.6A). Extension of the elastic I-band region in both titin isoforms supports myocardial passive relaxation during diastole. Post-translational modifications of total titin and its specific segments rapidly alter cardiomyocyte passive stiffness ($F_{passive}$; Figure 1.6B). In HFpEF patients, hypophosphorylation of the N2B isoform and reduced PKG activity are associated with an increased $F_{passive}$[52,53]. Interestingly, PKG activity is reduced in HFpEF as a result of reduced NO bioavailability due to oxidative stress, leading to impaired NO/cGMP/PKG signalling[50]. This suggests that oxidative stress, NO bioavailability, and PKG play a crucial role in regulating $F_{passive}$. Furthermore, other protein kinases, such as PKA, PKC, extracellular signal-regulated kinase-2 (ERK2), and Ca^{2+}/calmodulin-dependent kinase-II (CAMKII), also modify $F_{passive}$[51]. HFpEF patients showed increased site-specific titin phosphorylation on PEVK (a region rich in specific amino acids) S11878 and reduced phosphorylation on N2B unique sequence (N2Bus) S4185, which were associated with an increased $F_{passive}$[54]. In addition to these post-translational modifications of titin, alterations of the N2BA/N2B isoform ratios occur in pathologies[55]. Despite this, HFpEF patients do not consistently show isoform changes, with only some patients exhibiting increased stiff N2B isoform levels[56]. Altogether, increased cardiomyocyte $F_{passive}$ in HFpEF is mediated by **post-**

translational modifications in the short term, which are interconnected to the oxidative state, and to **isotype switching** in the long term.

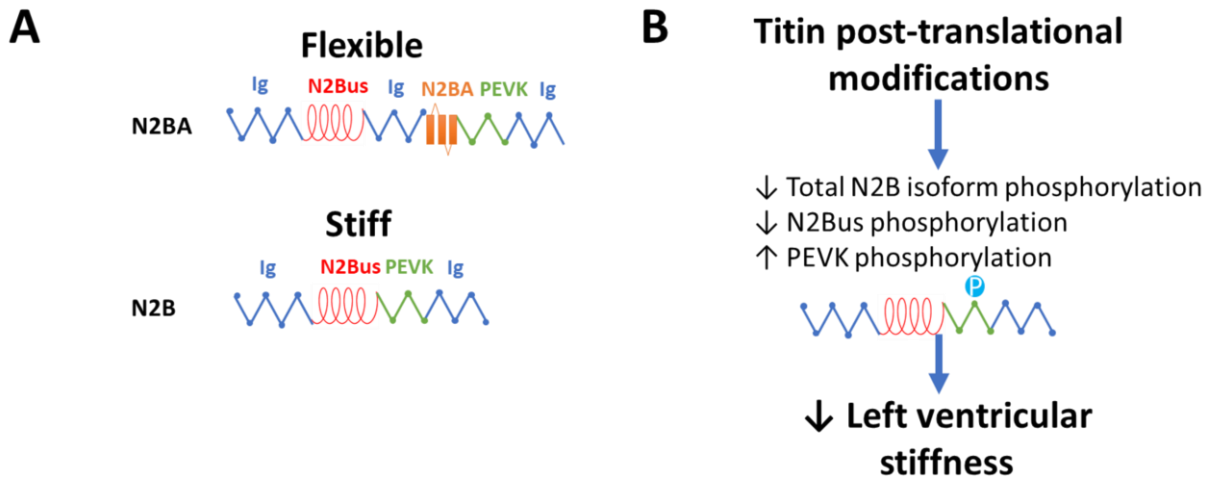

Figure 1.6- Titin modulates left ventricular stiffness. ***A)*** *Structure of the more flexible N2BA and stiff N2B isoforms of titin.* ***B)*** *Post-translational modifications of titin during HFpEF. Ig, immunoglobulin; N2Bus, N2B unique sequence. Adapted from Steven J Simmonds et al. 2020*[57].

1.3.2. Collagen quantity, type, and cross-linking are altered during HFpEF

Myocardial fibrosis and extracellular matrix accumulation are hallmarks of adverse cardiac remodelling associated with HFpEF and its comorbidities[54,58-63]. The **quantity**, **type**, and degree of **cross-linking** of collagen influences tissue stiffness. Increased collagen deposition, switching from more flexible collagen III to stiffer collagen I, and collagen cross-linking are all associated with worsening of diastolic function in HFpEF patients[54,58,60].

Lysyl oxidases (LOXs) are the main enzymes involved in collagen and elastin cross-linking during cardiac remodelling[64]. Upregulation of LOX expression and collagen cross-linking is associated with impaired diastolic tissue Doppler parameters (e.g. E/E') in HFpEF patients[58]. Furthermore, advanced glycation end product-mediated cross-linking of collagen was also observed in aged and T2DM patients, resulting in reduced vascular elasticity and myocardial flexibility, which contributes to vascular and myocardial stiffness and ultimately diastolic dysfunction[65]. Cardiac fibrosis is also associated with a reduced cardiac microvascular density in HFpEF patients, indicating that insufficient cardiac perfusion may cause excessive collagen

deposition[60]. Pro-inflammatory mediators, such as interleukin 6 (IL-6), tumor necrosis factor alpha (TNFα), C-C motif chemokine ligand 2 (CCL2), and TGFβ, participate in fibrosis regulation and pharmacological prevention of cardiac infiltration of pro-inflammatory monocytes attenuated fibrosis development in murine hypertension[66]. However, specific cytokine regulation of cardiac fibrosis is debated.

1.4 Coronary microvascular dysfunction and rarefaction in HFpEF

Endothelial cells constitute the major non-cardiomyocyte cell population in the healthy heart and therefore cardiac endothelial abnormalities have a large impact on cardiac health. The **microvascular paradigm** proposes endothelial dysfunction as the central mediator connecting systemic inflammation with myocardial dysfunction and remodelling in HFpEF (Figure 1.5)[50]. Decreased NO bioavailability, oxidative stress, neurohormonal activation, and/or increased leukocyte infiltration, trigger coronary microvascular endothelial dysfunction, which adversely impacts cardiac perfusion observed in most HFpEF comorbidities[50,67].

Coronary microvascular dysfunction is determined by **endothelium-dependent and/or -independent mechanisms**. Endothelium-dependent dysfunction develops due to an imbalance between endothelium-derived relaxing factors (e.g. NO, ATP) and constrictors (e.g. endothelin-1)[68]. In HFpEF patients, plasma levels of NO metabolites were lower compared to HFrEF subjects, indicating a reduced NO bioavailability[69]. Furthermore, HFpEF patients showed increased levels of endothelin-1, a predictor of 1-year HF hospitalisation associated with long-term mortality[70]. Endothelium-dependent coronary microvascular dysfunction was present in 29% of the HFpEF patients, as measured by changes in coronary flow reserve after infusion of acetylcholine[71]. Notably patients presenting with a greater burden of T2DM and reduced high-density lipoprotein (HDL) levels had an increased prevalence of endothelium-dependent coronary microvascular dysfunction[71]. In line with these results, 76% of the HFpEF patients

showed endothelium-dependent dysfunction during the non-invasive evaluation of the coronary flow reserve using phase contrast cine-magnetic resonance imaging after the infusion of ATP[72]. On the other hand, endothelium-independent dysfunction is the result of changes in vascular tone mediated by an imbalance between vasoconstrictors (e.g. angiotensin II) and vasodilators (e.g. adenosine) acting on vascular smooth muscle cells (vSMCs). A recent study showed that 33% of the HFpEF patients (mostly older, hypertensive subjects) displayed endothelium-independent dysfunction, as reflected by a decreased coronary flow reserve after adenosine administration[71]. Interestingly, endothelium-independent microvascular dysfunction was associated with a worsened diastolic function and increased mortality[71]. Both a swine model of metabolic risk factors (e.g. hypercholesterolaemia, T2DM, and chronic kidney disease) and T2DM patients showed reduced coronary flow reserve after infusion of adenosine as a result of increased basal blood flow due to perturbations in myocardial efficiency[73-75]. Of note, the increased basal myocardial blood flow correlated with diastolic dysfunction in female T2DM patients, while coronary flow reserve did not correlate with diastolic dysfunction[74]. As such, basal myocardial blood flow could represent a superior marker of coronary microvascular dysfunction in certain pathological settings[76]. Nevertheless, while administration of vSMC relaxants, such as sodium nitroprusside, improves endothelium-independent vasodilation in HFrEF, its use in HFpEF is debated[77]. In short, as myocardial capillaries are the primary determinant of the coronary flow reserve[78,79], capillary endothelial-dependent and -independent dysfunction are considered the major determinants of coronary microvascular dysfunction in HFpEF patients[80].

In parallel to these functional vascular alterations, a reduction in myocardial microvascular density per myocardial area, called **microvascular rarefaction**, is observed in HFpEF patients[60]. In-depth, the cardiac density of both capillaries and pre-capillary arterioles per myocardial area was decreased in the sub-epicardial, mid-myocardial, sub-endocardial, and

papillary muscle region in HFpEF patients compared to control subjects[60]. Similar findings were observed when only the cardiac capillary density per myocardial area was assessed between HFpEF patients and control subjects[60]. Cardiac capillary rarefaction is therefore considered as the major contributor of cardiac microvascular rarefaction in HFpEF patients[60,80]. Cardiac capillary rarefaction contributes to insufficient cardiac perfusion by impairing myocardial oxygen delivery in HFpEF patients[81]. In a multiple comorbidity swine model perturbations in myocardial blood flow and oxygen delivery were present, which resulted in increased myocardial oxygen extraction[73]. This increase in oxygen extraction occurred despite a reduction in cardiac capillary density, suggesting that rarefaction or dysfunction of cardiac resistance vessels (including small arteries and arterioles) was mainly responsible for the impaired myocardial blood flow and oxygen delivery[73]. Notably, reduced cardiac perfusion leads to local blood supply-demand imbalance and energy metabolite deficiency, causing cardiac metabolic reprogramming and dysfunction. Accordingly, more than 50% of the patients with coronary microvascular dysfunction had an impaired myocardial flow reserve, which was independently associated with a worsened diastolic function and increased hospitalisation for HFpEF[82].

Microvascular rarefaction may precede disease development, as HFpEF-associated comorbidities show capillary rarefaction. For example, myocardial capillary rarefaction per myocardial area was reported in end-stage HF patients with diabetes, a type 1 diabetes pig model, and a combined animal model of ageing, oestrogen depletion, and obesity[83,84]. Furthermore, skeletal capillary rarefaction impedes insulin delivery to muscles, contributing to poor insulin uptake, thereby promoting the development of insulin resistance[85,86]. In young adults with familial predisposition to hypertension and in patients with borderline or established hypertension, a reduced dermal capillary density per microscopic field has also been shown[87,88]. Interestingly, in obese patients, increased left ventricular filling pressure correlated with lower

coronary capillary density per myocardial area, potentially contributing to impaired cardiac metabolism underlying diastolic dysfunction[89]. Furthermore, increased subepicardial and pericoronary adipose tissue, as observed in obese, T2DM, and elderly patients, also correlated with impaired coronary flow reserve, microvasculature, and coronary function leading to deteriorated diastolic function[90]. Despite accumulating evidence for coronary microvascular dysfunction and capillary rarefaction during HFpEF development, its exact role in disease progression is still unknown.

1.4.1 Inflammation as a trigger for coronary vascular dysfunction

The most frequent HFpEF-associated comorbidities are all associated with **chronic systemic low-grade inflammation (**Figure 1.7**)**[91-94]. HFpEF patients showed elevated systemic inflammatory markers, such as acute inflammatory C-reactive protein (CRP), which increased with the number of comorbidities and raised circulating levels of neutrophils and monocytes[95-98]. *In vitro* culture of healthy donor monocytes with serum from HFpEF patients promoted alternative anti-inflammatory macrophage differentiation[98]. Consequently, chronic systemic low-grade inflammation is proposed as a major trigger, together with oxidative stress and NO dysregulation, for coronary microvascular dysfunction in HFpEF[50].

Both chronic systemic low-grade inflammation and activation of the renin-angiotensin-aldosterone axis by hypertension, insulin resistance, and expanding inflamed visceral and perivascular adipose tissue, lead to endothelial cell activation by upregulating adhesion molecules. In addition, elevated advanced glycation end products receptor signalling in T2DM stimulates the nuclear factor kappa B (NFκB) signalling pathway, inducing its receptor and pro-inflammatory genes, forming a vicious cycle of self-renewing pro-inflammatory signals[99]. HFpEF patients showed increased expression of adhesion molecules on the coronary endothelium, together with elevated myocardial infiltration of $CD45^+$ leukocytes and $CD3^+$ T-

lymphocytes[100]. Furthermore, there was a positive correlation between echocardiographic indices of diastolic dysfunction (E/E') and splenic activation, suggesting a role of increased splenic myeloid cell oversupply in HFpEF patients[97]. However, while both systemic and cardiac inflammation have been observed in HFpEF patients, the causal involvement of inflammation in coronary microvascular dysfunction in HFpEF has never been investigated.

1.4.2. Oxidative stress as a trigger for coronary vascular dysfunction

Oxidative stress is induced by increased ROS production and/or reduced antioxidant enzyme levels, leading to both endothelial and cardiac dysfunction (Figure 1.7). As cardiomyocytes are rich in mitochondria, they have an elevated baseline ROS production compared to other cell types. Of note, risk factors for HFpEF stimulate ROS production[67,101-104]. For example, advanced glycation end product signalling in T2DM directly induces oxidative stress by activating nicotinamide adenine dinucleotide phosphate oxidases (NOXs)[105]. Consequently, chronic systemic low-grade inflammation is proposed as a major trigger, together with oxidative stress and NO dysregulation, for coronary microvascular dysfunction in HFpEF[50].

Within vascular endothelial cells, elevated ROS production triggers canonical NFκB signalling, leading to cytokine production and proteasome and inflammasome activation, which may cause endothelial cell apoptosis and pyroptosis **(**Figure 1.7**)**[67]. Furthermore, endothelial oxidative stress reduces the NO bioavailability due to superoxide anion (O_2^-)-mediated peroxynitrite ($ONOO^-$) formation, thereby promoting protein nitrosylation, resulting in endothelial dysfunction and cell death **(**Figure 1.7**)**[106]. Increased cardiac levels of hydrogen peroxide (H_2O_2) and reactive oxidative metabolites, endothelial nitric oxide synthase (eNOS) uncoupling, and macrophage and endothelial NOX2 expression and reduced NO levels, all indicate the presence of myocardial oxidative stress in HFpEF patients[107]. Beyond oxidation, hyperglycaemia-induced inhibition of NO production could reduce NO bioavailability by elevating asymmetric

dimethyl-L-arginine (ADMA) levels, an eNOS inhibitor, thereby contributing to endothelium-dependent dysfunction associated with a worsened prognosis of HFpEF[108].

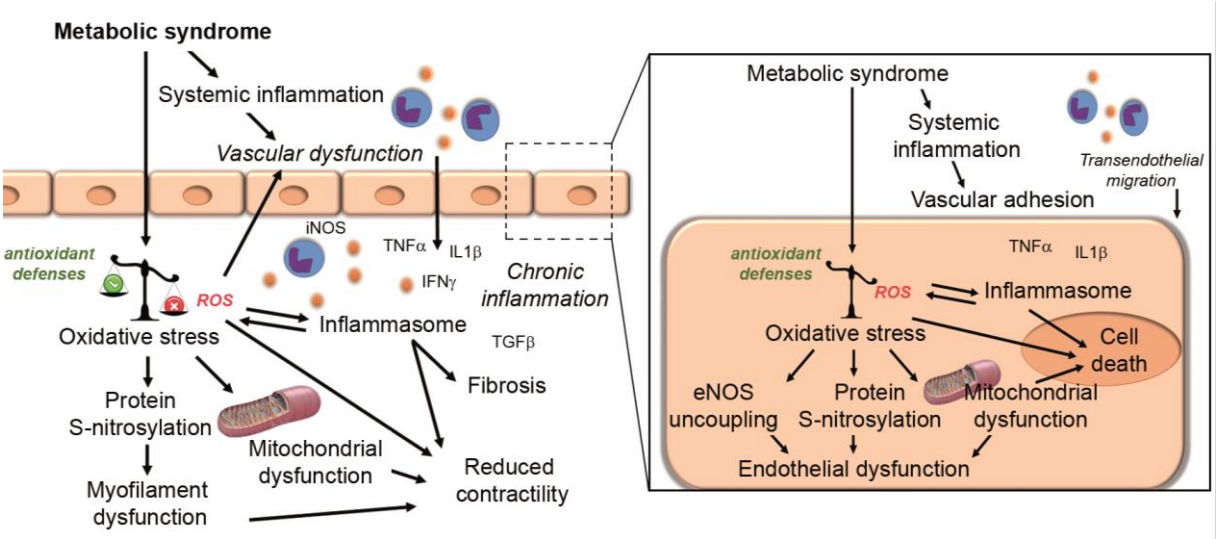

Figure 1.7- Cardiac and vascular oxidative stress and inflammation in HFpEF. *The metabolic syndrome induces chronic systemic low-grade inflammation and direct deleterious effects in the myocardium (left) and in its endothelium (right). Chronic cardiac inflammation develops due to increased immune cell transmigration across activated endothelial cells. Endothelial and cardiomyocyte oxidative stress result from an imbalance between antioxidant defenses and excessive reactive oxygen species (ROS) production induced by immune mediators. Prolonged ROS-mediated inflammasome activation and increased transforming growth factor beta (TGFβ) levels contribute to cardiac fibrosis. Severe oxidative stress also causes mitochondrial dysfunction resulting in reduced cardiac contractility and endothelial dysfunction. ROS-induced protein modifications (e.g. S-nitrosylation) lead to sarcomeric myofilament dysfunction and reduced endothelial nitric oxide synthase (eNOS)-mediated NO production. Oxidative stress also leads to eNOS uncoupling, contributing to poor flow-mediated vasodilation and cardiac perfusion. Furthermore, increased myocardial activation of inducible nitric oxide synthase (iNOS) leads to increased nitrosative stress. Finally, persistent inflammation and oxidative stress may induce endothelial cell death, contributing to vascular rarefaction and reduced cardiac perfusion. Figure from Cuijpers I et al. 2020*[109]

1.4.3 Microvessel wall barrier dysfunction in HFpEF

The microvascular endothelium barrier opposes free exchange between blood and tissues and tightly regulates transport of plasma constituents and immune cells. Events such as ischemia in HFrEF cause increased vascular endothelial growth factor (VEGF)-A levels, leading to vascular barrier breakdown, increased extravasation of immune cells, and oedema. In addition, there is also accumulating evidence of **microvascular wall barrier dysfunction** in HFpEF-associated comorbidities[110-113].

The **endothelial glycocalyx** covers the luminal surface of endothelial cells and serves as a barrier for solute and macromolecule exchanges. It is also a mechanotransducer, sensing endothelial shear stress from the flowing blood, attenuating coagulation and leukocyte adhesion, and affecting vasoregulatory responses to flow. Thinning of the glycocalyx occurs in several HFpEF-associated comorbidities[114-117], resulting in adherence of immune cells to the endothelium **(**Figure 1.8**)**[118]. In HFpEF patients, increased circulating levels of the glycocalyx shedding marker syndecan-1 were associated with endothelial dysfunction and increased risk of all-cause mortality and rehospitalisation[119]. Interestingly, exogenous NO administration during reperfusion preserved vascular integrity and attenuated cardiac oedema formation through protection of the glycocalyx in experimental ischemia/reperfusion injury[120].

Vascular endothelial hyperpermeability occurs in the peripheral microvasculature of hypertensive or diabetic patients, as well as obese or elderly rodent models[110-113]. Disruption and remodelling of cell-cell junctions is a major cause of vascular barrier integrity loss and occurs in murine models of diastolic dysfunction and MetS and in aged endothelial cells **(**Figure 1.8**)**[112,121-123]. A number of pro-permeabilizing stimuli, including VEGF-A and inflammatory agents (e.g. histamine), stimulate hyperphosphorylation of VE-cadherin, resulting in the breakdown of junctional contacts[124]. Moreover, the VEGF-A-, histamine-, and serotonin-induced formation of trans-endothelial channels from coalesced vesicles or vacuoles, called **vesiculo-vacuolar organelles**, is another proposed route of transcytosis-mediated extravasation during vascular leakage **(**Figure 1.8). Vascular hyperpermeability by trans- or paracellular pathways leads to increased influx of solutes, macromolecules, and immune cells to the interstitium.

Beyond endothelial cells, **pericytes**, mural cells around microvessels, are crucial for regulating vascular blood flow and microvascular stability. Cardiac pericytes are involved in many processes regulating cardiac homeostasis, such as vascular maturation, supply of trophic

substances, fibrosis, and blood flow. Interestingly, HFpEF-diseased ZSF1 rats showed both disorganized accumulation of vascular pericytes in subendocardial hyperproliferative (inflamed) foci and reduced vascular pericyte coverage[125].

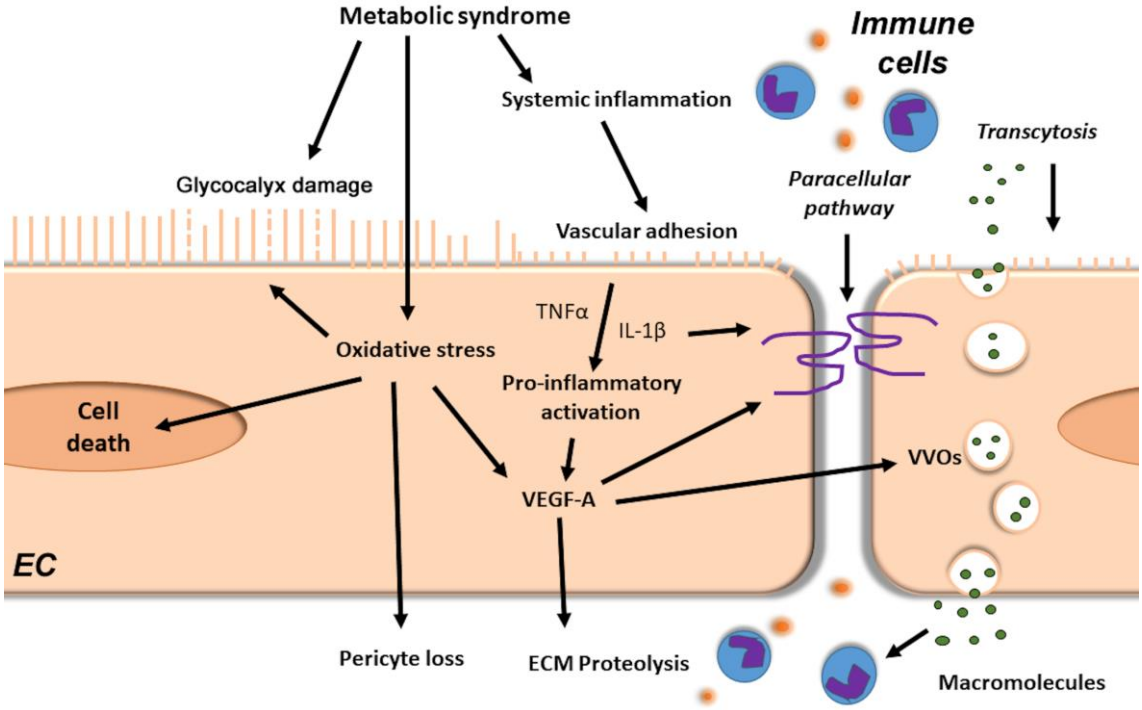

Figure 1.8 - Microvessel wall barrier dysfunction in HFpEF. *The metabolic syndrome induces via chronic systemic low-grade inflammation deleterious effects in coronary endothelial cells (EC). It leads to the degradation of the endothelial glycocalyx layer, thereby promoting endothelial immune cell transmigration. Metabolic syndrome-induced cellular oxidative stress may lead to glycocalyx damage and cell death of both endothelial and mural cells. In addition, pro-inflammatory mediators, such as tumor necrosis factor alpha (TNFα) and interleukin 1beta (IL-1β), together with oxidative stress, increase vascular growth factor-A (VEGF-A) levels. This weakens vascular barriers (e.g. loss of cell-cell junctions), which facilitates paracellular passage of immune cells and trans-vascular transport by transcellular vesiculo-vascular organ (VVO) formation. VEGF-A also stimulates vascular basement membrane remodelling through extracellular matrix (ECM) protease activation, leading to reduced vascular stability and vascular regression. Figure from Cuijpers I et al. 2020*[109]

In short, microvascular dysfunction, rarefaction, inflammation, oxidative stress, and vascular barrier dysfunction occur in HFpEF. However, when these pathological processes occur with respect to the development of HFpEF is unknown. Furthermore, triggers for cardiac microvascular dysfunction and rarefaction have never been investigated in HFpEF.

1.5 Experimental animal models for HFpEF

The development of effective therapeutics for HFpEF patients is hampered by the absence of appropriate animal models, that accurately mimic the heterogeneous human pathology. Rodents represent the majority of the developed HFpEF animal models, as for example the low costs for housing and maintenance allow the inclusion of a larger number of animals in studies. Most of the currently available rodent models suffer from one of the HFpEF-associated comorbidities, specifically hypertension, obesity, diabetes mellitus, and/or ageing[126]. Here, we discuss some of the most currently used HFpEF rodent models (Table 1.1.).

1.5.1 Hypertension-induced HFpEF rodent models

Hypertension is a major risk factor for the development of HFpEF with a prevalence of 55-86% in HFpEF patients[127]. The Dahl salt-sensitive rat represents the most published hypertension-induced HFpEF model. When these animals are fed a high-salt diet (8%) at six to eight weeks of age, the animals develop hypertension, renal failure, left ventricular concentric hypertrophy, cardiac fibrosis, inflammation, capillary rarefaction per myocardial area, and diastolic dysfunction[128-130]. However, continued exposure to the high salt diet (~26 weeks) or administration of the diet at an older age results in the development of HFrEF[128]. Chronic stimulation with pro-hypertrophic agents, such as angiotensin II, also results in the development cardiac remodelling (hypertrophy, inflammation, capillary rarefaction per myocardial area, and fibrosis) and diastolic dysfunction, both in the presence and absence of hypertension[131-134]. Transverse aortic constriction initially results in the development of cardiac inflammation, fibrosis, and increased capillary density per myocardial area, left ventricular concentric hypertrophy, and diastolic dysfunction, followed by cardiac ventricular enlargement and left ventricular eccentric hypertrophy, resulting in further deterioration of the systolic function, thereby reducing the ejection fraction[135].

1.5.2 T2DM- and obesity-induced HFpEF rodent models

More than two-third of the HFpEF patients are obese or overweight[136] and approximately one-third of the HFpEF patients has T2DM[137]. Several models have been developed to recapitulate the obese and T2DM phenotype in HFpEF patients, including the leptin deficient *ob/ob* mouse ($Lep^{ob/ob}$) and leptin receptor deficient *db/db* mouse ($Lepr^{db/db}$), in which the altered leptin homeostasis leads to obesity, hyperglycaemia, hyperinsulinemia, insulin resistance, and diabetic complications. *Ob/ob* mice develop diastolic dysfunction possible due to cardiac lipid accumulation[138]. Furthermore, these mice develop cardiac hypertrophy, fibrosis, and inflammation[139], without changes in cardiac vascular density per myocardial area[140]. However, progressively this animal model develops diabetic cardiomyopathy with impaired cardiac contractility and relaxation[141]. *Db/db* mice develop oxidative stress, cardiac fibrosis, capillary rarefaction per myocardial area, concentric hypertrophy, and diastolic dysfunction, while the ejection fraction remains preserved even after 6 months of age[142]. Similar to the *db/db* mouse, the Zucker diabetic fatty (ZDF) rat is deficient for the leptin receptor (+/*lepr fa*) and develops T2DM, obesity, moderate hypertension, renal damage, cardiac fibrosis, inflammation, capillary rarefaction per myocardial area, and diastolic dysfunction at 45 weeks of age, while cardiac hypertrophy and systolic dysfunction are absent[143-145].

1.5.3 Age-induced HFpEF rodent models

Among women older than 65 years, 85% of the HF cases are HFpEF[146]. An example of an ageing model is the senescence-accelerated mouse-prone 8 (*Samp8*) mouse model, which has a reduced life span due to accelerated senescence[147]. High-fat diet-fed *Samp8* mice have been shown develop diastolic dysfunction and cardiac interstitial fibrosis, hypertrophy, and endothelial activation (ICAM-1), while systolic function was not affected[148]. Another ageing model, the Fischer 344 ageing rat, has been reported to develop more prominent diastolic

dysfunction in females, while males were heavier and had increased cardiac hypertrophy and fibrosis[149].

1.5.4. The multiple comorbidity-induced HFpEF model: the obese ZSF1 rat

Zucker fatty spontaneously hypertensive heart failure F1 hybrid (ZSF1) rats are developed by crossing rat strains with two different types of leptin receptor mutations, the lean female Zucker diabetic fatty rat (ZDF; +/*lepr fa*) and the lean male spontaneously hypertensive heart failure (*SHHF/Mcc*; +/*lepr facp*) rat. The obese ZSF1 rat offspring are homozygous for the leptin receptor mutation (*lepr fa/lepr facp*) and inherit the hypertensive gene, resulting in the combined development of T2DM, hypertension, hyperlipidaemia, and obesity[150]. In contrary, lean littermates are heterozygous for the leptin receptor (*lepr fa/+* or *lepr facp/+*), but do inherit the hypertensive gene resulting exclusively in the development of hypertension[150]. Obese ZSF1 rats develop diastolic dysfunction, left ventricular hypertrophy, cardiac fibrosis, inflammation, increased cardiomyocyte stiffness, and renal failure[125,151].

Table 1.1: Pathological characteristics of rodent HFpEF animal models

	Hypertension			**T2DM and obesity**			**Ageing**		**Multiple factors**
	Dahl SS rat	AngII Infusion	TAC	Ob/ob mouse	Db/db mouse	ZDF rat	SAMP8	Fischer 344 rat	Obese ZSF1 rat
Risk factors									
Hypertension	Yes	Yes/No	Yes	No	No	Yes	N/A	No	Yes
Obesity	No	No	No	Yes	Yes	Yes	No	No	Yes
T2DM	No	No	No	Yes	Yes	Yes	No	No	Yes
Ageing	No	No	No	No	No	No	Yes	Yes	No
Cardiac remodelling									
Hypertrophy	Yes	Yes	Yes	Yes	Yes	No	Yes	Yes/No	Yes
Fibrosis	Yes	Yes	Yes	Yes	Yes	Yes	Yes	Yes/No	Yes
Inflammation	Yes	Yes	Yes	Yes	N/A	Yes	No	N/A	Yes
Capillary rarefaction	Yes	Yes	No	No	Yes	Yes	N/A	No	N/A
Diastolic dysfunction	Yes	Yes	Yes	Yes	Yes	Yes	Yes	Yes	Yes
Systolic dysfunction	Yes, at older age	Yes, at older age	Yes, at older age	Yes, at older age	No	No	No	No	No

ANGII, angiotensin II; N/A, not available; SAMP8, senescence-accelerated mouse-prone 8; TAC, transverse aortic constriction; T2DM, type 2 diabetes mellitus; ZDF, Zucker diabetic fatty; ZSF1, Zucker fatty spontaneously hypertensive heart failure F1 hybrid.

1.6 Therapeutic options for patients with HFpEF

In contrast to the therapeutic advances in HFrEF, established HF and novel therapeutics have failed to improve the prognosis of HFpEF. As such, there is an urgent need for an **improved clinical definition** of HFpEF and **novel diagnostic tools and methods**. Tailored approaches **targeting multiple pathways** involved during HFpEF might ameliorate or even treat HFpEF (Figure 1.9).

1.6.1 Treatment of HFpEF-associated comorbidities and risk factors

Most currently available treatments **ameliorate HFpEF-associated comorbidities**. **Physical activity** and **caloric restriction** are important non-pharmacological approaches that have beneficial prognostic effects in HFpEF. Physical activity reduced diastolic dysfunction and HF hospitalisation and improved quality of life[152,153]. Importantly, additive beneficial effects were observed when anaerobic exercise training was combined with a low caloric diet[154]. **Diabetic pharmacological interventions**, such as and insulin-sensitizing or glucose lowering agents, e.g. metformin, dipeptidyl peptidase-4 (DPP-4) inhibitors, and glucagon-like peptide-1 (GLP-1) and glucose-dependent insulinotropic peptide (GIP) receptor agonists, all improved murine diastolic function[155]. The **sodium-glucose transport protein 2 (SGLT2) inhibitor** Dapagliflozin, used for the treatment of both type 1 and 2 diabetes, attenuated left ventricular concentric remodelling without improving diastolic dysfunction in a combined hypertension- and hyperlipidaemia-induced HFpEF pig model[156]. The therapeutic benefit of two SGLT2 inhibitors (Dapagliflozin and Empagliflozin) is currently being studied in patients with HFpEF (NCT03619213, NCT03057951).

Hypertension can cause recurring HFpEF hospitalisations. However, while targeting the renin-angiotensin-aldosterone axis activation by counteracting the deleterious effects of angiotensin II on the cardiovascular system by **angiotensin-converting enzyme inhibitors** and

angiotensin receptor blockers improved the outcome in HFrEF, this was not observed in HFpEF[157-159]. The angiotensin receptor neprilysin inhibitor sacubitril/valsartan LCZ696 only reduced HF hospitalisation in female HFpEF patients and those with ejection fraction of 45-57%, including both HFmrEF and HFpEF patients[160,161]. Debatable, **mineralocorticoid receptor antagonists** improved cardiac fibrosis markers and diastolic function patients with asymptomatic diastolic dysfunction or HFpEF[162], while the TOPCAT trial only demonstrated survival benefit in HFrEF, but not HFpEF patients[163].

Other comorbidities, such as atrial fibrillation and anaemia due to iron deficiency, often co-exist with HFpEF. In a small retrospective analysis, **catheter ablation** prevented arrhythmia recurrence and improved symptoms in HFpEF patients[164]. Currently, two randomized-controlled trials (NCT03074591, NCT03833336) investigate the effect of intravenously administered **iron** on mortality in HFpEF patients. In short, as HFpEF patients often represent with multiple comorbidities, targeting multiple comorbidities at once could prevent or delay HFpEF development.

1.6.2 Anti-inflammatory therapy for patients with HFpEF

Given the plethora of cardiac detrimental effect triggered by chronic low-grade inflammation, the use of **cytokine inhibitors** has been extensively investigated in HF patients[165]. However, the ability to translate this to a drug has not met with success and in some cases led to worsening of HF and/or even increased mortality[165]. Nevertheless, IL-1α and -1β blockage (Anakinra), for example, improved aerobic exercise capacity in HFpEF patients and is currently investigated in a phase 2 clinical trial (NCT02173548)[166]. In addition to anti-cytokine therapies, lipid-lowering **statins** have anti-inflammatory effects and are associated with a reduced rehospitalisation and mortality in HFpEF patients[167]. Despite this, currently no approved effective anti-inflammatory drug has been approved for the treatment or prevention of HFpEF.

1.6.3 Anti-oxidative stress therapy for patients with HFpEF

Anti-oxidative stress therapies aim to either (i) **inhibit oxidative stress producers**, (ii) **improve endogenous antioxidant capacity**, and/or (iii) **supplement exogeneous antioxidants**. The mitochondria-target antioxidant Szeto-Schiller-31 (SS-31; Elamipretide) attenuated cardiac remodelling in hypertensive cardiomyopathy and is currently investigated as a novel therapeutic for HFpEF in phase II trials (NCT02814097)[168]. Treatment with other mitochondria-targeted antioxidants (e.g. MitoTEMPO or N-acetylcysteine) also prevented diastolic dysfunction in rodent models of diabetes and hypertensive cardiomyopathy[169,170]. Interestingly, supplementation with an antioxidant cocktail, containing alpha lipoic acid, vitamin C and E, reduced systemic inflammation and improved endothelium-dependent vasodilation in HFpEF patients[171].

1.6.4 Drugs improving NO bioavailability for patients with HFpEF

NO-inducing drugs include (i) **organic nitrates**, (ii) **inorganic nitrite/nitrates**, (iii) **eNOS activators**, (iv) **β_3 adrenergic receptor-selective agonists**, (v) **stimulators of soluble guanylate cyclase**, or (vi) compounds that prevent the breakdown of cGMP downstream of NO by **phosphodiesterases** (PDE) . Enhancement of eNOS attenuated experimental diastolic HF and coronary endothelial dysfunction[172,173]. However, administration of organic nitrate[174] (isosorbide mononitrate; NCT02053493), inorganic nitrite[175] (NCT02742129), the sGC stimulator Vericiguat[176] (NCT01951638), or PDE-5 inhibitors[177] (NCT00763867) had no clinical benefit in HFpEF patients. Mirabegron, a new β_3 adrenergic receptor-selective agonist, which increases NO synthesis and release, is currently investigated in HFpEF patients (NCT02599480).

1.6.5 Drugs improving left ventricular compliance for patients with HFpEF

To improve left ventricular compliance, several **anti-fibrotic therapeutics** were trailed in HFpEF patients. As discussed in section 1.6.1, the therapeutic effect of **mineralocorticoid receptor antagonist**, targeting the maladaptive induction of cardiac fibrosis in HFpEF by aldosterone, is debatable[162,163]. Reduction of advanced glycation end product-induced cross-linking of the extracellular matrix by **alagebrium chloride** (ALT-711) improved diastolic function by reducing cardiac stiffness in a pilot clinical trial with 23 elderly HFpEF patients[178]. However, larger clinical trials failed to demonstrate improvements in cardiac function and exercise tolerance in HFrEF patients and sedentary elderly subjects chronically treated with ALT-711[179,180]. Furthermore, reduction of pro-fibrotic TGFβ signalling by **Pirfenidone** is currently evaluated as an anti-fibrotic drug in HFpEF patients (NCT02932566). In addition, **reductions** in **cardiomyocyte $F_{passive}$** by modulating titin might improve left ventricular compliance. In murine diastolic dysfunction, inhibition of the RNA binding motif-20 (*Rbm20*) generated more compliant titin isoforms, resulting in improvement in diastolic function[181]. Furthermore, anti-diabetic treatment altered post-translational modification of titin in rodent T2DM and a HFpEF-like model[182-184]. Thus, therapeutic interventions targeting fibrosis have met with limited success up until now. Innovative approaches to the treatment of cardiac stiffening, targeting both fibrosis and titin, however, could provide significant advances in this area.

In short, while several therapeutics have been proven to be beneficial in HFrEF, therapies for HFpEF are still lacking due to incomplete understanding of the disease, underdiagnosis, and heterogeneity in the patient population. Therefore, there is an urgent need to further elucidate the disease development to improve early HFpEF diagnosis and develop targeted personal medicine.

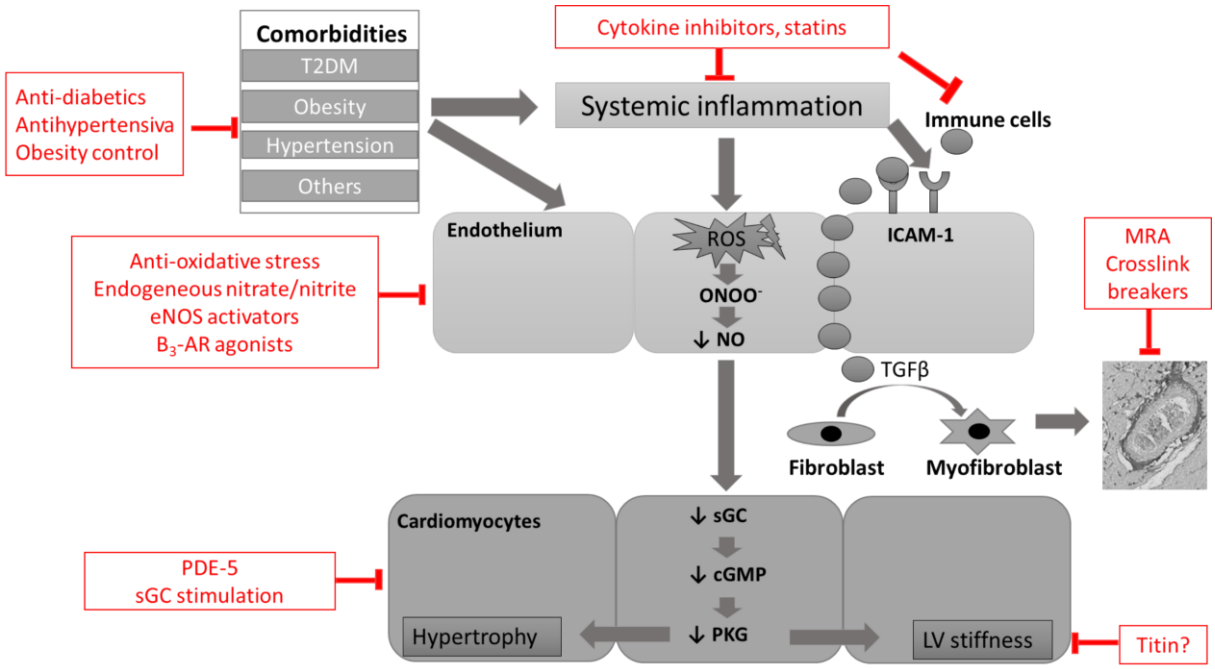

Figure 1.9- Potential therapies for HFpEF targeting comorbidities, inflammation, endothelial dysfunction, cardiac fibrosis, and/or cardiomyocyte dysfunction. β_3-AR, β_3 adrenergic receptor; *cGMP, cyclic guanosine monophosphate; eNOS, endothelial nitric oxide synthase; ICAM-1, intercellular adhesion molecule-1; MRA, mineralocorticoid receptor antagonist; NO, nitric oxide; ONOO$^-$, peroxynitrite; PDE-5, phosphodiesterase-5; PKG, protein kinase G; T2DM, type 2 diabetes mellitus; ROS, reactive oxygen species; sGC, soluble guanylate cyclase; TGFβ, transforming growth factor beta. Figure based on Paulus WJ et al. 2013*[50].

Chapter 2: Rationale and Aims

While the prevalence of HFpEF dramatically increases, evidence-based effective **treatment** and **prevention** strategies are **absent** due to **inadequate diagnosis**, **incomplete understanding of the pathology**, and **heterogeneity** in the patient population.

To improve the understanding of the pathology, we use an animal model, the obese ZSF1 rat, which mimics human HFpEF pathology. However, the use of anaesthetics to immobilize the animal is required for reduction of stress and reliable and reproducible echocardiography recordings. **Anaesthesia** is well known to affect cardiac contractility, hemodynamic, pre- and afterload. However, the effects on cardiac function, especially diastolic dysfunction, have never been investigated in HFpEF rodent models**.**

Objective 1: We aimed to examine the effect of the most commonly used anaesthetics for rodent models, isoflurane and ketamine/xylazine, during echocardiography acquisition on cardiac function in HFpEF-diseased obese ZSF1 rats and lean controls (Chapter 3).

Recently, a paradigm has proposed **endothelial dysfunction** as the central mediator in HFpEF driving myocardial dysfunction and remodelling[50]. Interestingly, a reduced cardiac microvascular density (capillaries and pre-capillary arterioles) per cardiomyocyte area, also called microvascular rarefaction, was reported in HFpEF patients[60]. Rarefaction is a dynamic process that occurs both under physiological and pathological conditions[185] and can be caused by decreased angiogenesis or increased vessel regression. However, when rarefaction occurs with respect to the development of HFpEF is not known. Furthermore, triggers for cardiac microvascular regression have not been investigated in HFpEF.

Objective 2: Establish the role of cardiac microvascular rarefaction in HFpEF development (Chapter 4).

- ***a) Investigate whether cardiac microvascular rarefaction precedes, coincides with, or follows the development of HFpEF.***
- ***b) Identify the trigger(s) for cardiac microvascular rarefaction in HFpEF to allow for effective and specific treatment strategies and early biomarkers for HFpEF.***

Increased left ventricular stiffness is the earliest manifestation of diastolic dysfunction. Left ventricular stiffness is determined by the extracellular matrix and cardiomyocyte $F_{passive}$[107]. Impaired cardiomyocyte relaxation is the first affected determinant of left ventricular stiffness and precedes the excessive deposition of cardiac fibrosis[186,187]. Cardiac stiffening is determined by increased cardiomyocyte $F_{passive}$[56,188-190], mainly due to modifications of titin. Diastolic dysfunction and left ventricular stiffening are associated with **increased circulating DPP-4** levels in obese and T2DM patients[191-193]. **Linagliptin**, a **DPP-4 inhibitor**, is used for the treatment of T2DM by controlling blood glucose levels. While linagliptin also has beneficial effects on the heart independently of their glucose-lowering effects[194-200], its protective effects on left ventricular stiffness and diastolic dysfunction have not been investigated in the MetS.

Objective 3: Determine whether the anti-diabetic drug linagliptin prevents the development of left ventricular stiffening, assessing both extracellular matrix- and cardiomyocyte-derived stiffness, in metabolic-risk induced cardiovascular disease (Chapter 5).

Chapter 3: The effect of different anaesthetics on echocardiographic evaluation of diastolic dysfunction in a HFpEF model.

I. Cuijpers, P. Carai, P. Mendes-Ferreira, S.J. Simmonds, P. Mulder, D. Miranda-Silva, D. De Giorgio, P. Pokreisz, S. Heymans, and E.A.V. Jones.

Minor revision Nature Scientific Reports

3.1 Abstract

There is currently no treatment for HFpEF. Therapeutics development demands effective diagnosis of diastolic dysfunction in animal models mimicking human pathology, which requires appropriate anaesthetics. Here, we investigated which anaesthetic, ketamine/xylazine or isoflurane, could be used to reveal diastolic dysfunction in HFpEF-diseased obese ZSF1 rats by echocardiography. First, diastolic dysfunction was confirmed by PV loops in obese compared to lean control ZSF1 rats. In echocardiography, ketamine/xylazine, unlike isoflurane, was able to demonstrate impaired relaxation in obese ZSF1 rats, as reflected by impaired E and A filling peak velocities, decreased E/A ratio, and a prolonged deceleration and isovolumic relaxation time. Interestingly, ketamine/xylazine induced a wider separation of both tissue and pulsed wave Doppler-derived echocardiographic waves required for diastolic dysfunction diagnosis, potentially by reducing the HR, while isoflurane resulted in merged waves. To assess whether HR-lowering alone explained the differences between the anaesthetics, echocardiography measurements under isoflurane with and without the HR-lowering drug ivabradine were compared. However, diastolic dysfunction could not be diagnosed in ivabradine-treated obese ZSF1 rats. In summary, ketamine/xylazine compared to isoflurane is the anaesthetic of choice to detect diastolic dysfunction by echocardiography in rodent HFpEF.

3.2 Introduction

HFpEF is a complex heterogeneous cardiovascular syndrome characterised by diastolic dysfunction and cardiac remodelling (stiffening, inflammation, and hypertrophy) in the presence of a preserved ejection fraction (≥50%). Due to the ageing population, as well as an improved survival of patients with comorbidities, such as obesity, T2DM, and hypertension, the prevalence of HFpEF is steadily rising, accounting for more than 50% of incident HF overall[17]. Despite the improved management of HFrEF over the last two decades, little advancement has been made in identifying evidence-based treatments for HFpEF. Treatment of HFpEF has been especially complicated by incomplete understanding of the pathophysiology, patient population heterogeneity, and inadequate diagnosis[24].

Animal models are essential for understanding HFpEF disease progression and treatment. Obese ZSF1 rats are an established HFpEF model associated with cardiometabolic risks, including obesity, T2DM, and hypertension[150]. Echocardiography is crucial for the differential diagnosis of diastolic function in these rats, however the use of anaesthetics is required for reduction of stress and reliable and reproducible recordings[201]. Anaesthetics are well known to affect cardiac preload, afterload, myocardial contractility, and hemodynamics (e.g. HR)[202]. However, their effects on cardiac function, including systolic function, hemodynamics, left ventricular dimensions, and especially diastolic function, have never been investigated in a HFpEF rodent model. Accordingly, this study examined the effect of the most commonly used anaesthetics for rodent models, isoflurane and ketamine/xylazine, on cardiac function during echocardiography acquisition in obese and lean control ZSF1 rats.

3.3 Materials and Methods

3.3.1 Experimental animals

Experiments were performed according to the European Directive (2010/63/EU) and approved by the Animal Care and Use Committee of KU Leuven (Project 168/2016). Male ZSF1 rats, including obese and lean control littermates, were obtained from Charles River Laboratories (#strain code 378 and 379, respectively). ZSF1 rats are developed by crossing rat strains with two different types of leptin receptor mutations (*leprfa* and *lepr facp*), the lean female ZDF (+/*lepr fa*) and the lean male SHHF (*SHHF/Mcc*; +/*lepr facp*) rat. The obese ZSF1 rat offspring are homozygous for the leptin receptor mutation (*lepr fa /lepr facp*) and inherit the hypertensive gene (*SHHF/Mcc*), resulting in the combined development of T2DM, hypertension, hyperlipidaemia, ultimately leading to the development of metabolic risk induced-HFpEF, characterised by diastolic dysfunction, increased left ventricular myocardial stiffness and hypertrophy, and a preserved ejection fraction (≥50%) at 20 weeks[151]. In contrast to obese ZSF1 rats, lean littermates are heterozygous for the leptin receptor mutation (*lepr fa/+* or *lepr facp/+*), but inherit the hypertensive gene (*SHHF/Mcc*). Lean ZSF1 rats therefore only develop hypertension, thereby serving as non-HFpEF diseased controls[151]. Animals were housed and acclimated under a 12-hour light-dark cycle with access to water and chow diet *ad libitum* (#V1534-000, Ssniff Spezialdiäten GmbH, Germany). As diastolic dysfunction has previously been reported in obese ZSF1 rats at 20 weeks[151], echocardiography with isoflurane or ketamine/xylazine was performed on 20 weeks old lean and obese ZSF1 (n=7/group). After one week of recovery, fourteen of those animals underwent subsequently PV loops at 21 weeks. One obese ZSF1 rat died during the PV loop acquisition. On a different set of animals, including seven lean and eight obese ZSF1 rats per group (20 weeks old; kindly provided by Prof. Paul Mulder), echocardiography was performed with or without intraperitoneal (IP) administration of 0.3 mg/kg of the HR-lowering drug ivabradine in combination with 1.5% inhaled isoflurane.

3.3.2 PV loops

Lean and obese ZSF1 rats were anaesthetised with isoflurane, 8% for induction and 2-3.5% for maintenance (Ecuphar, Belgium). Animals were endotracheally intubated (14G) and mechanically ventilated (Rovent, Kent Scientific Corporation, USA) using 100% oxygen, while maintaining positive end-expiratory pressure at 5 cm H_2O. Proper sedation was confirmed by assessing the pedal withdraw reflex in the hind limbs, and the toe pinch and eyelid reflex[203].

Body temperature was controlled using a homeothermic blanket system to prevent anaesthesia-induced hypothermia and cardiac electrical activity was monitored using an electrocardiogram (ECG; Bio Amplifier, FE136, AD Instruments Ltd., UK). Using an open chest approach, a SPR-838 pressure-volume catheter (Millar Instruments, USA) was inserted in the left ventricle through the apex. Fluid loss was compensated by infusion of warmed 0.9% saline at a rate of 32 ml/kg/h through the femoral vein (25G IV catheter, B. Braun Melsungen AG, Germany). Bolus injections of 50 µl hypertonic saline (10% NaCl) were administered to determine parallel conductance. Slope factor α was determined by dividing the PV loop- and echocardiographic-derived cardiac output (CO). Pressure and volume signals were continuously acquired using a Millar Ultra Pressure Volume system (Millar Instruments, USA), digitally recorded using a Power lab 16/35 data acquisition system, and analysed using Lab Chart 8 (both AD Instruments Ltd., UK). After a 15 minutes stabilization period, baseline acquisitions were recorded at suspended end-expiration. Transient occlusions of the inferior vena cava using a 3-0 silk lace were achieved to obtain load-independent indexes. Hemodynamic parameters included HR, CO, ejection fraction (EF), end-diastolic and -systolic pressures (EDP and ESP) and volumes (EDV and ESV), logarithmic isovolumic relaxation time constant tau (logistic method), dp/dt_{min}, dp/dt_{max}, preload-recruitable stroke work (PRSW), arterial elastance (Ea), as well as the slope of ESPVR and EDPVR, called end-systolic and end-diastolic stiffness (elastance). The catheter was subsequently positioned in the ascending aorta to measure systolic and

diastolic arterial pressures (SAP and DAP). Mean arterial pressure (MAP) was calculated, whereby MAP equals 2/3 DAP plus 1/3 SAP. Heparinized blood was collected for conductance-based volume calibration (#910-1048, Millar Instruments, USA). As the body weight of obese ZSF1 rats is significantly higher than the lean control ZSF1 rats, volumes were indexed for body surface area (BSA), estimated as 9.1 * body weight in grams$^{2/3}$, to account for differences in body weight between the groups[151,204]. Both the indexed and non-indexed volumes for PV loops are presented. After the procedure, animals were euthanized by anaesthetics overdose using 50 mg/kg ketamine (Nimatek, Eurovet, Netherlands) and 5 mg/kg xylazine (Xyl-M®, V.M.D. nv/sa, Belgium) dissolved in 0.9% NaCl. Death was confirmed by absence of an ECG signal.

3.3.3 Transthoracic echocardiography

Lean and obese ZSF1 rats were randomized for echocardiography and anaesthetised with either an IP injection of 50 mg/kg ketamine (Nimatek, Eurovet, Netherlands) and 5 mg/kg xylazine (Xyl-M®, V.M.D. nv/sa, Belgium) (Ket/Xyl) dissolved in 0.9% NaCl (n=7/group) or 5% inhaled isoflurane (cuphar, Belgium) for induction followed by 1.5% inhaled isoflurane for maintenance (n=7/group).

To assess the effect of HR-lowering, 7 lean and 8 obese ZSF1 rats were randomly assigned to isoflurane (5% for induction and 1.5% for maintenance) with IP administration of 0.3 mg/kg ivabradine in 0.9% saline (Procoralan, Servier, France) or 0.9% saline (vehicle control). Echocardiography was performed during two days with a washout period for ivabradine for at least 24h after the previous acquisition.

Similar to PV loops, proper sedation was confirmed by assessing the pedal withdraw reflex in the hind limbs, and the toe pinch and eyelid reflex[203]. The time between anaesthetic induction and image acquisition was similar, approximately 5-10 minutes, in all the experimental groups.

2-D M-mode echocardiography was performed using a MS 250 transducer (13-24 MHz) connected to a Vevo 2100 echocardiograph (Visual Sonics, Canada). Animals were placed in a supine position on a heating pad to maintain the core body temperature between 37.5-37.7 °C, measured using a rectal probe. Body temperature was monitored during the whole procedure to prevent anaesthesia-induced hypothermia and to assess the anaesthesia depth. ECG recordings were performed to monitor the heart and breathing rate. Anaesthesia dosage was modified if needed to ensure similar heart and breathing rates between all animals. HR, end-diastolic- and systolic diameters (EDD and ESD), as well as left ventricular anterior wall thickness (AW) and posterior wall thicknesses (PW) in diastole and systole, were acquired on the parasternal short-axis using M-mode imaging. Stroke volume (SV), fractional shortening (FS), left ventricular mass (corrected and uncorrected), EF, CO, as well as ESV and EDV (Teichholz formula), were calculated based on M-mode images. Left ventricular filling was assessed by pulsed wave Doppler trans-mitral flow tracings (gate size 0.29 mm and Doppler angle -25°), including E, A, IVRT, mitral valve deceleration time, isovolumic contraction time (IVCT), and aortic ejection time (AET), just above the tip of the mitral valve leaflets using an apical view. Non-flow time (NFT) was the sum of IVCT, IVRT, and AET. Systolic peak wave (S'), E', and A' were measured with tissue Doppler imaging (gate size 0.29 mm and Doppler angle 0°) at the lateral mitral annulus using an apical view. To assess diastolic function, E/A, E/E', E'/A', and E/E'/SV ratios were calculated. Myocardial performance index (MPI), an indicator for systolic and diastolic function, was calculated by dividing summed IVCT and IVRT by AET. In addition to presenting the non-indexed values, cardiac volumes were corrected for BSA to account for differences in body weight between the obese and lean ZSF1 rats. At least three stable cardiac cycles were averaged for all measurements. After the procedure, ketamine/xylazine-anaesthetised animals were recovered by an IP injection with 0.1 mg/kg Atipamezole

(Antisedan, Elanco Animal Health, Antwerpen, Belgium) intraperitoneally, while maintaining their body temperature between 37.5-37.7 °C to prevent anaesthesia-induced hypothermia.

3.3.4 Statistical analysis

Results are presented as mean ± SD. Statistical analysis was performed using GraphPad software V7 (San Diego, CA, USA). Normal distribution of all continuous variables was tested according to the D'Agostino & Pearson omnibus normality test. Normal distributed PV loop data were analysed using a two-tailed unpaired Student t-test, while non-normally distributed data were analysed by a Mann-Whitney U test. Echocardiography parameters were analysed by regular two-way analysis of variance (ANOVA) with Šídák's multiple comparison post hoc test. P-values of <0.05 were considered statistically significant.

3.4 Results

3.4.1 Diastolic dysfunction in obese ZSF1 rats confirmed by PV loops

To confirm the in literature-reported development of diastolic dysfunction in 20-week-old obese ZSF1 rats[151], we performed golden standard PV loops in obese and lean control ZSF1 rats at 21 weeks. Obese ZSF1 rats showed a significantly decreased HR and increased non-BSA-indexed SV compared to lean ZSF1 rats, while cardiac index (CI) and BSA-indexed SV and CO were similar between lean and obese ZSF1 rats (Table 3.1). Furthermore, obese ZSF1 rats showed a worsened hypertensive profile, reflected by significantly increased SAP and MAP, while DAP was modestly, albeit not significantly (p=0.06), increased compared to lean ZSF1 rats (Table 3.1). Obese ZSF1 rats had an increased EDP and tau, confirming an impaired diastolic function in obese compared to lean ZSF1 rats (Figure 3.1A-C and Table 3.1). BSA-indexed end-diastolic stiffness (also called end-diastolic elastance) was modestly, although non-significantly (p=0.06), increased in obese compared to lean ZSF1 rats (Figure 3.1D and Table 3.1). Similarly, non-indexed end-diastolic stiffness was not significantly different

between lean and obese ZSF1 rats (Table 3.1). dP/dt_{min} and BSA-indexed and non-indexed EDV were similar in lean and obese ZSF1 rats (Table 3.1). Systolic parameters, including EF (>50%), dP/dt_{max}, PRSW, and BSA-indexed and non-indexed ESV, Ea, and end-systolic stiffness (also called end-systolic elastance) were comparable in lean and obese ZSF1 rats (Table 3.1). In summary, PV loops confirmed diastolic dysfunction in presence of a preserved EF in 21-week-old obese ZSF1 rats compared to age-matched lean ZSF1 rats.

Table 3.1- PV loops in left ventricle and aorta of lean and obese ZSF1 rats at 21 weeks

Parameter	Lean (n=7)	Obese (n=6)	P-value
Baseline			
Body weight (g)	371 ± 38	534 ± 21	**0.0012**
BSA (cm^2)	470 ± 33	599 ± 16	**0.0012**
HR (bpm)	313 ± 18	277 ± 33	**0.0307**
SV (µl)	178 ± 11	221 ± 13	**0.0271**
SV, i ($µl/cm^2$)	0.38 ± 0.07	0.37 ± 0.02	0.7207
CO (ml/min)	56 ± 7.1	61 ± 12	0.3167
CI ($ml/min/cm^2$)	0.12 ± 0.02	0.10 ± 0.02	0.1623
EF (%)	56 ± 7.8	62 ± 14	0.2921
ESP (mmHg)	143 ± 13	169 ± 17	**0.0098**
ESV (µl)	174 ± 47	187 ± 83	0.7265
ESV, i ($µl/cm^2$)	0.37 ± 0.10	0.31 ± 0.14	0.3884
dP/dt_{max} (mmHg/s)	8532 ± 1127	8695 ± 556	0.7545
Ea (mmHg/µl)	0.82 ± 0.19	0.75 ± 0.13	0.4316
Ea, i ($mmHg/µl/cm^2$)	389 ± 96	449 ± 80	0.2495
EDP (mmHg)	9.7 ± 3.5	14.4 ± 3.68	**0.0393**
EDV (µl)	335 ± 21	385 ± 30	0.1985
EDV, i ($µl/cm^2$)	0.72 ± 0.14	0.64 ± 0.12	0.3272
dP/dt_{min} (mmHg/s)	-9758 ± 1382	-9231 ± 1003	0.4557
Tau Logistic (ms)	8.0 ± 0.4	11 ± 1.4	**0.0006**
Occlusion			
PRSW (mmHg)	75 ± 24	75 ± 36	0.9992
End-systolic stiffness (mmHg/µl)	0.62 ± 0.22	0.50 ± 0.23	0.3896
End-systolic stiffness, i ($mmHg/µl/cm^2$)	289 ± 107	301 ± 137	0.8696
End-diastolic stiffness (mmHg/µl)	0.009 ± 0.004	0.01 ± 0.0005	0.2763
End-diastolic stiffness, i ($µl/cm^2$)	4.1 ± 1.8	7.0 ± 3.2	0.0616
Aortic parameters			
SAP (mmHg)	143 ± 13	167 ± 16	**0.0131**
DAP (mmHg)	99 ± 15	116 ± 15	0.0632
MAP (mmHg)	121 ± 15	141 ± 15	**0.0339**

*Values are presented as mean ± SD. BSA, body surface area; CI, cardiac index; CO, cardiac output; DAP, diastolic blood pressure; dP/dt_{max}, maximum rate of pressure change in the left ventricle; dP/dt_{min}, minimum rate of pressure change in the left ventricle; Ea, arterial elastance; EDP, end-diastolic pressure; EDV, end-diastolic volume; EF, ejection fraction; ESP, end-systolic pressure; ESV, end-systolic volume; HR, heart rate; i, indexed for body surface area, calculated as 9.1 * body weight in $grams^{2/3}$; MAP, mean arterial pressure; PRSW, preload recruitable stroke work; PV; pressure-volume; SAP, systolic arterial pressure; SV, stroke volume. Normal distributed pressure-volume loop data were analysed using a two-tailed unpaired Student t-test, while non-normally distributed data were analysed by a Mann-Whitney U test.*

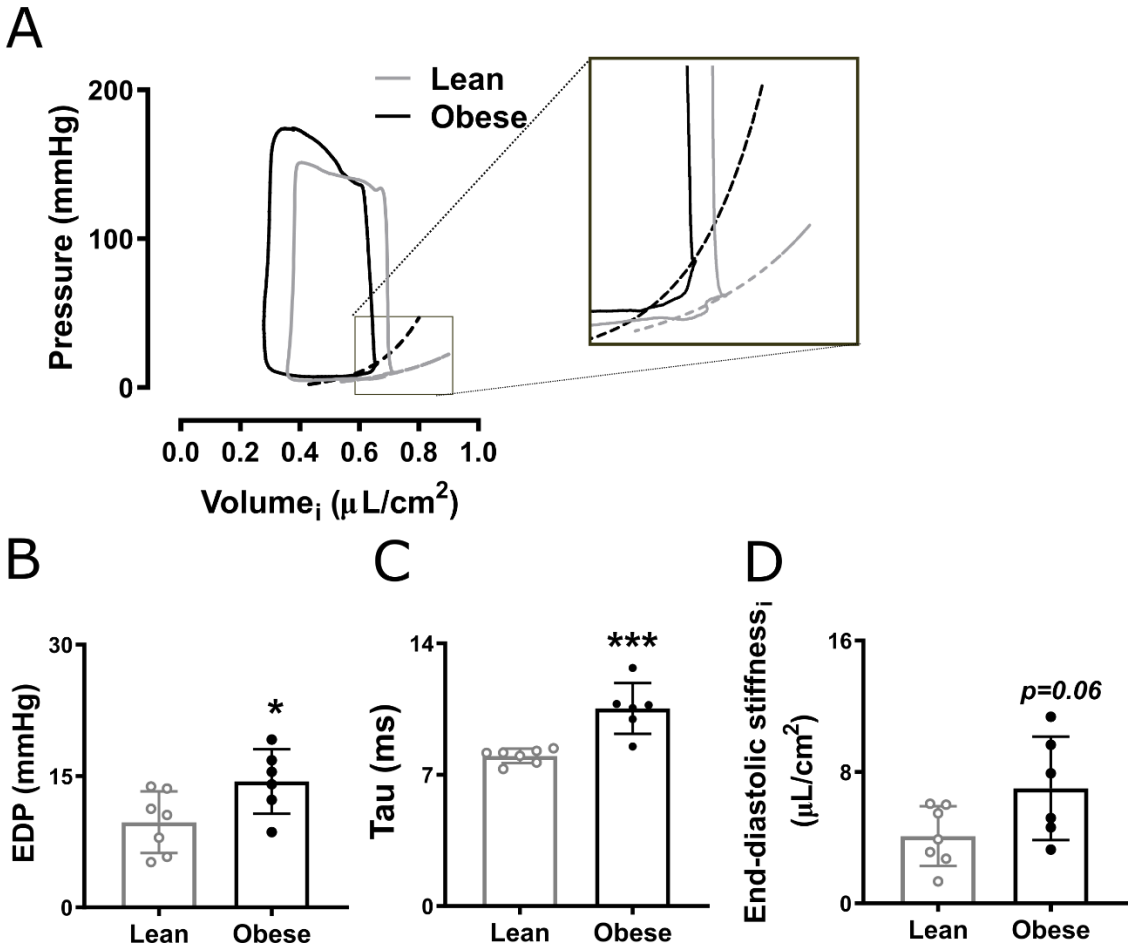

Figure 3.1- Diastolic dysfunction in obese ZSF1 rats assessed by pressure-volume loops. *Pressure-volume loops indexed for body surface area (**A**), EDP (**B**), tau (**C**), and end-diastolic stiffness indexed for body surface area (**D**) in 6 obese and 7 lean ZSF1 rats at 21 weeks. Values are presented as mean ± SD. Panel B-D were analysed using a two-tailed unpaired Student t-test with*P<0.05 and ***<0.001. EDP, end-diastolic pressure; i, indexed for body surface area, calculated as 9.1 * body weight in grams$^{2/3}$.*

3.4.2 Diastolic dysfunction in obese ZSF1 rats is detectable by echocardiography using ketamine/xylazine

To assess whether diastolic dysfunction could be diagnosed by echocardiography using isoflurane or ketamine/xylazine, we performed pulsed wave and tissue Doppler echocardiography in lean and obese ZSF1 rats at 20 weeks. A clear separation of both E and A waves in pulsed wave Doppler and early E' and A' waves in tissue Doppler was observed in both lean and obese ZSF1 rats anaesthetised with ketamine/xylazine (Figure 3.2 and 3.3, lower panels). In contrast to ketamine/xylazine, anaesthesia with isoflurane superimposed E and A waves, as well as E' and A' waves, on each other, thereby impeding the reliable assessment of diastolic function (Figure 3.2 and 3.3, upper panels).

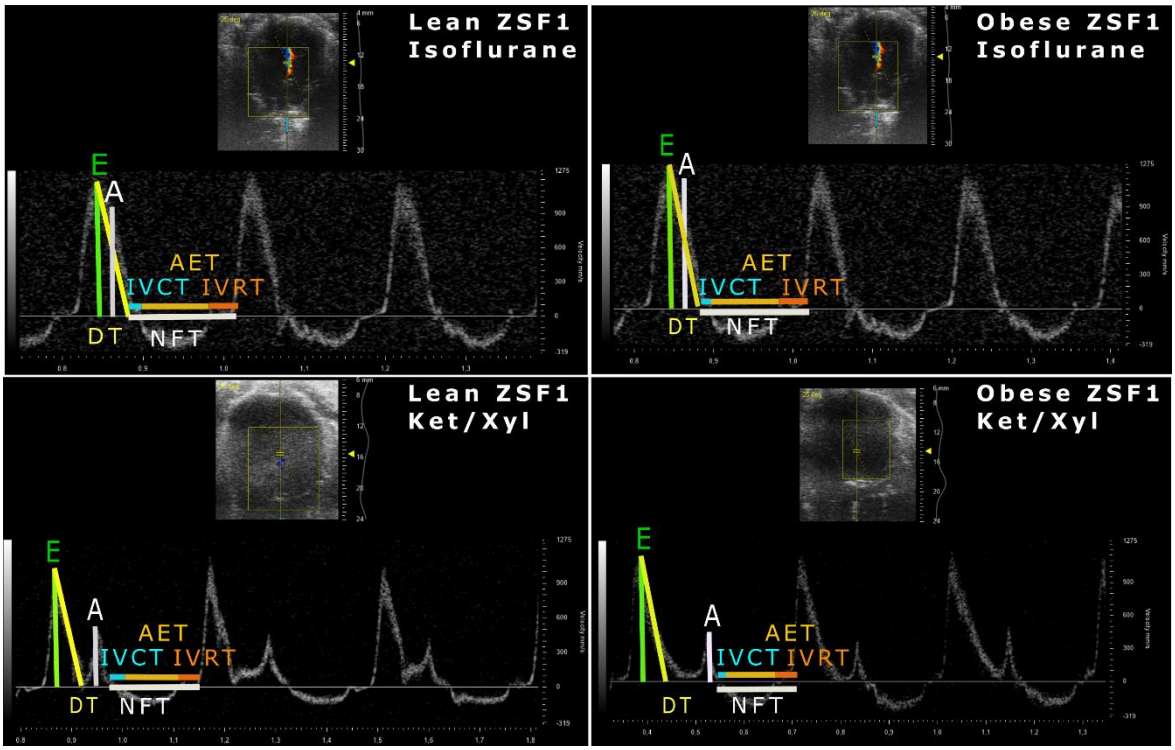

Figure 3.2- Ketamine/xylazine resulted in a more distinct separation of pulsed wave Doppler waves in both obese and lean ZSF1 rats. *Pulsed wave Doppler images of isoflurane- and ketamine/xylazine-anaesthetised 20-week-old lean and obese ZSF1 rats (n=7 per group). A, late mitral inflow peak velocity; AET, aortic ejection time; DT, mitral valve deceleration time; E, early mitral inflow peak velocity; IVCT, isovolumic contraction time; IVRT, isovolumic relaxation time; Ket/Xyl, ketamine/xylazine; NFT, non-flow time.*

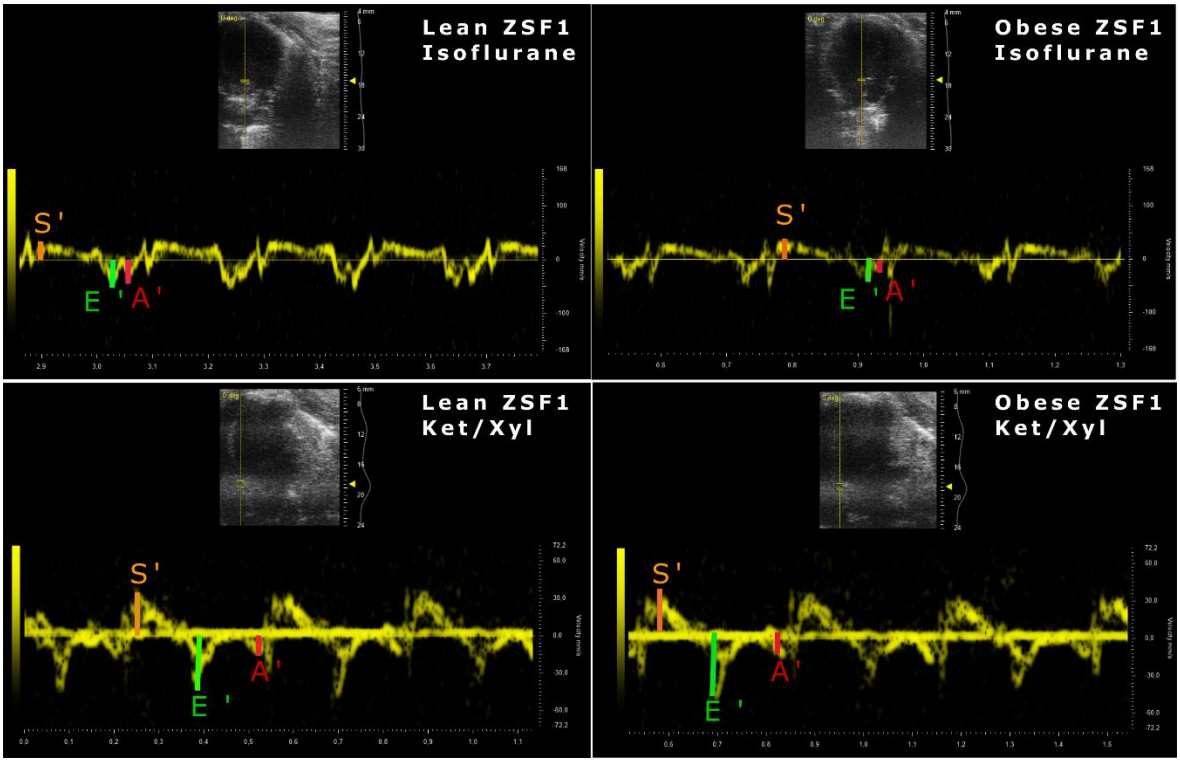

Figure 3.3- Ketamine/xylazine induced a more distinct separation of tissue Doppler waves in lean and obese ZSF1 rats. *Tissue Doppler images of 20-week-old isoflurane- and ketamine/xylazine-anaesthetised lean and obese ZSF1 rats (n=7 per group). A', late mitral annulus peak velocity; E', early diastolic mitral annulus peak velocity; Ket/Xyl, ketamine/xylazine; S', systolic peak velocity.*

Ketamine/xylazine significantly decreased E peak velocities in lean ZSF1 rats, while decreasing A peak velocities in both lean and obese ZSF1 rats, resulting in significantly increased E/A ratios in both lean and obese ZSF1 rats compared to isoflurane-anaesthetized ZSF1 rats (Figure 3.4A-C). In obese ZSF1 rats, ketamine/xylazine increased mitral valve deceleration time, IVRT, and NFT compared to isoflurane (Figure 3.4D-E and Table 3.2). Furthermore, ketamine/xylazine decreased E' peak velocities in lean ZSF1 rats, while it reduced A' peak velocities in both lean and obese ZSF1 rats compared to isoflurane (Figure 3.4F-G). In obese ZSF1 rats, ketamine/xylazine increased E'/A' compared to isoflurane, while in lean ZSF1 rats, it increased both the operant diastolic elastance (E/E'/SV) and the E/E' ratio (Figure 3.4H-I and Table 3.2). Importantly, diastolic dysfunction could only be diagnosed when using ketamine/xylazine in obese ZSF1 rats, as reflected by a decreased E/A ratio, operant diastolic elastance (E/E'/SV), and MPI, and increased E and A peak velocities, mitral valve deceleration time, IVRT, NFT, and E'/A' ratio compared to lean ZSF1 rats (Figure 3.4A-E and H and Table 3.2). In contrast to ketamine/xylazine, isoflurane only increased A peak velocities in obese compared to lean ZSF1 rats, showing the inability to detect diastolic dysfunction when using isoflurane as an anaesthetic (Figure 3.4A-I and Table 3.2).

Taken together, diastolic dysfunction in obese ZSF1 rats is detectable when using ketamine/xylazine but cannot be identified when isoflurane is administered as an anaesthetic.

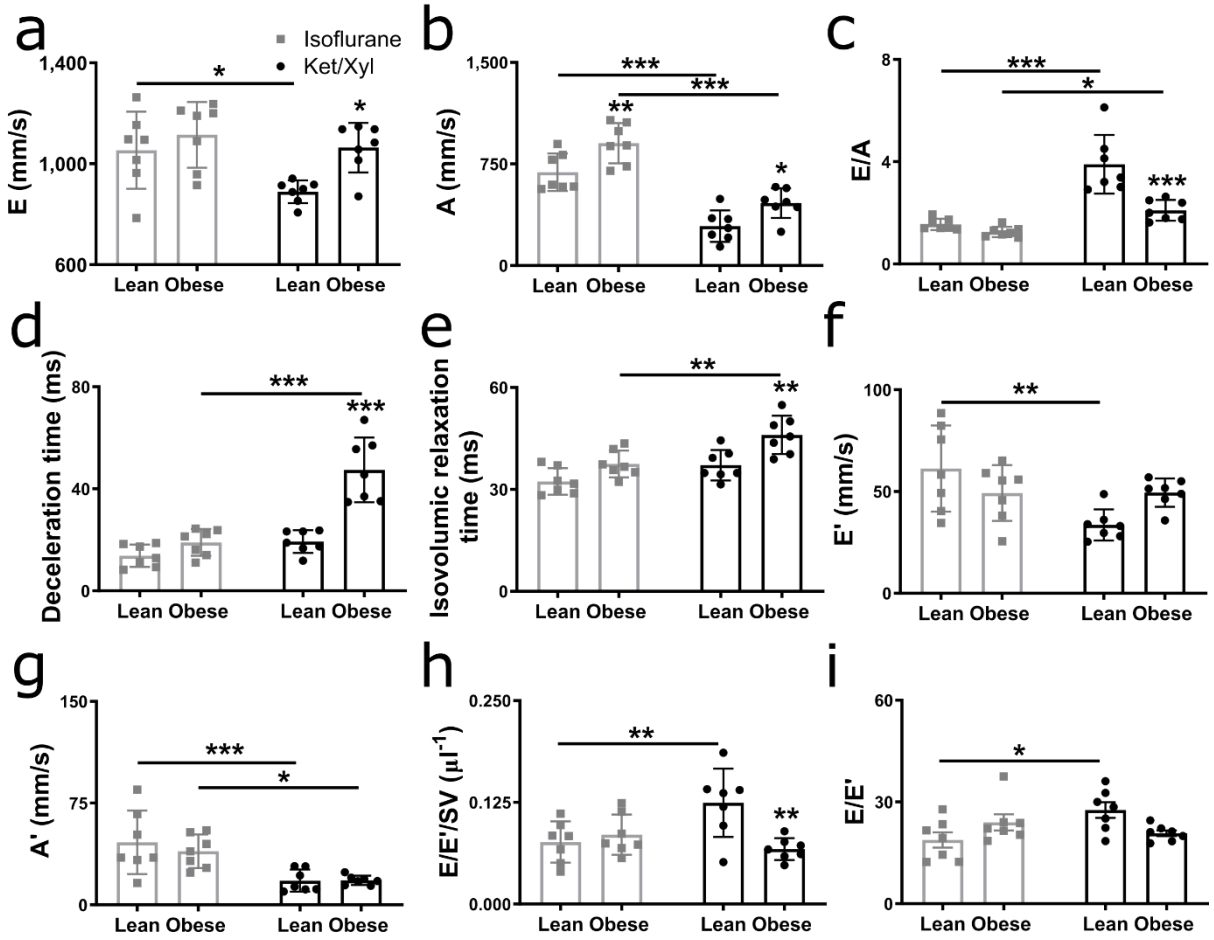

Figure 3.4- Diastolic dysfunction in obese ZSF1 rats is detectable when ketamine/xylazine is used as an anaesthetic. *E and A peak velocities (**A-B**), E/A ratio (**C**), mitral valve deceleration time (**D**), isovolumic relaxation time (**E**), E' and A' peak velocities (**F-G**), and E/E'/SV (**H**) and E/E' ratios (**I**) in 20-week-old isoflurane- or ketamine/xylazine-anaesthetised lean and obese ZSF1 rats (n=7 per group). Values are presented as mean ± SD. Significance was assessed by a regular two-way analysis of ANOVA followed by a Šídák's multiple comparisons test with *p<0.05, **<0.01, and ***<0.001. A, late mitral inflow peak velocity; A', late mitral annulus peak velocity; E, early mitral inflow peak velocity; E', early diastolic mitral annulus peak velocity; Ket/Xyl, ketamine/xylazine; SV, stroke volume.*

Table 3.2- Echocardiography parameters in isoflurane- or ketamine/xylazine-anaesthetised lean and obese ZSF1 rats

Parameter	Lean-Isoflurane (n=7)	Obese-Isoflurane (n=7)	Lean-Ket/Xyl (n=7)	Obese-Ket/Xyl (n=7)
Body weight (g)	406 ± 13	552 ± 25***	371 ± 38$^{\#}$	536 ± 20***
BSA (cm^2)	499 ± 13	612 ± 19***	470 ± 33$^{\#}$	601 ± 15***
LV mass (mg)	1199 ± 199	1618 ± 369**	1297 ± 204	1500 ± 152
Corrected LV mass (mg)	959 ± 159	1294 ± 296**	1037 ± 163	1200 ± 122
HR (bpm)	360 ± 20	310 ± 26***	243 ± 25$^{\#\#\#}$	200 ± 20$^{**,\#\#\#}$
SV (µl)	252 ± 43	287 ± 41	230 ± 42	314 ± 46**
SV, $_i$ (µl/cm^2)	0.51 ± 0.09	0.47 ± 0.07	0.50 ± 0.14	0.52 ± 0.08
CO (ml/min)	90 ± 12	88 ± 14	55 ± 7.3$^{\#\#\#}$	63 ± 12$^{\#\#}$
CI (ml/min/cm^2)	0.18 ± 0.02	0.14 ± 0.03*	0.12 ± 0.02$^{\#\#\#}$	0.11 ± 0.02$^{\#\#}$
AW$_d$ (mm)	1.9 ± 0.3	2.1 ± 0.3	2.3 ± 0.4$^{\#}$	2.0 ± 0.3
AW$_s$ (mm)	3.4 ± 0.3	3.8 ± 0.5	3.5 ± 0.4	3.6 ± 0.5
EDD (mm)	8.0 ± 0.8	8.5 ± 0.8	7.7 ± 0.7	8.7 ± 0.4*
ESD (mm)	4.5 ± 0.8	4.7 ± 0.7	4.4 ± 0.8	4.7 ± 0.6
PW$_d$ (mm)	1.9 ± 0.3	2.2 ± 0.2	1.9 ± 0.4	2.0 ± 0.3
PW$_s$ (mm)	3.0 ± 0.3	3.2 ± 0.3	2.8 ± 0.5	3.3 ± 0.3*
EDV (µl)	350 ± 78	391 ± 61	316 ± 66	419 ± 39
EDV, $_i$ (µl/cm^2)	0.70 ± 0.16	0.64 ± 0.11	0.68 ± 0.20	0.70 ± 0.06
ESV (µl)	97 ± 42	107 ± 37	85 ± 34	105 ± 31
ESV, $_i$ (µl/cm^2)	0.20 ± 0.08	0.18 ± 0.06	0.18 ± 0.08	0.10 ± 0.05
EF (%)	73 ± 6.0	73 ± 5.7	74 ± 7.4	75 ± 7.5
FS (%)	44 ± 4.9	44 ± 4.8	45 ± 6.7	46 ± 6.8
AET (ms)	74 ± 7.5	84 ± 7.4	74 ± 9.9	103 ± 13$^{***,\#\#}$
IVCT (ms)	19 ± 3.0	19 ± 2.8	15 ± 3.3	18 ± 2.8
NFT (ms)	125 ± 14	141 ± 11	127 ± 13	167 ± 14$^{***,\#\#}$
MPI (AU)	0.69 ± 0.05	0.67 ± 0.05	0.68 ± 0.04	0.62 ± 0.04*
S' (mm/s)	45 ± 13	37 ± 4.0	40 ± 3.0	33 ± 9.8
E'/A'	1.7 ± 0.8	1.3 ± 0.4	2.3 ± 0.84	3.0 ± 0.53$^{*,\#\#\#}$

*Values are presented as mean ± SD. A', late mitral annulus peak velocity; AET, aortic ejection time; AW, anterior wall; CI, cardiac index; CO, cardiac output; d, in diastole; E', early diastolic mitral annulus peak velocity; EDD, end-diastolic diameter; EDV, end-diastolic volume; EF, ejection fraction; ESD, end-systolic diameter; ESV, end-systolic volume; FS, fractional shortening; HR, heart rate; i, indexed for body surface area, calculated as 9.1 * body weight in grams$^{2/3}$; IVCT, isovolumic contraction time; Ket/Xyl; ketamine/xylazine; LV, left ventricular; MPI, myocardial performance index; NFT, non-flow time; PW, posterior wall; s, in systole; S', systolic peak wave; SV, stroke volume. Significance was assessed by a regular two-way analysis of ANOVA followed by a Šídák's multiple comparisons test. *P<0.05, **<0.01, and ***<0.001 comparing ketamine/xylazine- or isoflurane-anaesthetised Lean versus Obese rats. $^{\#}$P<0.05, $^{\#\#}$<0.01, and $^{\#\#\#}$P<0.001 comparing isoflurane- versus ketamine/xylazine-anaesthetised in each group of rats (either Lean or Obese*

3.4.3 Ketamine/xylazine has a cardiodepressive effect without affecting systolic parameters in both obese and lean ZSF1 rats

We subsequently investigated the anaesthetic's effects on left ventricular dimensions, hemodynamics, and systolic function. Ketamine/xylazine had cardiodepressive effects in both lean and obese ZSF1 rats, as reflected by a drop in HR and CO (Figure 3.5A-C). Similar to PV loops, a decreased HR was observed in obese compared to lean ZSF1 rats, regardless of the

type of anaesthetic (Figure 3.5B). SV was only increased in ketamine/xylazine-anaesthetised obese compared to lean ZSF1 rats, while correction for BSA resulted in similar SV in all groups (Figure 3.5D and Table 3.2). CI was significantly reduced in isoflurane-anaesthetised obese compared to lean ZSF1 rats, while ketamine/xylazine significantly reduced CI in both lean and obese ZSF1 rats compared to isoflurane (Table 3.2).

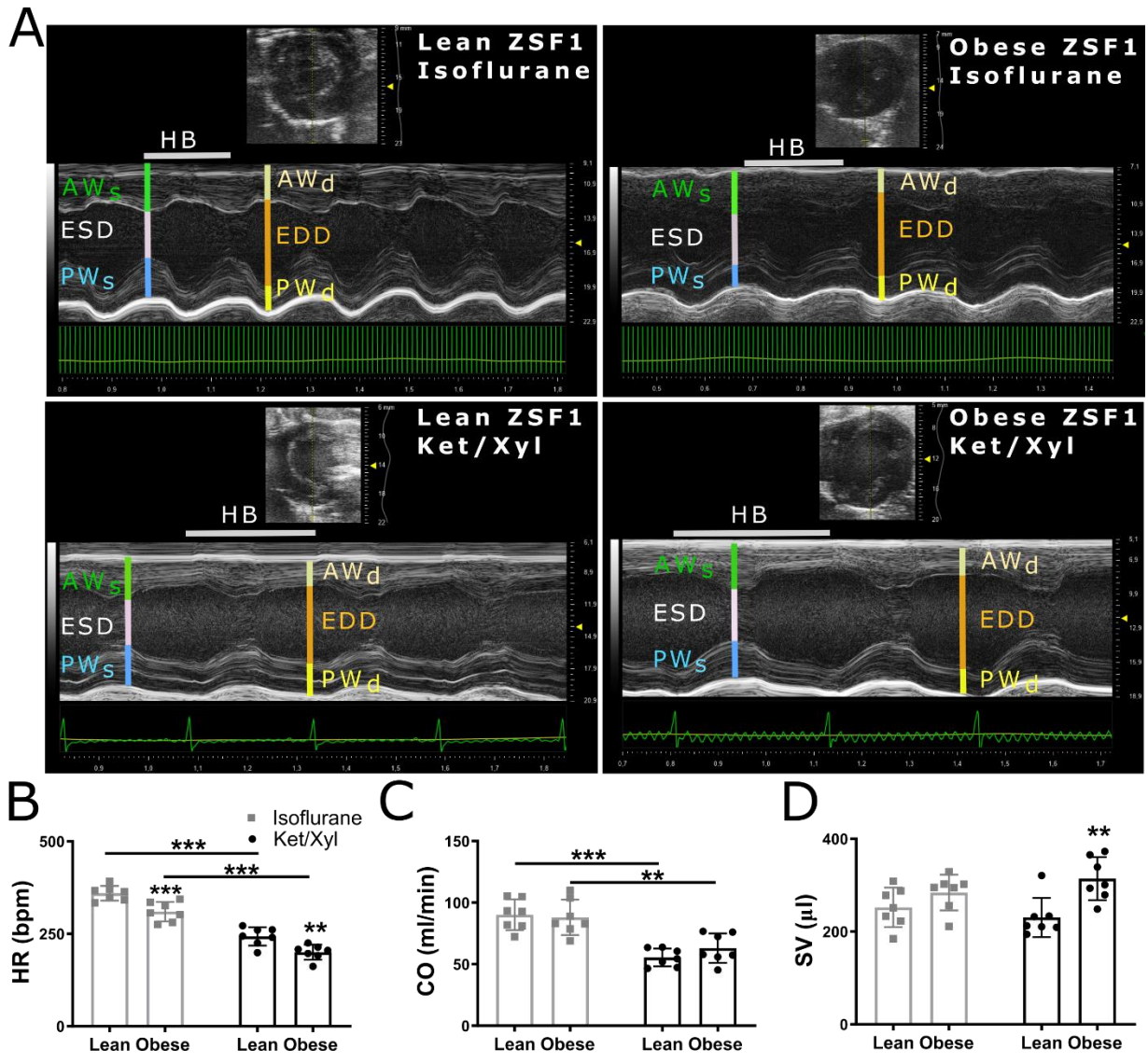

Figure 3.5- Ketamine/xylazine was cardiodepressive in both lean and obese ZSF1 rats. *M-mode images of 20-weeks-old isoflurane- and ketamine/xylazine-anaesthetised lean and obese ZSF1 rats (n=7 per group) (**A**). HR (**B**), CO (**C**), and SV (**D**) in 20-week-old isoflurane- or ketamine/xylazine-anaesthetised lean and obese ZSF1 rats. Values are presented as mean ± SD. Significance was assessed by a regular two-way analysis of ANOVA followed by a Šídák's multiple comparisons test with **p<0.01 and ***<0.001. AW, anterior wall; CO, cardiac output; EDD, end-diastolic diameter; ESD, end-systolic diameter; HB, heartbeat; HR, Heart rate; Ket/Xyl, ketamine/xylazine; PW, posterior wall; SV, stroke volume.*

Parameters of systolic function (EF, FS, S', and IVCT) and AW_s and ESD were not affected by the type of anaesthetic (Figure 3.6A-D and Table 3.2). Ketamine/xylazine significantly increased measurements of PW_s and EDD in obese compared to lean ZSF1 rats, while lean ZSF1 rats showed an increased AW_d when measured using ketamine/xylazine compared to isoflurane (Figure 3.6E-G and Table 3.2). Measurements of PW_d and non-indexed and indexed ESV and EDV were not affected by the type of anaesthetic (Figure 3.6H-I and Table 3.2). These findings demonstrated that ketamine/xylazine had a cardiodepressive effect but did not differently affect systolic function and measurements of left ventricular volumes.

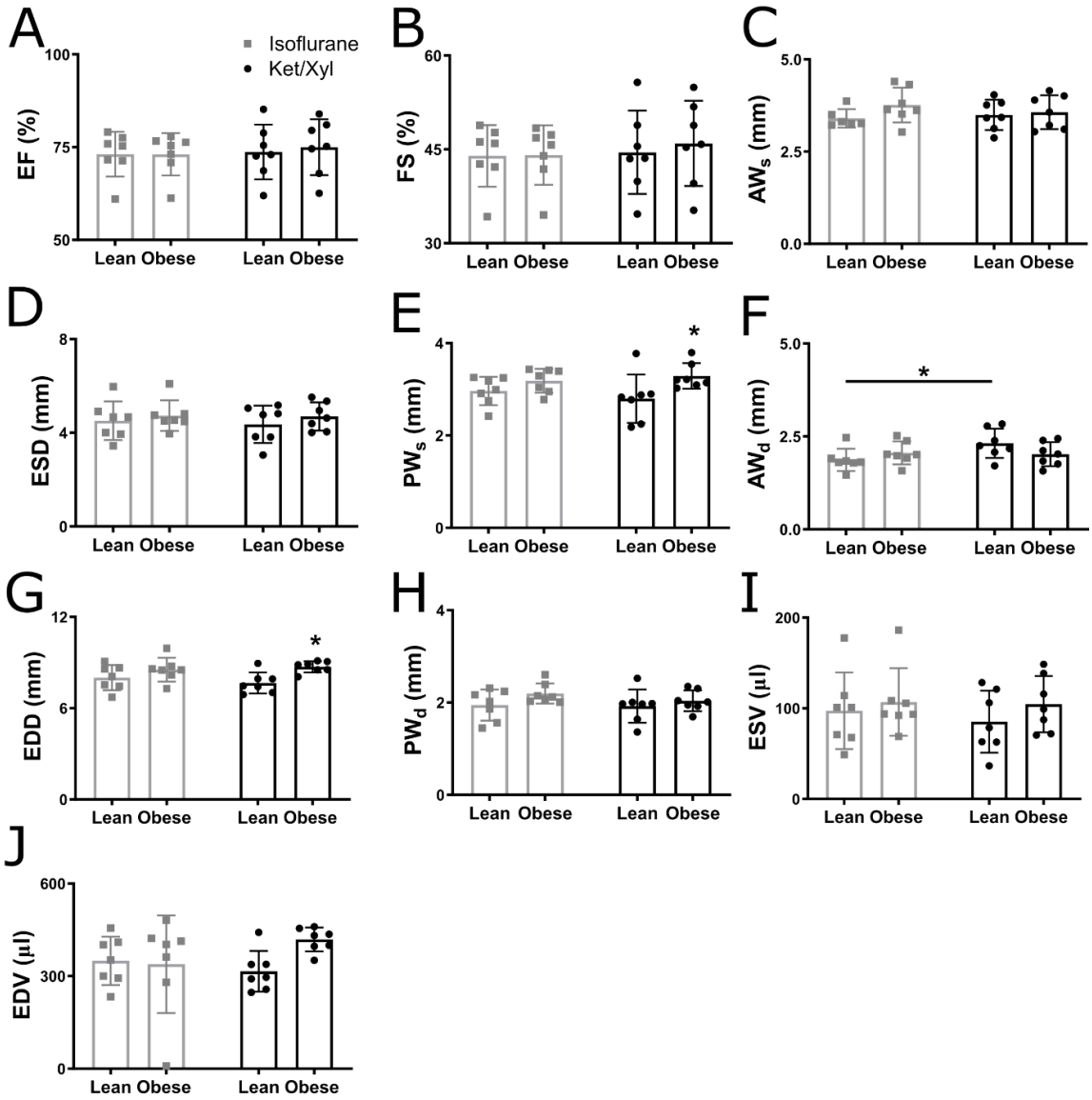

Figure 3.6- The effects of ketamine/xylazine on systolic function and left ventricular dimension and volumes. *EF (**A**), FS (**B**), AWs (**C**), ESD (**D**), PWs (**E**), AWd (**F**), EDD (**G**), PWd (**H**), ESV (**I**) EDV (**J**) in in 20-week-old isoflurane- or ketamine/xylazine-anaesthetised lean and obese ZSF1 rats (n=7 per group). Values are presented*

*as mean ± SD. Significance was assessed by a regular two-way analysis of ANOVA followed by a Šídák's multiple comparisons test with *p<0.05. AW, anterior wall; d, in diastole; EDD; end-diastolic diameter; EDV, end-diastolic volume; EF, ejection fraction; ESD, end-systolic diameter; ESV, end-systolic volume; FS, fractional shortening; Ket/Xyl, ketamine/xylazine; PW, posterior wall; s, in systole*

3.4.4 HR-lowering alone does not allow diagnosis of diastolic dysfunction in isoflurane-anaesthetised obese ZSF1 rats

To assess whether the negative chronotropic (HR-lowering) effects of ketamine/xylazine were responsible for the ability to detect diastolic dysfunction in obese ZSF1 rats, we used ivabradine – having solely negative chronotropic effects – along with isoflurane anaesthesia. Ivabradine significantly reduced the HR in both lean and obese ZSF1 rats, while in obese ZSF1 rats, it reduced CO compared to saline, all showing its HR-reducing effect (Table 3.3). Ivabradine decreased EF and FS due to an increased EDV in obese compared to lean ZSF1 rats, but this decrease in EF was still within the definition of "preserved EF" (≥50%; Table 3.3). Furthermore, other systolic parameters, including IVCT and S', were similar in ivabradine-treated lean and obese ZSF1 rats (Table 3.3). Interestingly, separation of pulsed wave and tissue Doppler waves was improved in both lean and obese ZSF1 rats treated with ivabradine. However, E, A, and E/A ratio were similar between ivabradine-treated obese and lean ZSF1 rats, indicating the inability to detect diastolic dysfunction (Figure 3.7A-C). Ivabradine-treated obese ZSF1 rats showed an increased mitral valve deceleration time, IVRT, NFT, and E'/A' ratio and a reduced MPI compared to lean ZSF1 rats (Figure 3.7D-E and Table 3.3). Furthermore, E', A', E/E'/SV, and E/E' were similar in lean and obese ZSF1 rats treated with ivabradine (Figure 3.7F-I). Thus, despite improved separation of the waves in pulsed wave and tissue Doppler, heart rate reduction did not result in the detection of diastolic dysfunction in isoflurane-anaesthetised obese ZSF1 rats.

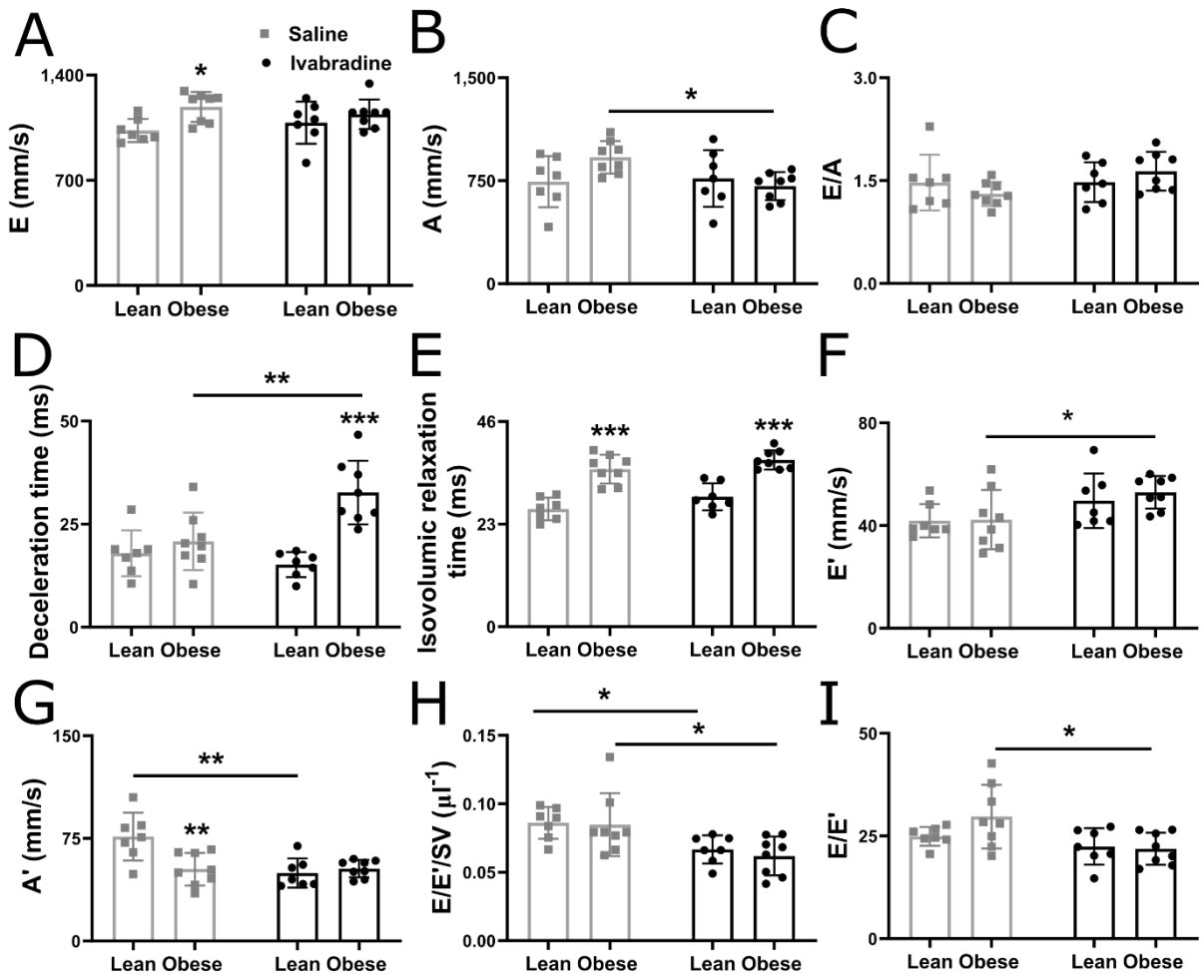

Figure 3.7- Heart rate reduction does not allow diagnosis of diastolic dysfunction in obese ZSF1 rats. *E and A peak velocities (**A-B**), E/A ratio (**C**), deceleration time (**D**), isovolumic relaxation time (**E**), E' and A' peak velocities (**F-G**), and E/E'/SV (**H**) and E/E' ratios (**I**) in 20-week-old isoflurane-anaesthetised lean and obese ZSF1 rats (n=7 and 8 per group, respectively) administered with ivabradine or saline (vehicle control). Values are presented as mean ± SD. Significance was assessed by a regular two-way analysis of ANOVA followed by a Šídák's multiple comparisons test with *p<0.05, **<0.01, and ***<0.001. A, late mitral inflow peak velocity; A', late mitral annulus peak velocity; E, early mitral inflow peak velocity; E', early diastolic mitral annulus peak velocity; SV, stroke volume.*

Table 3.3- Echocardiography parameters of isoflurane-anaesthetised lean and obese ZSF1 rats treated with or without ivabradine.

Parameter	Lean Saline (n=7)	Obese Saline (n=8)	Lean +Ivabradine (n=7)	Obese +Ivabradine (n=8)
Body weight (g)	477 ± 15	574 ± 33***	476 ± 15	574 ± 33***
BSA (cm^2)	555 ± 12	628 ± 24	555 ± 12	628 ± 24
LV mass (mg)	1402 ± 226	1524 ± 83	1440 ± 102	1618 ± 134*
Corrected LV mass (mg)	1122 ± 181	1219 ± 66	1152 ± 82	1294 ± 107*
HR (bpm)	369 ± 47	317 ± 28*	302 ± 41$^{\#\#\#}$	258 ± 19$^{*,\#\#\#}$
SV (µl)	291 ± 18	328 ± 31	399 ± 62$^{\#}$	359 ± 31
SV, $_i$ (µl/cm^2)	0.53 ± 0.04	0.50 ± 0.09	0.61 ± 0.11	0.54 ± 0.10
CO (ml/min)	108 ± 16	104 ± 12	101 ± 23	93 ± 8.7$^{\#}$
CI (ml/min/cm^2)	0.19 ± 0.03	0.16 ± 0.03	0.18 ± 0.04	0.14 ± 0.03*
AW$_d$ (mm)	2.1 ± 0.2	2.1 ± 0.2	2.1 ± 0.3	2.1 ± 0.1
AW$_s$ (mm)	4.1 ± 0.3	3.9 ± 0.3	4.0 ± 0.3	3.8 ± 0.3
EDD (mm)	8.1 ± 0.1	8.8 ± 0.3**	8.5 ± 0.6	9.1 ± 0.3*
ESD (mm)	3.7 ± 0.3	4.4 ± 0.2**	3.9 ± 0.5	4.7 ± 0.4***
PW$_d$ (mm)	2.1 ± 0.4	2.0 ± 0.2	2.0 ± 0.2	2.0 ± 0.2
PW$_s$ (mm)	3.4 ± 0.4	3.2 ± 0.2	3.5 ± 0.2	3.3 ± 0.2
EDV (µl)	352 ± 12	421 ± 32**	398 ± 63	460 ± 36*
EDV, $_i$ (µl/cm^2)	0.63 ± 0.03	0.64 ± 0.10	0.72 ± 0.12	0.69 ± 0.11
ESV (µl)	61 ± 11	93 ± 13**	66 ± 19	101 ± 19***
ESV, $_i$ (µl/cm^2)	0.11 ± 0.02	0.14 ± 0.02*	0.12 ± 0.03	0.15 ± 0.02
EF (%)	83 ± 3.3	79 ± 2.3	84 ± 3.6	78 ± 3.5**
FS (%)	54 ± 3.7	50 ± 2.3	55 ± 4.3	48 ± 4.0**
IVCT (ms)	17 ± 2.3	16 ± 2.4	17 ± 3.0	17 ± 3.4
AET (ms)	63 ± 6.0	82 ± 2.3***	66 ± 4.3	90 ± 3.5$^{***,\#\#\#}$
NFT (ms)	106 ± 7.8	133 ± 3.7***	112 ± 5.2$^{\#}$	143 ± 3.8$^{***,\#\#\#}$
MPI	0.70 ± 0.08	0.63 ± 0.05	0.70 ± 0.08	0.61 ± 0.06*
E'/A'	0.60 ± 0.17	0.86 ± 0.40	0.69 ± 0.14	1.2 ± 0.3**
S' (mm/s)	42 ± 12	38 ± 5.7	48 ± 15	41 ± 5.1

*Values are presented as mean ± SD. A', late mitral annulus peak velocity; AET, aortic ejection time; AW, anterior wall; CI, cardiac index; CO, cardiac output; d, in diastole; E', early diastolic mitral annulus peak velocity; EDD, end-diastolic diameter; EDV, end-diastolic volume; EF, ejection fraction; ESD, end-systolic diameter; ESV, end-systolic volume; FS, fractional shortening; HR, heart rate; i , indexed for body surface area, calculated as 9.1 * body weight in grams$^{2/3}$; IVCT, isovolumic contraction time; LV, left ventricular; MPI, myocardial performance index; NFT, non-flow time; PW, posterior wall; s, in systole; S', systolic peak wave; SV, stroke volume. Significance was assessed by a regular two-way analysis of ANOVA followed by a Šídák's multiple comparisons test. *P<0.05, **<0.01, and ***<0.001 comparing either isoflurane-anaesthetised Lean and Obese treated with saline or isoflurane-anaesthetised Lean and Obese rats treated with ivabradine. $^{\#}$P<0.05, $^{\#\#\#}$<0.01, and $^{\#\#\#}$P<0.001 comparing ivabradine- versus saline-treated isoflurane-anaesthetised in each group of rats (either Lean or Obese).*

3.5 Discussion

Animal models allow us to understand cardiac molecular, cellular, physiological, and functional changes during HFpEF development, leading to the discovery of novel therapeutics. Echocardiography is widely used for the diagnosis of pre-clinal and clinical HFpEF with the advantage of being non-invasive, safe, repeatable, widely available, and inexpensive. Anaesthetics usage during echocardiography acquisition in rodent models and clinical perioperative phases is generally accepted, despite their poorly understood mechanism and impact on cardiac function. While all anaesthetics have some hemodynamic effects, the key is to identify the anaesthetic that can be used to diagnose the disease of interest. The best clinical practice to perform echocardiography in humans is to preserve the HR in a normal range between 60-100 bpm for adults. In rats, the normal HR is on average around 300-450 bpm, consequently the best strategy in rats is not necessarily the same as in humans. In fact, our results show that ketamine/xylazine improved the ability to diagnose diastolic dysfunction in obese ZSF1 rats over isoflurane. The inability to detect diastolic dysfunction in obese ZSF1 rats, when using isoflurane in combination with the HR-lowering drug ivabradine, showed that the detection of diastolic dysfunction in obese ZSF1 rats using ketamine/xylazine is not due to a pure chronotropic effect, but is also mediated by ketamine/xylazine's inotropic effects.

Ketamine/xylazine allowed for a clear separation of both E and A waves in pulsed wave Doppler and E' and A' waves in tissue Doppler compared to isoflurane. Importantly, the consequence of inaccurate separation of these waves, includes possible overestimation of A and A' peak velocities, while underestimating mitral valve deceleration time and E/A ratio. This inaccurate separation translated in the inability to reliably diagnose diastolic dysfunction in isoflurane-anaesthetised obese ZSF1 rats. We showed that ketamine/xylazine, unlike isoflurane, was able to demonstrate diastolic dysfunction in obese ZSF1 rats. Ketamine/xylazine significantly decreased A peak velocities in both lean and obese ZSF1 rats

and E peak velocities in lean ZSF1 rats, resulting in increased E/A ratios in lean and obese ZSF1 rats compared to isoflurane-anaesthetised rats. In rats with chronic aortic valve regurgitation, ketamine/xylazine (0.1 and 0.75 mg/kg, respectively) significantly decreased E peak velocities, while modestly, albeit non-significantly, decreasing A peak velocities (p=0.05) and E/A ratio (p=0.07) compared to 1.5% isoflurane[205]. In healthy Fischer 344 rats, ketamine/xylazine increased IVRT without affecting E and A peak velocities, E/A ratio, and mitral valve deceleration time compared to 1.5% isoflurane[206]. However, in Wistar rats, ketamine/xylazine (0.1 and 0.75 mg/kg, respectively) reduced E and A peak velocities without affecting E/A ratio compared to 1.5% isoflurane, while a higher dose of ketamine/xylazine (40 and 8 mg/kg, respectively) decreased A and preserved E, resulting in an increased E/A ratio compared to 1.5% isoflurane[205,207]. Literature with regard to influence of ketamine/xylazine *versus* isoflurane on echocardiography parameters in mice is scarce and mostly focusses on systolic function and cardiac diameters, while the differential effects of these anaesthetics on diastolic function have never been reported[208,209]. In preoperative echocardiography, inhaled anaesthetics (sevoflurane, isoflurane, and desflurane) improved diastolic function by decreasing E and A peak velocities in patients with diastolic dysfunction[210-212], all providing a possible explanation for the inability to detect diastolic dysfunction when using isoflurane.

HR can affect diastolic function, and this is one of the reasons that waking HRs are preferred for echocardiography measurements. In our study, ketamine/xylazine had cardiodepressive effects (reduced HR and CO), but did not affect EF, as shown before[205-207,213,214]. Therefore, the improved diagnosis using ketamine/xylazine could be the result of a decreased HR (negative chronotropy) and/or cardiac contraction (negative inotropy). However, while the selective negative chronotropic drug ivabradine induced an improved separation of pulsed wave and tissue Doppler waves, diastolic dysfunction could not be detected in isoflurane-anaesthetised obese ZSF1 rats. This indicates that the detection of diastolic dysfunction in obese ZSF1 rats

using ketamine/xylazine is not due to a pure chronotropic effect, but that both negative chronotropic and inotropic effects of ketamine/xylazine are required to unveil diastolic dysfunction. This inotropic effect could be mediated by the interference of anaesthetics with the intracellular calcium flow and re-uptake in the sarcoplasmic reticulum (SR). Xylazine acts as an alpha 2 receptor agonist, reducing cardiac intracellular cyclic adenosine monophosphate (cAMP), decreasing the influx of extracellular calcium, the SR-mediated uptake of calcium, and the sensitivity of the contractile proteins to calcium, ultimately leading to reduced cardiac contractility[215]. Ketamine has both a positive inotropic effect, by increasing myocardial calcium influx, and negative inotropic effect by impairing calcium flux in the SR[216,217]. In addition, ketamine affects a wide range of other processes, such as non-competitive blockage of N-methyl-D-aspartate (NMDA) channels and nicotinic receptors, activation of L-arginine/NO/cGMP signalling, and promotion of the release of noradrenaline[218-220], all indicating that ketamine/xylazine can affect diastolic function by a wide range of effects.

Overall, given all our data, depth of anaesthesia is critical for accurate assessment of diastolic dysfunction. The doses proposed here should not be blindly applied to other strains, sexes, or ages. In other rodent models, a dose-response curve needs to be performed, with special attention to obese models, as anaesthetics can accumulate in adipose tissue layers. Anaesthetic induction and image acquisition should always be performed within the same range of time for all the experimental animals. ECG recording can be used to monitor the breathing rate, which is a measurement for anaesthetic depth; a reduced breathing rate and superficial breathing indicate a too light anaesthesia depth, while an increased breathing rate and gasping (heavily breathing) indicate a too deep anaesthesia depth. In addition, ECG acquisition is crucial for ensuring the reduction in HR, which is required for a proper separation of the pulsed wave and tissue Doppler waves. HR should be monitored during the whole echocardiography procedure. A HR above 300 bpm does not allow the separation of the waves in pulsed wave and tissue

Doppler. Optimally the HR should be between 220-260 bpm to allow the separation of the waves in pulsed wave and tissue Doppler.

We have presented both indexed and non-indexed volumes, as it is debated whether indexing is appropriate for the diagnosis of diastolic dysfunction in rodents. BSA is the most widely used parameter for indexing cardiac volumes in preclinical and clinical settings[221,222], however, it has several limitations. First of all, correct BSA calculation is complex and different formulae are available[223]. Clinical calculations of BSA take into account both height and body mass[223], however, common rodent calculations are much simpler and only use the rodent's body mass to estimate BSA. Given that the presence of obesity can stunt growth, the simplified calculation of BSA based on purely mass may underestimate the prevalence of cardiac pathology (e.g. hypertrophy, dilation, etc.) in overweight and obese rodents[221]. Furthermore, animal research is more controlled (e.g. all same age, background, gender etc.) compared to clinical research. As such, while indexing for BSA in patients is required to obtain more standardized values, which can be compared between the different experimental groups, the same concerns may not apply to rodent models.

Limitations

Different animals were used for each type of anaesthetic, due to concerns that the physiological stress induced by the anaesthetics could affect the measurement of cardiac function, specifically diastolic function. The administration of a single anaesthetic was already difficult, as the obese ZSF1 rats were diseased and susceptible to death. As such, we did not use the same animals for both anaesthetics, even though common practice is to use the same animals. We assessed the effect of isoflurane and ketamine/xylazine only in one HFpEF rodent model, as this is currently the most accepted HFpEF rodent model, which mimics human pathology. We only used male

ZSF1 rats, as the model was established in males and few studies have investigated HFpEF development in female rats[224]. However, we do not rule out that females might respond differently. PV loops were obtained only under isoflurane, as a stable anaesthesia depth is required over a long period of time, and ketamine/xylazine results in an inconstant anaesthesia depth, which gradually declines over time. For echocardiography, only a limited amount of time is required, which ensures that the anaesthesia depth is more stable.

In conclusion, the frequently used anaesthetics isoflurane and ketamine/xylazine differently affect echocardiography-derived cardiac hemodynamics and diastolic function both in HFpEF-diseased obese and control lean ZSF1 rats. Diastolic dysfunction could only be detected in obese ZSF1 rats anaesthetised with ketamine/xylazine. As the prevalence of HFpEF and surgical procedures increase steadily with ageing, the impact of anaesthetics on diastolic function should be taken in consideration and further investigated in both animal models and patients.

Chapter 4: Capillary regression triggered by pericyte loss is an early event in the development of HFpEF

I. Cuijpers, S.J. Simmonds, P. Carai, L. Vertommen, A.P. Papageorgiou, S. Heymans, and E.A.V. Jones

In preparation

4.1 Abstract

HFpEF is a complex heterogeneous disease for which treatments are lacking due to limited understanding of the pathophysiology. Reduced cardiac microvascular density (rarefaction) is present in established HFpEF, however the onset and triggers remain unknown. Here, we used the obese ZSF1 rat as a HFpEF model to investigate cardiac microvascular rarefaction in relation to key pathological features of HFpEF. HFpEF-associated risk factors developed early (6 and 13 weeks) triggering capillary endothelial abnormalities (activation and junctional remodelling) and cardiomyocyte hypertrophy as early as 14 weeks. Though capillary rarefaction was not observed until 21 weeks, active capillary regression was present at 14 weeks, as indicated by the presence of empty collagen sleeves. Systemic and cardiac inflammation, fibrosis, and fully established grade I diastolic dysfunction (also called impaired relaxation) were not yet present at 14 weeks. Investigating triggers of active regression, we found a significant reduction in pericyte coverage in obese ZSF1 rats. Stimulation of pericytes or endothelial cells with metabolic stressors (either high glucose, low-density lipoprotein, or H_2O_2) caused more gene expression changes in pericytes compared to endothelial cells (2655 *versus* 551 genes). Furthermore, 23 genes were similarly regulated by two of the stressors in pericytes, whereas there were only 7 genes in endothelial cells. Our findings show that cardiac capillary regression is an active process in HFpEF, occurring before the onset of other pathological processes. Reduced pericyte coverage is the result of the increased susceptibility

of pericytes to metabolic stressors, as such treatments aiming at preserving pericytes could prevent the development of HFpEF.

4.2 Introduction

More than half of the HF patients suffer from HFpEF, a complex cardiovascular syndrome characterised by diastolic dysfunction and cardiac inflammation, fibrosis, hypertrophy, and endothelial dysfunction[225]. HFpEF development is strongly associated with the presence of comorbidities (e.g. T2DM, obesity, and hypertension)[226]. However, evidence-based effective treatment and prevention strategies are absent due to the incomplete understanding of the pathology.

In recent years, endothelial dysfunction has been proposed to contribute to HFpEF development[50]. Furthermore, HFpEF patients show reduced cardiac microvascular density per myocardial area, called microvascular rarefaction[60], while in HFpEF-associated comorbidities, such as T2DM and hypertension, microvascular rarefaction precedes disease development and has been even suggested to cause disease progression[85-88]. Vessel density can be reduced either because of reduced angiogenesis (i.e. cardiomyocyte hypertrophy without compensatory angiogenesis) or due to vessel regression. Vessel regression is being recognized as an active process that is initiated by pro-regression signals, rather than representing dying cells[185]. Regression can occur even in the presence of pro-angiogenic signals, therefore attempts to induce angiogenesis are futile if pro-regression signals are present[227]. As such, active capillary regression is especially increasingly being recognized as important in vascular physiology and pathology, although molecular mechanisms are poorly understood.

Pericytes, mural cells wrapped around capillary vessels, play an important role in maintaining the vascular integrity. Pericyte dysfunction has been reported in cardiovascular and

neurological diseases, diabetes, inflammation, and cancer[228-230]. Detachment of pericytes from capillaries leads to unstable vessels prone to rarefaction[231].

Here, we investigated the timing of vascular changes in relation to the development of the key pathological features of HFpEF (diastolic dysfunction, fibrosis, hypertrophy, and inflammation). We further investigated triggers for rarefaction in obese ZSF1 rats, a model mimicking the presence of chronic comorbidities as observed in human HFpEF development[150].

4.3 Materials and Methods

4.3.1 Experimental animals

Experiments were performed according to the European Directive on the Care and Use of Experimental Animals (2010/63/EU) and approved by the Animal Care and Use Committee of KU Leuven (Project 178/2016). Male lean and obese ZSF1 rats, developed by crossing a female ZDF1 rat (+/*lepr fa*) with a lean male SHHF (*SHHF/Mcc*; +/*lepr facp*) rat, were obtained at the youngest as possible age (5 weeks) from Charles River Laboratories (#379 and 378, respectively). The obese ZSF1 rat offspring are homozygous for the leptin receptor mutation (*lepr fa /lepr facp*) and inherit the hypertensive gene (*SHHF/Mcc*), resulting in the combined development of T2DM, hypertension, obesity, and hyperlipidaemia[151]. This cluster of comorbidities in the obese ZSF1 rats has previously reported to result in the development of diastolic dysfunction, left ventricular hypertrophy, cardiac fibrosis, inflammation, increased cardiomyocyte stiffness, and renal failure[125,151]. Lean littermates are only hypertensive (*fa/+* or *facp* and *SHHF/Mcc*), thereby serving as non-HFpEF diseased controls[151]. Animals were housed and acclimated under a 12-hour light-dark cycle with access to water and chow diet *ad libitum* (#V1534-000, Ssniff Spezialdiäten GmbH, Germany). A schematic overview is given in Figure 4.1.

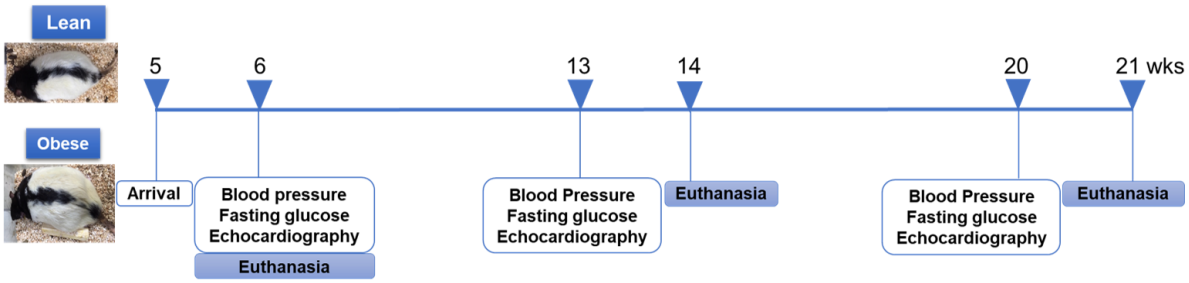

Figure 4.1- Schematic presentation of the in vivo study set up. *5 weeks-old lean and obese ZSF1 rats were purchased. Blood pressure (n=7/group), fasting glucose (n=12/group), and echocardiography (n=9 lean and 11 obese) measurements were performed over time. Animals were euthanized at 6, 14, and 21 weeks of age (n=7 per group; except 1 lean died at 6 weeks). Blood and organs were collected for flow cytometric, histological, and molecular analyses.*

4.3.2 Blood pressure and fasting glucose measurements

At 6, 13, and 20 weeks, blood pressure in lean and obese conscious ZSF1 rats (n=7 per group) was assessed using the non-invasive CODA tail-cuff system (Kent Scientific, CT, USA). For two days, animals were placed in the restrainer to acclimatize. The next day animals were acclimatized to the blood pressure machine. On the day of measurement, 10 cycles were recorded to acclimatize the animal, followed by at least 20 cycles for analysis. To assess fasting glucose levels, lean and obese ZSF1 rats (n=12 per group) were fasted for 16 hours, placed in the restrainer, and glucose levels were assessed via tail vein puncture with Glucomen LX plus (A. Menarini Diagnostics, Italy).

4.3.3 Transthoracic echocardiography

At 6, 13, and 20 weeks, ZSF1 lean (n=9) and obese (n=11) rats were anaesthetised with an IP injection of 50 mg/kg ketamine (Nimatek, Eurovet, Netherlands) and 5 mg/kg xylazine (Xyl-M®, V.M.D. nv/sa, Belgium) dissolved in 0.9% NaCl. Echocardiography was performed using a MS 250 transducer (13-24 MHz) connected to a Vevo 2100 echocardiograph (Visual Sonics, Canada). Animals were placed in a supine position on a heating pad to maintain the core body temperature between 37.5-37.7 °C. HR, ESV, EDV, AW, EDD, ESD, and PW were assessed

by parasternal short-axis M-mode imaging. CO, SV, EF, FS, as well as ESV and EDV (Teichholz formula), were calculated based on parasternal short-axis M-mode recordings. Left ventricular filling was assessed by pulsed wave Doppler trans-mitral flow velocity tracings, including E, A, mitral valve deceleration time, IVRT, NFT, AET, IVCT, just above the tip of the mitral leaflets and MPI was calculated. Myocardial movements, E' and A' were measured by tissue Doppler imaging at the lateral mitral annulus. E/A and E/E' ratios were calculated. As the body weight of obese ZSF1 rats is significantly higher than the lean control ZSF1 rats, volumes were also indexed for BSA, estimated as 9.1 * body weight in grams$^{2/3}$, to account for differences in body weight between the groups[151,204]. At least three stable cardiac cycles were averaged for all measurements.

4.3.4 Organ and blood collection

At 6, 14, and 21 weeks, 7 lean (except n=6 at 6 weeks) and 7 obese ZSF1 rats were anaesthetised by IP injection of 50 mg/kg ketamine (Nimatek, Eurovet, Netherlands) and 5 mg/kg xylazine (Xyl-M®, V.M.D. nv/sa, Belgium) dissolved in 0.9% NaCl. Blood samples were collected in EDTA-coated vacutainer tubes (BD Biosciences, Belgium) from the posterior vena cava. Rats were then perfused with 20 ml PBS by inserting a butterfly needle in the left ventricle, while making a cut in the right atrium. Rats were euthanized by excision of the heart and organs were collected and weights were normalized by tibia length (TL).

4.3.5 Flow cytometry

Systemic and cardiac inflammation was assessed in lean and obese ZSF1 rats (n=4-7/ per group) by flow cytometry on the day of organ and blood collection. For circulating cells, whole blood was lysed in red blood cell lysis buffer (157 mM NH_4Cl, 10 mM $NaHCO_3$, 0.1 mM EDTA, pH 7.3) and the pellet was dissolved in PBS containing 0.1% BSA and 2 mM EDTA. For cardiac

cells, heart tissue was minced, enzymatically digested (0.25% Collagenase I, 20% FBS, PBS), mechanically dispersed and filtered (40 µm) and debris was removed (#130-109-398, Miltenyi Biotec, Netherlands). For both sample types, non-specific blinding was blocked using CD16/32 FCR Block (1/100; clone d34-485, #BD550271, BD Biosciences, Belgium) and immune cells were stained (Table 4.1), and transferred to Trucount tubes (#340334, BD Biosciences, Belgium). Absolute numbers of systemic leukocytes ($CD45^+$), B-cells ($CD45^+B220^+$), T-cells ($CD45^+CD3^+$), T-helper cells ($CD45^+CD3^+CD4^+$), granulocytes ($CD45^+B220^-CD3^-SSC^+$), and total ($CD45^+B220^-CD3^-SSC^-CD8^-$), pro-inflammatory ($CD45^+B220^-CD3^-SSC^-CD8^-$ $CD4^-CD43^+HIS48^+$), and anti-inflammatory ($CD45^+B220^-CD3^-SSC^-CD8^-CD43^{++}HIS48^{low/int}CD4^+$) monocytes were assessed. Similarly, cardiac leukocytes, B-cells, total and T-helper cells, granulocytes ($CD45^+B220^-CD3^-HIS36^-$ $HIS48^+SSC^+$), macrophages ($CD45^+B220^-CD3^-$ $HIS36^+$), and total ($CD45^+B220^-CD3^-SSC^-HIS36^-$), pro-inflammatory ($CD45^+B220^-CD3^-SSC^-$ $HIS36^-HIS48^+CD4^-$) and anti-inflammatory ($CD45^+B220^-CD3^-SSC^-HIS36^-$ $HIS48^{int}CD4^-$) monocytes were assessed. All immune cells were measured on FACS Canto II (BD Biosciences, Belgium) and analysed with FCS express 6.0 (De Novo Software, CA, USA).

Table 4.1: Antibody list for flow cytometery

Antibody	Dilution	Clone	Catalogue number and distributer
CD45-PerCP	1/100	Ox1	202203, Biolegend
B220-PE-Cy7	1/100	His24	25-0460-82, eBioscience
CD3-APC	1/100	Ebiog4.18	17-0030-82, eBioscience
CD4-APC-Cy7	1/100	Ox35	550296, BD Biosciences
CD8-V50	1/100	Ox8	561614, BD Biosciences
His48-FITC	1/100	His48	11-0570-82, eBioscience
CD43-PE	1/100	W3/13	202812, Biolegend
His36-PE	1/100	His36	12-0660-82, eBioscience

4.3.6 Cardiac histology

Cardiac tissue was fixed in 1% paraformaldehyde at 4 °C for 24 hours and embedded in paraffin. Four µm sections were stained with Picro Sirius Red (fibrosis) or anti-Laminin A antibodies (cardiomyocyte size; 1/400, # L9393, Sigma-Aldrich, Belgium). Images were acquired using an Axiovert 200M microscope (Zeiss, Germany) and analysis was performed using Image J software. The amount of total and perivascular cardiac fibrosis was quantified as the percentage Sirius red positive area per total and perivascular cardiac area, respectively. Interstitial fibrosis (total - perivascular fibrosis) was expressed as percentage of total fibrosis. The largest diameter of the fibrotic tissue in the tunica adventitia (perivascular fibrosis thickness) around each vessel diameter class was quantified. Cardiomyocyte hypertrophy was assessed by calculating the myocyte cross-sectional area (CSA) based on the inner circumference of at least 240 myocytes per laminin-stained section.

Frozen cardiac tissue (10 µm) was stained with anti-Collagen IV (1/400, #2150-1470, Biorad, Belgium), VE-Cadherin (1/50, #AF1002, R&D systems, UK), VCAM-1 (1/100, #AF643, R&D systems, UK), Ki-67 (1/50, #14-5698-82, eBioscience, US), Isolectin GS-IB_4 Alexa Fluor 488 (1/50; #I21411, Invitrogen, Belgium; isolectin binds to the sugar residues in the glycocalyx of blood vessels), neuron-glial antigen 2 (NG2; 1/100, #Ab5320, EMD Millipore, Belgium), or alpha smooth muscle actin (αSMA)-Cy3 (1/200, #C6198, Sigma-Aldrich, Belgium). Images were acquired and analysed using a Zeiss LSM700 confocal microscope (Zeiss, Germany) and Image J software, respectively. Capillary density was assessed by counting the number of VE-Cadherin$^+$ vessels per mm^2 myocardial area, while microvascular regression (%) was calculated by dividing the number of empty sleeves (Collagen IV$^+$ VE-Cadherin$^-$) by the total number of VE-Cadherin$^+$ vessels [232]. The percentage of VCAM-1$^+$ vessels of total larger vessel (diameter > 10 µm) was assessed by dividing the number of VCAM-1$^+$isolectin$^+$ vessels by the total number of isolectin$^+$ vessels with a diameter greater than 10 µm. The absolute number of α-

SMA^+ $isolectin^+$ vessels per mm^2 myocardial area and the percentage of α-SMA^+ $isolectin^+$ vessels of the total $isolectin^+$ vessels was quantified. Furthermore, α-SMA area (μm^2) was assessed per diameter vessel class (10-20, 21-50, 51-100, and >100 µm). Pericyte coverage (%) was assessed by dividing the number of $NG2^+$ $isolectin^+$ by the total number of $isolectin^+$ vessels. Endothelial cell proliferation was assessed by diving the number of $Ki67^+$ VE-$Cadherin^+$ vessels by the number of total VE-$Cadherin^+$ vessels.

4.3.7 In vitro stimulation of endothelial cells and pericytes

Human umbilical vein endothelial cells (HUVECs, passage 5; #C2517A, Lonza, Belgium) and human immortalized pericytes (#CL 05008-CLTH, Celther, Poland) were cultured in endothelial cell growth medium MV2 (#C-22121, PromoCell, Germany) or DMEM high glucose (#41965039, Thermofisher, Belgium) supplemented with penicillin/streptomycin, respectively. For the stimulation of HUVECs and pericytes, endothelial cell growth medium MV2 and DMEM normal glucose (#21885025, Gibco, Thermofisher, Belgium) were used, respectively. The media with factor was made up separately for each individual sample for all conditions and cells were treated for three days. To mimic hyperglycaemia, HUVECs and pericytes were stimulated with either high D-glucose (30 mM) or normal D-glucose (5.5 mM) containing 24.5 mM mannitol[233,234]. The medium was changed every day to maintain the desired glucose concentration[235]. To mimic hyperlipidaemia, HUVECs and pericytes were stimulated with or without 50 µg/ml human low-density lipoprotein (LDL; #LP2-2MG, Sigma-Aldrich, Belgium)[236,237]. To mimic oxidative stress, HUVECs and pericytes were stimulated with or without 100 µM H_2O_2 (#H1009-500ML, Sigma-Aldrich, Belgium)[238,239], which was changed every eight hours. Four samples per condition (except three for HUVECs exposed to H_2O_2) were lysed using Qiazol (#t9306, Qiagen, Belgium) and RNA quantity and purity were determined using Nanodrop ND-100. Three samples per condition were stained with Annexin V (1/9; #A13202, Thermofisher, Belgium) to assess the number of apoptotic cells.

4.3.8 RNA sequencing and data analysis

RNA sequencing was performed by the Genomics Core (KU Leuven, Belgium). Sequence libraries were prepared with the Lexogen QuantSeq 3' mRNA-Seq Library prep. Samples were indexed to allow for multiplexing. Library quality and size range was assessed using a Bioanalyser with the DNA 1000 kit (Agilent Technologies, CA, USA). Libraries were diluted to a final concentration of 2nM and subsequently sequenced on an Illumina HiSeq4000 platform (Illumina, CA, USA). Single end reads of 50bp length were produced with a minimum of 1M reads per sample.

Quality control of raw reads was performed with FastQC v0.11.7[240]. Adapters were filtered with ea-utils fastq-mcf v1.05[241]. Splice-aware alignment was accomplished using HISAT2 (http://daehwankimlab.github.io/hisat2/) against the human reference genome hg38 using default parameters. Reads mapping to multiple loci in the reference genome were discarded. Resulting BAM alignment files were handled with Samtools v1.5[242]. Reads per gene were quantified by HT-seq Count v2.7.14. Count-based differential expression analysis was assessed with R-based Bioconductor package DESeq2[243]. P-values were adjusted for multiple testing with the Benjamini-Hochberg procedure. Similar differentially expressed genes (DEGs) in two conditions in the stimulated endothelial cells or pericytes (adjusted p-value <0.05) were presented in heat maps (GraphPad Software, CA, USA). Venn diagrams were made using R Statistical software (Austria).

4.3.9 Statistical analysis

Results are presented as mean ± SEM. Statistical analysis was performed using GraphPad software V8 (CA, USA). *In vivo* data were analysed using a two-way ANOVA with Šídák's comparison post hoc test. P-values of <0.05 were statistically significant.

4.4 Results

4.4.1 Metabolic risk factors develop early, leading to diastolic dysfunction

HFpEF-associated risk factors were assessed at baseline (5/6 weeks), mid-term (13 weeks), and in literature-established HFpEF (21 weeks)[151] in obese ZSF1 rats and their control lean littermates. Increased body weight was already present in obese ZSF1 rats at 5 weeks, while increased liver weight/TL was observed in obese ZSF1 rats at 14 weeks (Figure 4.2A-B). Hyperglycaemia (fasting glucose >7 mM) developed in obese ZSF1 rats at 13 weeks (Figure 4.2C). Established hypertension (diastolic and systolic blood pressure > 90 and 140 mm Hg, respectively[244]) was already present in obese ZSF1 rats at 6 weeks (Figure 4.2D-E).

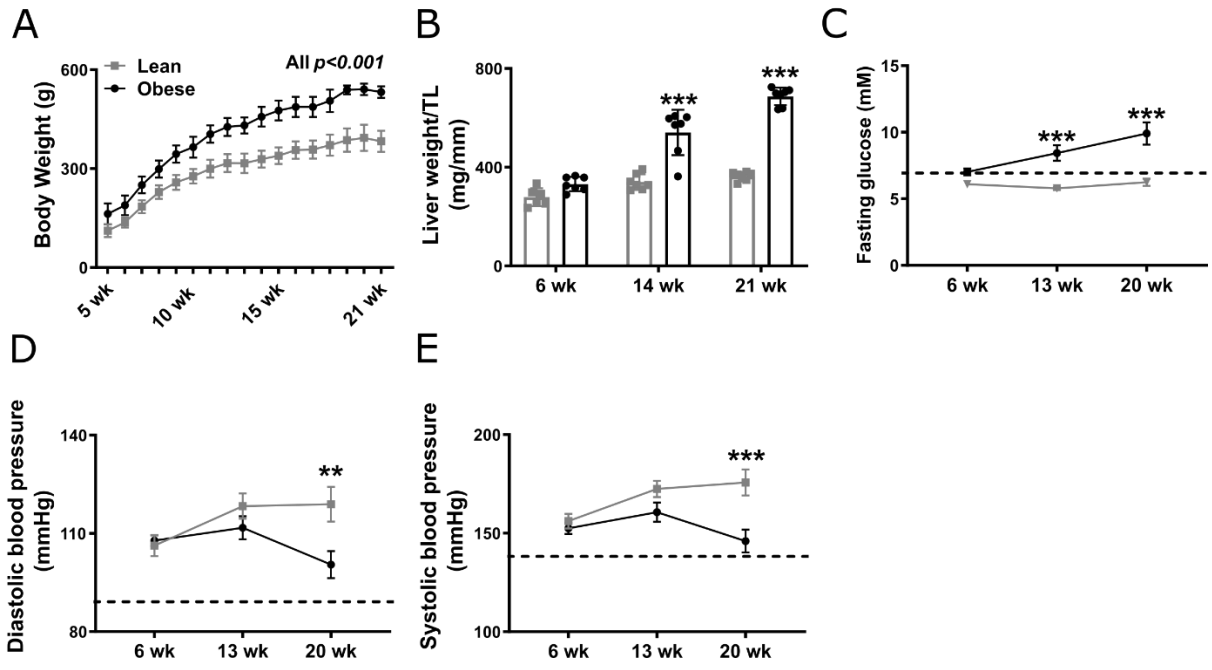

Figure 4.2- Metabolic risk factors develop early in obese ZSF1 rats. *Body weight (**A**; n=11/group), liver weight to tibia length (**B**; TL, n=6-7/group), fasting glucose levels (**C**; n=12/group), diastolic (**D**) and systolic (**E**) blood pressure (both n=7/group) in lean and obese ZSF1 rats over time. Dashed lines indicate the cut off values for hyperglycaemia (**C**; 7 mM) and established hypertension (**D** and **E**; 90 and 140 mmHg, respectively). Values are presented as mean ± SEM. For panel A and C-E, significance between lean and obese ZSF1 rats at each time point is assessed by a paired two-way ANOVA followed by Šídák's multiple comparisons test, while in panel B a non-paired two-way ANOVA followed by Šídák's multiple comparisons test was used with **p<0.01 and ***<0.001.*

We subsequently assessed the development of diastolic dysfunction in lean and obese ZSF1 rats using echocardiography. Grade I diastolic dysfunction grade (impaired relaxation) in obese ZSF1 rats was first identified at 20 weeks, as reflected increased E, A, deceleration time, IVRT,

NFT, and E', and reduced E/A ratio, while having a preserved E/E' ratio (Figure 4.3A-H). Some parameters indicative of diastolic dysfunction did change earlier than 20 weeks. E' was already increased at 6 weeks, however returned to the same values as lean counterparts at 13 weeks (Figure 4.3G). More consistent changes were observed from 13 weeks onwards, including increased deceleration time, IVRT, and NFT (Figure 4.3D-F). Systolic function was preserved in obese ZSF1 rats at all time points, reflected by a preserved EF (>50%), FS, and IVCT compared to lean ZSF1 rats (Figure 4.2I and Table 4.2). In short, grade I diastolic dysfunction (requiring a combination of a decreased E/A ratio, increased IVRT and deceleration time, and preserved E/E' ratio) together with a preserved EF develops at 20 weeks.

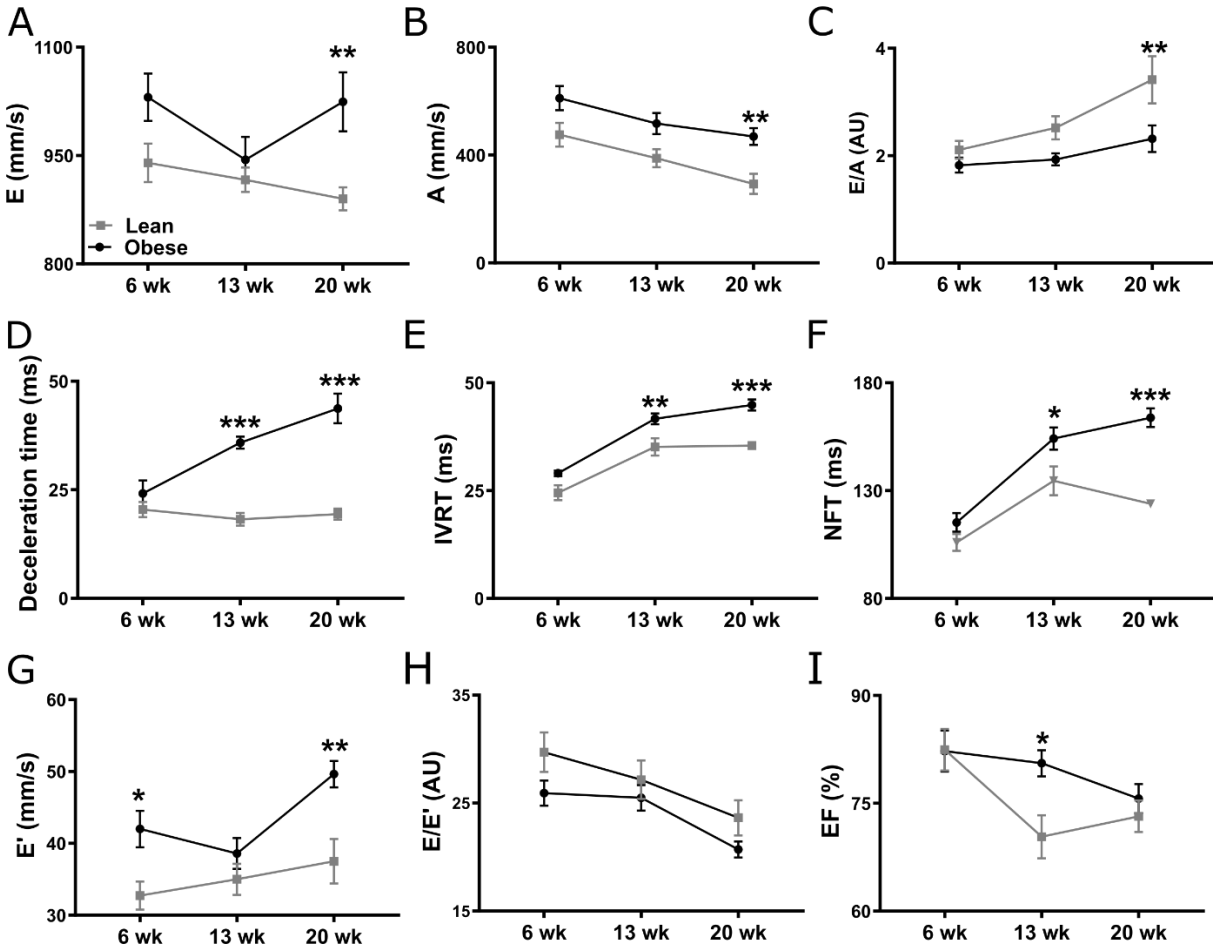

Figure 4.3 – Fully established grade I diastolic dysfunction with preserved ejection fraction develops in obese ZSF1 rats at 21 weeks. *E (**A**), A (**B**), E/A ratio (**C**), deceleration time (**D**), IVRT (**E**), NFT (**F**), E' (**G**), E/E' ratio (**H**), and EF (**I**) in lean and obese ZSF1 rats (n=9 and 11, respectively) over time. Values are presented as mean ± SEM. Significance between lean and obese ZSF1 rats at each time point is assessed by a paired two-way ANOVA followed by Šídák's multiple comparisons test with *p<0.05, **<0.01, and ***<0.001. A, late mitral inflow peak velocity; E, early mitral inflow peak velocity; E', early diastolic annulus peak velocity; EF, ejection fraction; IVRT, isovolumic relaxation time; NFT, non-flow time.*

Table 4.2: Echocardiography parameters in lean and obese ZSF1 rats over time.

	6 weeks		13 weeks		20 weeks	
	Lean (n=9)	Obese (n=11)	Lean (n=9)	Obese (n=11)	Lean (n=9)	Obese (n=11)
Body weight (g)	155 ± 8.9	197 ± 7.1**	315 ± 10	437 ± 5.1***	385 ± 14	540 ± 5.6***
BSA (cm^2)	261 ± 10	308 ± 7.4***	421 ± 9.6	524 ± 4.1***	481 ± 12	603 ± 4.2***
LV mass (mg)	645 ± 29	660 ± 42	1023 ± 49	1373 ± 51***	1306 ± 59	1548 ± 47**
Corrected LV mass (mg)	516 ± 23	526 ± 34	819 ± 39	1124 ± 50***	1045 ± 48	1238 ± 38**
HR (bpm)	316 ± 5.6	317 ± 11	243 ± 6.8	217 ± 6.7	241 ± 7.7	202 ± 5.8**
SV (µl)	175 ± 18	196 ± 13	217 ± 13	221 ± 13	229 ± 12	309 ± 16**
SV, $_i$ ($\mu l/cm^2$)	0.66 ± 0.05	0.64 ± 0.04	0.52 ± 0.03	0.42 ± 0.03**	0.48 ± 0.04	0.51 ± 0.02
CO (ml/min)	54 ± 5.0	62 ± 4.3	53 ± 3.7	48 ± 2.8	55 ± 2.3	62 ± 3.9
CI ($ml/min/cm^2$)	0.20 ± 0.01	0.20 ± 0.01	0.13 ± 0.01	0.09 ± 0.01*	0.11 ± 0.01	0.10 ± 0.01
AW_d (mm)	1.7 ± 0.1	1.5 ± 0.1	1.9 ± 0.1	2.4 ± 0.2*	2.3 ± 0.1	2.1 ± 0.1
AW_s (mm)	3.2 ± 0.1	3.1 ± 0.5	3.0 ± 0.2	4.1 ± 0.2***	3.6 ± 0.1	3.8 ± 0.1
EDD (mm)	6.7 ± 0.2	6.9 ± 0.2	7.6 ± 0.2	7.2 ± 0.2	7.7 ± 0.2	8.6 ± 0.2**
ESD (mm)	3.3 ± 0.2	3.5 ± 0.5	4.5 ± 0.3	3.5 ± 0.2	4.4 ± 0.2	4.6 ± 0.2
PW_d (mm)	1.6 ± 0.1	1.7 ± 0.2	1.7 ± 0.1	2.3 ± 0.1**	2.0 ± 0.1	2.1 ± 0.1
PW_s (mm)	2.3 ± 0.1	2.6 ± 0.1	2.5 ± 0.1	3.2 ± 0.1	2.7 ± 0.2	3.2 ± 0.1
EDV (µl)	213 ± 22	244 ± 20	311 ±19	275 ± 17	315 ± 19	409 ± 21**
EDV, $_i$ ($\mu l/cm^2$)	0.81 ± 0.07	0.79 ± 0.06	0.75 ± 0.06	0.53 ± 0.03*	0.67 ± 0.06	0.68 ± 0.03
ESV (µl)	45 ± 4.8	47 ± 10.7	106 ± 23	55 ± 7.1*	98 ± 12	100 ± 11
ESV, $_i$ ($\mu l/cm^2$)	0.17 ± 0.02	0.15 ± 0.04	0.26 ± 0.05	0.10 ± 0.01	0.18 ± 0.02	0.17 ± 0.02
FS (%)	51 ± 2.0	54 ± 2.9	42 ± 2.7	51 ± 1.9*	44 ± 2.0	47 ± 2.0
AET (ms)	65 ± 2.3	70 ± 3.0	41 ± 4.6	54 ± 1.6***	72 ± 1.4	96 ± 3.0***
IVCT (ms)	14 ± 0.7	16 ± 1.7	22 ± 2.6	18 ± 2.3	16 ± 1.1	19 ± 0.8
A' (mm/s)	23 ± 3.1*	30 ± 2.5	22 ± 2.8	19 ± 1.2	17 ± 2.4	18 ± 1.0

*Values are presented ± SEM. A', late mitral annulus peak velocity; AET, aortic ejection time; AW, anterior wall; CO, cardiac output; CI, cardiac index; d, in diastole; EDD, end-diastolic diameter; EDV, end-diastolic volume; ESD, end-systolic diameter; ESV, end-systolic volume; FS, fractional shortening; HR, heart rate; $_i$, indexed for body surface area, calculated as 9.1 * body weight in grams$^{2/3}$; IVCT, isovolumic contraction time; LV, left ventricular; PW, posterior wall; s, in systole; SV, stroke volume. Significance between lean and obese ZSF1 rats at each time point is assessed by a paired two-way ANOVA followed by Šídák's multiple comparisons test with *p<0.05, **<0.01, and ***<0.001.*

4.4.2 Very little inflammation is present either systemically or in the heart

HFpEF-associated risk factors have been associated with systemic low-grade chronic inflammation[91,93,94]. We therefore quantified absolute circulating immune cells by flow cytometry. Exclusively at 21 weeks, circulating granulocytes and total, pro-inflammatory, and anti-inflammatory monocytes were increased in obese ZSF1 rats (Figure 4.4A-D). Circulating B-cells were decreased at 6 weeks, while other circulating immune cells, including total leukocytes, T-cells, and T-helper cells, were similar between lean and obese ZSF1 rats at all the time points (Figure 4.4E-H). This all indicates that while metabolic risk factors develop early, systemic inflammation occurs at a later stage in HFpEF development in obese ZSF1 rats.

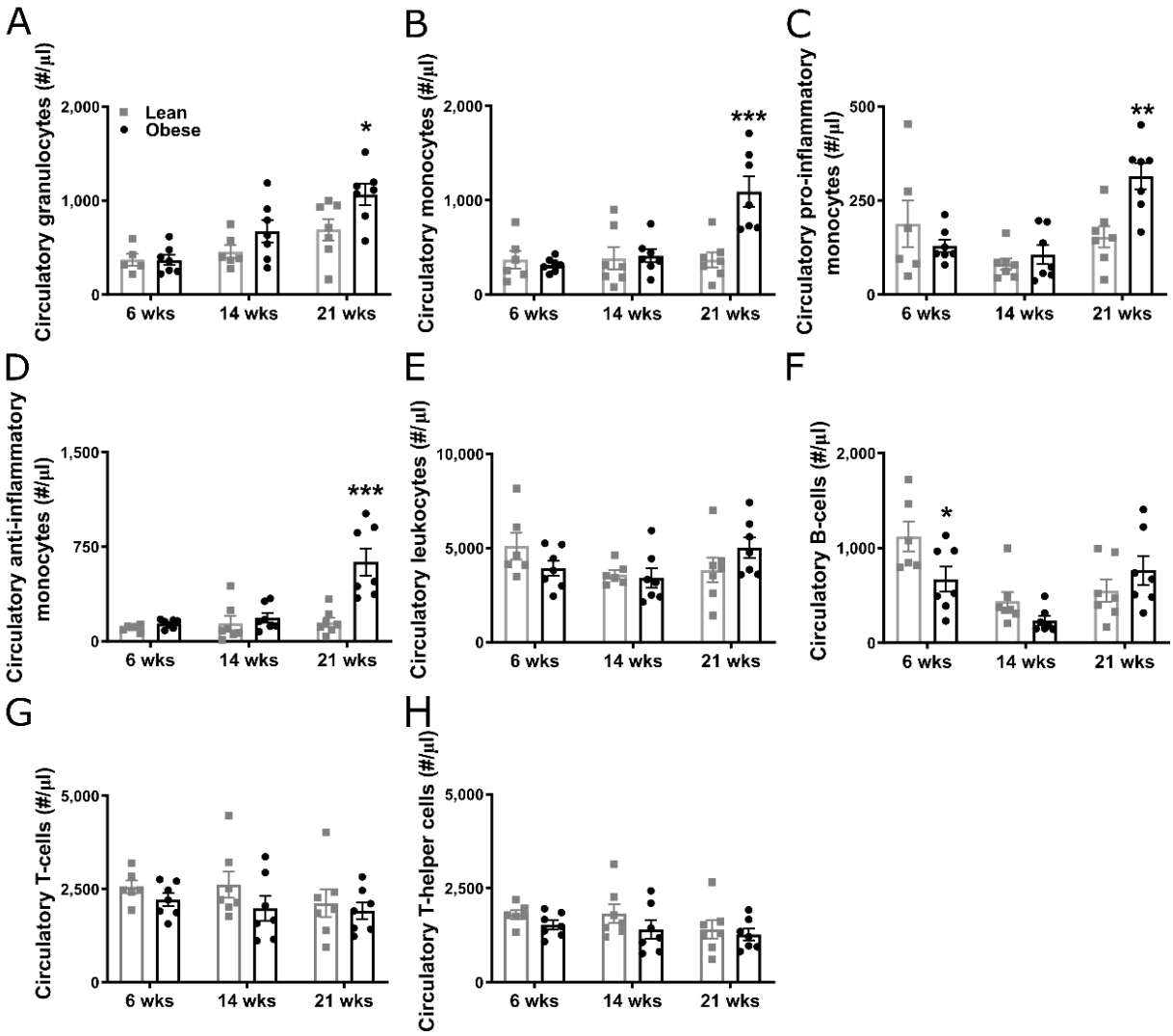

Figure 4.4- Absolute circulating immune cell levels during HFpEF development. *Absolute granulocytes (**A**) and total (**B**), pro-inflammatory (**C**), and anti-inflammatory (**D**) monocytes, leukocytes (**E**), B-cells (**F**), T-cells (**G**), and T-helper cells (**H**) in lean and obese ZSF1 rats over time (all n=4-7/group). Values are presented as mean ± SEM. Significance between lean and obese ZSF1 rats at each time point is assessed by a non-paired two-way ANOVA followed by Šídák's multiple comparisons test with *p<0.05, **<0.01, and ***<0.001.*

We also investigated infiltration of inflammatory cells into the heart. Cardiac granulocytes were significantly decreased in obese ZSF1 rats at 6 weeks and macrophages were increased at 14 weeks (Figure 4.5A-B). Both changes were small and present only at one stage. All other immune cells, including total leukocytes, B-cells, T-cells, T-helper cells, and total, pro-inflammatory, and anti-inflammatory monocytes were similar in lean and obese ZSF1 rats at all time points (Figure 4.5C-I).

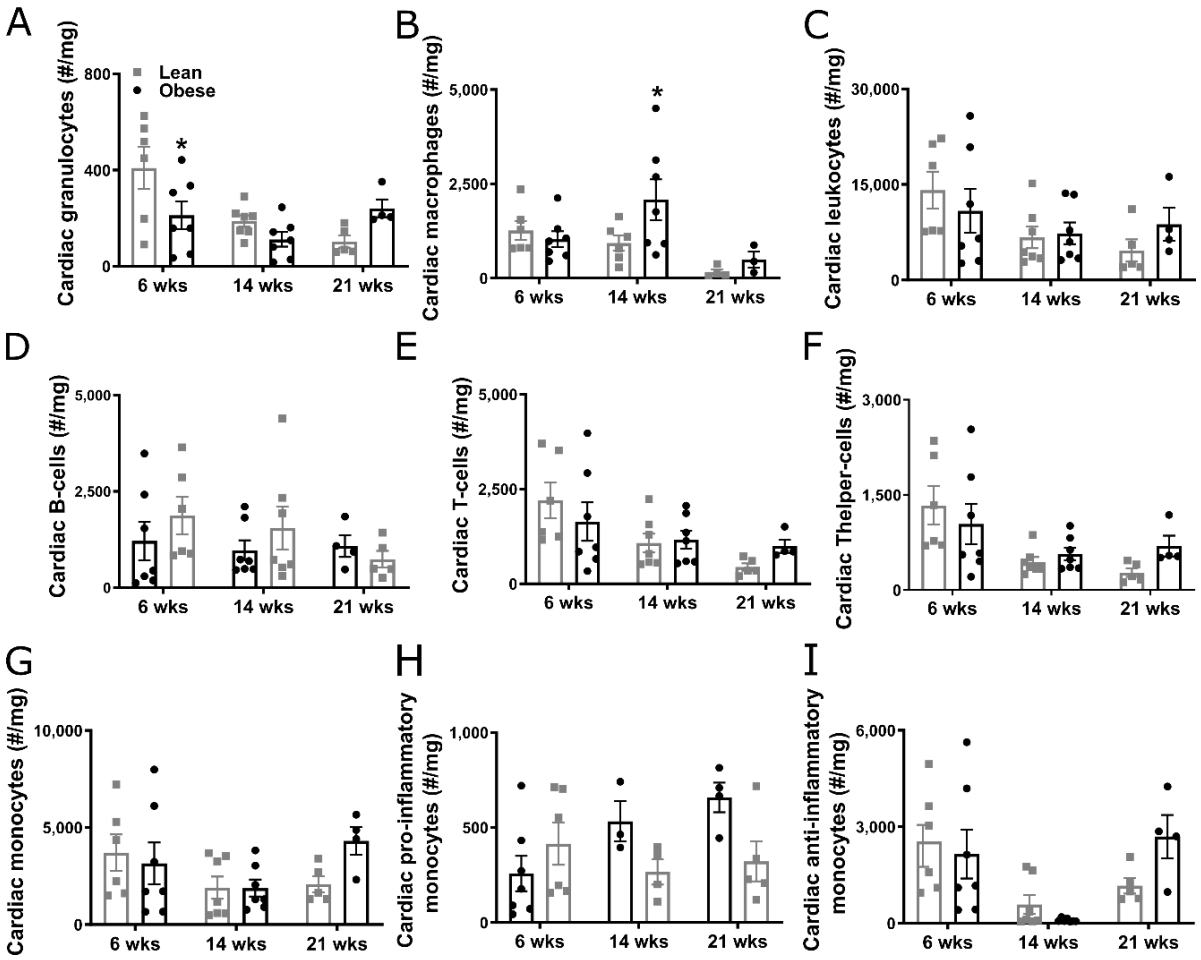

Figure 4.5- Cardiac immune cells in lean and obese ZSF1 rats over time. *Absolute cardiac granulocytes (**A**), macrophages (**B**), leukocytes (**C**), B-cells (**D**), T-cells (**E**), T-helper cells (**F**), and total (**G**), pro-inflammatory (**H**), and anti-inflammatory (**I**) monocytes in lean and obese ZSF1 rats (n=4-7/group) over time. Values are presented as mean ± SEM. Significance between lean and obese ZSF1 rats at each time point is assessed by a non-paired two-way ANOVA followed by Šídák's multiple comparisons test with *p<0.05.*

4.4.3 Cardiac hypertrophy develops with first signs of diastolic dysfunction

We next assessed the development of cardiac fibrosis and hypertrophy. Cardiac total and interstitial fibrosis, as assessed by Sirius red staining, were similar in lean and obese ZSF1 rats at all time points, while perivascular fibrosis thickness was increased around mid-sized (diameter 76 µm) and larger (>76-100 µm) cardiac vessels in obese ZSF1 rats at 21 weeks (Figure 4.6A-E). Cardiomyocyte size, as assessed by laminin staining, was significantly increased in obese ZSF1 rats at 14 weeks (Figure 4.6F-G). Heart weight/TL, another marker of cardiac hypertrophy, was only increased at 21 weeks, however (Figure 4.6H). In short, differences in cardiomyocyte size were first detected at 14 weeks, before echocardiographic

signs of fully established grade I diastolic dysfunction (also called impaired relaxation), whereas gross cardiac hypertrophy and perivascular fibrosis around mid-sized and large vessels were late events in disease development.

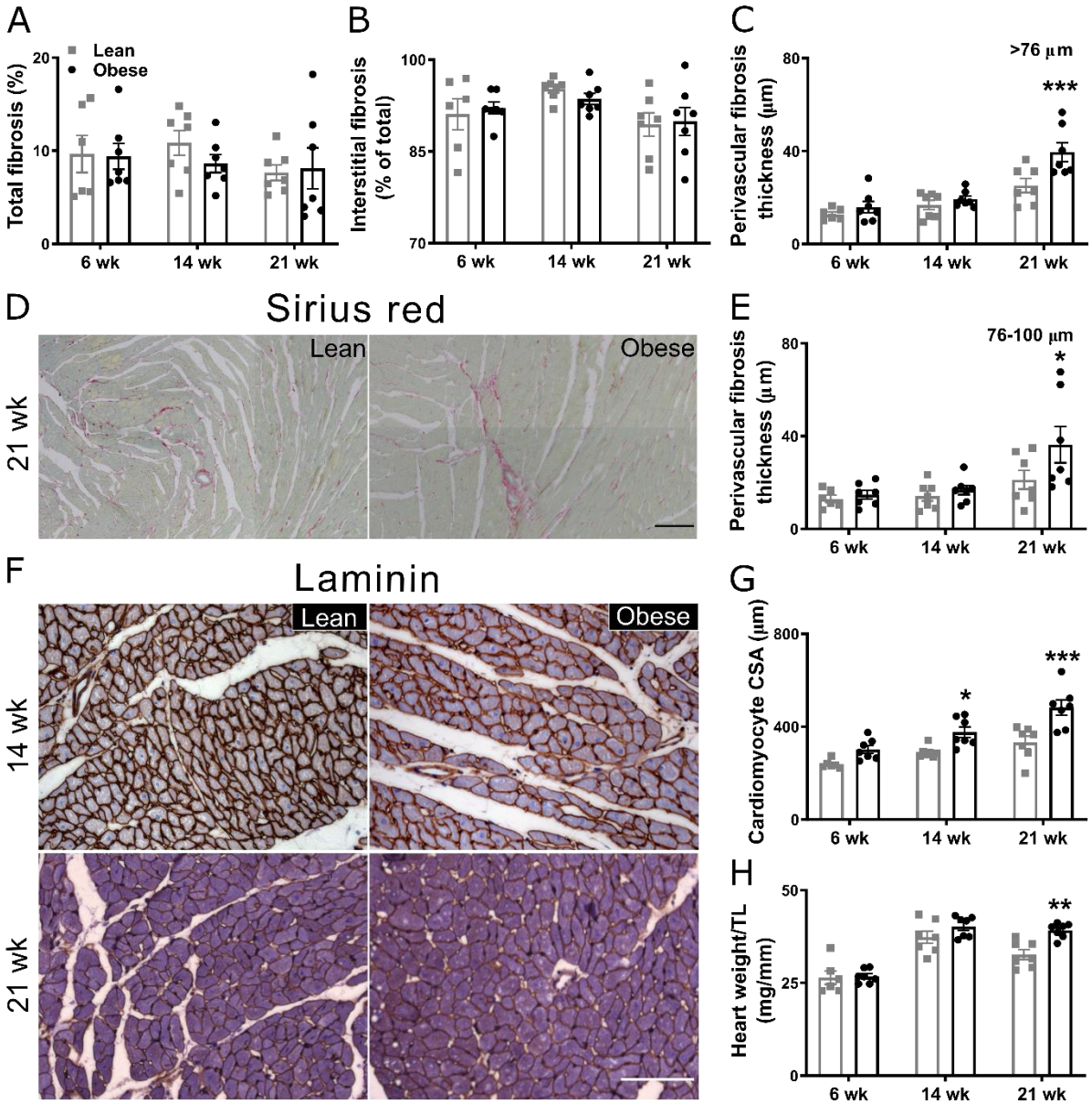

Figure 4.6- Cardiac hypertrophy, but not fibrosis, develops before the onset of diastolic dysfunction in obese ZSF1 rats. *Cardiac total (**A**) and interstitial fibrosis (**B**), Sirius red staining (**C**; scale bar 2000 µm), perivascular fibrosis thickness around vessels with a diameter of 51-75 µm (**D**) and >76 µm (**E**), cardiac laminin staining (**F**; scale bar 100 µm), cardiomyocyte cross-sectional area (**G**), and heart weight to tibia length (**H**) in obese and lean ZSF1 rats over time (n=7/group; except 6 lean at 6 weeks). Values are presented as mean ± SEM. Significance between lean and obese ZSF1 rats at each time point is assessed by non-paired two-way ANOVA followed by Šídák's multiple comparisons test with *p<0.05, **<0.01, and ***<0.001. CSA, cross-sectional area; TL, tibia length.*

4.4.4 Endothelial activation, junctional remodelling, and capillary regression are early events in HFpEF development

We subsequently investigated changes in the vasculature. Endothelial expression of the cell surface adhesion molecule VCAM-1 was increased in obese ZSF1 rats at 14 and 21 weeks, indicating endothelial cell activation (Figure 4.7A). In line with these findings, "jagged" disassembled VE-Cadherin junctions[245], also called remodelling junctions, were observed in obese ZSF rats at 14 and 21 weeks, but were absent at 6 weeks (Figure 4.7B). In contrast to obese ZSF1 rats, lean ZSF1 rats showed linear nicely assembled VE-Cadherin junctions at 6, 14, and 21 weeks (Figure 4.7B). Cardiac capillary rarefaction, shown by a reduced capillary density (VE-Cadherin$^+$) per myocardial area, occurred only at 21 weeks in obese ZSF1 rats (Figure 4.7C and D). Interestingly, obese ZSF1 rats showed active capillary regression, reflected by the presence of empty collagen sleeves (VE-Cadherin$^-$ Collagen IV$^+$)[246] at 14 weeks (Figure 4.7C and E). Endothelial proliferation did not show any differences between lean and obese ZSF1 rats over time (Figure 4.8A), further showing that active regression, rather than a decrease in proliferation, induced rarefaction.

We also assessed whether any changes in the density of arteries and arterioles were present by co-staining for isolectin and the vSMC marker α-SMA. Total cardiac density and percentage of α-SMA$^+$ vessels were similar between lean and obese ZSF1 rats at all the time points (Figure 4.8B-C), indicating that rarefaction is limited to capillary vessels. In T2DM and hypertension, vSMCs switch from the contractile α-SMA-expressing phenotype to a synthetic, migratory, and proliferative phenotype, characterised by the disappearance of α-SMA and other proteins associated with the contractile phenotype[247-250]. We therefore investigated changes in the cross-sectional area of α-SMA around different vessel diameter classes. No difference was observed between lean and obese ZSF1 rats at all time points (Figure 4.8D-F).

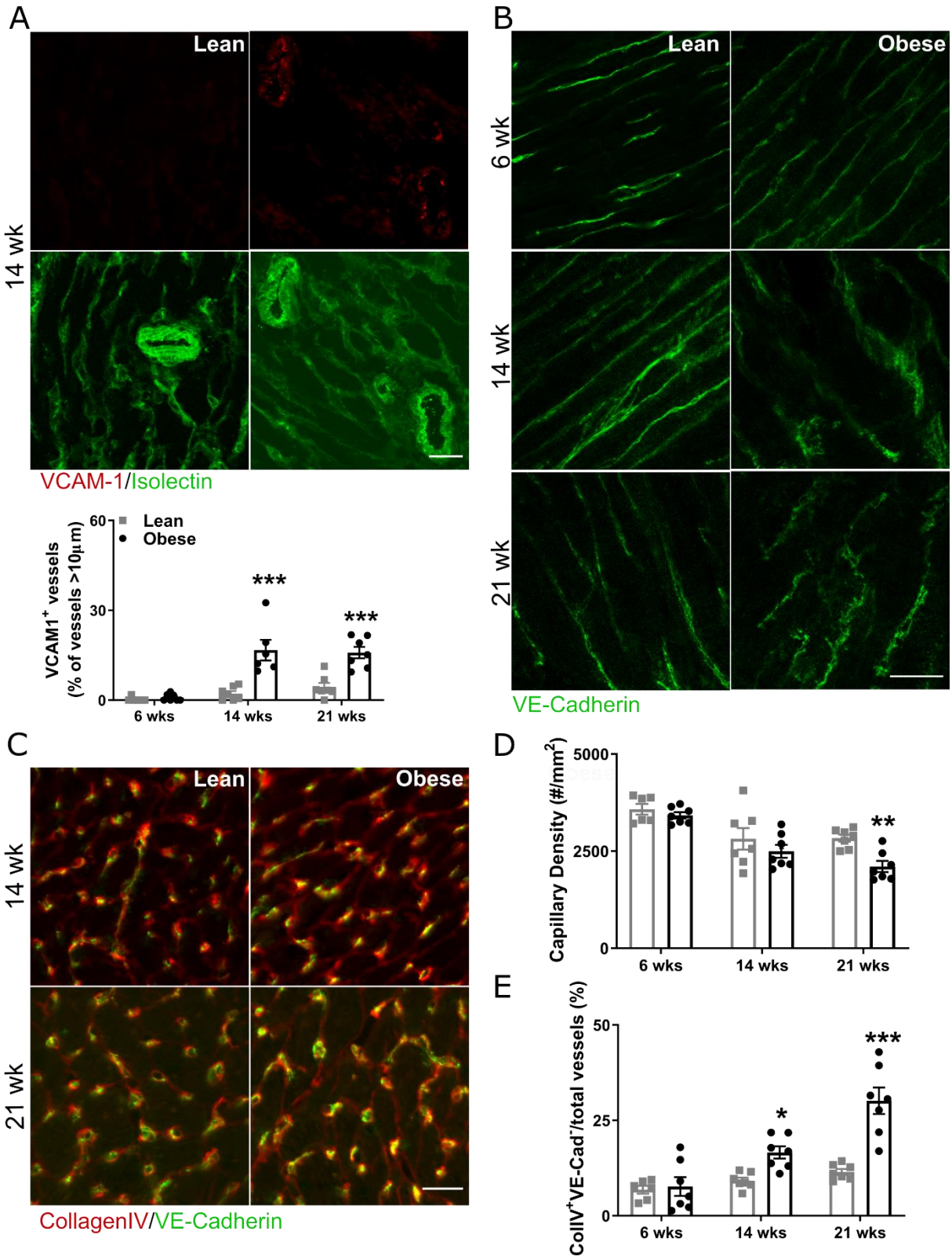

Figure 4.7- Cardiac endothelial activation, junctional remodelling, and capillary regression develop before the onset of fully established grade I diastolic dysfunction in obese ZSF1 rats. ***A****) Double staining for the endothelial activation marker vascular cell adhesion molecule-1 (VCAM-1; red) and isolectin (green; binds to sugar residues in the glycocalyx of blood vessels) in the heart of lean and obese ZSF1 rats at 14 weeks (scale bar 25 µm). Percentage of VCAM-1^{+} vessels of total larger vessel (diameter > 10 µm) in lean and obese ZSF1 rats over time (n=7/group; except 6 lean at 6 weeks).* ***B****) VE-Cadherin staining in elongated vessels in the heart of lean and obese ZSF1 rats at 6, 14, and 21 weeks (scale bar 25 µm).* ***C****) Cardiac endothelial cell (VE-Cadherin; green) and basement membrane Collagen IV (red) double staining in lean and obese ZSF1 rats at 14 and 21 weeks (scale bar*

*50 µm). **D**) Cardiac capillary density (VE-Cadherin$^+$) and **E**) vessel regression (VE-Cadherin$^-$Collagen IV$^+$; empty collagen sleeves) in lean and obese ZSF1 rats over time (n=7/group; except 6 lean at 6 weeks). Values are presented as mean ± SEM. Significance between lean and obese ZSF1 rats at each time point is assessed by non-paired two-way ANOVA followed by Šídák's multiple comparisons test with *p<0.05, **<0.01, and ***<0.001. CollIV, collagen IV; VE-Cad, vascular endothelial-Cadherin*

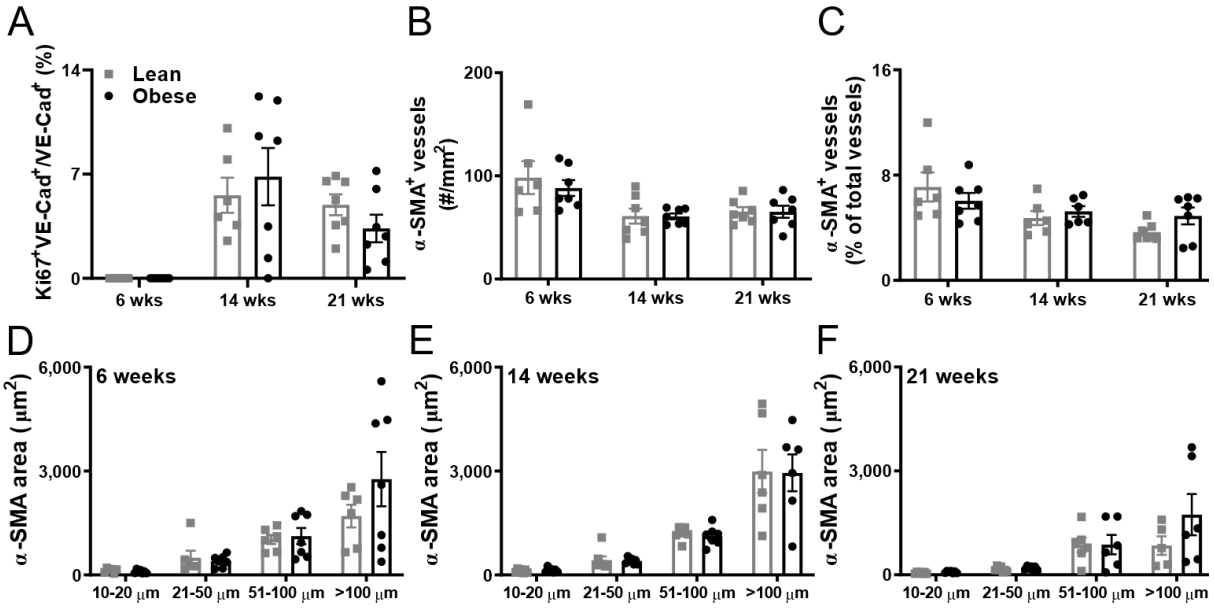

Figure 4.8- Endothelial proliferation and α-SMA$^+$ vessels in lean and obese ZSF1 rats over time. ***A**) Percentage of proliferating (Ki67$^+$VE-cadherin$^+$) of total endothelial cells (VE-cadherin$^+$) in lean and obese ZSF1 rats over time (n=7/group). Total density (**B**) and percentage of alpha-smooth muscle actin-positive (α-SMA$^+$) vessels (**C**) in lean and obese ZSF1 rats over time (n=7/group; except 6 lean at 6 weeks). **D-F**) α-SMA$^+$ surface around the different vessel diameter classes in lean and obese ZSF1 rats at 6, 14, and 21 weeks, respectively (n=7/group; except 6 lean at 6 weeks). Significance between lean and obese ZSF1 rats at each time point is assessed by non-paired two-way ANOVA followed by Šídák's multiple comparisons test with *p<0.05.*

4.4.5 Reduced pericyte coverage is present due to high vulnerability of pericytes to metabolic risks and oxidative stress

Capillary regression is associated with vessel destabilization. Pericytes are important in the maintenance of the endothelial barrier and capillary stability and integrity. Loss of endothelial cell pericyte coverage leads to unstable and dysfunctional vessels prone to rarefaction[251]. We found that pericyte coverage was dramatically decreased in obese ZSF1 rats, reflected by 41% reduction already at 14 weeks (Figure 4.9A-B).

We investigated the effects of conditions mimicking HFpEF-associated comorbidities and the resultant oxidative stress on pericytes and endothelial cells *in vitro* (Figure 4.9C). Pericyte cell apoptosis was increased after stimulation with any of the metabolic stressors (high glucose, LDL, and H_2O_2), while the number of apoptotic endothelial cells was only increased after stimulation with H_2O_2 (Figure 4.9D). Similarly, stimulated pericytes showed a higher number of DEGs compared to stimulated endothelial cells (2655 *versus* 551 DEGs) (Figure 4.10A-C). More DEGs were similarly regulated by two different experimental conditions in pericytes compared to endothelial cells (23 *versus* 7 DEGs) (Figure 4.10A). Interestingly, DEGs similarly regulated by more than one experimental condition in pericytes are involved in prostaglandin signalling, including prostaglandin E synthase 1 (*Ptges-1*), aldo-keto reductase family 1 member B1 (*Akr1b1*), immediate early response 3 (*Ier3*), prolyl-4-hydroxylase subunit alpha 1 *(P4ha1*) (Figure 4.10B). Endothelial genes regulated by more than one experimental condition, included angiopoietin 2 (*Angpt2*), that has been shown to induce pericyte detachment (Figure 4.10C)[252].

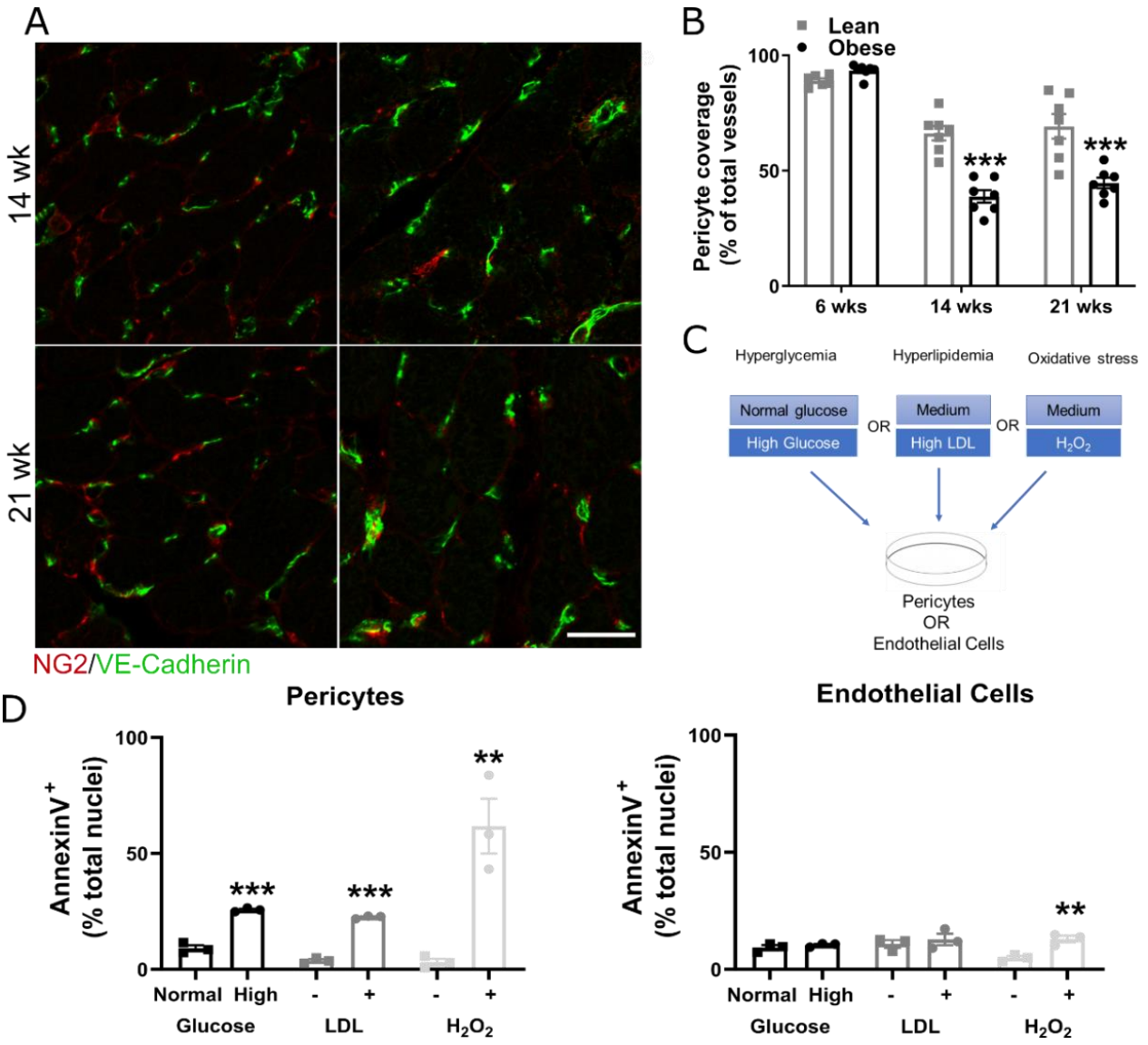

Figure 4.9- Reduced pericyte/endothelial cell coverage due to increased vulnerability of pericytes to metabolic stimuli. A*) Double staining for the pericyte marker neuron-glial antigen 2 (NG2; red) and endothelial marker VE-Cadherin (green; scale bar 25 µm) and* ***B****) quantification of pericyte coverage (NG2$^+$VE-Cadherin$^+$) of total vessels (VE-Cadherin$^+$)in lean and obese ZSF1 rats (n=7/group; except 6 lean at 6 weeks) over time.* ***C****) Pericytes and endothelial cell were stimulated with high glucose, low-density lipoprotein (LDL), hydrogen peroxide (H_2O_2) or control medium for three days.* ***D****) Percentage of apoptotic cells (Annexin V$^+$) of the total number of pericytes (left panel) and endothelial cells (right panel) stimulated with the different conditions. For panel B, significance between lean and obese ZSF1 rats at each time point is assessed by non-paired two-way ANOVA followed by Šídák's multiple comparisons test, while in panel D a non-paired Student t-test was used with *p<0.05, with *p<0.05, **<0.01, and ***<0.001.*

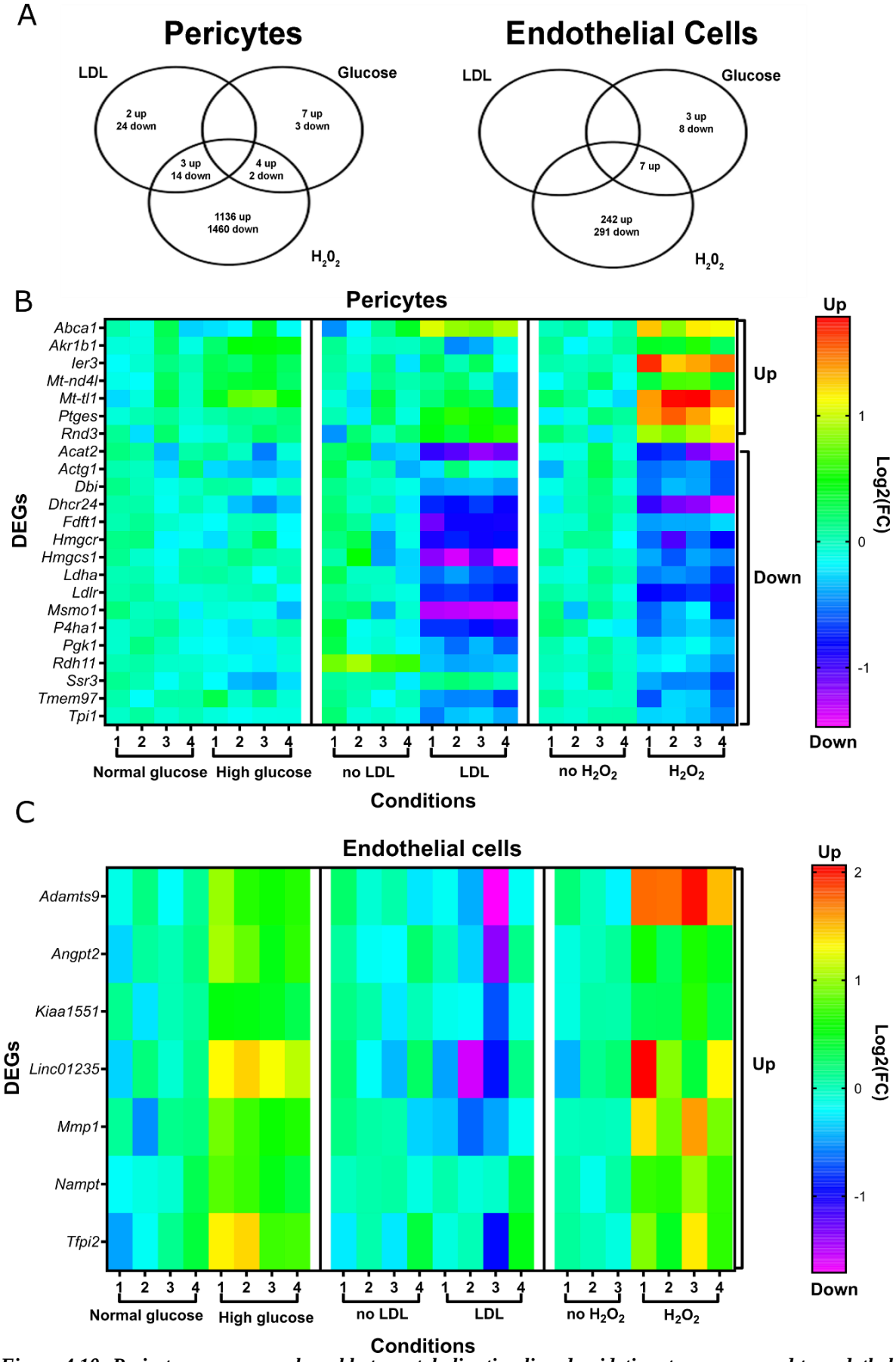

Figure 4.10- Pericytes are more vulnerable to metabolic stimuli and oxidative stress compared to endothelial cells. A) *Venn diagram showing the overlap between the differentially expressed genes (DEGs) after stimulation*

*of pericytes (left) or endothelial cells (right) with the different conditions. Heat map displaying fold changes of the DEGs similarly regulated by two differential experimental conditions in pericytes (**B**) and endothelial cells (**C**). The colours represent the log2(FC) and are ranging from purple (FC<-1.0) to light blue (FC=0) to red (FC>1.0). DEGs had an adjusted p-value below 0.05.*

4.5 Discussion

Here, we show that active cardiac capillary regression is an early event in HFpEF development, leading to rarefaction in established HFpEF. Reduced pericyte coverage of capillaries was present when active capillary regression was observed. Furthermore, our *in vitro* results suggest that pericytes are more susceptible to hyperglycaemia, hyperlipidaemia, and oxidative stress compared to endothelial cells. Furthermore, other vascular abnormalities, including junctional remodelling and endothelial activation, were already present before the establishment of key pathological processes in HFpEF. Coronary capillary abnormalities have been scarcely investigated in HFpEF and most studies focused on established HFpEF. Much of the work has focussed on vasodilation and contraction, and thus investigated arteriole function. HFpEF patients showed for example both endothelium-dependent and -independent dysfunction in arteriolar contractility, and these dysfunctions were associated with increased mortality and worsened diastolic function[71]. Established HFpEF patients do also show cardiac rarefaction of arterioles and capillaries[60], and this was shown to contribute to perfusion insufficiencies and impaired oxygen delivery to the heart[81]. In a multiple comorbidity swine model, impaired myocardial blood flow and oxygen delivery occurred without reductions in coronary capillary density, suggesting rarefaction or dysfunction of larger resistance vessels in the heart[73]. In contrast to this study, we show that endothelial dysfunction, including endothelial activation, junctional remodelling, and active regression, is an early event in the development of HFpEF and that rarefaction is limited to the capillary vasculature, that are devoid of vSMC coverage.

In the healthy heart, alterations in hemodynamic and mechanical factors, as well as hypoxia, stimulate the release of angiogenic growth factors (e.g. VEGF) from cardiomyocytes to induce parallel growth of the nutrient- and oxygen-supplying vasculature[253]. *Vice versa*, endothelial

cells release signalling factors (e.g. NO and endothelin-1), which regulate cardiac function and morphology[253]. However, dysfunctional endothelial or cardiomyocyte signalling can lead to pathological cardiomyocyte hypertrophy without physiological compensatory increases in vessel formation, resulting in rarefaction. We observed that capillary rarefaction occurred simultaneously with the onset of cardiomyocyte hypertrophy. We cannot establish whether one causes the other, however, it is likely that they exacerbate each other. Though the reduction of capillary density can occur purely by increases in cardiomyocyte size, e.g. the cardiomyocyte size increases resulting in less cardiomyocytes and capillaries per surface area, that effect does not explain the increased presence of empty collagen sleeves (active regression of capillaries), endothelial activation, junctional remodelling, and/or the loss of pericytes observed at 14 weeks. In HFpEF patients, rarefaction of capillaries and arterioles was positively associated with cardiomyocyte hypertrophy in HFpEF patients[60]. Though others have found that cardiomyocyte stiffness changes before deviations in vascular contractility are observed, these groups investigated arteriolar function and not capillaries as investigated here[254].

Pericytes, mural cells surrounding endothelial cells in capillaries, are crucial for ensuring stability of capillaries, preventing regression, and regulating blood flow, angiogenesis, vessel maturation, and permeability[255]. As such, pericyte-endothelial crosstalk is essential in both quiescent vasculature and remodelling and disruption of this complex crosstalk often occurs in vascular disease. Pericyte loss is one of the earliest hallmarks of diabetes-associated vascular diseases, including retinopathy, nephropathy, and neuropathy, where it causes capillary regression, leading to leaking of fluids, leukocyte infiltration, and hypoxia in the damaged area[229,256]. Similarly, reduced pericyte coverage is observed in cardiac ischemia/reperfusion injury due to modifications of the pericyte architecture[257]. Specific pericyte ablation was recently reported to cause severe blood-brain barrier disruption, tight and adherens junctional remodelling, oedema, reduced cerebral blood flow, neuron loss, and behavioural changes in

mice[258]. Interestingly, disorganized pericyte/endothelial structures were also reported in obese ZSF1 rats with advanced HFpEF[125]. Here, we showed that cardiac pericyte loss occurred exclusively in obese ZSF1 rats before the establishment of key pathological processes of HFpEF, including diastolic dysfunction, inflammation, and fibrosis. *In vitro*, we also showed that pericytes stimulated with high glucose, LDL, or H_2O_2 were more vulnerable compared to stimulated endothelial cells, further underlining that metabolic stresses induce pericyte loss leading to capillary regression, dysfunction, and rarefaction.

In line with our *in vivo* and *in vitro* observations, pericytes have been shown to be vulnerable to HFpEF-associated risk factors, including obesity, hyperlipidaemia, and T2DM, and the resultant oxidative stress[256,259-262]. For example, hyperlipidaemia reduced pericyte/endothelial cell coverage in *apoe*$^{-/-}$ mice by attenuating the expression of the junctional protein N-cadherin, which mediates pericyte/endothelial interaction[260]. High LDL concentrations also lead to pericyte vasoconstriction resulting in impaired blood flow and capillary regression[246,263]. Hyperglycaemia can induce also pericyte loss by (i) increased formation of advanced glycation end products, (ii) PKC activation, (iii) capillary contraction due to reduced vasodilator (e.g. endothelium-derived hyperpolarization factor) production, and/or (iv) excessive production of ROS[261,264-266].

Limitations

We only used male ZSF1 rats, as the model was established in males and few studies have investigated HFpEF development in female rats[224]. However, we do not rule out that the development of HFpEF in females might differ from males. In this study, we have assessed microvascular abnormalities only in one HFpEF rodent model, as this is currently the most accepted HFpEF rodent model, which mimics human pathology. Nevertheless, our preliminary

data shows pericyte loss occurs in different mouse models of HFpEF, including the published L-Name and HFD-treated mouse model[267] and *db/db* mice treated with a low dose of salt. Furthermore, we did not show a causal involvement of pericyte loss in the development of HFpEF. To establish whether pericyte loss causes HFpEF development, diastolic dysfunction and cardiac remodelling should be assessed in an animal model with pericyte loss, such as the double *Ng2*/ platelet-derived growth factor beta receptor (*Pdgfβr*) knock out mouse model[258].

In conclusion, pericyte loss is an early event in the development of HFpEF, which causes capillary regression, rarefaction, and dysfunction. Targeting pericytes could be an attractive therapeutic approach for preventing the development of HFpEF.

Chapter 5: Linagliptin prevents left ventricular stiffening by reducing titin cleavage and hypophosphorylation

Ilona Cuijpers[*], *Anna-Pia Papageorgiou*[*], *Paolo Carai1, Melissa Herwig, Andreas Mügge, Thomas Klein, Nazha Hamdani*[#], *Elizabeth A. V. Jones*[#], *Stephane Heymans*[#]

*,[#] *Authors contributed equally; In revision for Journal of Molecular and Cellular Medicine*

5.1 Abstract

The MetS is an escalating problem worldwide, causing left ventricular stiffening, an early characteristic of diastolic dysfunction, for which no treatments exists. Increased circulating DPP-4 levels are associated with diastolic dysfunction and stiffening in MetS patients. However, whether DPP-4 inhibition improves left ventricular dysfunction is unclear. Here, we investigate whether the DPP-4 inhibitor linagliptin reduces left ventricular stiffness in MetS-induced cardiovascular disease. Sixteen-week old obese ZSF1 rats, displaying the MetS and left ventricular stiffness, received linagliptin-supplemented diet or placebo chow for four weeks. Linagliptin significantly reduced obesity, hyperlipidaemia and -glycaemia, and improved left ventricular relaxation, the latter indicated by decreased E/E' and mitral valve deceleration time. The reduced left ventricular stiffness *in vivo* after linagliptin treatment was related to decreased cardiac fibrosis and cardiomyocyte passive stiffness. This reduced cardiomyocyte passive stiffness was the result of titin isoform switching from the stiff N2B isoform to the more flexible N2BA titin isoform and increased phosphorylation of total titin and specifically its N2Bus region (S4080 and S3391). Importantly, DPP-4 directly cleaved titin *in vitro*, resulting in an increased cardiomyocyte passive stiffness, which was prevented by simultaneous administration of linagliptin. Linagliptin treatment improves left ventricular stiffness in obese ZSF1 rats by preventing direct DPP4-mediated titin cleavage, as well as by modulating both titin isoform levels and phosphorylation. Reducing left ventricular stiffness by administering the clinically used linagliptin might prevent metabolic risk-induced early diastolic dysfunction in humans.

5.1 Introduction

The MetS –a cluster of hyperglycaemia, insulin resistance, obesity, hyperlipidaemia, and hypertension– is one of the most progressively escalating public health problems affecting children, adolescents, and adults worldwide. The MetS may cause left ventricular stiffening, an early manifestation of diastolic dysfunction[268]. Impaired cardiomyocyte relaxation is the first affected determinant of left ventricular stiffness and precedes the excessive deposition of cardiac fibrosis[186,187]. However, therapies to prevent the progression of MetS towards left ventricular stiffening are lacking.

Cardiac stiffening involves increased cardiomyocyte $F_{passive}$[188], mainly due to modifications of the giant spring titin, which forms a continuous filament network in the sarcomeres of striated myocytes. Cardiac titin consists of two isoforms: the short, stiff N2B and the longer, more flexible N2BA isoform. Extension of the elastic I-band segment in both isoforms allows for passive cardiomyocyte relaxation in diastole. Cardiomyocyte stiffness and left ventricular relaxation are modulated by isoform switching and phosphorylation of titin[51].

Diastolic dysfunction and left ventricular stiffening are positively associated with elevated DPP-4 levels in T2DM and obese patients[191-193]. The DPP-4 inhibitor linagliptin is clinically used as an anti-diabetic drug, as it improves blood glucose regulation by preventing the degradation of GLP-1 and GIP[195]. Still the cardiovascular protective properties of DPP-4 inhibitors remain a matter of debate[269] and their protective effects on left ventricular stiffness and diastolic dysfunction are unclear. Here, we revealed that DPP-4 inhibition reduces left ventricular stiffening in a rat model of combined T2DM, hypertension, and obesity, in part by modulating titin cleavage, isoform switching, and phosphorylation. Linagliptin might be a potential strategy for the prevention and treatment of metabolic risk-induced cardiac diastolic dysfunction in humans.

5.3 Materials and Methods

5.3.1 Experimental animals

Experiments were performed according to the European Directive on the Care and Use of Experimental Animals (2010/63/EU) and approved by the Animal Care and Use Committee of KU Leuven (Project 283/2014). Eight weights old male obese ZSF1 rats (n=14; *SHHF/Mcc*; *lepr fa* /*lepr facp*), which develop left ventricular stiffness, secondary to T2DM, obesity, and hypertension, were purchased from Charles River Laboratories (#strain code 379, MA)[151]. Animals were housed and acclimated under a 12-hour light-dark cycle with access to water and chow diet *ad libitum* (#V1534-000, Ssniff Spezialdiäten GmbH, Germany) until 16 weeks of age. At 16 weeks of age, 7 obese ZSF1 rats (Obese + Lina) were randomised for linagliptin-supplemented (83 mg/kg; Boehringer Ingelheim GmbH, Germany) chow diet (#1534-0, Ssniff Spezialdiäten GmbH, Germany), while 7 obese ZSF1 rats (Obese) received the non-supplemented chow diet *ad libitum* (#1534-0, Ssniff Spezialdiäten GmbH, Germany) for 4 weeks. At 20 weeks, blood glucose was assessed with Glucomen LX plus (A. Menarini Diagnostics, Belgium) after 16 hours fasting. Complete 2D echocardiography was performed in 20-week-old linagliptin-treated and control obese ZSF1 rats. The day after, rats were anaesthetised with an IP injection with 50 mg/kg ketamine (Nimatek, Eurovet Animal Health BV, Netherlands) and 5 mg/kg xylazine (Xyl-M®, V.M.D. nv/sa, Belgium). Blood samples were collected and the rats were then perfused with 20 ml PBS. Organs were collected and weighted. Plasma lipid levels (UZ Leuven, Belgium) and DPP-4 and active GLP-1 and GIP (Boehringer Ingelheim GmbH, Germany)[270,271] were measured. The heart was collected for histological, mechanical, and molecular analyses. A schematic overview is given in Figure 5.1

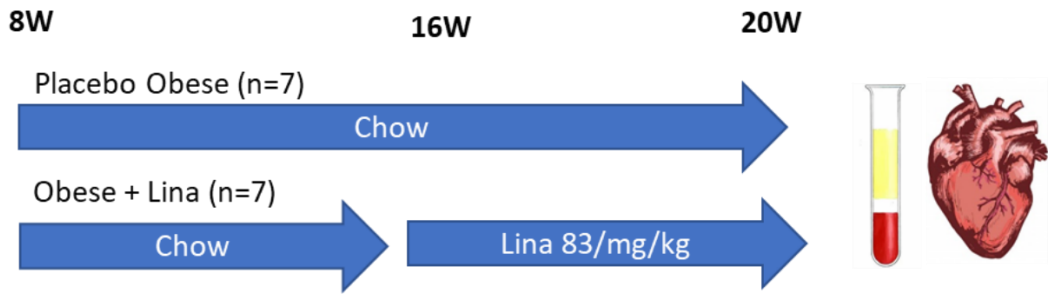

Figure 5.1- Schematic presentation of the in vivo study set up. *Eight weeks old male obese ZSF1 rats were purchased and were fed a chow diet. At 16 weeks of age, the animals either received linagliptin-supplemented chow diet (83 mg/kg) or placebo chow diet (n=7/group). At 20 weeks of age, echocardiography measurements were performed and blood and organs were collected. The heart was collected for histological, mechanical, and molecular analyses.*

5.3.2 Transthoracic echocardiography

Rats were anaesthetised by inhaling 5% inhaled isoflurane (Ecuphar, Netherlands) for induction followed by 2% inhaled isoflurane for maintenance. Complete transthoracic echocardiography was performed using a MS 250 transducer (13-24 MHz) connected to a Vevo 2100 echocardiograph (Visual Sonics, Canada). HR, ESV and EDV, and cardiac dimensions, AW, EDD, ESD, and PW, were assessed on the parasternal short-axis B-mode. CO, SV, EF, and FS were calculated based on parasternal short-axis B-mode recordings. Left ventricular filling was assessed by pulsed wave Doppler trans-mitral flow velocity tracings, including E and A peak velocities, mitral valve deceleration time, NFT, AET, IVCT, IVRT, and MPI, just above the tip of the mitral leaflets. E' and A' peak velocities were measured by tissue Doppler imaging at the lateral mitral annulus. E/A, E/E', and E/deceleration time ratios were calculated. Echocardiography-derived volumes were also indexed for BSA, estimated as 9.1 * body weight in grams$^{2/3}$, to account for differences in body weight between the groups[151,204]. At least three stable cardiac cycles were averaged for all measurements.

5.3.3 RNA isolation and quantitative RT-PCR

Cardiac total RNA was isolated (miRVana kit, Thermofisher, Belgium), cDNA was generated (miScript II RT kit, Qiagen, Netherlands), and transcript levels in 5 ng cDNA were quantified

using SYBR Green PCR Master Mix and Applied Biosystems QuantStudio 3 (both Thermofisher, Belgium). Primers were designed to span exon-exon junctions using Primer3 software and synthesised IDT (Belgium). Relative gene expression levels were calculated using the $2^{-\Delta\Delta Ct}$ method.

Gene	**Forward primer (5'-3')**	**Reverse primer (5'-3')**
Collagen 1a1 (Col1a1)	aggagagagtgccaactcca	gtagggagcagcaagag
Collagen 3a1 (Col3a1)	ggcaatcctgatcttcctga	gcctgatccatgtaggcaat
Metalloproteinase 2 (Mmp2)	ggaracaggrgrgccaaggt	gcagtgtggtggaaaactga
Metalloproteinase (Mmp9)	agcctgtggttggtcagaag	ataaaagggccggtaaggtg
Tissue inhibitor of metalloproteinases (Timp1)	tcccttgcaaactggagagt	gtcatcgagaccccaaggta
Tissue inhibitor of metalloproteinases (Timp2)	ccctccaaccagtgtttcat	ggggaagagagaggaaggaa
Gapdh	gtggacctcatggcctacat	tgtgagggagatgctcagtg

5.3.4 Histology

Cardiac tissue was fixed in 1% PFA at 4 °C for 24 hours and imbedded in paraffin (Leica TP1020; Leica Biosystems, Belgium). Sections (4 μm) were stained with Picro Sirius Red (fibrosis) and rabbit anti-Laminin A antibodies (1/400; #L9393, Sigma-Aldrich, Belgium). Images were acquired and analysed using an Axiovert 200M microscope (Zeiss, Germany) and Image J software, respectively. Total and perivascular fibrosis was quantified as the percentage Sirius red positive area per total and perivascular cardiac area, respectively. Interstitial fibrosis was expressed as percentage of total fibrosis. Cardiomyocyte hypertrophy was assessed by calculating the myocyte CSA based on the inner circumference of at least 240 myocytes per laminin-stained section.

5.3.5 Force measurements in isolated cardiomyocytes ex vivo

Cardiac tissue of linagliptin- and placebo-treated obese ZSF1 rats was incubated in relaxation buffer supplemented with 1% Triton X-100 overnight to remove membrane structures. Isolated cardiomyocytes were attached between a force transducer and length monitor (1600A; Aurora Scientific, Canada) and $F_{passive}$ was measured between 1.8 and 2.4 µm sarcomere length[151].

5.3.6 Myocardial kinase activity

Myocardial kinase activities were measured using a Cyclex CAMKII (#CY-1173, MBL International, MA), non-radioactive PKA and PKC (#ADI-EKS-390A and -420A, Enzo Life Sciences, Germany) and, home-made radiolabelled ATP PKG activity kit[53] according manufacturer's instructions.

5.3.7 Titin isoform levels and phosphorylation

To determine titin isoform protein levels, left ventricular samples were mechanically homogenised, heated, and separated on an agarose-strengthened 1.8% SDS-PAGE gel for titin separation combined with a second 10% SDS-PAGE gel for separation of small proteins at 2 mA overnight for at least 12 hours[272]. Proteins were transferred on a polyvinylidene difluoride (PVDF) membranes and stained with Coomassie Blue. Titin and myosin heavy chain (MHC) bands were analysed[273] and titin isoform levels were normalised to MHC protein levels. Anti-phospho serine (Ser)/threonine antibody (Thr) (dilution 1:500; #PP2551, ECM Biosciences LLC, KY) was used to assess N2B phosphorylation. Both titin isoform and phosphorylation levels were normalised to placebo-treated obese ZSF1 rats.

To determine site-specific titin phosphorylation, previously validated custom-made, affinity-purified, phospho site-specific anti-titin antibodies (Eurogentec, Belgium) were used[151,254,272,274]:

- anti-phospho-N2Bus (Ser3991) against EEGKS(PO3H2)LSFPLA (dilution 1:500);
- anti-phospho-N2Bus (Ser4043) against QELLS(PO3H2)KETLFP (dilution 1:100) and anti-mouse-N2Bus-titin against mouse sequence QELLSKETLFP (dilution 1:500)
- anti-phospho-N2Bus (Ser4080) against LFS(PO3H2)EWLRNI (dilution 1:500);
- anti-phospho-PEVK (Ser12742) against EVVLKS(PO3H2)VLRK (dilution 1:100);
- anti-phospho-PEVK (Ser12884) against KLRPGS(PO3H2)GGEKPP (dilution 1:500) and anti-PEVK-domain against (cross-species conserved) sequence KLRPGSGGEKPP (1:100).

Primary antibody binding was visualised using secondary horseradish peroxidase (HRP)-labelled goat anti-rabbit antibody (1/10,000; #P044801-2, Dako Cytomation, Denmark) and enhanced chemiluminescence (ECL Western blotting detection; Amersham Biosciences, France). Stainings were visualised using the LAS-4000 Image Reader and analysed with Multi Gauge V3.2 software (both from FUJIFILM Corp, Japan). Signals obtained from phospho-specific antibodies were normalised to signals obtained from PVDF stains referring to the entire protein amount transferred.

5.3.8 In vitro human titin experiments

Left ventricular tissue of five male non-failing human donors (average age, 40 years), who died due to a non-cardiac related death, was collected in cardioplegic solution and stored in liquid nitrogen until use. All procedures were performed according to the Declaration of Helsinki (1997) and were approved by the local ethics committee (OKAR/1066/2008/OKAR). Human cardiac biopsies were incubated overnight in relaxing solution supplemented with 1% triton X-

100. Isolated cardiomyocytes were subsequently incubated with (i) 300 ng/ml recombinant his-tagged DPP-4 (#50718-M08H; Sino Biological, Eschborn, Germany), (ii) 300 ng/ml recombinant DPP-4 and 100 nmol/L linagliptin (Boehringer Ingelheim GmbH, Biberbach, Germany), or (iii) PBS/DMSO (control) for 30 minutes to assess $F_{passive}$ *in vitro.* To assess titin cleavage *in vitro*, human isolated cardiomyocytes were incubated with (i) 300 ng/ml recombinant DPP-4, (ii) 100 nmol/L linagliptin, (iii) 300 ng/ml DPP-4 and 100 nmol/L linagliptin, (iv) or PBS/DMSO (control) at 37 °C for 2 hours. Isolated cardiomyocytes were incubated with 300 ng/ml DPP-4 to assess the direct effect of DPP-4 on titin over time. Samples were subsequently run on an agarose strengthened 1.8% SDS-PAGE gel on top of a 10% acrylamide SDS-PAGE gel at 2 mA overnight for at least 12 hours. Cleavages of total titin were visualised by Coomassie Blue staining. Segment-specific titin cleavage was assessed by western blotting using custom-made, affinity-purified antibodies, including the anti-N2Bus domain against mouse sequence QELLSKETLFP and anti-PEVK domain against (cross-species conserved) sequence KLRPGSGGEKPP (both Eurogentec, Seraing, Belgium).

5.3.9 Statistical analysis

Data are expressed as mean ± SEM. All analysis was performed using GraphPad Prism 7.0. Normal distribution of all continuous variables was tested using the Shapiro-Wilk normality test. Normally distributed data were analysed using a two-tailed unpaired Student t-test, while non-normally distributed data were analysed using a Mann-Whitney U test. *P<0.05, ** P<0.01, and ***P<0.001.

5.4 Results

5.4.1 Linagliptin improves cardiac relaxation in cardiometabolic disease

Four weeks of linagliptin supplementation significantly reduced fasting glucose levels by reducing DPP-4 activity, resulting in decreased breakdown of systemic active GIP and GLP-1 (Figure 5.2A-D). Furthermore, linagliptin-treated rats had significantly decreased body weight, organ (liver and spleen) weight/TL ratio, plasma triglycerides, and non-HDL cholesterol levels, while HDL cholesterol was increased (Figure 5.2E-G and Table 5.1). In addition to its well-established anti-diabetic, -obesity, and -hyperlipidaemic effects[195,275], linagliptin is suggested to have beneficial cardiac effects[200]. Interestingly, mitral valve deceleration time and E/E', the non-invasive parameter for left ventricular stiffness, were significantly reduced in linagliptin-treated obese ZSF1 rats (Figure 5.2H-I and Table 5.2), indicating decreased left ventricular stiffness and improved relaxation. Thus, linagliptin decreases cardiometabolic risk factors, including obesity, hyperglycaemia, and hyperlipidaemia, and improved left ventricular relaxation in obese ZSF1 rats.

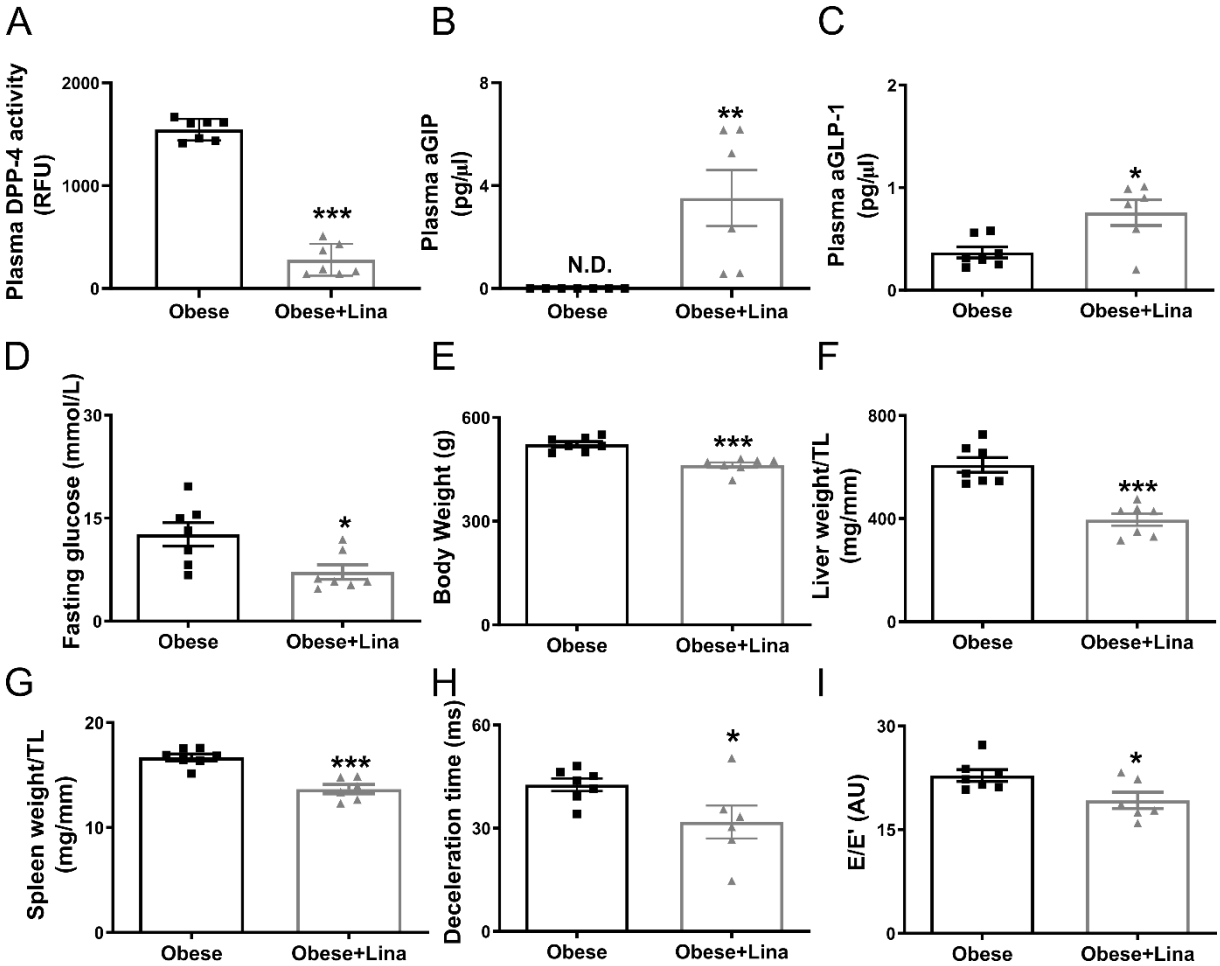

Figure 5.2- Linagliptin improves left ventricular relaxation in obese ZSF1 rats. *Plasma DPP-4 activity (**A**), aGIP (**B**) and GLP-1 levels (**C**), fasting glucose (**D**), body weight (**E**), liver (**F**) and spleen weight to tibia length (**G**), mitral valve deceleration time (**H**), and E/E' ratio (**I**) in 20-week-old linagliptin- (Obese+Lina) and placebo-treated obese (Obese) ZSF1 rats (n=7 per group). aGIP, active glucose-dependent insulinotropic peptide; aGLP-1, active glucagon-like peptide 1; DPP-4, dipeptidyl peptidase-4; E, early mitral inflow peak velocity; E', early diastolic mitral annulus peak velocity; ND, not detected; RFU, relative fluorescence units; TL, tibia length. Data are expressed as mean ± SEM. All data were analysed using a two-tailed unpaired Student t-test, except H was analysed by a Mann-Whitney U test. * Indicates P<0.05, ** P<0.01, and ***P<0.001.*

Table 5.1: Plasma lipid levels in linagliptin- and placebo-treated obese ZSF1 rats

	Obese (n=7)	Obese + Lina (n=7)
Triglycerides (mg/dl)	471 ± 50.7	227 ± 23.4***
Cholesterol (mg/dl)	104 ± 6.32	91.7 ± 10.3
HDL-cholesterol (mg/dl)	19.4 ± 1.49	34.0 ± 4.53**
Non-HDL cholesterol (mg/dl)	84.1 ± 6.16	57.9 ± 8.13*

*Values are presented as mean ± SEM. HDL indicates high-density lipoprotein. All data were analysed using a two-tailed unpaired Student t-test. * Indicates P<0.05, ** P<0.01, *** P<0.001 comparing linagliptin- (Obese+Lina) and placebo-treated obese (Obese) ZSF1 rats (both n=7).*

Table 5.2: Echocardiography in placebo-and linagliptin-treated obese ZSF1 rats

Parameter	Obese (n=7)	Obese + Lina (n=7)
Body weight (g)	501 ± 11	449 ± 8.3**
BSA (cm^2)	574 ± 8.6	534 ± 6.6**
LV mass (mg)	1475 ± 48	1483 ± 78
Corrected LV mass (mg)	1180 ± 38	1186 ± 62
HR (bpm)	291 ± 7.34	283 ± 5.93
SV (µl)	408 ± 37.0	420 ± 30.9
SV, $_i$ (µl/cm^2)	0.71 ± 0.06	0.79 ± 0.05
CO (ml/min)	120 ± 12.9	118 ± 8.16
CI (ml/min/cm^2)	0.21 ± 0.02	0.22 ± 0.01
AWd (mm)	1.95 ± 0.09	1.83 ± 0.10
AWs (mm)	2.90 ± 0.09	2.71 ± 0.19
EDD (mm)	8.77 ± 0.36	9.13 ± 0.35
ESD (mm)	5.89 ± 0.29	6.46 ± 0.41
PWd (mm)	2.06 ± 0.11	1.99 ± 0.09
PWs (mm)	2.90 ± 0.10	2.64 ± 0.16
EDV (µl)	680 ± 54.8	755 ± 61.6
EDV, $_i$ (µl/cm^2)	1.18 ± 0.21	1.41 ± 0.29
ESV (µl)	273 ± 30.5	335 ± 39.9
ESV, $_i$ (µl/cm^2)	0.47 ± 0.13	0.63 ± 0.07
EF (%)	60.0 ± 2.81	56.3 ± 2.87
FS (%)	32.9 ± 1.86	29.6 ± 2.46
E (mm/s)	1070 ± 50.0	947 ± 32.2
A (mm/s)	513 ± 33.2	501 ±47.1
E/A (AU)	2.13 ± 0.16	1.96 ±0.16
Deceleration time (ms)	42.6 ± 1.79	31.8 ± 4.77*
E/deceleration time	28.8 ± 1.81	39.9 ± 6.25
IVRT (ms)	32.4 ± 1.22	36.9 ± 0.81*
IVCT (ms)	20.0 ± 1.40	16.5 ± 0.70
AET (ms)	74.4 ± 2.79	78.9 ± 3.86
NFT (ms)	127 ± 4.61	135 ± 3.63
E' (mm/s)	46.9 ± 1.41	50.3 ± 3.71
A' (mm/s)	31.0 ± 1.58	36.4 ± 3.23
E/E' (AU)	22.8 ± 0.84	19.2 ± 1.19*
MPI (AU)	0.70 ± 0.01	0.72 ± 0.06

*Data are presented as mean ± SEM. A, arterial or "late" mitral inflow peak velocity; A', late diastolic mitral annulus peak velocity; AET, aortic ejection time; AW, anterior wall; CO, cardiac output; CI, cardiac index; d, diastole; E, early mitral inflow peak velocity; E', early diastolic mitral annulus peak velocity; EDD, end-diastolic diameter; EDV, end-diastolic volume; EF, ejection fraction; ESD, end-systolic diameter; ESV, end-systolic volume; FS, fractional shortening; HR, heart rate; $_i$, indexed for body surface area, calculated as 9.1 * body weight in grams$^{2/3}$; IVCT, isovolumic contraction time; IVRT, isovolumic relaxation time; Lina, linagliptin; LV, left ventricular; MPI, myocardial performance index; NFT, non-flow time; PW, posterior wall; s, systole; SV, stroke volume. Normally distributed data were analysed using a two-tailed unpaired Student t-test, while non-normally distributed data were analysed using a Mann-Whitney U test. * Indicates P<0.05, **P<0.01, ***P<0.001 comparing linagliptin- (Obese+Lina) and placebo-treated obese (Obese) ZSF1 rats (both n=7).*

5.4.2 Linagliptin has cardiac anti-fibrotic effects in obese ZSF1 rats

Increased left ventricular stiffness may in part be determined by extracellular matrix-mediated stiffness, caused by elevated cardiac fibrosis[51]. Linagliptin significantly reduced total, perivascular, and interstitial cardiac fibrosis in obese ZSF1 rats (Figure 5.3A-D). Cardiac transcript levels of genes involved in fibrosis, including *Col1a1*, *Col3a1*, and *Timp1* were also significantly decreased after linagliptin treatment, while *Mmp2*, *Mmp9* were mildly reduced (albeit not significant; p=0.08 and 0.09, respectively) and *Timp2* levels was not significantly different between linagliptin- and placebo-treated obese ZSF1 rats (Figure 5.3E-J).

Linagliptin also mildly reduced heart weight/TL ratio and cardiomyocyte size, without reaching statistical significance (*p*=0.07 and 0.05, respectively, Figure 5.4A-C). This indicates both anti-fibrotic and mild anti-hypertrophic effects, in line with previous rodent studies[276,277].

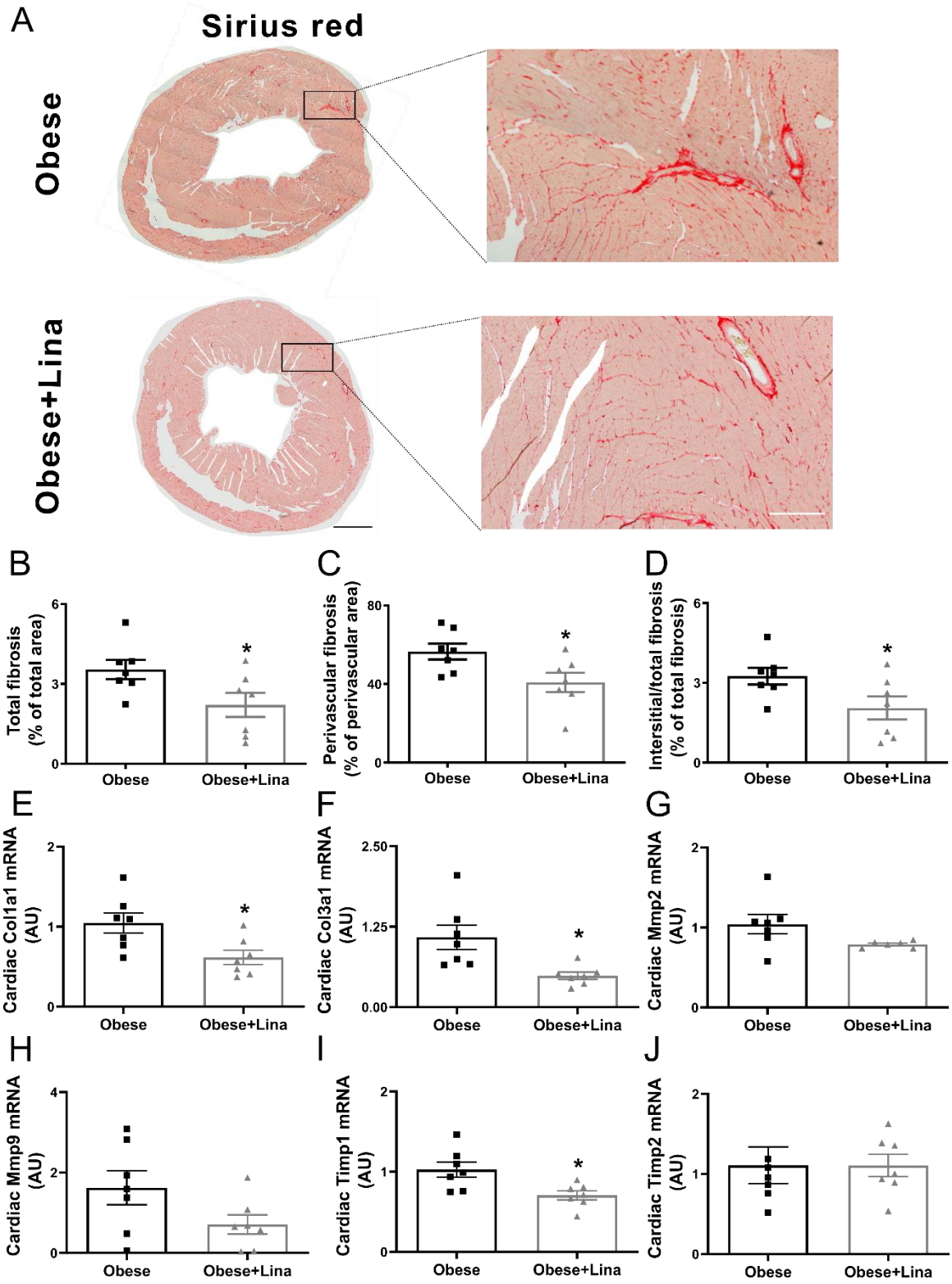

Figure 5.3- Linagliptin has anti-fibrotic effects in obese ZSF1 rats. A*) Representative images of cardiac fibrosis of Sirius red-stained sections in 20-weeks-old linagliptin- (Obese+Lina) and placebo-treated obese (Obese) ZSF1 rats (scale bar = 750 µm). The framed area represents the location for the zoomed images presented in the panel on the right (scale bar = 150 µm). Cardiac total (**B**), perivascular (**C**), and interstitial fibrosis (**D**) and gene expression levels of Col1a1 (**E**), Col3a1 (**F**), Mmp2 (**G**), Mmp9 (**H**), Timp1 (**I**), and Timp2 (**J**) in linagliptin- (Obese+Lina) and placebo-treated obese (Obese) ZSF1 rats at 20 weeks (both =7). Col, collagen; Mmp, matrix metalloproteinase; Timp, tissue inhibitor of matrix metalloproteinase. Data are expressed as mean ± SEM. All graphs were analysed using a two-tailed unpaired Student t-test, except J was analysed by a Mann-Whitney U test. * Indicates P<0.05.*

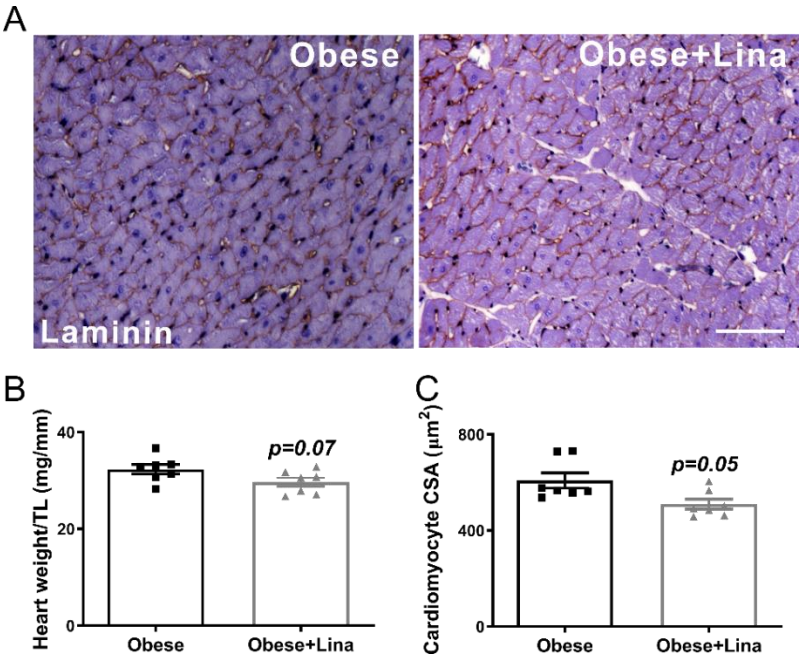

Figure 5.4- Linagliptin has anti-fibrotic effects without changing cardiomyocyte hypertrophy in obese ZSF1 rats. *Laminin-stained cardiac sections (**A**; scale bar = 100 µm) (A), heart weight/tibia length (**B**; TL), and cardiomyocyte cross-sectional area (**C**; CSA) in linagliptin- (Obese+Lina) and placebo-treated obese (Obese) ZSF1 rats (both n=7). Data are expressed as mean ± SEM. B and C were analysed by a Mann-Whitney U test.*

5.4.3 Linagliptin reduces cardiomyocyte passive stiffness by isoform switching to more flexible N2BA and post-translational modifications

The primary determinant of left ventricular stiffness in early diastolic dysfunction is an increased cardiomyocyte $F_{passive}$, mainly determined by modifications of the giant spring protein titin[51]. In the adult heart, titin has two predominant isoforms: the longer and more compliant N2BA isoform and the shorter and stiffer N2B isoform (Figure 5.5A). The adult human myocardium contains roughly similar amounts of the more compliant N2BA and stiffer N2B isoforms, while N2B is the predominant isoform in the rodent myocardium[278,279]. Titin isoform switching from the N2BA to the N2B isoform (reduced N2BA:N2B ratio) increases $F_{passive}$, as observed in diastolic dysfunction in HFpEF, while the inverse reduces $F_{passive}$, as shown in dilated cardiomyopathy (DCM) and hypothyroidism (HT) (Figure 5.5B)[280]. Linagliptin significantly reduced $F_{passive}$ in isolated cardiomyocytes from obese ZSF1 rats (Figure 5.5C), along with titin isoform switching from the stiffer N2B to the more flexible N2BA isoform (Figure 5.5D-E), resulting in an increased N2BA/N2B ratio (Figure 5.5F).

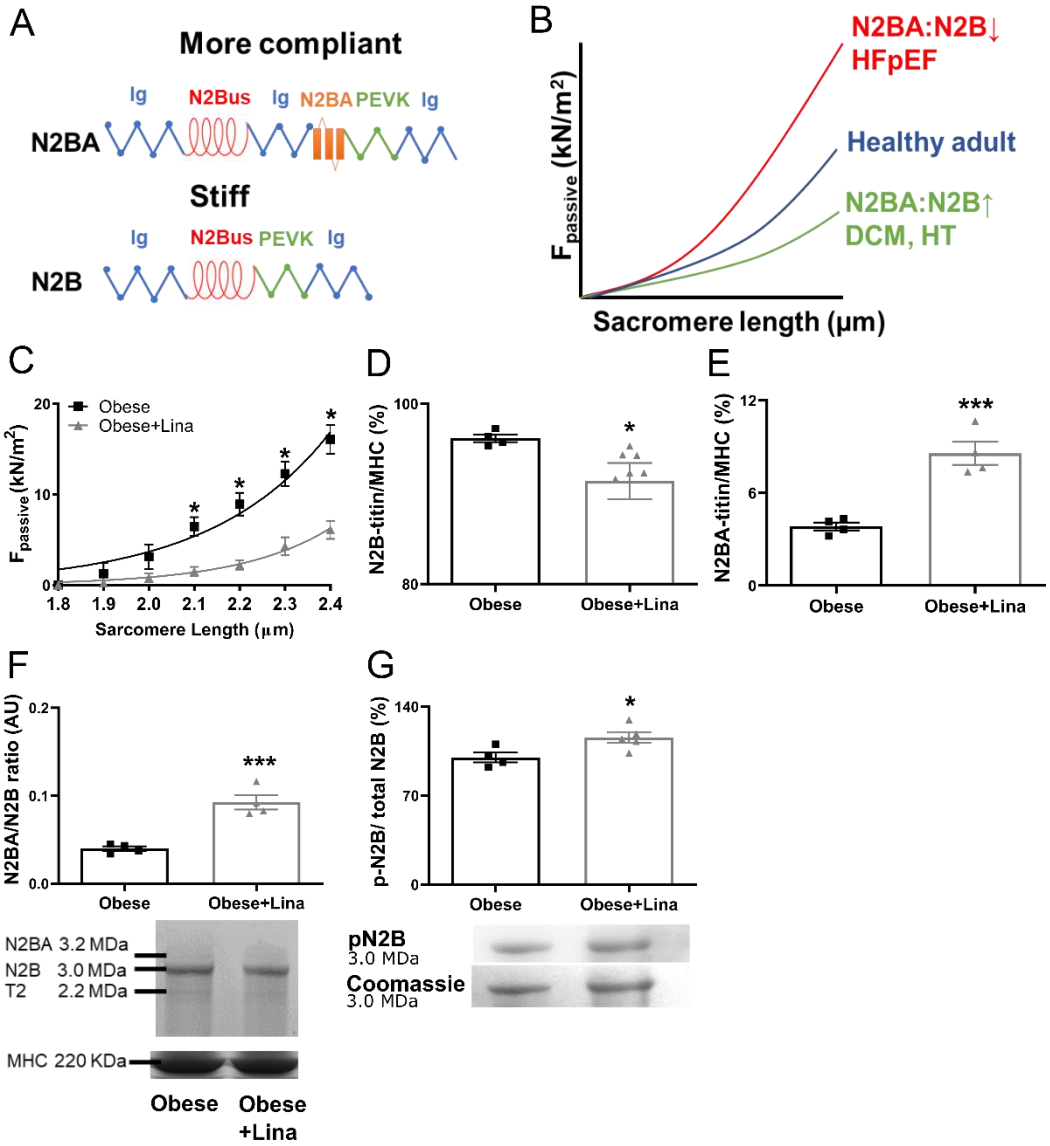

Figure 5.5- Linagliptin induces isoform switching and total titin phosphorylation in obese ZSF1 rats. A) *Composition of the I-band of the more compliant N2BA and stiffer N2B titin isoform. Blue, immunoglobulin (Ig) domain; red, N2B unique sequence (N2Bus) domain; green, PEVK domain; orange, N2BA domain.* ***B)*** *Consequence of isotype switching on $F_{passive}$. Titin isoform switching from the N2BA to the N2B isoform (reduced N2BA:N2B ratio) increases $F_{passive}$, as observed HFpEF, while the inverse reduces $F_{passive}$, as shown in dilated DCM and HT.* ***C)*** *$F_{passive}$ in isolated cardiomyocytes of linagliptin- (Obese+Lina) and placebo-treated obese (Obese) ZSF1 rats at 20 weeks (n=3 different left ventricular tissues and n=12 cardiomyocytes/tissue for each condition). N2B (**D**) and N2BA levels (**E**), N2BA/N2B titin isoform ratio and representative Coomassie Blue stained-PVDF membranes containing bands of N2BA, N2B, and titin-2 (T2; known degradation product), and loading control myosin heavy chain (MHC) (**F**) and total N2B titin phosphorylation and representative Coomassie Blue stained-PVDF membranes (**G**) in linagliptin- (Obese+Lina) and placebo-treated obese (Obese) ZSF1 rats at 20 weeks (n=4-7 per group). DCM, dilated cardiomyopathy; $F_{passive}$, passive stiffness; HFpEF, heart failure with preserved ejection fraction; HT, hypothyroidism; MHC, myosin heavy chain. Data are expressed as mean ± SEM. All data were analysed using a two-tailed unpaired Student t-test. * Indicates P<0.05 and ***P<0.001.*

In addition to isoform switching, phosphorylation of titin is also an important modulator of $F_{passive}$. Hypophosphorylation of the N2B titin isoform occurs in patients and animals with diastolic dysfunction[52,151]. Linagliptin increased titin N2B isoform phosphorylation in obese

ZSF1 rats (Figure 5.5G). The cardiac specific isoform N2B can be phosphorylated at the N2Bus and/or PEVK region within the I-band by various protein kinases, such as PKA, PKCα, PKG, and CAMKII. PKG phosphorylates the N2Bus segment at S4080 (conserved; called S4099 in humans) and hypophosphorylation is associated with increased $F_{passive}$ in patients with dilated and hypertrophic cardiomyopathy and canine HFpEF (Figure 5.6A)[274,281]. Linagliptin significantly increased cardiac PKG activity and thereby increased N2Bus S4080 phosphorylation in obese ZSF1 rats, implying a potential mechanism for the reduced $F_{passive}$ (Figure 5.6B-C). PKA phosphorylates titin at the N2Bus segment at S3991 (conserved; referred to S4010 in humans) and hypophosphorylation is associated with increased $F_{passive}$ (Figure 5.5A)[151]. Linagliptin also significantly increased cardiac PKA activity and PKA-dependent phosphorylation of the N2Bus S3391, which is associated with a reduced $F_{passive}$ (Figure 5.6D-E). In addition, titin is phosphorylated by CAMKII at the N2Bus region on S4043 (conserved; called S4062 in humans) and hypophosphorylation is associated with an increased $F_{passive}$ (Figure 5.6A)[282]. PKCα can also phosphorylate titin at PEVK S12742 (conserved; named S11878 in humans) and hyperphosphorylation is associated with an increased $F_{passive}$ (Figure 5.6A)[283]. Lastly, both CAMKII and PKCα phosphorylate titin at the PEVK region on S12884 (conserved; S12022 in humans) and CAMKII-mediated hypophosphorylation is associated with an increased $F_{passive}$ (Figure 5.6A)[151,282]. Linagliptin significantly reduced cardiac CAMKII and PKC activity in obese ZSF1 rats, while CAMKII-dependent phosphorylation at N2Bus S4043 and PEVK S12884 and PKC-dependent PEVK S12742 phosphorylation were not affected (Figure 5.6F-J). Thus, linagliptin reduces $F_{passive}$ by inducing isoform switching from the stiff N2B to the more flexible N2BA isoform and post-translational modifications of the giant spring protein titin, including increased phosphorylation of total titin, and PKG- and PKA-dependent site-specific phosphorylation of N2Bus S4080 and S3391, respectively.

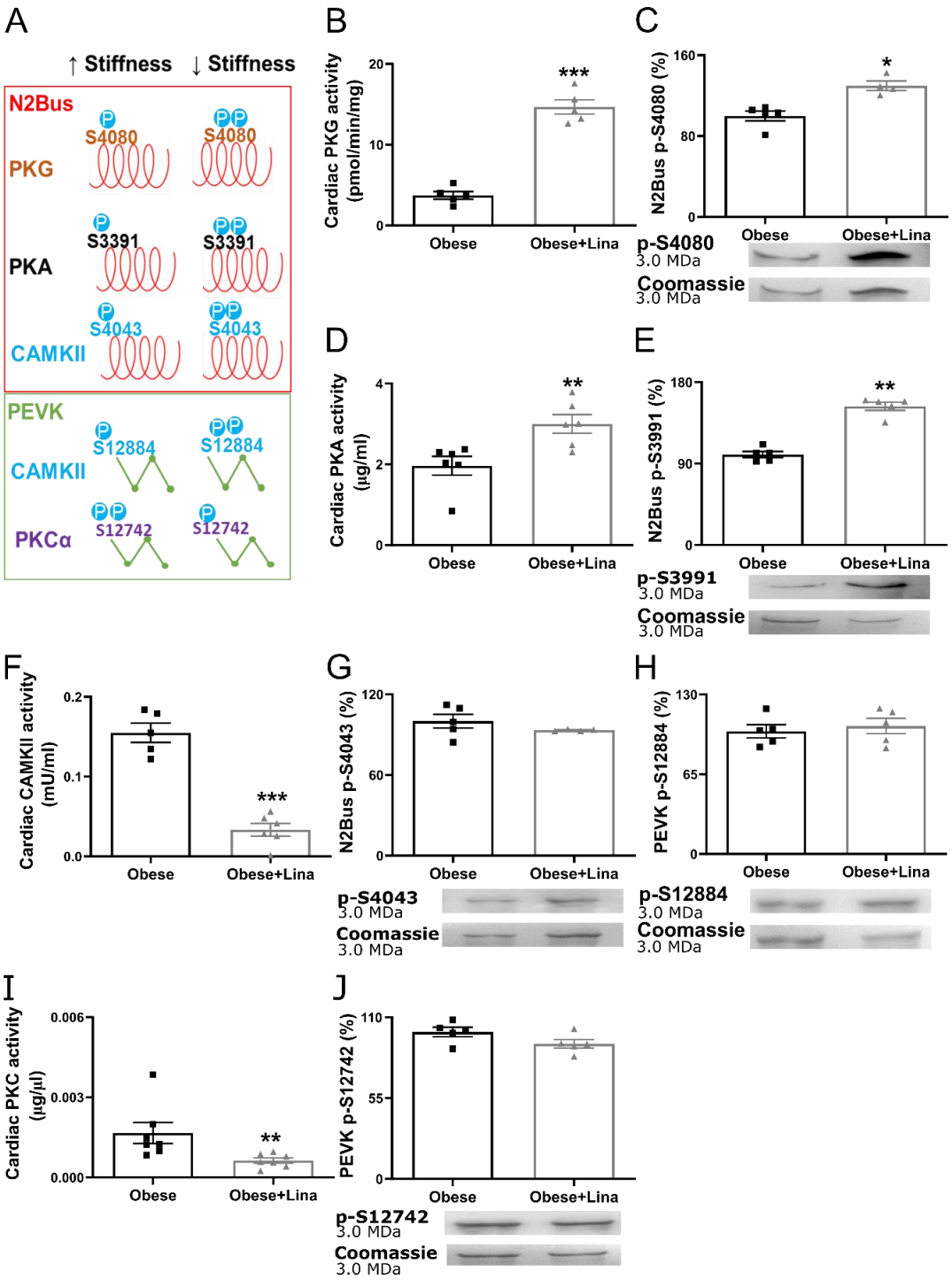

Figure 5.6- Linagliptin prevents N2Bus segment hypophosphorylation in obese ZSF1 rats. ***A****) Site-specific phosphorylation by protein kinases alters cardiomyocyte passive stiffness. Cardiac PKG activity (****B****), PKG-dependent N2Bus S4080 phosphorylation and representative Coomassie Blue stained-PVDF membranes (****C****), cardiac PKA activity (****D****), PKA-mediated N2Bus S3991 phosphorylation and representative Coomassie Blue stained-PVDF membranes (****E****), cardiac CAMKII activity (****F****), and CAMKII-mediated N2Bus S4043 phosphorylation and representative Coomassie Blue stained-PVDF membranes (****G****), and PEVK S12884 phosphorylation and representative Coomassie Blue stained-PVDF membranes (****H****), and PKC activity (****I****) and PKC-mediated PEVK S12742 phosphorylation and representative Coomassie Blue stained-PVDF membranes (****J****) in 20 week-old linagliptin- (Obese+Lina) and placebo-treated obese (Obese) ZSF1 rats (both n=5-7). CAMKII, calcium/calmodulin-dependent protein kinase II; N2Bus, N2B unique sequence; P, phosphorylation; PKA, protein kinase A; PKC, protein kinase C; PKG, protein kinase G. Data are expressed as mean ± SEM. B, F, G, and H were analysed using a two-tailed unpaired Student t-test, C-E and I were analysed by a Mann-Whitney U test. * Indicates P<0.05, **P<0.01, and ***P<0.001.*

5.4.4 Linagliptin prevents DPP-4-mediated titin cleavage in human cardiomyocytes

In addition to linagliptin's indirect cardioprotective effects by decreasing cardiometabolic risk factors, DPP-4 inhibitors may also have direct effects. While DPP-4 is predominantly expressed by coronary capillaries and immune cells, some cardiomyocytes also express DPP-4 within the cytosol[284,285]. Furthermore, gliptins (saxagliptin and sitagliptin) are internalized by cardiomyocytes and are subsequently localized in the cytosol[286,287]. As such, we investigated whether linagliptin could directly affect cardiomyocyte stiffness *in vitro*, in the absence of cardiometabolic risk factors. We incubated isolated human cardiomyocytes with either DPP-4, linagliptin and DPP-4, or vehicle control. Incubation with DPP-4 resulted in an increased $F_{passive}$ compared to control, while addition of linagliptin completely prevented the DPP-4-induced increase in $F_{passive}$ (Figure 5.7A). Importantly, treating cardiomyocytes with DPP-4 induced titin cleavage *in vitro*, while simultaneous linagliptin administration with DDP-4 prevented this (Figure 5.7B; cleavage products indicated with red asterisks). Visualization of titin protein levels at the full N2Bus and anti-PEVK domain of human N2B titin form revealed cleavage products after administration of DPP-4 *in vitro*, while simultaneous linagliptin and DPP-4 treatment prevented titin cleavage at both the full N2Bus and PEVK region (Figure 5.7C-D; cleavage products indicated with red asterisks). Thus, linagliptin may also prevent elevated passive stiffness in part by directly inhibiting DPP-4-mediated titin cleavage.

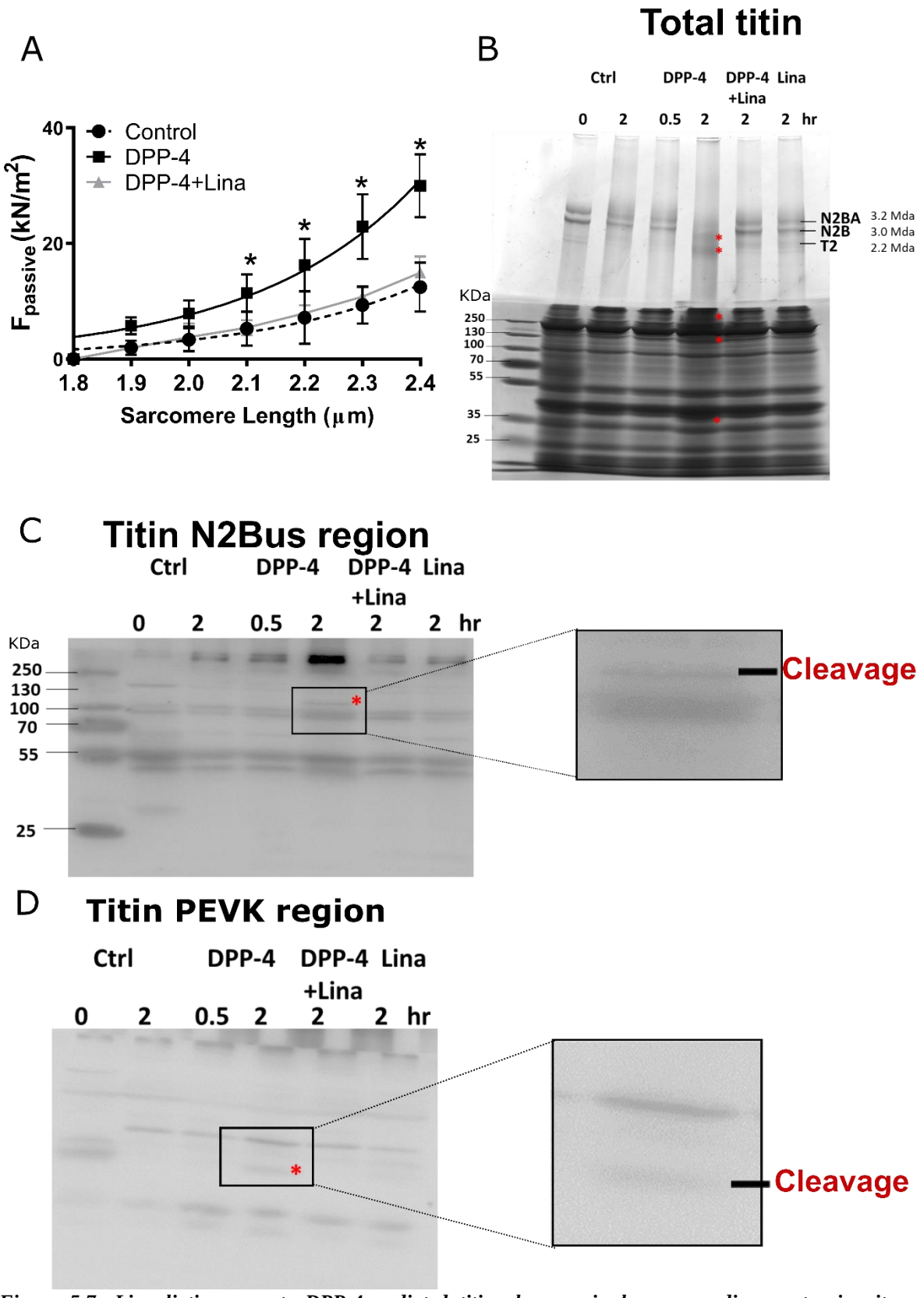

Figure 5.7- Linagliptin prevents DPP-4-mediated titin cleavage in human cardiomyocytes in vitro. A) *Cardiomyocyte passive stiffness in human cardiomyocytes treated with 300 ng/ml DPP-4, 100 nmol/L linagliptin and 300 ng/ml DPP-4, or control (DMSO/PBS) for 30 minutes (n=3 different left ventricular tissues measuring at least 12 cardiomyocytes from each left ventricular tissue per condition).* ***B)*** *Western blots of total titin, containing the two isoforms N2BA and N2B and the known degradation product titin-2 (T2) of human cardiomyocytes exposed to control PBS/DMSO (Ctrl) for 0 or 2 hours (lane 1 and 2, respectively), 300 ng/ml DPP-4 for 30 minutes and 2*

*hours (lane 3 and 4, respectively), 300 ng/ml DPP-4 and 100 nmol/L linagliptin for 2 hours (lane 5), or 100 nmol/L linagliptin alone for 2 hours (lane 6) (n=3 different left ventricular tissues). Titin cleavage is indicated by red asterisks. Western blots of the specific N2Bus region (**C**; cross-species conserved sequence QELLSKETLFP) and PEVK region (**D**; cross-species conserved sequence KLRPGSGGEKPP) of human cardiomyocytes exposed to control PBS/DMSO (Ctrl) for 0 or 2 hours (lane 1 and 2, respectively), 300 ng/ml DPP-4 for 30 minutes and 2 hours (lane 3 and 4, respectively), 300 ng/ml DPP-4 and 100 nmol/L linagliptin for 2 hours (lane 5), or 100 nmol/L linagliptin alone for 2 hours (lane 6) (n=3 different left ventricular tissues). Titin cleavage is indicated by red asterisks. The framed area represents the location for the zoomed images presented on the right side. Ctrl, control; DPP-4, dipeptidyl peptidase-4; $F_{passive}$, passive stiffness; Lina, linagliptin; N2Bus, N2B unique sequence. Data are expressed as mean ± SEM. Panel A was analysed using a two-tailed unpaired Student t-test with * indicating $P<0.05$*

5.5 Discussion

Here, linagliptin, a commonly used oral drug for the treatment of T2DM, significantly decreased left ventricular passive stiffness in a rat model of MetS-induced left ventricular dysfunction (Figure 5.8). The improvement of left ventricular passive stiffness upon linagliptin treatment was mainly caused by decreasing the first and main determinant of left ventricular stiffness, called cardiomyocyte $F_{passive}$. This reduced cardiomyocyte $F_{passive}$ was the result of the prevention of DPP-4 mediated-titin cleavage *in vitro*, as well as isotype switching from the stiff N2B isoform towards the more flexible N2BA titin isoform and increased total and site-specific phosphorylation of N2Bus titin at S4080 and S3391 *in vivo*. In addition, cardiac fibrosis, another determinant of left ventricular stiffening, which develops after cardiomyocyte stiffening, was decreased by linagliptin, as described before in individual models of either T2DM, obesity, or hypertension[276,277,288].

In addition to linagliptin's cardioprotective effects mediated by reducing metabolic risk factors (e.g. hyperglycaemia and hyperlipidaemia), we found that linagliptin directly prevented DPP-4-mediated cleavage of titin, specifically in the N2Bus and PEVK regions, resulting in decreased cardiomyocyte $F_{passive}$ *in vitro*. Breakdown of titin may predispose cardiomyocytes to diastolic dysfunction, myofilament instability, and cell death[289]. Our findings are in line with previous studies, where titin cleavage had been associated with cardiac stiffening and failure in humans[290] and targeted deletion of the N2Bus or PEVK region of the N2B titin isoform led to

increased $F_{passive}$ and diastolic dysfunction in mice[291,292]. Thus, part of the beneficial effect of linagliptin treatment on $F_{passive}$ and diastolic dysfunction may be explained by preventing DPP4-mediated titin cleavage.

The beneficial effect of linagliptin on cardiomyocyte stiffness *in vivo* was also accompanied by isoform switching from the stiff N2B isoform to the more compliant N2BA titin isoform in obese ZSF1 rats, most probably as a result of its positive effect on the components of the MetS, especially T2DM[293]. Interestingly, linagliptin is the first anti-cardiometabolic risk therapy that induces isotype switching to the more flexible N2BA isoform, while other therapies, like metformin[182] and exercise training[294], did not shown any changes in titin isoforms and another DPP-4 inhibitor sitagliptin even induced switching to the stiffer N2B isoform[184].

Linagliptin also increased total and site-specific phosphorylation of titin at N2Bus S3391 and S4080 in obese ZSF1 rats. In contrast to isoform switching, post-translational modifications of titin, including phosphorylation by kinases (e.g. PKG and PKA), provide a faster mechanism to change cardiomyocyte $F_{passive}$. Hypophosphorylation of the total N2B isoform contributes to increased $F_{passive}$ in human and animal hearts of HFpEF[151,189], while site-specific hypophosphorylation of N2Bus S3991 and S4080 occurs in rodent HFpEF[151,182] and T2DM models[183]. In line with our results, diabetic mice treated with sitagliptin had increased total titin phosphorylation, which were suggested to be partly mediated by stimulatory effects on the myocardial PKG pathway[184]. However, sitagliptin's effects on site-specific phosphorylation and cleavage of titin were not assessed in this study. Furthermore, as patients suffering from the MetS often represent with renal impairments, linagliptin is preferred as it is uniquely primarily eliminated via a non-renal route[295], while sitagliptin is predominantly excreted via the kidneys and requires dose adjustments in patients with renal dysfunction[296]. Altogether, linagliptin reduces cardiomyocyte stiffness by increasing titin total and site-specific phosphorylation at N2Bus S4080 and S3991.

Limitations

We only used male ZSF1 rats, as the model was established in males and few studies have investigated HFpEF development in female rats[224]. However, we do not rule out that females might respond differently. While in chapter 3, the usage of isoflurane as an anaesthetic during echocardiography is debated, this study was performed before the time that the critical influences of anaesthesia on echocardiography parameters became clear. As such, we could only make limited conclusions about the cardiac function. Nevertheless, obese ZSF1 rats (n=7) showed signs of diastolic dysfunction, including an increased IVRT and deceleration time, a trend towards increased E/E' ratio, and a unaffected E/A ratio compared to a small group of lean control ZSF1 rats (n=4). This suggests that the obese ZSF1 rats suffered from an intermediate grade of diastolic dysfunction between grade I impaired relaxation and grade II pseudonormal relaxation. This impaired cardiac relaxation was also in line with the increased cardiomyocyte stiffness observed in obese compared to lean ZSF1 rats. Furthermore, we did not assess the effect of linagliptin on hypertension. Nevertheless, several previously published articles reported that linagliptin did not affect the diastolic and systolic blood pressure in patients with T2DM[297] and salt-sensitive hypertensive rats[277].

In short, linagliptin decreased left ventricular stiffness in metabolic risk-induced cardiovascular disease. Linagliptin reduced cardiomyocyte $F_{passive}$ by modifying titin's isoform levels and total and site-specific phosphorylation indirectly via its beneficial effect on the metabolic risk factors. Importantly, linagliptin also directly reduces cardiomyocyte $F_{passive}$ by preventing DPP-4 mediated titin cleavage. Whereas in human clinical studies DPP-4 inhibition does not prevent HF hospitalisations, it remains unknown whether it may prevent the development of early diastolic dysfunction and the progression towards HFpEF. Reducing left ventricular stiffness

by administering linagliptin might therefore be considered as a potential strategy for the prevention and treatment of metabolic risk-induced cardiac diastolic dysfunction in humans.

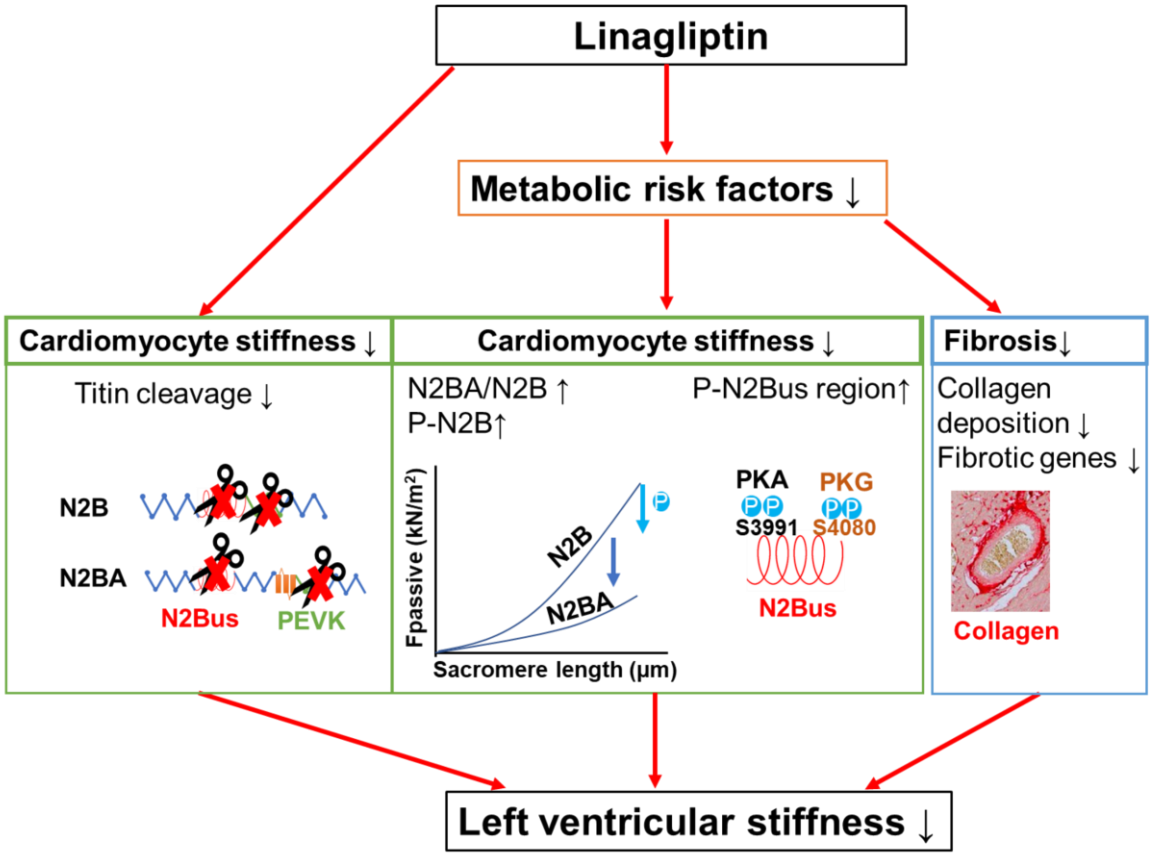

Figure 5.8- Proposed mechanism underlying the reduced left ventricular stiffening in metabolic syndrome-induced cardiac disease after linagliptin administration. *$F_{passive}$, passive stiffness; N2Bus, N2B unique sequence; PKA, protein kinase A; PKG, protein kinase G.*

Chapter 6: General discussion and conclusion

Inappropriate diagnosis, incomplete understanding of the pathophysiology, and patient heterogeneity hamper the development of effective therapeutics for HFpEF. In this thesis, we provide (i) awareness for the usage of anaesthetics in echocardiography, (ii) novel insights in the pathological development of HFpEF, and (iii) a potential novel therapy for increased left ventricular stiffness, as observed in HFpEF.

6.1 Development of animal models mimicking human pathophysiology is crucial

A critical obstacle in the therapeutic innovation in HFpEF is the absence of animal models that accurately mimic the heterogenic complexity of human pathology. Most of the developed animal models focus on using one HFpEF-associated comorbidity to induce one of the key pathological processes (e.g. diastolic dysfunction), rather than using a multiple systemic approach in which a **plethora of HFpEF comorbidities**, such as in the obese ZSF1 rats, induces **multiple key pathological processes**. As a result, the disease mechanisms that are discovered may be influenced by the short comings to account for comorbidities, age, gender, and hormonal status of current experimental animal models. Furthermore, HFpEF-associated comorbidities are often induced using non-physiological genetic (e.g. leptin receptor, hypertensive gene mutations), surgical (e.g. aortic banding), and/or pharmacological manipulations (e.g. L-Name, streptozotocin), rather than mimicking the **natural development** of these comorbidities in HFpEF patients[126]. Moreover, most of the HFpEF animal models are rodents, due to their ease to handle and house, inexpensiveness, short gestation time, and possibility of genetic manipulation. Despite their widespread use, rodents are phylogenetically very distant from humans and (patho)physiological features (e.g. higher HR) and responses to treatments may differ substantially[142,298]. For example, HFpEF rodent models often progress towards HFrEF, while this is uncommon in HFpEF patients[126]. In contrast to small rodent

models, larger animal's cardiac (patho)physiology is more similar to humans, however, high costs, ethical concerns, and difficulties in transgenesis and handling still limit their usage. Given that HFpEF is such a clinically heterogeneous disease, there may therefore **not** be one **single uniting pathological mechanism** driving the disease and thus having **multiple physiological pre-clinical animal models** that can be compared to human pathophysiology is critical.

6.2 An urgent need for an improved diagnosis of HFpEF

Another hurdle in the therapeutic innovation is the inadequate and late diagnosis, as symptoms of HFpEF are not-disease specific and are often difficult to interpret in patients suffering from multiple comorbidities[27-29,299]. Echocardiography is the preferred method for quantitative diagnosis of patients with suspected HFpEF patients and animal models mimicking human HFpEF[25], but the lack of standardization of echocardiography may result in unreliable and non-repeatable results[300]. Furthermore, as the prevalence of HFpEF and the number of surgical procedures dramatically increases with ageing, the need for perioperative echocardiography-mediated diagnosis of diastolic dysfunction requiring anaesthetics increases. In line with our findings in rodent HFpEF (Chapter 3), the usage anaesthesia (e.g. sevoflurane and isoflurane) resulted in underdiagnosis in patients with diastolic dysfunction[210,211]. This further underlines that **well-considered evaluation of anaesthetics** during **perioperative echocardiography-mediated diagnosis of diastolic dysfunction** is required in patients[212,301].

While multiple algorithms and definitions have been proposed, risk stratification of HFpEF is still not achieved[30]. However, as HFpEF is very heterogenous, there could be questions whether HFpEF should be considered as one disease or rather or spectrum of many diseases[302]. As such, there is an urgent need for an **improved clinical definition** of HFpEF, likely to be driven by the development of novel diagnostic tools, such as cardiac and non-cardiac imaging strategies

(e.g. MRI, Glycocheck) to assess microvascular regression as an early biomarker for risk stratification (Chapter 4).

6.3 A novel paradigm for HFpEF

While HFpEF was defined for the first time at the start of 2000, it took almost 10 years before the first hypothetical description on the development of HFpEF was published by Paulus et al.[50]. The pathological description of HFpEF development in this paradigm was merely based on established HFpEF in rodents and patients, rather than disease progression and early characteristics of HFpEF (Chapter 4). In **our revised paradigm** (Figure 6.1), we introduce for the first time the importance of **active microvascular regression** due to **decreased pericyte coverage** in the progression towards HFpEF. In contrast to the paradigm of Paulus et al., we show that both **systemic and cardiac inflammation** are rather **late events** in the development of HFpEF and this therefore rejects the hypothesis that systemic inflammation is the major driver for endothelial dysfunction. Moreover, we show that cardiomyocyte hypertrophy and microvascular dysfunction (activation, junctional remodelling, pericyte loss, and active regression) occur simultaneously before the development of diastolic dysfunction, fibrosis, and inflammation. Previous findings in young pre-diabetic rats showed that diastolic dysfunction and cardiomyocyte stiffening were present without any alterations in endothelium-dependent function[254]. However, this study focused on arteriolar function within the microcirculation and did not investigate capillary vessels. In addition to the importance of microvascular dysfunction, we showed the deteriorating direct role of **DPP-4** in increasing cardiomyocyte stiffness by inducing **titin cleavage** (Chapter 5). While titin truncation and cleavage has been reported in dilated cardiomyopathy and myocardial ischaemia/reperfusion injury, respectively[303,304], its role in diastolic dysfunction and HFpEF was never shown before.

In short, while the paradigm of Paulus et al. gives a comprehensive overview of the involved pathological processes in HFpEF, revised evaluation of both the time frame and triggers of these processes is required. As such, the development of pathological processes (e.g. vascular abnormalities, inflammation, fibrosis, hypertrophy, cardiomyocyte stiffness, titin changes, and diastolic dysfunction) should be assessed over time in multiple physiological pre-clinical animal models with different HFpEF-associated comorbidities that can be compared to human pathophysiology. In addition, the causal involvement of each of these pathological processes in the development of HFpEF should be investigated. For example, to determine whether pericyte loss is the driving factor of HFpEF development, a mouse model with cardiac-specific pericyte loss should be created and the development of HFpEF should be assessed over time.

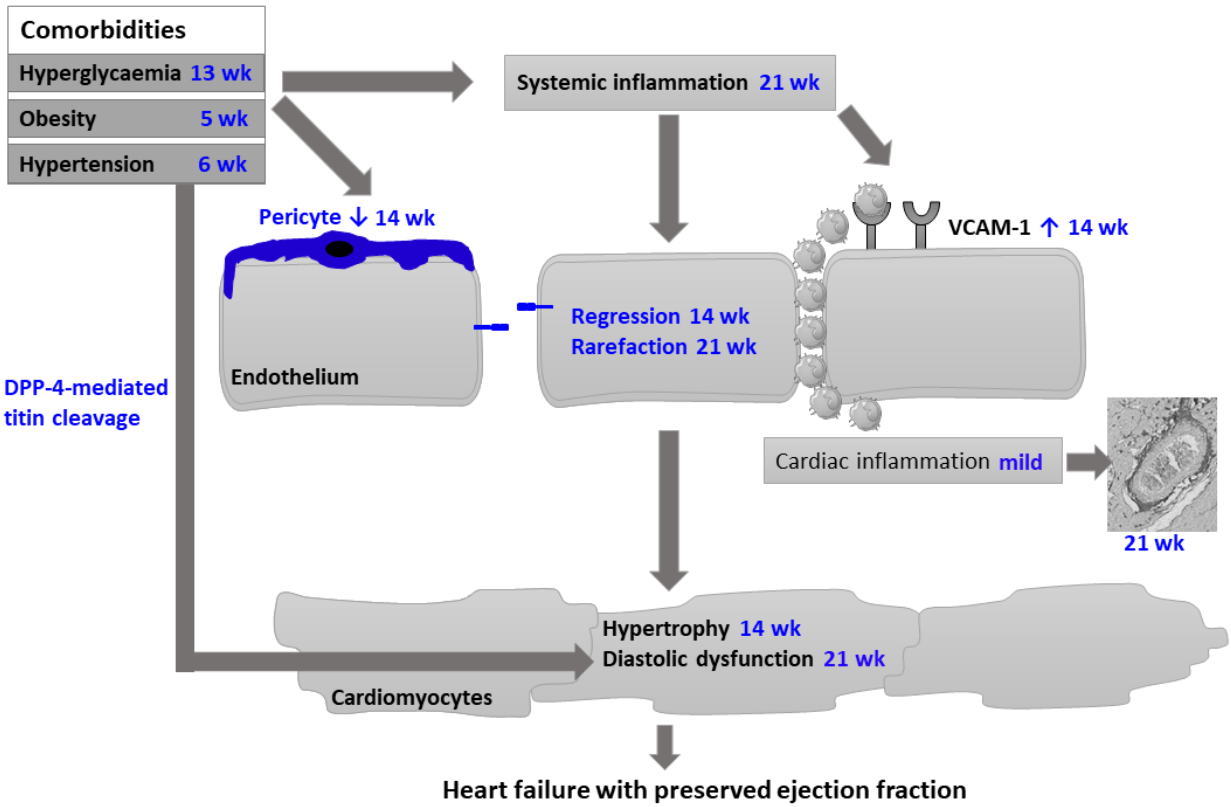

Figure 6.1- Novel paradigm for HFpEF. *Cardiac microvascular endothelial abnormalities induced by a cluster of HFpEF-associated risk factors (obesity, hypertension, and T2DM) are the central mediator of HFpEF development. These microvascular endothelial abnormalities are characterised by junctional remodelling, endothelial activation (VCAM-1 expression), reduced pericyte coverage, active regression, ultimately leading to microvascular rarefaction in established HFpEF. These cardiac microvascular endothelial abnormalities coincide with cardiomyocyte hypertrophy and occur before the development of systemic inflammation and cardiac abnormalities (inflammation, fibrosis, and diastolic dysfunction). Increased dipeptidyl-peptidase-4 levels associated with the comorbidities induce directly diastolic dysfunction by inducing titin cleavage. Time points*

indicate at which age, an established HFpEF rodent model, the obese ZSF1 rat, the corresponding key pathological process developed. New mechanistical insights discovered in this thesis are given in blue.

6.4 A step ahead towards effective therapy for HFpEF

In this thesis, we provide novel therapeutic targets and approaches for HFpEF. First, we showed that the currently used anti-T2DM drug **linagliptin prevented left ventricular stiffening**, an early characteristic of diastolic dysfunction (Chapter 4). As such, linagliptin might be a potential therapeutic strategy for metabolic risk-induced diastolic dysfunction in HFpEF.

In addition, we showed that **pericyte loss** plays an important role in HFpEF disease progression (Chapter 4). However, only a few therapeutic strategies targeting pericytes exist, including pericyte **transplantation** and **interference with pericyte signalling**, such as **PDGFβ/PDGFβR** and **ANGPT1/2**, have been investigated. Pericyte transplantation in murine myocardial infarction decreased cardiac fibrosis, immune infiltration, and increased angiogenesis resulting in improved cardiac contractility[305]. Similarly, transplantation of human adipose-derived pericytes protected against diabetic retinopathy by promoting angiogenesis and vascular support[306]. Although autologous transplantation is preferable to use, pericytes may be deficient in number and/or function in HFpEF-associated risk factors, such as T2DM[307,308]. Enhancement of PDGFβR signalling has also been proposed as a therapy, as it is important for pericyte recruitment to blood vessels and survival. **Thalidomide**, an immunomodulating agent applied in cancer and rheumatic disease, has been proposed to induce pericyte proliferation and recruitment to capillaries by increasing *Pdgfβr* expression[309]. Thalidomide has been shown to reduce blood-brain-barrier permeability, vascular malformations, and cardiotoxicity in experimental models of Alzheimer Disease, hereditary haemorrhagic telangiectasia, and sunitinib-induced cardiotoxicity, respectively[309-311]. However, thalidomide is associated with cardiovascular complications (bradycardia, peripheral oedema, orthostatic hypertension, thrombosis)[312]. Furthermore, *Pdgfβr* expression is not limited to pericytes but is also expressed

on fibroblasts and vSMCs[313] and increased PDGFβR activation is associated with elevated pericyte differentiation in myofibroblast, resulting in excessive renal fibrosis and injury *in vivo*[314]. In addition to PDGFβ/ PDGFβR signalling, ANGPT1/ANGPT2 mediates vascular stability: ANGPT1 stabilises vessels by inducing the release of pericyte recruitment factors from endothelial cell, while endothelial expression of ANGPT2 promotes vessel destabilization and is associated with poor pericyte coverage. In line with these findings, we observed increased *Angpt2* expression in endothelial cells stimulated with high glucose or H_2O_2 (Chapter 4). Interestingly, endothelial-specific depletion of *Angpt2* attenuated pericyte detachment and ameliorated post ischaemic cardiovascular remodeling[252], suggesting ANGPT2 inhibition as a potential therapy.

In Chapter 4, we observed dysregulation of genes (*Ptges1*, *Akr1b1*, *P4ha1*, and *Ier3*) involved in the **prostaglandin pathway** in pericytes in either an oxidative stress, hyperlipidaemic, or hyperglycaemic environment. Elevated Ptges-mediated prostaglandin E2 (PGE2) synthesis is associated with inflammation, vasodilation, vascular permeability, and endothelial dysfunction[315,316]. On the other hand, Akr1b1-mediated prostaglandin F2alpha (PGF2α) synthesis promotes inflammation, vasoconstriction, hypertension, and myocardial fibrosis and hypertrophy[317]. Interestingly, PGF2α protein expression is increased in HFpEF-associated comorbidities, including obesity, T2DM, elderly and decreased PGF2α protein expression is associated with a lower susceptibility to cardiovascular diseases[318-321]. Targeting the prostaglandin pathway by inhibiting PTGES1 and/or AKR1B1 might potentially prevent microvascular and cardiac remodelling and dysfunction.

In short, while several therapeutics have been investigated, no specific pericyte therapy is investigated in clinical studies. This is particularly hampered by (i) the **scarcity of tools to study pericytes**, (ii) **off-target effects** of the above proposed medicines, (iii) **non-specific delivery** to the target organ, and (iv) the pericyte **microenvironment**. The limited tools to study

pericytes have been especially complicated by the fact that there is no single unique molecular marker that can be used to unequivocally identify pericytes. Current strategies to identify pericytes therefore mostly rely on their morphology, proximity to the endothelium, and assessment of several well-established markers (e.g. NG2, PDGFβR). Recently, an inducible pericyte-specific Cre mouse line was developed using a double promotor approach with *Ng2* and *Pdgfβr* in which pericyte-specific cell death could be induced by crossing with iDTR mice followed with diphtheria toxin[258]. Furthermore, as pericytes are present around all microvessels in all organs, targeted delivery of pericytes itself or therapeutic agents stimulating pericyte recruitment, is essential to prevent accumulation of pericytes, which is associated with aggressive cancers[322]. Lastly, the efficiency of pericyte therapy is highly dependent on the capacity of pericytes to survive and function within the hyperglycaemic, hyperlipidaemic, and oxidative cardiac environment[262], therefore combining pericyte therapy with additional therapies that could ameliorate the comorbidities (e.g. linagliptin) is expected to be more efficient.

Scientific Acknowledgements

Aspects of introduction were written in collaboration with Dr. S. Simonds, the LYMIT-DIS network, and ESC working group. We acknowledge Prof. B. de Geest and P. Herijgers (KU Leuven) for the PV loop and blood pressure machine, respectively. I thank P. Carai (KU Leuven) for echocardiographical image acquisition; P. Mendes-Ferreira and D. Miranda-Silva (University of Porto, Portugal) for the PV loop acquisition; Prof. P. Mulder (University of Rouen, France) for the supply of ZSF1 rats and ivabradine; Prof. N Hamdani and M. Herwig and Prof. A Mügge (Ruhr University Bochum, Germany) for the titin experiments. I would like to thank L. Vertommen (KU Leuven) for her technical assistance during her master thesis internship. I would like to thank P. Carai (KU Leuven) and S. Simmonds (KU Leuven) for their technical assistance and helpful discussions for the Chapters. I would like to thank A. Tabibian (KU Leuven) for the discussions about cell culture. Lastly, I would like to thank Prof. A. Luttun (KU Leuven) for the supply of antibodies. H. Peacock (KU Leuven) proofread Chapter 3 and 5. Co-authors on papers edited the manuscripts. Prof. Dr. E.A.V. Jones (KU Leuven) edited this thesis manuscript.

This work was supported by Fonds Wetenschappelijk Onderzoek grant [1160718N, 9091018N], the European Research Area Network Cardiovascular disease [LYMIT-DIS 2016, MacroERA], IMI2-CARDIATEAM [N° 821508], Netherlands Organization for Scientific Research [NWO Vidi 91796338], and the Dutch Heart Foundation [CVON2016-Early HFPEF, CVON She-PREDICTS, CVON Arena-PRIME]. Chapter 5 was supported by Boehringer Ingelheim International GmbH [DE 811138149].

Personal Contribution

Together with Prof. E.A.V. Jones (Chapter 3-5) or Dr. Anna-Pia Papageorgiou and Prof. S. Heymans (Chapter 5), I designed, organised, performed, and analysed all the experiments and wrote the manuscript, except where indicated. For the linagliptin study, parts were already performed before the start of my PhD. However, I was responsible for the analysis, finishing up, and design of new experiments. I was responsible for writing all the manuscripts and reviews and this thesis.

Conflict of Interest Statement

The are no conflicts of interest to be reported.

Valorisation

Socio-economic Relevance

HF is the most prominent cause of hospitalisation globally, with 3.6 million newly diagnosed patients annually[1], and its prevalence is expected to increase by 46% in 2030[323]. More than half of these HF patients suffer from HFpEF and this number is expected to rise even further due to the ageing population and increased survival of patients with non-cardiac comorbidities[324]. HFpEF prognosis is poor with a severely impaired quality of life and high hospital readmission and mortality rate[20,21], resulting in soaring long-term cost are due to increasing emergency rehospitalisations[22]. While significant advancements have been made in the treatment of HFrEF, to date no specific efficient treatments are available for HFpEF due to incomplete pathophysiological understanding, patient population heterogeneity, and inadequate diagnosis[23,24].

Our results are a first step forward in improved therapy for HFpEF patients by a) better understanding of anaesthesia in **diagnosis**, b) **elucidating the understanding of the pathophysiology**, b) and c) identifying novel **prevention/treatment strategies** using a rodent model mimicking human HFpEF.

Echocardiography is the preferred method for diagnosis of patients with suspected HFpEF patients animal models mimicking human HFpEF. In Chapter 3, we show that the **type of anaesthetic** can **influence** the **diagnosis** of **diastolic dysfunction** in a HFpEF-diseased rodent model. Anaesthetic usage during echocardiography acquisition to assess HFpEF progression in animal models is essential. Furthermore, as the prevalence of HFpEF and the number of surgical procedures increases dramatically with ageing, perioperative echocardiography-mediated diagnosis of diastolic dysfunction requiring anaesthetics increases proportionally[301]. This underlines that **well-considered evaluation of anaesthetics** during **echocardiographical**

diagnosis of diastolic dysfunction is required both in **patients** and **pre-clinical animal models**.

Chapter 4 shows for the first time that cardiac microvascular regression is an early event in the development of HFpEF, occurring before the onset of diastolic dysfunction**.** These new insights underline that the **microvascular paradigm originally proposed by Paulus et al.** should be **revised,** and further research should be executed regarding the role of microvascular regression in HFpEF. **Diagnosis of microvascular regression** by usage of **advanced imaging techniques** (e.g. MRI, optical coherence angiography, Glycocheck etc; Horizon2020, E.A.V. Jones) will allow us to **earlier diagnose** HFpEF in suspected patients. Furthermore, we show that cardiac microvascular regression is associated with a reduced coverage of cells that stabilise the small blood vessels, also called pericytes. **Prevention of pericyte loss** in the heart of susceptible patients could **prevent disease progression** to HFpEF.

Chapter 5 shows that linagliptin significantly reduces cardiometabolic risk-induced left ventricular stiffness by reducing titin cleavage and hypophosphorylation. This is the first study showing the importance of titin cleavage in diastolic dysfunction, indicating that the microvascular paradigm originally proposed by Paulus et al. should be revised. Reducing left ventricular stiffness by **linagliptin** might be a potential **prevention and treatment strategy for HFpEF**. Currently, Boehringer investigates linagliptin as a treatment for HFpEF in clinical trials.

Target Groups, Products, Activities, and Future Directives

First of all, the effect of anaesthesia on diastolic dysfunction diagnosis are poorly known. In Chapter 3, we create more awareness for the effect of anaesthesia on diastolic function assessment. Furthermore, the pathophysiology underlying HFpEF is currently poorly

understood. Most research focusses on established HFpEF, while early stages are poorly investigated. In Chapter 4, we provide new insights in the development of HFpEF, using a rodent model mimicking human early, intermediate, and established HFpEF. It crucially underlines that the microvascular hypothesis for HFpEF development needs to be revised, thereby stimulating the **scientific community** to further investigate early stages of HFpEF. Lastly, in Chapter 5 we show the importance of drug repurposing in HFpEF prevention. In order to reach the scientific community, we have published our observations in peer-reviewed scientific journals and discussed the data at several national and international congresses.

Especially **patients suffering from a cluster of non-cardiac comorbidities** and **elderly**, **predominantly female subjects**, have an increased risk of developing HFpEF. As the number of surgical procedures dramatically increases with ageing, caution should be taken when diastolic dysfunction is assessed during perioperative echocardiography using anaesthesia. Furthermore, assessment of microvascular regression in these high-risk patients could provide an early diagnosis strategy. Currently, the diagnostic potential of microvascular regression is investigated by Prof. E.A.V. Jones (Horizon2020 project) aiming to non-invasively diagnose HFpEF patients at an early stage. If these susceptible patients represent with an increased microvascular regression, pericyte-targeted therapies, preventing microvascular regression, in combination with linagliptin, reducing left ventricular stiffness, could prevent the progression towards HFpEF. In established HFpEF patients, linagliptin and pericyte-targeted therapies might prevent deterioration of the disease. In order to explain our findings to the general public and patients, I presented our research at the Pint of Science festival Belgium in 2019 and joined the organization to improve science communication to the general public.

The involvement of microvascular regression is increasingly becoming more apparent in various **other cardiovascular (e.g. HFrEF), renal (e.g. chronic kidney disease), retinal (e.g. diabetic retinopathy), and neurological diseases (e.g. vascular cognitive impairment,**

dementia), while underlying causal triggers of microvascular regression and the resultant molecular pathways are poorly understood. The Horizon2020 grant aims to identify molecular mechanisms (reduced pericyte coverage) underlying microvascular regression and to assess whether microvascular regression could be used as a non-invasive diagnostic marker for vascular cognitive impairment. Thus, this thesis provides far-reaching insides in microvascular regression development beyond HFpEF and the cardiology community. Furthermore, patients with diabetic cardiomyopathy, hypertensive cardiomyopathy, hypertrophic cardiomyopathy, aortic stenosis, and dilated cardiomyopathy show an increased left ventricular stiffness[183,325-327], however linagliptin's potential benefit on left ventricular stiffness in these cardiovascular diseases has never investigated. This thesis could therefore provide potential prevention strategies for other cardiovascular diseases.

List of References

1 Ambrosy, A. P. *et al.* The global health and economic burden of hospitalizations for heart failure: lessons learned from hospitalized heart failure registries. *J Am Coll Cardiol* **63**, 1123-1133, doi:10.1016/j.jacc.2013.11.053 (2014).

2 He, J. *et al.* Risk factors for congestive heart failure in US men and women: NHANES I epidemiologic follow-up study. *Arch Intern Med* **161**, 996-1002, doi:10.1001/archinte.161.7.996 (2001).

3 Vedin, O. *et al.* Significance of Ischemic Heart Disease in Patients With Heart Failure and Preserved, Midrange, and Reduced Ejection Fraction: A Nationwide Cohort Study. *Circ Heart Fail* **10**, doi:10.1161/CIRCHEARTFAILURE.117.003875 (2017).

4 Koh, A. S. *et al.* A comprehensive population-based characterization of heart failure with mid-range ejection fraction. *Eur J Heart Fail* **19**, 1624-1634, doi:10.1002/ejhf.945 (2017).

5 Kapoor, J. R. *et al.* Precipitating Clinical Factors, Heart Failure Characterization, and Outcomes in Patients Hospitalized With Heart Failure With Reduced, Borderline, and Preserved Ejection Fraction. *JACC Heart Fail* **4**, 464-472, doi:10.1016/j.jchf.2016.02.017 (2016).

6 Jeong, E. M. & Dudley, S. C., Jr. Diastolic dysfunction. *Circ J* **79**, 470-477, doi:10.1253/circj.CJ-15-0064 (2015).

7 Ho, J. E. *et al.* Predictors of new-onset heart failure: differences in preserved versus reduced ejection fraction. *Circ Heart Fail* **6**, 279-286, doi:10.1161/CIRCHEARTFAILURE.112.972828 (2013).

8 Ergatoudes, C. *et al.* Non-cardiac comorbidities and mortality in patients with heart failure with reduced vs. preserved ejection fraction: a study using the Swedish Heart Failure Registry. *Clin Res Cardiol* **108**, 1025-1033, doi:10.1007/s00392-019-01430-0 (2019).

9 Streng, K. W. *et al.* Non-cardiac comorbidities in heart failure with reduced, mid-range and preserved ejection fraction. *Int J Cardiol* **271**, 132-139, doi:10.1016/j.ijcard.2018.04.001 (2018).

10 Davis, J. M., 3rd *et al.* Five-year changes in cardiac structure and function in patients with rheumatoid arthritis compared with the general population. *Int J Cardiol* **240**, 379-385, doi:10.1016/j.ijcard.2017.03.108 (2017).

11 Lee, D. S. *et al.* Relation of disease pathogenesis and risk factors to heart failure with preserved or reduced ejection fraction: insights from the framingham heart study of the national heart, lung, and blood institute. *Circulation* **119**, 3070-3077, doi:10.1161/CIRCULATIONAHA.108.815944 (2009).

12 Duca, F. *et al.* Gender-related differences in heart failure with preserved ejection fraction. *Sci Rep* **8**, 1080, doi:10.1038/s41598-018-19507-7 (2018).

13 Krumholz, H. M., Larson, M. & Levy, D. Sex differences in cardiac adaptation to isolated systolic hypertension. *Am J Cardiol* **72**, 310-313, doi:10.1016/0002-9149(93)90678-6 (1993).

14 Li, S. & Gupte, A. A. The Role of Estrogen in Cardiac Metabolism and Diastolic Function. *Methodist Debakey Cardiovasc J* **13**, 4-8, doi:10.14797/mdcj-13-1-4 (2017).

15 Matthews, K. A. *et al.* Are changes in cardiovascular disease risk factors in midlife women due to chronological aging or to the menopausal transition? *J Am Coll Cardiol* **54**, 2366-2373, doi:10.1016/j.jacc.2009.10.009 (2009).

16 Bokslag, A. *et al.* Early-onset preeclampsia predisposes to preclinical diastolic left ventricular dysfunction in the fifth decade of life: An observational study. *PLoS One* **13**, e0198908, doi:10.1371/journal.pone.0198908 (2018).

17 Pfeffer, M. A., Shah, A. M. & Borlaug, B. A. Heart Failure With Preserved Ejection Fraction In Perspective. *Circ Res* **124**, 1598-1617, doi:10.1161/CIRCRESAHA.119.313572 (2019).

18 Tsao, C. W. *et al.* Temporal Trends in the Incidence of and Mortality Associated With Heart Failure With Preserved and Reduced Ejection Fraction. *JACC Heart Fail* **6**, 678-685, doi:10.1016/j.jchf.2018.03.006 (2018).

19 Shah, A. M. *et al.* Heart Failure Stages Among Older Adults in the Community: The Atherosclerosis Risk in Communities Study. *Circulation* **135**, 224-240, doi:10.1161/CIRCULATIONAHA.116.023361 (2017).

20 Savarese, G. & Lund, L. H. Global Public Health Burden of Heart Failure. *Card Fail Rev* **3**, 7-11, doi:10.15420/cfr.2016:25:2 (2017).

21 Lewis, E. F. *et al.* Characterization of health-related quality of life in heart failure patients with preserved versus low ejection fraction in CHARM. *Eur J Heart Fail* **9**, 83-91, doi:10.1016/j.ejheart.2006.10.012 (2007).

22 Murphy, T. M. *et al.* A comparison of HFrEF vs HFpEF's clinical workload and cost in the first year following hospitalization and enrollment in a disease management program. *Int J Cardiol* **232**, 330-335, doi:10.1016/j.ijcard.2016.12.057 (2017).

23 Kass, D. A., Bronzwaer, J. G. & Paulus, W. J. What mechanisms underlie diastolic dysfunction in heart failure? *Circ Res* **94**, 1533-1542, doi:10.1161/01.RES.0000129254.25507.d6 (2004).

24 Senni, M. *et al.* New strategies for heart failure with preserved ejection fraction: the importance of targeted therapies for heart failure phenotypes. *Eur Heart J* **35**, 2797-2815, doi:10.1093/eurheartj/ehu204 (2014).

25 Ponikowski, P. *et al.* 2016 ESC Guidelines for the diagnosis and treatment of acute and chronic heart failure: The Task Force for the diagnosis and treatment of acute and chronic heart failure of the European Society of Cardiology (ESC). Developed with the special contribution of the Heart Failure Association (HFA) of the ESC. *Eur J Heart Fail* **18**, 891-975, doi:10.1002/ejhf.592 (2016).

26 Kitzman, D. W. *et al.* Pathophysiological characterization of isolated diastolic heart failure in comparison to systolic heart failure. *JAMA* **288**, 2144-2150, doi:10.1001/jama.288.17.2144 (2002).

27 Daniels, L. B. *et al.* How obesity affects the cut-points for B-type natriuretic peptide in the diagnosis of acute heart failure. Results from the Breathing Not Properly Multinational Study. *Am Heart J* **151**, 999-1005, doi:10.1016/j.ahj.2005.10.011 (2006).

28 Hawkins, N. M. *et al.* Heart failure and chronic obstructive pulmonary disease: diagnostic pitfalls and epidemiology. *Eur J Heart Fail* **11**, 130-139, doi:10.1093/eurjhf/hfn013 (2009).

29 Rutten, F. H. *et al.* Recognising heart failure in elderly patients with stable chronic obstructive pulmonary disease in primary care: cross sectional diagnostic study. *BMJ* **331**, 1379, doi:10.1136/bmj.38664.661181.55 (2005).

30 Pieske, B. *et al.* How to diagnose heart failure with preserved ejection fraction: the HFA-PEFF diagnostic algorithm: a consensus recommendation from the Heart Failure Association (HFA) of the European Society of Cardiology (ESC). *Eur Heart J* **40**, 3297-3317, doi:10.1093/eurheartj/ehz641 (2019).

31 Tromp, J. *et al.* Age-Related Characteristics and Outcomes of Patients With Heart Failure With Preserved Ejection Fraction. *J Am Coll Cardiol* **74**, 601-612, doi:10.1016/j.jacc.2019.05.052 (2019).

32 Solomon, S. D. in *ssential Echocardiography. Contemporary Cardiology.* Vol. Totowa (eds S.D. Solomon & B. Bulwer) 3-17 (Humana Press, 2007).

33 Ho, C. Y. in *Contemporary Cardiology: Essential Echocardiography* (ed S.D. Solomon) 119-131 (Humana Press, 2007).

34 Ho, C. Y. in *Contemporary Cardiology: Essential Echocardiography* (Solomon, S. (Ed), Totawa, NJ, Humana Press, 2007).

35 Vermeiren, G. L., Malbrain, M. L. & Walpot, J. M. Cardiac Ultrasonography in the critical care setting: a practical approach to asses cardiac function and preload for the "non-cardiologist". *Anaesthesiol Intensive Ther* **47 Spec No**, s89-104, doi:10.5603/AIT.a2015.0074 (2015).

36 Shah, A. M. *et al.* Contemporary Assessment of Left Ventricular Diastolic Function in Older Adults: The Atherosclerosis Risk in Communities Study. *Circulation* **135**, 426-439, doi:10.1161/CIRCULATIONAHA.116.024825 (2017).

37 Kane, G. C. *et al.* Progression of left ventricular diastolic dysfunction and risk of heart failure. *JAMA* **306**, 856-863, doi:10.1001/jama.2011.1201 (2011).

38 Abudiab, M. M. *et al.* Cardiac output response to exercise in relation to metabolic demand in heart failure with preserved ejection fraction. *Eur J Heart Fail* **15**, 776-785, doi:10.1093/eurjhf/hft026 (2013).
39 Borlaug, B. A. The pathophysiology of heart failure with preserved ejection fraction. *Nat Rev Cardiol* **11**, 507-515, doi:10.1038/nrcardio.2014.83 (2014).
40 Borlaug, B. A., Kane, G. C., Melenovsky, V. & Olson, T. P. Abnormal right ventricular-pulmonary artery coupling with exercise in heart failure with preserved ejection fraction. *Eur Heart J* **37**, 3293-3302, doi:10.1093/eurheartj/ehw241 (2016).
41 Borlaug, B. A. & Reddy, Y. N. V. The Role of the Pericardium in Heart Failure: Implications for Pathophysiology and Treatment. *JACC Heart Fail* **7**, 574-585, doi:10.1016/j.jchf.2019.03.021 (2019).
42 Borlaug, B. A. *et al.* Global cardiovascular reserve dysfunction in heart failure with preserved ejection fraction. *J Am Coll Cardiol* **56**, 845-854, doi:10.1016/j.jacc.2010.03.077 (2010).
43 Obokata, M. *et al.* Haemodynamics, dyspnoea, and pulmonary reserve in heart failure with preserved ejection fraction. *Eur Heart J* **39**, 2810-2821, doi:10.1093/eurheartj/ehy268 (2018).
44 Adamson, P. B. *et al.* Wireless pulmonary artery pressure monitoring guides management to reduce decompensation in heart failure with preserved ejection fraction. *Circ Heart Fail* **7**, 935-944, doi:10.1161/CIRCHEARTFAILURE.113.001229 (2014).
45 Dorfs, S. *et al.* Pulmonary capillary wedge pressure during exercise and long-term mortality in patients with suspected heart failure with preserved ejection fraction. *Eur Heart J* **35**, 3103-3112, doi:10.1093/eurheartj/ehu315 (2014).
46 Reddy, Y. N. V., Carter, R. E., Obokata, M., Redfield, M. M. & Borlaug, B. A. A Simple, Evidence-Based Approach to Help Guide Diagnosis of Heart Failure With Preserved Ejection Fraction. *Circulation* **138**, 861-870, doi:10.1161/CIRCULATIONAHA.118.034646 (2018).
47 Konecny, F. *Tools & Techniques for Pressure-Volume Hemodynamic Studies*. 1-145 (Dros, C.J. , 2017).
48 Paulus, W. J. *et al.* How to diagnose diastolic heart failure: a consensus statement on the diagnosis of heart failure with normal left ventricular ejection fraction by the Heart Failure and Echocardiography Associations of the European Society of Cardiology. *Eur Heart J* **28**, 2539-2550, doi:10.1093/eurheartj/ehm037 (2007).
49 Penicka, M. *et al.* Heart failure with preserved ejection fraction in outpatients with unexplained dyspnea: a pressure-volume loop analysis. *J Am Coll Cardiol* **55**, 1701-1710, doi:10.1016/j.jacc.2009.11.076 (2010).
50 Paulus, W. J. & Tschope, C. A novel paradigm for heart failure with preserved ejection fraction: comorbidities drive myocardial dysfunction and remodeling through coronary microvascular endothelial inflammation. *J Am Coll Cardiol* **62**, 263-271, doi:10.1016/j.jacc.2013.02.092 (2013).
51 Franssen, C. & Gonzalez Miqueo, A. The role of titin and extracellular matrix remodelling in heart failure with preserved ejection fraction. *Neth Heart J* **24**, 259-267, doi:10.1007/s12471-016-0812-z (2016).
52 Borbely, A. *et al.* Hypophosphorylation of the Stiff N2B titin isoform raises cardiomyocyte resting tension in failing human myocardium. *Circ Res* **104**, 780-786, doi:10.1161/CIRCRESAHA.108.193326 (2009).
53 van Heerebeek, L. *et al.* Low myocardial protein kinase G activity in heart failure with preserved ejection fraction. *Circulation* **126**, 830-839, doi:10.1161/CIRCULATIONAHA.111.076075 (2012).
54 Zile, M. R. *et al.* Myocardial stiffness in patients with heart failure and a preserved ejection fraction: contributions of collagen and titin. *Circulation* **131**, 1247-1259, doi:10.1161/CIRCULATIONAHA.114.013215 (2015).
55 Makarenko, I. *et al.* Passive stiffness changes caused by upregulation of compliant titin isoforms in human dilated cardiomyopathy hearts. *Circ Res* **95**, 708-716, doi:10.1161/01.RES.0000143901.37063.2f (2004).
56 van Heerebeek, L. *et al.* Myocardial structure and function differ in systolic and diastolic heart failure. *Circulation* **113**, 1966-1973, doi:10.1161/CIRCULATIONAHA.105.587519 (2006).

57 Simmonds, S. J., Cuijpers, I., Heymans, S. & Jones, E. A. V. Cellular and Molecular Differences between HFpEF and HFrEF: A Step Ahead in an Improved Pathological Understanding. *Cells* **9**, doi:10.3390/cells9010242 (2020).

58 Kasner, M. *et al.* Diastolic tissue Doppler indexes correlate with the degree of collagen expression and cross-linking in heart failure and normal ejection fraction. *J Am Coll Cardiol* **57**, 977-985, doi:10.1016/j.jacc.2010.10.024 (2011).

59 Regan, T. J. *et al.* Evidence for cardiomyopathy in familial diabetes mellitus. *J Clin Invest* **60**, 884-899, doi:10.1172/JCI108843 (1977).

60 Mohammed, S. F. *et al.* Coronary microvascular rarefaction and myocardial fibrosis in heart failure with preserved ejection fraction. *Circulation* **131**, 550-559, doi:10.1161/CIRCULATIONAHA.114.009625 (2015).

61 Oliveira-Junior, S. A. *et al.* AT1 receptor blockade attenuates insulin resistance and myocardial remodeling in rats with diet-induced obesity. *PLoS One* **9**, e86447, doi:10.1371/journal.pone.0086447 (2014).

62 Song, Y., Yao, Q., Zhu, J., Luo, B. & Liang, S. Age-related variation in the interstitial tissues of the cardiac conduction system; and autopsy study of 230 Han Chinese. *Forensic Sci Int* **104**, 133-142, doi:10.1016/s0379-0738(99)00103-6 (1999).

63 Querejeta, R. *et al.* Increased collagen type I synthesis in patients with heart failure of hypertensive origin: relation to myocardial fibrosis. *Circulation* **110**, 1263-1268, doi:10.1161/01.CIR.0000140973.60992.9A (2004).

64 Rodriguez, C. & Martinez-Gonzalez, J. The Role of Lysyl Oxidase Enzymes in Cardiac Function and Remodeling. *Cells* **8**, doi:10.3390/cells8121483 (2019).

65 Deluyker, D. *et al.* Cross-linking versus RAGE: How do high molecular weight advanced glycation products induce cardiac dysfunction? *Int J Cardiol* **210**, 100-108, doi:10.1016/j.ijcard.2016.02.095 (2016).

66 Falkenham, A. *et al.* Nonclassical resident macrophages are important determinants in the development of myocardial fibrosis. *Am J Pathol* **185**, 927-942, doi:10.1016/j.ajpath.2014.11.027 (2015).

67 Forrester, S. J., Kikuchi, D. S., Hernandes, M. S., Xu, Q. & Griendling, K. K. Reactive Oxygen Species in Metabolic and Inflammatory Signaling. *Circ Res* **122**, 877-902, doi:10.1161/CIRCRESAHA.117.311401 (2018).

68 Versari, D., Daghini, E., Virdis, A., Ghiadoni, L. & Taddei, S. Endothelium-dependent contractions and endothelial dysfunction in human hypertension. *Br J Pharmacol* **157**, 527-536, doi:10.1111/j.1476-5381.2009.00240.x (2009).

69 Chirinos, J. A. *et al.* Heart Failure, Left Ventricular Remodeling, and Circulating Nitric Oxide Metabolites. *J Am Heart Assoc* **5**, doi:10.1161/JAHA.116.004133 (2016).

70 Chowdhury, M. A. *et al.* Endothelin 1 Is Associated with Heart Failure Hospitalization and Long-Term Mortality in Patients with Heart Failure with Preserved Ejection Fraction and Pulmonary Hypertension. *Cardiology* **143**, 124-133, doi:10.1159/000501100 (2019).

71 Yang, J. H. *et al.* Endothelium-dependent and independent coronary microvascular dysfunction in patients with heart failure with preserved ejection fraction. *Eur J Heart Fail* **22**, 432-441, doi:10.1002/ejhf.1671 (2020).

72 Kato, S. *et al.* Impairment of Coronary Flow Reserve Evaluated by Phase Contrast Cine-Magnetic Resonance Imaging in Patients With Heart Failure With Preserved Ejection Fraction. *J Am Heart Assoc* **5**, doi:10.1161/JAHA.115.002649 (2016).

73 van de Wouw, J. *et al.* Perturbations in myocardial perfusion and oxygen balance in swine with multiple risk factors: a novel model of ischemia and no obstructive coronary artery disease. *Basic Res Cardiol* **115**, 21, doi:10.1007/s00395-020-0778-2 (2020).

74 Haas, A. V. *et al.* Sex Differences in Coronary Microvascular Function in Individuals With Type 2 Diabetes. *Diabetes* **68**, 631-636, doi:10.2337/db18-0650 (2019).

75 Picchi, A. *et al.* Increased basal coronary blood flow as a cause of reduced coronary flow reserve in diabetic patients. *Am J Physiol Heart Circ Physiol* **301**, H2279-2284, doi:10.1152/ajpheart.00615.2011 (2011).

76 Bender, S. B. Linking Coronary Microvascular and Cardiac Diastolic Dysfunction in Diabetes: Are Women More Vulnerable? *Diabetes* **68**, 474-475, doi:10.2337/dbi18-0053 (2019).
77 Schwartzenberg, S. *et al.* Effects of vasodilation in heart failure with preserved or reduced ejection fraction implications of distinct pathophysiologies on response to therapy. *J Am Coll Cardiol* **59**, 442-451, doi:10.1016/j.jacc.2011.09.062 (2012).
78 Kaul, S. & Jayaweera, A. R. Myocardial capillaries and coronary flow reserve. *J Am Coll Cardiol* **52**, 1399-1401, doi:10.1016/j.jacc.2008.07.039 (2008).
79 Tsagalou, E. P. *et al.* Depressed coronary flow reserve is associated with decreased myocardial capillary density in patients with heart failure due to idiopathic dilated cardiomyopathy. *J Am Coll Cardiol* **52**, 1391-1398, doi:10.1016/j.jacc.2008.05.064 (2008).
80 Zeng, H. & Chen, J. X. Microvascular Rarefaction and Heart Failure With Preserved Ejection Fraction. *Front Cardiovasc Med* **6**, 15, doi:10.3389/fcvm.2019.00015 (2019).
81 van Empel, V. P., Mariani, J., Borlaug, B. A. & Kaye, D. M. Impaired myocardial oxygen availability contributes to abnormal exercise hemodynamics in heart failure with preserved ejection fraction. *J Am Heart Assoc* **3**, e001293, doi:10.1161/JAHA.114.001293 (2014).
82 Taqueti, V. R. *et al.* Coronary microvascular dysfunction and future risk of heart failure with preserved ejection fraction. *Eur Heart J* **39**, 840-849, doi:10.1093/eurheartj/ehx721 (2018).
83 Hinkel, R. *et al.* Diabetes Mellitus-Induced Microvascular Destabilization in the Myocardium. *J Am Coll Cardiol* **69**, 131-143, doi:10.1016/j.jacc.2016.10.058 (2017).
84 Loredo-Mendoza, M. L. *et al.* The role of inflammation in driving left ventricular remodeling in a pre-HFpEF model. *Exp Biol Med (Maywood)* **245**, 748-757, doi:10.1177/1535370220912699 (2020).
85 Baron, A. D. *et al.* Interaction between insulin sensitivity and muscle perfusion on glucose uptake in human skeletal muscle: evidence for capillary recruitment. *Diabetes* **49**, 768-774 (2000).
86 Bonner, J. S. *et al.* Muscle-specific vascular endothelial growth factor deletion induces muscle capillary rarefaction creating muscle insulin resistance. *Diabetes* **62**, 572-580, doi:10.2337/db12-0354 (2013).
87 Antonios, T. F. *et al.* Maximization of skin capillaries during intravital video-microscopy in essential hypertension: comparison between venous congestion, reactive hyperaemia and core heat load tests. *Clin Sci (Lond)* **97**, 523-528 (1999).
88 Noon, J. P. *et al.* Impaired microvascular dilatation and capillary rarefaction in young adults with a predisposition to high blood pressure. *J Clin Invest* **99**, 1873-1879, doi:10.1172/JCI119354 (1997).
89 Campbell, D. J. *et al.* Obesity is associated with lower coronary microvascular density. *PLoS One* **8**, e81798, doi:10.1371/journal.pone.0081798 (2013).
90 Nakanishi, K. *et al.* Relationships Between Periventricular Epicardial Adipose Tissue Accumulation, Coronary Microcirculation, and Left Ventricular Diastolic Dysfunction. *Can J Cardiol* **33**, 1489-1497, doi:10.1016/j.cjca.2017.08.001 (2017).
91 Pitsavos, C. *et al.* Association Between Low-Grade Systemic Inflammation and Type 2 Diabetes Mellitus Among Men and Women from the ATTICA Study. *Rev Diabet Stud* **4**, 98-104, doi:10.1900/RDS.2007.4.98 (2007).
92 Bruunsgaard, H. *et al.* Predicting death from tumour necrosis factor-alpha and interleukin-6 in 80-year-old people. *Clin Exp Immunol* **132**, 24-31, doi:10.1046/j.1365-2249.2003.02137.x (2003).
93 Sung, K. C. *et al.* High sensitivity C-reactive protein as an independent risk factor for essential hypertension. *Am J Hypertens* **16**, 429-433, doi:10.1016/s0895-7061(03)00566-1 (2003).
94 Illan-Gomez, F. *et al.* Obesity and inflammation: change in adiponectin, C-reactive protein, tumour necrosis factor-alpha and interleukin-6 after bariatric surgery. *Obes Surg* **22**, 950-955, doi:10.1007/s11695-012-0643-y (2012).
95 Collier, P. *et al.* Can emerging biomarkers of myocardial remodelling identify asymptomatic hypertensive patients at risk for diastolic dysfunction and diastolic heart failure? *Eur J Heart Fail* **13**, 1087-1095, doi:10.1093/eurjhf/hfr079 (2011).

96 DuBrock, H. M., AbouEzzeddine, O. F. & Redfield, M. M. High-sensitivity C-reactive protein in heart failure with preserved ejection fraction. *PLoS One* **13**, e0201836, doi:10.1371/journal.pone.0201836 (2018).
97 Hulsmans, M. *et al.* Cardiac macrophages promote diastolic dysfunction. *J Exp Med* **215**, 423-440, doi:10.1084/jem.20171274 (2018).
98 Glezeva, N. *et al.* Exaggerated inflammation and monocytosis associate with diastolic dysfunction in heart failure with preserved ejection fraction: evidence of M2 macrophage activation in disease pathogenesis. *J Card Fail* **21**, 167-177, doi:10.1016/j.cardfail.2014.11.004 (2015).
99 Bierhaus, A. *et al.* Understanding RAGE, the receptor for advanced glycation end products. *J Mol Med (Berl)* **83**, 876-886, doi:10.1007/s00109-005-0688-7 (2005).
100 Westermann, D. *et al.* Cardiac inflammation contributes to changes in the extracellular matrix in patients with heart failure and normal ejection fraction. *Circ Heart Fail* **4**, 44-52, doi:10.1161/CIRCHEARTFAILURE.109.931451 (2011).
101 Inoguchi, T. *et al.* High glucose level and free fatty acid stimulate reactive oxygen species production through protein kinase C--dependent activation of NAD(P)H oxidase in cultured vascular cells. *Diabetes* **49**, 1939-1945 (2000).
102 Oliver, C. N., Ahn, B. W., Moerman, E. J., Goldstein, S. & Stadtman, E. R. Age-related changes in oxidized proteins. *J Biol Chem* **262**, 5488-5491 (1987).
103 Chabrashvili, T. *et al.* Effects of ANG II type 1 and 2 receptors on oxidative stress, renal NADPH oxidase, and SOD expression. *Am J Physiol Regul Integr Comp Physiol* **285**, R117-124, doi:10.1152/ajpregu.00476.2002 (2003).
104 Furukawa, S. *et al.* Increased oxidative stress in obesity and its impact on metabolic syndrome. *J Clin Invest* **114**, 1752-1761, doi:10.1172/JCI21625 (2004).
105 Ramasamy, R. *et al.* Advanced glycation end products and RAGE: a common thread in aging, diabetes, neurodegeneration, and inflammation. *Glycobiology* **15**, 16R-28R, doi:10.1093/glycob/cwi053 (2005).
106 Incalza, M. A. *et al.* Oxidative stress and reactive oxygen species in endothelial dysfunction associated with cardiovascular and metabolic diseases. *Vascul Pharmacol* **100**, 1-19, doi:10.1016/j.vph.2017.05.005 (2018).
107 Franssen, C. *et al.* Myocardial Microvascular Inflammatory Endothelial Activation in Heart Failure With Preserved Ejection Fraction. *JACC Heart Fail* **4**, 312-324, doi:10.1016/j.jchf.2015.10.007 (2016).
108 Babes, E. E. & Babes, V. V. ADMA and prognosis in patients with heart failure and preserved ejection fraction *Eur Heart J* **34**, P1491, doi:https://doi.org/10.1093/eurheartj/eht308.P1491 (2013).
109 Cuijpers, I. *et al.* Microvascular and lymphatic dysfunction in HFpEF and its associated comorbidities. *Basic Res Cardiol* **115**, 39, doi:10.1007/s00395-020-0798-y (2020).
110 Viazzi, F. *et al.* Vascular permeability, blood pressure, and organ damage in primary hypertension. *Hypertens Res* **31**, 873-879, doi:10.1291/hypres.31.873 (2008).
111 Mathews, M. K., Merges, C., McLeod, D. S. & Lutty, G. A. Vascular endothelial growth factor and vascular permeability changes in human diabetic retinopathy. *Invest Ophthalmol Vis Sci* **38**, 2729-2741 (1997).
112 Jia, G. *et al.* Enhanced endothelium epithelial sodium channel signaling prompts left ventricular diastolic dysfunction in obese female mice. *Metabolism* **78**, 69-79, doi:10.1016/j.metabol.2017.08.008 (2018).
113 Blau, C. W. *et al.* The age-related deficit in LTP is associated with changes in perfusion and blood-brain barrier permeability. *Neurobiol Aging* **33**, 1005 e1023-1035, doi:10.1016/j.neurobiolaging.2011.09.035 (2012).
114 Ikonomidis, I. *et al.* Association of impaired endothelial glycocalyx with arterial stiffness, coronary microcirculatory dysfunction, and abnormal myocardial deformation in untreated hypertensives. *J Clin Hypertens (Greenwich)* **20**, 672-679, doi:10.1111/jch.13236 (2018).
115 Machin, D. R. *et al.* Advanced age results in a diminished endothelial glycocalyx. *Am J Physiol Heart Circ Physiol* **315**, H531-H539, doi:10.1152/ajpheart.00104.2018 (2018).

116 Eskens, B. J., Leurgans, T. M., Vink, H. & Vanteeffelen, J. W. Early impairment of skeletal muscle endothelial glycocalyx barrier properties in diet-induced obesity in mice. *Physiol Rep* **2**, e00194, doi:10.1002/phy2.194 (2014).
117 Nieuwdorp, M. *et al.* Loss of endothelial glycocalyx during acute hyperglycemia coincides with endothelial dysfunction and coagulation activation in vivo. *Diabetes* **55**, 480-486 (2006).
118 Jacob, M. *et al.* Albumin augmentation improves condition of guinea pig hearts after 4 hr of cold ischemia. *Transplantation* **87**, 956-965, doi:10.1097/TP.0b013e31819c83b5 (2009).
119 Tromp, J. *et al.* Fibrosis marker syndecan-1 and outcome in patients with heart failure with reduced and preserved ejection fraction. *Circ Heart Fail* **7**, 457-462, doi:10.1161/CIRCHEARTFAILURE.113.000846 (2014).
120 Bruegger, D. *et al.* Exogenous nitric oxide requires an endothelial glycocalyx to prevent postischemic coronary vascular leak in guinea pig hearts. *Crit Care* **12**, R73, doi:10.1186/cc6913 (2008).
121 Krouwer, V. J., Hekking, L. H., Langelaar-Makkinje, M., Regan-Klapisz, E. & Post, J. A. Endothelial cell senescence is associated with disrupted cell-cell junctions and increased monolayer permeability. *Vasc Cell* **4**, 12, doi:10.1186/2045-824X-4-12 (2012).
122 Oku, H., Kodama, T., Sakagami, K. & Puro, D. G. Diabetes-induced disruption of gap junction pathways within the retinal microvasculature. *Invest Ophthalmol Vis Sci* **42**, 1915-1920 (2001).
123 Rummery, N. M. & Hill, C. E. Vascular gap junctions and implications for hypertension. *Clin Exp Pharmacol Physiol* **31**, 659-667, doi:10.1111/j.1440-1681.2004.04071.x (2004).
124 Claesson-Welsh, L. Vascular permeability--the essentials. *Ups J Med Sci* **120**, 135-143, doi:10.3109/03009734.2015.1064501 (2015).
125 van Dijk, C. G. *et al.* Distinct Endothelial Cell Responses in the Heart and Kidney Microvasculature Characterize the Progression of Heart Failure With Preserved Ejection Fraction in the Obese ZSF1 Rat With Cardiorenal Metabolic Syndrome. *Circ Heart Fail* **9**, e002760, doi:10.1161/CIRCHEARTFAILURE.115.002760 (2016).
126 Conceicao, G., Heinonen, I., Lourenco, A. P., Duncker, D. J. & Falcao-Pires, I. Animal models of heart failure with preserved ejection fraction. *Neth Heart J* **24**, 275-286, doi:10.1007/s12471-016-0815-9 (2016).
127 Oktay, A. A. & Shah, S. J. Current perspectives on systemic hypertension in heart failure with preserved ejection fraction. *Curr Cardiol Rep* **16**, 545, doi:10.1007/s11886-014-0545-9 (2014).
128 Doi, R. *et al.* Development of different phenotypes of hypertensive heart failure: systolic versus diastolic failure in Dahl salt-sensitive rats. *J Hypertens* **18**, 111-120, doi:10.1097/00004872-200018010-00016 (2000).
129 Esposito, G. *et al.* Sitagliptin reduces inflammation, fibrosis and preserves diastolic function in a rat model of heart failure with preserved ejection fraction. *Br J Pharmacol* **174**, 4070-4086, doi:10.1111/bph.13686 (2017).
130 Miyachi, M. *et al.* Exercise training alters left ventricular geometry and attenuates heart failure in dahl salt-sensitive hypertensive rats. *Hypertension* **53**, 701-707, doi:10.1161/HYPERTENSIONAHA.108.127290 (2009).
131 Regan, J. A. *et al.* A mouse model of heart failure with preserved ejection fraction due to chronic infusion of a low subpressor dose of angiotensin II. *Am J Physiol Heart Circ Physiol* **309**, H771-778, doi:10.1152/ajpheart.00282.2015 (2015).
132 Ichihara, S. *et al.* Angiotensin II type 2 receptor is essential for left ventricular hypertrophy and cardiac fibrosis in chronic angiotensin II-induced hypertension. *Circulation* **104**, 346-351, doi:10.1161/01.cir.104.3.346 (2001).
133 Qi, G. *et al.* Angiotensin II infusion-induced inflammation, monocytic fibroblast precursor infiltration, and cardiac fibrosis are pressure dependent. *Cardiovasc Toxicol* **11**, 157-167, doi:10.1007/s12012-011-9109-z (2011).
134 Sabri, A. *et al.* Microvasculature in angiotensin II-dependent cardiac hypertrophy in the rat. *Hypertension* **32**, 371-375, doi:10.1161/01.hyp.32.2.371 (1998).

135 Xia, Y. *et al.* Characterization of the inflammatory and fibrotic response in a mouse model of cardiac pressure overload. *Histochem Cell Biol* **131**, 471-481, doi:10.1007/s00418-008-0541-5 (2009).

136 Haass, M. *et al.* Body mass index and adverse cardiovascular outcomes in heart failure patients with preserved ejection fraction: results from the Irbesartan in Heart Failure with Preserved Ejection Fraction (I-PRESERVE) trial. *Circ Heart Fail* **4**, 324-331, doi:10.1161/CIRCHEARTFAILURE.110.959890 (2011).

137 Seferovic, P. M. *et al.* Type 2 diabetes mellitus and heart failure: a position statement from the Heart Failure Association of the European Society of Cardiology. *Eur J Heart Fail* **20**, 853-872, doi:10.1002/ejhf.1170 (2018).

138 Christoffersen, C. *et al.* Cardiac lipid accumulation associated with diastolic dysfunction in obese mice. *Endocrinology* **144**, 3483-3490, doi:10.1210/en.2003-0242 (2003).

139 An, H. S. *et al.* Caloric restriction reverses left ventricular hypertrophy through the regulation of cardiac iron homeostasis in impaired leptin signaling mice. *Sci Rep* **10**, 7176, doi:10.1038/s41598-020-64201-2 (2020).

140 Westergren, H. U. *et al.* Impaired Coronary and Renal Vascular Function in Spontaneously Type 2 Diabetic Leptin-Deficient Mice. *PLoS One* **10**, e0130648, doi:10.1371/journal.pone.0130648 (2015).

141 Van den Bergh, A. *et al.* Dyslipidaemia in type II diabetic mice does not aggravate contractile impairment but increases ventricular stiffness. *Cardiovasc Res* **77**, 371-379, doi:10.1093/cvr/cvm001 (2008).

142 Valero-Munoz, M., Backman, W. & Sam, F. Murine Models of Heart Failure with Preserved Ejection Fraction: a "Fishing Expedition". *JACC Basic Transl Sci* **2**, 770-789, doi:10.1016/j.jacbts.2017.07.013 (2017).

143 Daniels, A. *et al.* Long-term severe diabetes only leads to mild cardiac diastolic dysfunction in Zucker diabetic fatty rats. *Eur J Heart Fail* **14**, 193-201, doi:10.1093/eurjhf/hfr166 (2012).

144 Steven, S. *et al.* The SGLT2 inhibitor empagliflozin improves the primary diabetic complications in ZDF rats. *Redox Biol* **13**, 370-385, doi:10.1016/j.redox.2017.06.009 (2017).

145 Abuderman, A. Morphological quantification of myocardial pathology in the Zucker diabetic fatty rat. *Global Journal on Advances in Pure & Applied Sciences*, 1-12 (2016).

146 Kitzman, D. W., O'Neill, T. J. t. & Brubaker, P. H. Unraveling the Relationship Between Aging and Heart Failure With Preserved Ejection Fraction: The Importance of Exercise and Normative Reference Standards. *JACC Heart Fail* **5**, 356-358, doi:10.1016/j.jchf.2017.01.009 (2017).

147 Reed, A. L. *et al.* Diastolic dysfunction is associated with cardiac fibrosis in the senescence-accelerated mouse. *Am J Physiol Heart Circ Physiol* **301**, H824-831, doi:10.1152/ajpheart.00407.2010 (2011).

148 Gevaert, A. B. *et al.* Endothelial Senescence Contributes to Heart Failure With Preserved Ejection Fraction in an Aging Mouse Model. *Circ Heart Fail* **10**, doi:10.1161/CIRCHEARTFAILURE.116.003806 (2017).

149 Forman, D. E., Cittadini, A., Azhar, G., Douglas, P. S. & Wei, J. Y. Cardiac morphology and function in senescent rats: gender-related differences. *J Am Coll Cardiol* **30**, 1872-1877, doi:10.1016/s0735-1097(97)00411-7 (1997).

150 Leite, S. C., R J; Ibarrola, J; Fontoura, D; Fernández-Celis, A; Zannad, F; Falcão-Pires, I; Paulus, W J; Leite-Moreira, A F; Rossignol, P; López-Andrés, N; Lourenço, AP. Arterial Remodeling and Dysfunction in the ZSF1 Rat Model of Heart Failure With Preserved Ejection Fraction. *Circ Heart Fail* **12**, doi:https://doi.org/10.1161/CIRCHEARTFAILURE.118.005596 (2019).

151 Hamdani, N. *et al.* Myocardial titin hypophosphorylation importantly contributes to heart failure with preserved ejection fraction in a rat metabolic risk model. *Circ Heart Fail* **6**, 1239-1249, doi:10.1161/CIRCHEARTFAILURE.113.000539 (2013).

152 Hegde, S. M. *et al.* Physical Activity and Prognosis in the TOPCAT Trial (Treatment of Preserved Cardiac Function Heart Failure With an Aldosterone Antagonist). *Circulation* **136**, 982-992, doi:10.1161/CIRCULATIONAHA.117.028002 (2017).

153 Edelmann, F. *et al.* Exercise training improves exercise capacity and diastolic function in patients with heart failure with preserved ejection fraction: results of the Ex-DHF (Exercise training in Diastolic Heart Failure) pilot study. *J Am Coll Cardiol* **58**, 1780-1791, doi:10.1016/j.jacc.2011.06.054 (2011).
154 Kitzman, D. W. *et al.* Effect of Caloric Restriction or Aerobic Exercise Training on Peak Oxygen Consumption and Quality of Life in Obese Older Patients With Heart Failure With Preserved Ejection Fraction: A Randomized Clinical Trial. *JAMA* **315**, 36-46, doi:10.1001/jama.2015.17346 (2016).
155 Heggermont, W. A., Papageorgiou, A. P., Heymans, S. & van Bilsen, M. Metabolic support for the heart: complementary therapy for heart failure? *Eur J Heart Fail* **18**, 1420-1429, doi:10.1002/ejhf.678 (2016).
156 Zhang, N. *et al.* Dapagliflozin improves left ventricular remodeling and aorta sympathetic tone in a pig model of heart failure with preserved ejection fraction. *Cardiovasc Diabetol* **18**, 107, doi:10.1186/s12933-019-0914-1 (2019).
157 Zi, M., Carmichael, N. & Lye, M. The effect of quinapril on functional status of elderly patients with diastolic heart failure. *Cardiovasc Drugs Ther* **17**, 133-139, doi:10.1023/a:1025387702212 (2003).
158 Yusuf, S. *et al.* Effects of candesartan in patients with chronic heart failure and preserved left-ventricular ejection fraction: the CHARM-Preserved Trial. *Lancet* **362**, 777-781, doi:10.1016/S0140-6736(03)14285-7 (2003).
159 Massie, B. M. *et al.* Irbesartan in patients with heart failure and preserved ejection fraction. *N Engl J Med* **359**, 2456-2467, doi:10.1056/NEJMoa0805450 (2008).
160 McMurray, J. J. V. *et al.* Effects of Sacubitril-Valsartan Versus Valsartan in Women Compared With Men With Heart Failure and Preserved Ejection Fraction: Insights From PARAGON-HF. *Circulation* **141**, 338-351, doi:10.1161/CIRCULATIONAHA.119.044491 (2020).
161 Solomon, S. D. *et al.* Angiotensin-Neprilysin Inhibition in Heart Failure with Preserved Ejection Fraction. *N Engl J Med* **381**, 1609-1620, doi:10.1056/NEJMoa1908655 (2019).
162 Pandey, A. *et al.* Effect of Mineralocorticoid Receptor Antagonists on Cardiac Structure and Function in Patients With Diastolic Dysfunction and Heart Failure With Preserved Ejection Fraction: A Meta-Analysis and Systematic Review. *J Am Heart Assoc* **4**, e002137, doi:10.1161/JAHA.115.002137 (2015).
163 Kosmas, C. E., Silverio, D., Sourlas, A., Montan, P. D. & Guzman, E. Role of spironolactone in the treatment of heart failure with preserved ejection fraction. *Ann Transl Med* **6**, 461, doi:10.21037/atm.2018.11.16 (2018).
164 Black-Maier, E. *et al.* Catheter ablation of atrial fibrillation in patients with heart failure and preserved ejection fraction. *Heart Rhythm* **15**, 651-657, doi:10.1016/j.hrthm.2017.12.001 (2018).
165 Mann, D. L. Innate immunity and the failing heart: the cytokine hypothesis revisited. *Circ Res* **116**, 1254-1268, doi:10.1161/CIRCRESAHA.116.302317 (2015).
166 Van Tassell, B. W. *et al.* Effects of interleukin-1 blockade with anakinra on aerobic exercise capacity in patients with heart failure and preserved ejection fraction (from the D-HART pilot study). *Am J Cardiol* **113**, 321-327, doi:10.1016/j.amjcard.2013.08.047 (2014).
167 Marume, K. *et al.* Effect of Statins on Mortality in Heart Failure With Preserved Ejection Fraction Without Coronary Artery Disease- Report From the JASPER Study. *Circ J* **83**, 357-367, doi:10.1253/circj.CJ-18-0639 (2019).
168 Dai, D. F. *et al.* Mitochondrial targeted antioxidant Peptide ameliorates hypertensive cardiomyopathy. *J Am Coll Cardiol* **58**, 73-82, doi:10.1016/j.jacc.2010.12.044 (2011).
169 Luo, M. *et al.* Diabetes increases mortality after myocardial infarction by oxidizing CaMKII. *J Clin Invest* **123**, 1262-1274, doi:10.1172/JCI65268 (2013).
170 Wilder, T., Ryba, D. M., Wieczorek, D. F., Wolska, B. M. & Solaro, R. J. N-acetylcysteine reverses diastolic dysfunction and hypertrophy in familial hypertrophic cardiomyopathy. *Am J Physiol Heart Circ Physiol* **309**, H1720-1730, doi:10.1152/ajpheart.00339.2015 (2015).

171 Ratchford, S. M. *et al.* Impact of Acute Antioxidant Administration on Inflammation and Vascular Function in Heart Failure with Preserved Ejection Fraction. *FASEB J* **33**, No. 1_supplement.
172 Westermann, D. *et al.* Enhancement of the endothelial NO synthase attenuates experimental diastolic heart failure. *Basic Res Cardiol* **104**, 499-509, doi:10.1007/s00395-009-0014-6 (2009).
173 Xue, H. M., Yu, C. M., Underwood, M. J., Huang, J. H. & Yang, Q. AVE3085 protects coronary endothelium from the impairment of asymmetric dimethylarginine by activation and recoupling of eNOS. *Cardiovasc Drugs Ther* **26**, 383-392, doi:10.1007/s10557-012-6404-2 (2012).
174 Zakeri, R. *et al.* Nitrate's effect on activity tolerance in heart failure with preserved ejection fraction trial: rationale and design. *Circ Heart Fail* **8**, 221-228, doi:10.1161/CIRCHEARTFAILURE.114.001598 (2015).
175 Borlaug, B. A. *et al.* Effect of Inorganic Nitrite vs Placebo on Exercise Capacity Among Patients With Heart Failure With Preserved Ejection Fraction: The INDIE-HFpEF Randomized Clinical Trial. *JAMA* **320**, 1764-1773, doi:10.1001/jama.2018.14852 (2018).
176 Pieske, B. *et al.* Vericiguat in patients with worsening chronic heart failure and preserved ejection fraction: results of the SOluble guanylate Cyclase stimulatoR in heArT failurE patientS with PRESERVED EF (SOCRATES-PRESERVED) study. *Eur Heart J* **38**, 1119-1127, doi:10.1093/eurheartj/ehw593 (2017).
177 Redfield, M. M. *et al.* Effect of phosphodiesterase-5 inhibition on exercise capacity and clinical status in heart failure with preserved ejection fraction: a randomized clinical trial. *JAMA* **309**, 1268-1277, doi:10.1001/jama.2013.2024 (2013).
178 Little, W. C. *et al.* The effect of alagebrium chloride (ALT-711), a novel glucose cross-link breaker, in the treatment of elderly patients with diastolic heart failure. *J Card Fail* **11**, 191-195, doi:10.1016/j.cardfail.2004.09.010 (2005).
179 Hartog, J. W. *et al.* Effects of alagebrium, an advanced glycation endproduct breaker, on exercise tolerance and cardiac function in patients with chronic heart failure. *Eur J Heart Fail* **13**, 899-908, doi:10.1093/eurjhf/hfr067 (2011).
180 Fujimoto, N. *et al.* Cardiovascular effects of 1 year of alagebrium and endurance exercise training in healthy older individuals. *Circ Heart Fail* **6**, 1155-1164, doi:10.1161/CIRCHEARTFAILURE.113.000440 (2013).
181 Methawasin, M. *et al.* Experimentally Increasing the Compliance of Titin Through RNA Binding Motif-20 (RBM20) Inhibition Improves Diastolic Function In a Mouse Model of Heart Failure With Preserved Ejection Fraction. *Circulation* **134**, 1085-1099, doi:10.1161/CIRCULATIONAHA.116.023003 (2016).
182 Slater, R. E. *et al.* Metformin improves diastolic function in an HFpEF-like mouse model by increasing titin compliance. *J Gen Physiol* **151**, 42-52, doi:10.1085/jgp.201812259 (2019).
183 Hopf, A. E. *et al.* Diabetes-Induced Cardiomyocyte Passive Stiffening Is Caused by Impaired Insulin-Dependent Titin Modification and Can Be Modulated by Neuregulin-1. *Circ Res* **123**, 342-355, doi:10.1161/CIRCRESAHA.117.312166 (2018).
184 Hamdani, N. *et al.* Left ventricular diastolic dysfunction and myocardial stiffness in diabetic mice is attenuated by inhibition of dipeptidyl peptidase 4. *Cardiovasc Res* **104**, 423-431, doi:10.1093/cvr/cvu223 (2014).
185 Korn, C. & Augustin, H. G. Mechanisms of Vessel Pruning and Regression. *Dev Cell* **34**, 5-17, doi:10.1016/j.devcel.2015.06.004 (2015).
186 Linke, W. A. & Hamdani, N. Gigantic business: titin properties and function through thick and thin. *Circ Res* **114**, 1052-1068, doi:10.1161/CIRCRESAHA.114.301286 (2014).
187 de Boer, R. A. *et al.* Towards better definition, quantification and treatment of fibrosis in heart failure. A scientific roadmap by the Committee of Translational Research of the Heart Failure Association (HFA) of the European Society of Cardiology. *Eur J Heart Fail* **21**, 272-285, doi:10.1002/ejhf.1406 (2019).
188 van Heerebeek, L. *et al.* Diastolic stiffness of the failing diabetic heart: importance of fibrosis, advanced glycation end products, and myocyte resting tension. *Circulation* **117**, 43-51, doi:10.1161/CIRCULATIONAHA.107.728550 (2008).

189 Borbely, A. *et al.* Cardiomyocyte stiffness in diastolic heart failure. *Circulation* **111**, 774-781, doi:10.1161/01.CIR.0000155257.33485.6D (2005).
190 Leopoldo, A. S. *et al.* Cardiac remodeling in a rat model of diet-induced obesity. *Can J Cardiol* **26**, 423-429, doi:10.1016/s0828-282x(10)70440-2 (2010).
191 Stengel, A. *et al.* Obese patients have higher circulating protein levels of dipeptidyl peptidase IV. *Peptides* **61**, 75-82, doi:10.1016/j.peptides.2014.09.006 (2014).
192 Anoop, S. *et al.* High circulating plasma dipeptidyl peptidase- 4 levels in non-obese Asian Indians with type 2 diabetes correlate with fasting insulin and LDL-C levels, triceps skinfolds, total intra-abdominal adipose tissue volume and presence of diabetes: a case-control study. *BMJ Open Diabetes Res Care* **5**, e000393, doi:10.1136/bmjdrc-2017-000393 (2017).
193 dos Santos, L. *et al.* Circulating dipeptidyl peptidase IV activity correlates with cardiac dysfunction in human and experimental heart failure. *Circ Heart Fail* **6**, 1029-1038, doi:10.1161/CIRCHEARTFAILURE.112.000057 (2013).
194 Aroor, A. R. *et al.* Dipeptidylpeptidase inhibition is associated with improvement in blood pressure and diastolic function in insulin-resistant male Zucker obese rats. *Endocrinology* **154**, 2501-2513, doi:10.1210/en.2013-1096 (2013).
195 McGill, J. B. Linagliptin for type 2 diabetes mellitus: a review of the pivotal clinical trials. *Ther Adv Endocrinol Metab* **3**, 113-124, doi:10.1177/2042018812449406 (2012).
196 Hocher, B., Sharkovska, Y., Mark, M., Klein, T. & Pfab, T. The novel DPP-4 inhibitors linagliptin and BI 14361 reduce infarct size after myocardial ischemia/reperfusion in rats. *Int J Cardiol* **167**, 87-93, doi:10.1016/j.ijcard.2011.12.007 (2013).
197 Anagnostis, P. *et al.* Glucagon-like peptide-1-based therapies and cardiovascular disease: looking beyond glycaemic control. *Diabetes Obes Metab* **13**, 302-312, doi:10.1111/j.1463-1326.2010.01345.x (2011).
198 Jax, T. Treatment of patients with diabetes with GLP-1 analogues or DPP-4- inhibitors: a hot topic for cardiologists? *Clin Res Cardiol* **98**, 75-79, doi:10.1007/s00392-008-0725-y (2009).
199 Ussher, J. R. & Drucker, D. J. Cardiovascular biology of the incretin system. *Endocr Rev* **33**, 187-215, doi:10.1210/er.2011-1052 (2012).
200 Jose, T. & Inzucchi, S. E. Cardiovascular effects of the DPP-4 inhibitors. *Diab Vasc Dis Res* **9**, 109-116, doi:10.1177/1479164111436236 (2012).
201 Lairez, O. *et al.* Anesthetic regimen for cardiac function evaluation by echocardiography in mice: comparison between ketamine, etomidate and isoflurane versus conscious state. *Lab Anim* **47**, 284-290, doi:10.1177/0023677213496236 (2013).
202 Johnson J.S., L. M. K. in *Handbook of Cardiac Anatomy, Physiology, and Devices.* (Springer, Cham, 2015).
203 Buitrago, S., Martin, T. E., Tetens-Woodring, J., Belicha-Villanueva, A. & Wilding, G. E. Safety and efficacy of various combinations of injectable anesthetics in BALB/c mice. *J Am Assoc Lab Anim Sci* **47**, 11-17 (2008).
204 Borlaug, B. A. *et al.* Diastolic relaxation and compliance reserve during dynamic exercise in heart failure with preserved ejection fraction. *Heart* **97**, 964-969, doi:10.1136/hrt.2010.212787 (2011).
205 Plante, E. *et al.* Impact of anesthesia on echocardiographic evaluation of systolic and diastolic function in rats. *J Am Soc Echocardiogr* **19**, 1520-1525, doi:10.1016/j.echo.2006.06.011 (2006).
206 Stein, A. B. *et al.* Effects of anesthesia on echocardiographic assessment of left ventricular structure and function in rats. *Basic Res Cardiol* **102**, 28-41, doi:10.1007/s00395-006-0627-y (2007).
207 Droogmans, S. *et al.* Impact of anesthesia on valvular function in normal rats during echocardiography. *Ultrasound Med Biol* **34**, 1564-1572, doi:10.1016/j.ultrasmedbio.2008.02.017 (2008).
208 Roth, D. M., Swaney, J. S., Dalton, N. D., Gilpin, E. A. & Ross, J., Jr. Impact of anesthesia on cardiac function during echocardiography in mice. *Am J Physiol Heart Circ Physiol* **282**, H2134-2140, doi:10.1152/ajpheart.00845.2001 (2002).

209 Pachon, R. E., Scharf, B. A., Vatner, D. E. & Vatner, S. F. Best anesthetics for assessing left ventricular systolic function by echocardiography in mice. *Am J Physiol Heart Circ Physiol* **308**, H1525-1529, doi:10.1152/ajpheart.00890.2014 (2015).
210 Filipovic, M. *et al.* Effects of sevoflurane and propofol on left ventricular diastolic function in patients with pre-existing diastolic dysfunction. *Br J Anaesth* **98**, 12-18, doi:10.1093/bja/ael277 (2007).
211 Couture, P. *et al.* Effects of anesthetic induction in patients with diastolic dysfunction. *Can J Anaesth* **56**, 357-365, doi:10.1007/s12630-009-9068-z (2009).
212 Ryu, T. & Song, S. Y. Perioperative management of left ventricular diastolic dysfunction and heart failure: an anesthesiologist's perspective. *Korean J Anesthesiol* **70**, 3-12, doi:10.4097/kjae.2017.70.1.3 (2017).
213 Redfors, B., Shao, Y. & Omerovic, E. Influence of anesthetic agent, depth of anesthesia and body temperature on cardiovascular functional parameters in the rat. *Lab Anim* **48**, 6-14, doi:10.1177/0023677213502015 (2014).
214 Sano, Y. *et al.* Effects of various types of anesthesia on hemodynamics, cardiac function, and glucose and lipid metabolism in rats. *Am J Physiol Heart Circ Physiol* **311**, H1360-H1366, doi:10.1152/ajpheart.00181.2016 (2016).
215 Evans, D. B. Modulation of cAMP: mechanism for positive inotropic action. *J Cardiovasc Pharmacol* **8 Suppl 9**, S22-29 (1986).
216 Riou, B., Viars, P. & Lecarpentier, Y. Effects of ketamine on the cardiac papillary muscle of normal hamsters and those with cardiomyopathy. *Anesthesiology* **73**, 910-918, doi:10.1097/00000542-199011000-00019 (1990).
217 Kunst, G., Martin, E., Graf, B. M., Hagl, S. & Vahl, C. F. Actions of ketamine and its isomers on contractility and calcium transients in human myocardium. *Anesthesiology* **90**, 1363-1371, doi:10.1097/00000542-199905000-00021 (1999).
218 Romero, T. R. *et al.* Ketamine activates the L-arginine/Nitric oxide/cyclic guanosine monophosphate pathway to induce peripheral antinociception in rats. *Anesth Analg* **113**, 1254-1259, doi:10.1213/ANE.0b013e3182285dda (2011).
219 Anis, N. A., Berry, S. C., Burton, N. R. & Lodge, D. The dissociative anaesthetics, ketamine and phencyclidine, selectively reduce excitation of central mammalian neurones by N-methyl-aspartate. *Br J Pharmacol* **79**, 565-575 (1983).
220 Scheller, M. *et al.* Ketamine blocks currents through mammalian nicotinic acetylcholine receptor channels by interaction with both the open and the closed state. *Anesth Analg* **83**, 830-836 (1996).
221 Lang, R. M. *et al.* Recommendations for chamber quantification: a report from the American Society of Echocardiography's Guidelines and Standards Committee and the Chamber Quantification Writing Group, developed in conjunction with the European Association of Echocardiography, a branch of the European Society of Cardiology. *J Am Soc Echocardiogr* **18**, 1440-1463, doi:10.1016/j.echo.2005.10.005 (2005).
222 Ristow, B. *et al.* Predicting heart failure hospitalization and mortality by quantitative echocardiography: is body surface area the indexing method of choice? The Heart and Soul Study. *J Am Soc Echocardiogr* **23**, 406-413, doi:10.1016/j.echo.2010.01.019 (2010).
223 Redlarski, G., Palkowski, A. & Krawczuk, M. Body surface area formulae: an alarming ambiguity. *Sci Rep* **6**, 27966, doi:10.1038/srep27966 (2016).
224 Nguyen, I. T. N. *et al.* Both male and female obese ZSF1 rats develop cardiac dysfunction in obesity-induced heart failure with preserved ejection fraction. *PLoS One* **15**, e0232399, doi:10.1371/journal.pone.0232399 (2020).
225 Borlaug, B. A. & Paulus, W. J. Heart failure with preserved ejection fraction: pathophysiology, diagnosis, and treatment. *Eur Heart J* **32**, 670-679, doi:10.1093/eurheartj/ehq426 (2011).
226 Braunschweig, F., Cowie, M. R. & Auricchio, A. What are the costs of heart failure? *Europace* **13 Suppl 2**, ii13-17, doi:10.1093/europace/eur081 (2011).
227 Olfert, I. M. Physiological Capillary Regression is not Dependent on Reducing VEGF Expression. *Microcirculation* **23**, 146-156, doi:10.1111/micc.12263 (2016).

228 Su, X., Huang, L., Qu, Y., Xiao, D. & Mu, D. Pericytes in Cerebrovascular Diseases: An Emerging Therapeutic Target. *Front Cell Neurosci* **13**, 519, doi:10.3389/fncel.2019.00519 (2019).
229 Ferland-McCollough, D., Slater, S., Richard, J., Reni, C. & Mangialardi, G. Pericytes, an overlooked player in vascular pathobiology. *Pharmacol Ther* **171**, 30-42, doi:10.1016/j.pharmthera.2016.11.008 (2017).
230 Zhang, Z. S. *et al.* Research advances in pericyte function and their roles in diseases. *Chin J Traumatol* **23**, 89-95, doi:10.1016/j.cjtee.2020.02.006 (2020).
231 Simonavicius, N. *et al.* Pericytes promote selective vessel regression to regulate vascular patterning. *Blood* **120**, 1516-1527, doi:10.1182/blood-2011-01-332338 (2012).
232 Baffert, F. *et al.* Cellular changes in normal blood capillaries undergoing regression after inhibition of VEGF signaling. *Am J Physiol Heart Circ Physiol* **290**, H547-559, doi:10.1152/ajpheart.00616.2005 (2006).
233 Zhu, W. *et al.* Mesenchymal stem cells ameliorate hyperglycemia-induced endothelial injury through modulation of mitophagy. *Cell Death Dis* **9**, 837, doi:10.1038/s41419-018-0861-x (2018).
234 Trudeau, K., Molina, A. J. & Roy, S. High glucose induces mitochondrial morphology and metabolic changes in retinal pericytes. *Invest Ophthalmol Vis Sci* **52**, 8657-8664, doi:10.1167/iovs.11-7934 (2011).
235 Karbach, S. *et al.* Hyperglycemia and oxidative stress in cultured endothelial cells--a comparison of primary endothelial cells with an immortalized endothelial cell line. *J Diabetes Complications* **26**, 155-162, doi:10.1016/j.jdiacomp.2012.03.011 (2012).
236 Diffley, J. M. *et al.* Apoptosis induction by oxidized glycated LDL in human retinal capillary pericytes is independent of activation of MAPK signaling pathways. *Mol Vis* **15**, 135-145 (2009).
237 Peng, N. *et al.* An activator of mTOR inhibits oxLDL-induced autophagy and apoptosis in vascular endothelial cells and restricts atherosclerosis in apolipoprotein E(-)/(-) mice. *Sci Rep* **4**, 5519, doi:10.1038/srep05519 (2014).
238 Park, W. H. The effects of exogenous H2O2 on cell death, reactive oxygen species and glutathione levels in calf pulmonary artery and human umbilical vein endothelial cells. *Int J Mol Med* **31**, 471-476, doi:10.3892/ijmm.2012.1215 (2013).
239 Kamouchi, M. *et al.* Hydrogen peroxide-induced Ca2+ responses in CNS pericytes. *Neurosci Lett* **416**, 12-16, doi:10.1016/j.neulet.2007.01.039 (2007).
240 Andrews, S. *FastQC: a quality control tool for high throughput sequence data.* , <http://www.bioinformatics.babraham.ac.uk/projects/fastqc> (2010).
241 Aronesty, E. *Ea-Utils: Command-Line Tools for Processing Biological Sequencing Data.*, <https://github.com/ExpressionAnalysis/ea-utils> (2011).
242 Li, H. *et al.* The Sequence Alignment/Map format and SAMtools. *Bioinformatics* **25**, 2078-2079, doi:10.1093/bioinformatics/btp352 (2009).
243 Love, M. I., Huber, W. & Anders, S. Moderated estimation of fold change and dispersion for RNA-seq data with DESeq2. *Genome Biol* **15**, 550, doi:10.1186/s13059-014-0550-8 (2014).
244 Williams, B. *et al.* 2018 ESC/ESH Guidelines for the management of arterial hypertension. *Eur Heart J* **39**, 3021-3104, doi:10.1093/eurheartj/ehy339 (2018).
245 Huveneers, S. *et al.* Vinculin associates with endothelial VE-cadherin junctions to control force-dependent remodeling. *J Cell Biol* **196**, 641-652, doi:10.1083/jcb.201108120 (2012).
246 Franco, C. A. *et al.* Dynamic endothelial cell rearrangements drive developmental vessel regression. *PLoS Biol* **13**, e1002125, doi:10.1371/journal.pbio.1002125 (2015).
247 Rensen, S. S., Doevendans, P. A. & van Eys, G. J. Regulation and characteristics of vascular smooth muscle cell phenotypic diversity. *Neth Heart J* **15**, 100-108, doi:10.1007/BF03085963 (2007).
248 Louis, S. F. & Zahradka, P. Vascular smooth muscle cell motility: From migration to invasion. *Exp Clin Cardiol* **15**, e75-85 (2010).
249 Reddy, M. A. *et al.* Regulation of Vascular Smooth Muscle Cell Dysfunction Under Diabetic Conditions by miR-504. *Arterioscler Thromb Vasc Biol* **36**, 864-873, doi:10.1161/ATVBAHA.115.306770 (2016).

250 Arnold, C. *et al.* Hypertension-evoked RhoA activity in vascular smooth muscle cells requires RGS5. *FASEB J* **32**, 2021-2035, doi:10.1096/fj.201700384RR (2018).

251 Varga J, L. R. *Rheumatology*. 6th edn, Vol. 2 117-1189 (Mosby, 2015).

252 Lee, S. J. *et al.* Angiopoietin-2 exacerbates cardiac hypoxia and inflammation after myocardial infarction. *J Clin Invest* **128**, 5018-5033, doi:10.1172/JCI99659 (2018).

253 Gogiraju, R., Bochenek, M. L. & Schafer, K. Angiogenic Endothelial Cell Signaling in Cardiac Hypertrophy and Heart Failure. *Front Cardiovasc Med* **6**, 20, doi:10.3389/fcvm.2019.00020 (2019).

254 Waddingham, M. T. *et al.* Diastolic dysfunction is initiated by cardiomyocyte impairment ahead of endothelial dysfunction due to increased oxidative stress and inflammation in an experimental prediabetes model. *J Mol Cell Cardiol* **137**, 119-131, doi:10.1016/j.yjmcc.2019.10.005 (2019).

255 Avolio, E. & Madeddu, P. Discovering cardiac pericyte biology: From physiopathological mechanisms to potential therapeutic applications in ischemic heart disease. *Vascul Pharmacol* **86**, 53-63, doi:10.1016/j.vph.2016.05.009 (2016).

256 Warmke, N., Griffin, K. J. & Cubbon, R. M. Pericytes in diabetes-associated vascular disease. *J Diabetes Complications* **30**, 1643-1650, doi:10.1016/j.jdiacomp.2016.08.005 (2016).

257 Siao, C. J. *et al.* ProNGF, a cytokine induced after myocardial infarction in humans, targets pericytes to promote microvascular damage and activation. *J Exp Med* **209**, 2291-2305, doi:10.1084/jem.20111749 (2012).

258 Nikolakopoulou, A. M. *et al.* Pericyte loss leads to circulatory failure and pleiotrophin depletion causing neuron loss. *Nat Neurosci* **22**, 1089-1098, doi:10.1038/s41593-019-0434-z (2019).

259 Tucsek, Z. *et al.* Aging exacerbates obesity-induced cerebromicrovascular rarefaction, neurovascular uncoupling, and cognitive decline in mice. *J Gerontol A Biol Sci Med Sci* **69**, 1339-1352, doi:10.1093/gerona/glu080 (2014).

260 Zechariah, A. *et al.* Hyperlipidemia attenuates vascular endothelial growth factor-induced angiogenesis, impairs cerebral blood flow, and disturbs stroke recovery via decreased pericyte coverage of brain endothelial cells. *Arterioscler Thromb Vasc Biol* **33**, 1561-1567, doi:10.1161/ATVBAHA.112.300749 (2013).

261 Shah, G. N. *et al.* Pharmacological inhibition of mitochondrial carbonic anhydrases protects mouse cerebral pericytes from high glucose-induced oxidative stress and apoptosis. *J Pharmacol Exp Ther* **344**, 637-645, doi:10.1124/jpet.112.201400 (2013).

262 Nwadozi, E., Rudnicki, M. & Haas, T. L. Metabolic Coordination of Pericyte Phenotypes: Therapeutic Implications. *Front Cell Dev Biol* **8**, 77, doi:10.3389/fcell.2020.00077 (2020).

263 Skinner, S., Locher, R., Niederer, E. & Vetter, W. Can low density lipoprotein influence microvascular caliber? *Microvasc Res* **55**, 241-248, doi:10.1006/mvre.1998.2074 (1998).

264 Chibber, R., Molinatti, P. A., Rosatto, N., Lambourne, B. & Kohner, E. M. Toxic action of advanced glycation end products on cultured retinal capillary pericytes and endothelial cells: relevance to diabetic retinopathy. *Diabetologia* **40**, 156-164, doi:10.1007/s001250050657 (1997).

265 Geraldes, P. & King, G. L. Activation of protein kinase C isoforms and its impact on diabetic complications. *Circ Res* **106**, 1319-1331, doi:10.1161/CIRCRESAHA.110.217117 (2010).

266 Gao, X., Martinez-Lemus, L. A. & Zhang, C. Endothelium-derived hyperpolarizing factor and diabetes. *World J Cardiol* **3**, 25-31, doi:10.4330/wjc.v3.i1.25 (2011).

267 Schiattarella, G. G. *et al.* Nitrosative stress drives heart failure with preserved ejection fraction. *Nature* **568**, 351-356, doi:10.1038/s41586-019-1100-z (2019).

268 Schwarzl, M. *et al.* Risk factors for heart failure are associated with alterations of the LV end-diastolic pressure-volume relationship in non-heart failure individuals: data from a large-scale, population-based cohort. *Eur Heart J* **37**, 1807-1814, doi:10.1093/eurheartj/ehw120 (2016).

269 Dunlay, S. M. *et al.* Type 2 Diabetes Mellitus and Heart Failure: A Scientific Statement From the American Heart Association and the Heart Failure Society of America: This statement does not represent an update of the 2017 ACC/AHA/HFSA heart failure guideline update. *Circulation* **140**, e294-e324, doi:10.1161/CIR.0000000000000691 (2019).

270 Dietrich, N. *et al.* The DPP4 Inhibitor Linagliptin Protects from Experimental Diabetic Retinopathy. *PLoS One* **11**, e0167853, doi:10.1371/journal.pone.0167853 (2016).
271 Thomas, L. *et al.* (R)-8-(3-amino-piperidin-1-yl)-7-but-2-ynyl-3-methyl-1-(4-methyl-quinazolin-2-ylm ethyl)-3,7-dihydro-purine-2,6-dione (BI 1356), a novel xanthine-based dipeptidyl peptidase 4 inhibitor, has a superior potency and longer duration of action compared with other dipeptidyl peptidase-4 inhibitors. *J Pharmacol Exp Ther* **325**, 175-182, doi:10.1124/jpet.107.135723 (2008).
272 Krysiak, J. *et al.* Protein phosphatase 5 regulates titin phosphorylation and function at a sarcomere-associated mechanosensor complex in cardiomyocytes. *Nat Commun* **9**, 262, doi:10.1038/s41467-017-02483-3 (2018).
273 Granzier, H. L. & Irving, T. C. Passive tension in cardiac muscle: contribution of collagen, titin, microtubules, and intermediate filaments. *Biophys J* **68**, 1027-1044, doi:10.1016/S0006-3495(95)80278-X (1995).
274 Hamdani, N., Bishu, K. G., von Frieling-Salewsky, M., Redfield, M. M. & Linke, W. A. Deranged myofilament phosphorylation and function in experimental heart failure with preserved ejection fraction. *Cardiovasc Res* **97**, 464-471, doi:10.1093/cvr/cvs353 (2013).
275 Hansen, H. H. *et al.* The DPP-IV inhibitor linagliptin and GLP-1 induce synergistic effects on body weight loss and appetite suppression in the diet-induced obese rat. *Eur J Pharmacol* **741**, 254-263, doi:10.1016/j.ejphar.2014.08.010 (2014).
276 Habibi, J., Aroor, A. R., Klein, T., Mayoux, E. & DeMarco, V. G. Combination Linagliptin and Empagliflozin Therapy Improves Diastolic Function in Female Diabetic db/db Mice. *Diabetes* **67**, -, doi:https://doi.org/10.2337/db18-2016-P (2018).
277 Koibuchi, N. *et al.* DPP-4 inhibitor linagliptin ameliorates cardiovascular injury in salt-sensitive hypertensive rats independently of blood glucose and blood pressure. *Cardiovasc Diabetol* **13**, 157, doi:10.1186/s12933-014-0157-0 (2014).
278 Cazorla, O. *et al.* Differential expression of cardiac titin isoforms and modulation of cellular stiffness. *Circ Res* **86**, 59-67, doi:10.1161/01.res.86.1.59 (2000).
279 Helmes, M. *et al.* Mechanically driven contour-length adjustment in rat cardiac titin's unique N2B sequence: titin is an adjustable spring. *Circ Res* **84**, 1339-1352, doi:10.1161/01.res.84.11.1339 (1999).
280 Hamdani, N. & Paulus, W. J. Myocardial titin and collagen in cardiac diastolic dysfunction: partners in crime. *Circulation* **128**, 5-8, doi:10.1161/CIRCULATIONAHA.113.003437 (2013).
281 Kotter, S. *et al.* Differential changes in titin domain phosphorylation increase myofilament stiffness in failing human hearts. *Cardiovasc Res* **99**, 648-656, doi:10.1093/cvr/cvt144 (2013).
282 Hamdani, N. *et al.* Crucial role for Ca2(+)/calmodulin-dependent protein kinase-II in regulating diastolic stress of normal and failing hearts via titin phosphorylation. *Circ Res* **112**, 664-674, doi:10.1161/CIRCRESAHA.111.300105 (2013).
283 Hidalgo, C. *et al.* PKC phosphorylation of titin's PEVK element: a novel and conserved pathway for modulating myocardial stiffness. *Circ Res* **105**, 631-638, 617 p following 638, doi:10.1161/CIRCRESAHA.109.198465 (2009).
284 Ku, H. C., Chen, W. P. & Su, M. J. DPP4 deficiency exerts protective effect against H2O2 induced oxidative stress in isolated cardiomyocytes. *PLoS One* **8**, e54518, doi:10.1371/journal.pone.0054518 (2013).
285 Ma, Y. *et al.* DPP-4 inhibitor anagliptin protects against hypoxia-induced cytotoxicity in cardiac H9C2 cells. *Artif Cells Nanomed Biotechnol* **47**, 3823-3831, doi:10.1080/21691401.2019.1652624 (2019).
286 Koyani, C. N. *et al.* Dipeptidyl peptidase-4 independent cardiac dysfunction links saxagliptin to heart failure. *Biochem Pharmacol* **145**, 64-80, doi:10.1016/j.bcp.2017.08.021 (2017).
287 Koyani, C. N. *et al.* Saxagliptin but Not Sitagliptin Inhibits CaMKII and PKC via DPP9 Inhibition in Cardiomyocytes. *Front Physiol* **9**, 1622, doi:10.3389/fphys.2018.01622 (2018).
288 Aroor, A. R. *et al.* Dipeptidyl peptidase-4 (DPP-4) inhibition with linagliptin reduces western diet-induced myocardial TRAF3IP2 expression, inflammation and fibrosis in female mice. *Cardiovasc Diabetol* **16**, 61, doi:10.1186/s12933-017-0544-4 (2017).

289 Lim, C. C. *et al.* Anthracyclines induce calpain-dependent titin proteolysis and necrosis in cardiomyocytes. *J Biol Chem* **279**, 8290-8299, doi:10.1074/jbc.M308033200 (2004).
290 Morano, I. *et al.* Titin, myosin light chains and C-protein in the developing and failing human heart. *J Mol Cell Cardiol* **26**, 361-368, doi:10.1006/jmcc.1994.1045 (1994).
291 Ye, L. *et al.* Truncations of the titin Z-disc predispose to a heart failure with preserved ejection phenotype in the context of pressure overload. *PLoS One* **13**, e0201498, doi:10.1371/journal.pone.0201498 (2018).
292 Granzier, H. L. *et al.* Deleting titin's I-band/A-band junction reveals critical roles for titin in biomechanical sensing and cardiac function. *Proc Natl Acad Sci U S A* **111**, 14589-14594, doi:10.1073/pnas.1411493111 (2014).
293 Kruger, M., Babicz, K., von Frieling-Salewsky, M. & Linke, W. A. Insulin signaling regulates cardiac titin properties in heart development and diabetic cardiomyopathy. *J Mol Cell Cardiol* **48**, 910-916, doi:10.1016/j.yjmcc.2010.02.012 (2010).
294 Hidalgo, C., Saripalli, C. & Granzier, H. L. Effect of exercise training on post-translational and post-transcriptional regulation of titin stiffness in striated muscle of wild type and IG KO mice. *Arch Biochem Biophys* **552-553**, 100-107, doi:10.1016/j.abb.2014.02.010 (2014).
295 Deacon, C. F. Dipeptidyl peptidase-4 inhibitors in the treatment of type 2 diabetes: a comparative review. *Diabetes Obes Metab* **13**, 7-18, doi:10.1111/j.1463-1326.2010.01306.x (2011).
296 Graefe-Mody, U. *et al.* Effect of renal impairment on the pharmacokinetics of the dipeptidyl peptidase-4 inhibitor linagliptin(*). *Diabetes Obes Metab* **13**, 939-946, doi:10.1111/j.1463-1326.2011.01458.x (2011).
297 von Eynatten, M., Gong, Y., Emser, A. & Woerle, H. J. Efficacy and safety of linagliptin in type 2 diabetes subjects at high risk for renal and cardiovascular disease: a pooled analysis of six phase III clinical trials. *Cardiovasc Diabetol* **12**, 60, doi:10.1186/1475-2840-12-60 (2013).
298 Camacho, P., Fan, H., Liu, Z. & He, J. Q. Small mammalian animal models of heart disease. *Am J Cardiovasc Dis* **6**, 70-80 (2016).
299 Nadar, S. New Classification for Heart Failure with Mildly Reduced Ejection Fraction: Greater clarity or more confusion? *Sultan Qaboos Univ Med J* **17**, e23-e26, doi:10.18295/squmj.2016.17.01.005 (2017).
300 Zacchigna, S. *et al.* Toward standardization of echocardiography for the evaluation of left ventricular function in adult rodents: a position paper of the ESC Working Group on Myocardial Function. *Cardiovasc Res*, doi:10.1093/cvr/cvaa110 (2020).
301 Shillcutt, S. K. *et al.* Heart Failure With Preserved Ejection Fraction: A Perioperative Review. *J Cardiothorac Vasc Anesth* **31**, 1820-1830, doi:10.1053/j.jvca.2017.06.009 (2017).
302 Borlaug, B. A. Is HFpEF One Disease or Many? *J Am Coll Cardiol* **67**, 671-673, doi:10.1016/j.jacc.2015.11.045 (2016).
303 Verdonschot, J. A. J. *et al.* Titin cardiomyopathy leads to altered mitochondrial energetics, increased fibrosis and long-term life-threatening arrhythmias. *Eur Heart J* **39**, 864-873, doi:10.1093/eurheartj/ehx808 (2018).
304 Ali, M. A. *et al.* Titin is a target of matrix metalloproteinase-2: implications in myocardial ischemia/reperfusion injury. *Circulation* **122**, 2039-2047, doi:10.1161/CIRCULATIONAHA.109.930222 (2010).
305 Chen, C. W. *et al.* Human pericytes for ischemic heart repair. *Stem Cells* **31**, 305-316, doi:10.1002/stem.1285 (2013).
306 Mendel, T. A. *et al.* Pericytes derived from adipose-derived stem cells protect against retinal vasculopathy. *PLoS One* **8**, e65691, doi:10.1371/journal.pone.0065691 (2013).
307 Tilton, R. G., Hoffmann, P. L., Kilo, C. & Williamson, J. R. Pericyte degeneration and basement membrane thickening in skeletal muscle capillaries of human diabetics. *Diabetes* **30**, 326-334, doi:10.2337/diab.30.4.326 (1981).
308 Teng, S. & Huang, P. The effect of type 2 diabetes mellitus and obesity on muscle progenitor cell function. *Stem Cell Res Ther* **10**, 103, doi:10.1186/s13287-019-1186-0 (2019).
309 Lebrin, F. *et al.* Thalidomide stimulates vessel maturation and reduces epistaxis in individuals with hereditary hemorrhagic telangiectasia. *Nat Med* **16**, 420-428, doi:10.1038/nm.2131 (2010).

310 Ryu, J. K. & McLarnon, J. G. Thalidomide inhibition of perturbed vasculature and glial-derived tumor necrosis factor-alpha in an animal model of inflamed Alzheimer's disease brain. *Neurobiol Dis* **29**, 254-266, doi:10.1016/j.nbd.2007.08.019 (2008).
311 Chintalgattu, V. *et al.* Coronary microvascular pericytes are the cellular target of sunitinib malate-induced cardiotoxicity. *Sci Transl Med* **5**, 187ra169, doi:10.1126/scitranslmed.3005066 (2013).
312 Moudgil, R. & Yeh, E. T. Mechanisms of Cardiotoxicity of Cancer Chemotherapeutic Agents: Cardiomyopathy and Beyond. *Can J Cardiol* **32**, 863-870 e865, doi:10.1016/j.cjca.2016.01.027 (2016).
313 Armulik, A., Genove, G. & Betsholtz, C. Pericytes: developmental, physiological, and pathological perspectives, problems, and promises. *Dev Cell* **21**, 193-215, doi:10.1016/j.devcel.2011.07.001 (2011).
314 Chen, Y. T. *et al.* Platelet-derived growth factor receptor signaling activates pericyte-myofibroblast transition in obstructive and post-ischemic kidney fibrosis. *Kidney Int* **80**, 1170-1181, doi:10.1038/ki.2011.208 (2011).
315 Avendano, M. S. *et al.* mPGES-1 (Microsomal Prostaglandin E Synthase-1) Mediates Vascular Dysfunction in Hypertension Through Oxidative Stress. *Hypertension* **72**, 492-502, doi:10.1161/HYPERTENSIONAHA.118.10833 (2018).
316 Gomez, I., Foudi, N., Longrois, D. & Norel, X. The role of prostaglandin E2 in human vascular inflammation. *Prostaglandins Leukot Essent Fatty Acids* **89**, 55-63, doi:10.1016/j.plefa.2013.04.004 (2013).
317 Zhang, J., Gong, Y. & Yu, Y. PG F(2alpha) Receptor: A Promising Therapeutic Target for Cardiovascular Disease. *Front Pharmacol* **1**, 116, doi:10.3389/fphar.2010.00116 (2010).
318 Sinaiko, A. R. *et al.* Relation of body mass index and insulin resistance to cardiovascular risk factors, inflammatory factors, and oxidative stress during adolescence. *Circulation* **111**, 1985-1991, doi:10.1161/01.CIR.0000161837.23846.57 (2005).
319 Helmersson, J., Vessby, B., Larsson, A. & Basu, S. Association of type 2 diabetes with cyclooxygenase-mediated inflammation and oxidative stress in an elderly population. *Circulation* **109**, 1729-1734, doi:10.1161/01.CIR.0000124718.99562.91 (2004).
320 Wohlin, M. *et al.* Both cyclooxygenase- and cytokine-mediated inflammation are associated with carotid intima-media thickness. *Cytokine* **38**, 130-136, doi:10.1016/j.cyto.2007.05.014 (2007).
321 Helmersson, J., Arnlov, J., Axelsson, T. & Basu, S. A polymorphism in the cyclooxygenase 1 gene is associated with decreased inflammatory prostaglandin F2alpha formation and lower risk of cardiovascular disease. *Prostaglandins Leukot Essent Fatty Acids* **80**, 51-56, doi:10.1016/j.plefa.2008.11.001 (2009).
322 Furuhashi, M. *et al.* Platelet-derived growth factor production by B16 melanoma cells leads to increased pericyte abundance in tumors and an associated increase in tumor growth rate. *Cancer Res* **64**, 2725-2733, doi:10.1158/0008-5472.can-03-1489 (2004).
323 McHugh, K. *et al.* Heart Failure With Preserved Ejection Fraction and Diabetes: JACC State-of-the-Art Review. *J Am Coll Cardiol* **73**, 602-611, doi:10.1016/j.jacc.2018.11.033 (2019).
324 Owan, T. E. *et al.* Trends in prevalence and outcome of heart failure with preserved ejection fraction. *N Engl J Med* **355**, 251-259, doi:10.1056/NEJMoa052256 (2006).
325 Diez, J. *et al.* Losartan-dependent regression of myocardial fibrosis is associated with reduction of left ventricular chamber stiffness in hypertensive patients. *Circulation* **105**, 2512-2517, doi:10.1161/01.cir.0000017264.66561.3d (2002).
326 Ciampi, Q. *et al.* Effect of hypertrophy on left ventricular diastolic function in patients with hypertrophic cardiomyopathy. *Heart Int* **2**, 106, doi:10.4081/hi.2006.106 (2006).
327 Franssen, C., Kole, J., Musters, R., Hamdani, N. & Paulus, W. J. alpha-B Crystallin Reverses High Diastolic Stiffness of Failing Human Cardiomyocytes. *Circ Heart Fail* **10**, e003626, doi:10.1161/CIRCHEARTFAILURE.116.003626 (2017).

Curriculum Vitae

Ilona.cuijpers@kuleuven.be

+31 638749481

Donderveldstraat 3,
6367 XW, Voerendaal
Netherlands

Skills

- Persuasion, integrity, and flexibility
- Project and time management
- Leadership and coaching
- Oral and written communication
- Critical and analytical thinking
- Problem solving and creativity
- Networking and teamwork
- Molecular, histological, and cellular techniques
- Laboratory animal science
- Prism, Image J, Inkscape, Zeiss

Research Interests

- Cardiovascular Research
- Metabolic Syndrome

Ilona Cuijpers

Education

09/2016 – Present **Double degree PhD Biomedical Sciences**
Supervisors: Prof. E.A.V. Jones and S. Heymans

09/2014 – 09/2016 **MSc of Biomedical Sciences**
Maastricht University, Netherlands
Major: Clinical Molecular Sciences
Senior Thesis: Stanols as treatment for Niemann-Pick type C1 disease, Molecular genetics
Junior Thesis: The role of obesity-induced macrophages in non-alcoholic steatohepatitis, Internal Medicine

09/2011 – 09/2014 **BSc of Biomedical Sciences**
Maastricht University, Netherlands
Major: Molecular Life Sciences
Minors: Diseased cells and chronic inflammatory diseases
Thesis: 27-hydroxycholesterol as a treatment for Niemann-Pick type C1 disease, Molecular Genetics

Publications

Cuijpers I.*, Papageorgiou A.P.*, Carai P., Herwig M., Mügge A., Klein T., Hamdani N., Jones E.A.V., and Heymans S. Linagliptin prevents left ventricular stiffening by reducing titin cleavage and hypophosphorylation. Submitted to Cellular and Molecular Medicine.

Cuijpers I., Carai P., Mendes-Ferriera P., Simmonds S.J., Mulder P., Miranda-Silva D., De Giorgio D., Pokreisz P., Heymans S., and Jones E.A.V. The effect of different anaesthetics on echocardiographic evaluation of diastolic dysfunction in a heart failure with preserved ejection fraction model. Submitted to nature scientific reports.

Cuijpers I., Simmonds S.J., Carai P., Vertommen L., Papageorgiou A.P., Heymans S., Jones E.A.V. Capillary regression triggered by pericyte loss is an early event in the development of heart failure with preserved ejection fraction. In preparation.

Simmonds S.J.*, **Cuijpers I**.*, Heymans S. and Jones E.A.V. Cellular and Molecular Differences between HFpEF and HFrEF: A Step Ahead in an improved Pathological Understanding. Cells 9, (2020).

Cuijpers I.*, Simmonds S.J.*, van Bilsen M., Czarnowska E., González Miqeuo A., Heymans S. , Kuhn A.R., Mulder P., Ratajska A., Jones E.A.V., Brakenhielm E. Microvascular and lymphatic dysfunction in HFpEF and its associated comorbidities. Bas Res Cardiol 115, (2020).

Zacchigna S., Paldino A., Falcão-Pires I., Daskapoulus E.P., Dal Ferro M., Vodret S., Cannatà A., Miranda-Silva D., Lourenco A.P., Pinamonti B., Sinagra G., Wienberger F., Eschenhagen T., Carrier L. Kehat I. Tocchetti C.G., Russo M., Ghigo A., Cimino J., Hirsch E., Dawson D., Ciccarelli M., Oliverti M., Linke W.A., **Cuijpers I.,** et al. Towards standardization of echocardiography for the evaluation of left ventricular function in adult rodents: a position paper of the ESC working Group on Myocardial Function. Cardiovasc Res, (2020).

Rienks M,. Carai P., Bitsch N., Schellings M., Vanhaverbeke M., Verjans J., **Cuijpers I.**, Heymans S., Papageorgiou A. Sema3A Promotes the Resolution of Cardiac Inflammation after Myocardial Infarction. Basic Res Cardiol 112(4), (2017).

Caolo V., Roblain Q., Lecomte J., Carai P., Peters L., **Cuijpers I**., Robinson E.L., Derks K., Sergeys J., Noël A., Jones E.A.V., Moons L., Heymans S. Resistance to Retinopathy Development in Obese, Diabetic and Hypertensive ZSF1 rats: An Exciting Model to Identify Protective Genes. Sci Rep 9(8), (2018).

Bijnen M., Josefs T., **Cuijpers I.**, Maalsen C.J., van de Gaar J., Vroomen M., Wijnands E., Rensen S.S., Greve J.W.M., Hofker M.H., Biessen E.A.L., Stehouwer C.D.A., Schalkwijk C.G., Wouters K. Adipose Tissue Macrophages Induce Hepatic Neutrophil Recruitment and Macrophage Accumulation in Mice. Gut 67(7), (2018).

Awards

10/2017 – Present	Fonds Wetenschappelijk Onderzoek Vlaanderen PhD Grant (4 years)
03/2020	Healthy Heart Travel Fund
02/2018	European Society of Cardiology (ESC) travel grant
06/2017	Basic Science ESC Summer School Travel grant

Poster and oral presentations at scientific meetings and congresses

06/2019	Capillary rarefaction precedes HFpEF development in obese ZSF1 rats. *Center for Molecular and Cardiovascular Biology Department Event, Leuven, Belgium (Poster)*
01/2019	Capillary rarefaction precedes HFpEF development in obese ZSF1 rats. *ESC heart failure winter meeting, Les Diablerets, Switzerland (Poster)*
11/2018	Capillary rarefaction precedes HFpEF development in obese ZSF1 rats. *Dutch Heart Foundation Cardiac Function and Adaptation, Papendal, Netherlands (Poster)*
04/2018	Linagliptin prevents cardiac fibrosis, inflammation and hypertrophy in obese ZSF1 rats. *ESC Frontiers in Cardiovascular Biology, Vienna, Austria (Poster)*
06/2017	Linagliptin prevents cardiac fibrosis, inflammation and hypertrophy in obese diabetic hypertensive ZSF1 rats. *ESC Basic Summer School, Nice, France (Poster)*
05/2017	Linagliptin prevents cardiac fibrosis, inflammation and hypertrophy in obese diabetic hypertensive ZSF1 rats. *ESC working group of myocardial function, Varenna, Italy (Oral and Poster presentation)*
10/2016	Linagliptin ameliorates the metabolic syndrome and prevents HFpEF. *Dutch Heart Foundation, Vascular Biology, Papendal, Netherlands (Poster presentation)*
07/2016	Stanols a new ally in the battle against Niemann-Pick type C1 disease. *Mosa Conference Maastricht, Netherlands (Oral and Poster presentation)*

Teaching

09/2019 - 03/2020	Co-supervisor of international research student (Daria De Giorgio)
09/2018 – 07/2019	Co-supervisor of Bachelor Erasmus Student (Laura Florit González)
02/2017 - 06/2017	Supervisor of Master Student Group T (Liene Vertommen)

Courses

09/2019	Good Clinical Practice (GCP; KU Leuven)
06/2019	Drug Development Course (Maastricht)
05/2019	Leadership (KU Leuven)
05/2019	Medical writing for industry (Janssen R&D)
05/2019	Writing for Medical Journals (Lancet)
05/2019	Transmission microscopy (VIB)
05/2019	Severity Assessment Animal Science (KU Leuven)
03/2019	Research Integrity (KU Leuven)
12/2018	Management of the PhD (KU Leuven)
11/2018	Dutch Heart Foundation Cardiac function and adaptation
05/2018	State-of-the-art research methods in biology (KU Leuven)'
01/2018	Medical writing (ILT, KU Leuven)
06/2017	ESC Basic Summer School (European Society of Cardiology)
05/2017	Confocal and general Microscopy (KU Leuven)
11/2016	Dutch Heart Foundation Vascular Biology

Other scientific and Extracurricular Activities

09/2019 - Present	Organization Pint of Science Festival
01/2020	Good manufacturing practice (GMP; Advipro)
05/2019	Speaker at the Pint of Science Festival Leuven
08/2019	Reviewer for European Journal of Heart Failure
2018, 2019	Annual report for the ERA-CVD Lymit-Dys
03/2019	Final report for the fibrotargets project